

Università degli studi di Padova
Dipartimento di Fisica e Astronomia
Master Degree in Astrophysics and Cosmology

Modelling quasi- and non-linear effects in the redshift space two-point correlation function

Relatore:
Prof. Daniele Bertacca

Laureando:
Riccardo Mezzani



Year 2024-2025

*To my Family, for their constant and selfless support.
To my Friends, for their effort in lightening the path.
To my Masters, for their ability to set things in motion when I felt trapped.
To You who are reading these lines,
to remember that "one breath at the time" anyone can travel a long distance.*

~

*Alla mia Famiglia, per il loro costante e gratuito supporto.
Ai miei Amici, per il loro impegno nell'alleggerire il cammino.
Ai miei Maestri, per la loro abilità di smuovermi quando mi son sentito intrappolato.
A Te che stai leggendo queste righe,
per ricordarti che "un respiro alla volta" chiunque può arrivare lontano.*

Abstract

Current and future galaxy surveys will be used to measure baryonic acoustic oscillations (BAOs) with high significance. In this thesis, we study BAO anisotropies arising in the two-point correlation function (2PCF) of galaxy redshift space and we do so with a derivation of the configuration-space 2PCF using the streaming model (Peebles 1980; Fisher et al. 1994; Fisher 1995; Scoccimarro 2004). Following the approach discussed in Jeong et al. 2015 and applying the streaming model further developed in A. Taruya et al. 2010, we can exploit the non-linear anisotropies of BAOs in redshift space to extract the cosmological information contained in BAOs themselves.

Contents

Abstract	iii
1 Introduction	1
1.1 Cosmological Principle	2
1.2 Background Cosmology	5
1.2.1 Cosmological Redshift	7
1.3 On Matter Clustering	9
1.3.1 Evolution of Perturbations	11
1.4 On Galaxy Statistics	14
1.4.1 Two Point Correlation Function and Power Spectrum	17
1.4.2 The Matter Power Spectrum	20
1.5 On Baryon Acoustic Oscillations	21
1.5.1 BAOs as a Statistical Standard Ruler	24
1.5.2 Retrieving Cosmological Information From BAOs	26
2 Theoretical Models of Redshift Space Distortions	28
2.1 On Redshift Space Distortions	29
2.2 Plane-Parallel Approximation	30
2.3 Derivation of the Kaiser Formula	32
2.3.1 On the Bias Factor	36
2.4 RSDs: a Phenomenological Description	37
2.5 The Streaming Model	39
2.5.1 Pairwise Velocity Moments	45
2.5.2 The Large Scale Limit	49
2.5.3 The Power Spectrum in the Streaming Model	51
2.6 Multipole Expansion of the Redshift Power Spectrum	52
2.7 The TNS Model	55
2.7.1 Zeroth Order Power Spectra	61
2.7.2 First Order Power Spectra	64
2.7.3 Second Order Power Spectra	65
2.8 Comparison Between Different Models	68
2.8.1 A New Definition for the Generating Function	71

3	Nonlinear Description of the Redshift Space 2PCF	74
3.1	On the D. Jeong et al. Description of the Redshift Space 2PCF	74
3.2	Toward a Configuration Space Description of the TNS Model	78
3.2.1	The Redshift Space 2PCF from the TNS Model	83
3.3	The Reid & White Approach: A Bridge Between Streaming and TNS Models	87
3.4	Improving the Derivation Accounting for Nonlinear terms	91
3.4.1	Multipole Decomposition Accounting for Nonlinear Terms	93
3.5	The Shift of the BAO Peak	99
4	Conclusions	105
4.1	Summary	105
4.2	Outlook	107
	Appendix A: Velocity Moment Relation with 2PCF Multipoles	109
	First Derivative of the Mean Displacement	109
	First Derivative of the Velocity Dispersion	111
	Second Derivative of the Velocity Dispersion	112
	Appendix B: Reconstruction of the Redshift 2PCF Using Multipoles	115
	List of Abbreviations	117
	Bibliography	118

1. Introduction

The *Two-Point Correlation Function* (2PCF hereafter) of the galaxy density fields has been an important tool for modern cosmology. It has already provided important constraints, thanks to the large scales surveys like the Sloan Digital Sky Survey (SDSS) with eBOSS [16], WiggleZ [9] and VIPERS [15], to the current Λ CDM model. Measurements from large scales distribution of galaxies will be further improved with the future data release of surveys such as the ESA mission Euclid¹, where the 2PCF will continue to be the key observable from which extract cosmological information.

One of the main goals of cosmological surveys is to constrain the properties of *Dark Energy* (DE from now on) by exploiting *Baryonic Acoustic Oscillations* (BAOs) in the galaxy 2PCF as standard rulers. BAOs appear as a peak corresponding to a scale of $d_{BAO} \simeq 105.6 [h^{-1}\text{Mpc}]$ [34] in the galaxy 2PCF, which correspond to the comoving distance travelled by the baryon-photon fluid from the Big Bang to the recombination epoch at redshift $z \simeq 1080$ [72]. The distance of the peak can be determined by very simple physics once one has determined the epoch of recombination: the time when photons decoupled from the matter of the Universe and started their free travel in a transparent environment [72]. From the BAO acoustic peak of the 2PCF we can retrieve information about the angular diameter distance, $D_A(z)$, and expansion rate, $H(z)$, by looking respectively at the angular separation and redshift difference between galaxies. These measurements combined can then help constraining the energy density and equation of state of DE [54, 59].

Given the early difficulties detecting the BAO bump, the first works focused on the angular averaged 2PCF, namely the monopole contribution, to constrain DE properties. Today surveys, however, are already characterized with a much better signal-to-noise ratio, making us able to focus on more robust statistics such the quadrupole [37, 48]. This combined measures allow the independent determination of $D_A(z)$ and $H(z)$ [72]. Future missions will be able to detect BAOs with even higher significance, allowing the detection of the BAO bump as a function of the orientation with respect to the line of sight and improving even further the measurement of $D_A(z)$ and $H(z)$.

With this work we want to characterize the description of the 2PCF as a function of the redshift space separation parallel and orthogonal to the line of sight. Our major tools will be the streaming model as presented by R. Scoccimarro in [58] and its iteration proposed by Taruya, Nishimichi and Saito in 2010 [68], from which we will derive the behaviour of the correlation function and the BAO bump. In this first Chapter we collected the fundamental concepts from which this work has been developed; we divided it as follows

- In Section 1.1 we present the cosmological principle and the implications coming from its assumption, both on theoretical and philosophical level.

¹https://www.esa.int/Science_Exploration/Space_Science/Euclid

- In Section 1.2 we focus on the cosmological aspects which constitute the basis of this work, with a particular focus, in Section 1.2.1, for the definition of the cosmological redshift, which constitutes our access to the third dimension.
- Section 1.3 defines matter perturbations: the density contrast and velocity fields of galaxies. Through Section 1.3.1, we summarize the current state of play of their evolution in different regimes.
- In Section 1.4 we focus on galaxy clustering: we define spatial correlation functions starting from the phase space analysis, done by adapting plasma physics for an expanding Universe. In 1.4.1 we use those definitions to build up specifically the 2PCF and the *Power Spectrum* (PS), which constitute the fundamental functions to implement the analysis inside Chapters 2 and 3 later on.
- Finally, in Section 1.5 we describe the BAO phenomenon, its important qualities as a statistical standard ruler, Section 1.5.1, and how it is possible to retrieve cosmological information from its investigation, Section 1.5.2.

1.1 Cosmological Principle

Stated in its first form by Milne in the early 30s of the past century as the *Extended Principle of Relativity* [45], it quickly became the fundamental principle of the modern cosmology. Nowadays it refers to the assumption of homogeneity and isotropy of the Universe and its strength comes from the fact that, on one hand, it is able to simplify equations in such a way to make theoretical analysis treatable, while on the other hand it has also very profound philosophical merits. First, among those philosophical merits, comes the extreme advantage determined by an isotropic and homogeneous universe: it would be, indeed, nearly impossible trying to understand a universe where physical conditions or, in even more dramatic scenarios, physical laws keep changing as one moves from region to region [12].

A more physical oriented validation of the Cosmological Principle came with the advent of general relativity: within Einstein's new theory of gravitation, isotropic and homogeneous universes possess what have been called *Cosmological Horizon*, a theoretical spherical surface that can be drawn around any event and describes the limit of causal connection. In other words, given an event in the Universe and its cosmological horizon, a second event could have been in causal connection to the first one only if it took place within the above mentioned cosmological horizon. The validation of the Cosmological Principle then comes from the analysis of the largest available cosmological scales, like for example the *Cosmic Microwave Background* (CMB), the radiation coming from the last scattering surface where photons decoupled from matter and started their free path in a transparent environment: if we fix a point on the CMB, the cosmological horizon will be a circle subtending an angle of approximately 1° ; at the same time however, for any point in the CMB surface we see a temperature which deviates from the mean value of the order of 10^{-5} [K] [1], even from regions of CMB well beyond a 1° separation [42]. This "agreement" between causal disconnected regions can be explained by either a re-evaluation of the cosmological horizon, like it is done in inflationary models, or by enforcing the Cosmological

Principle² [12].

With homogeneity we refer to the ability of a given field, and its statistical properties, to be invariant under translation of spatial coordinates, while isotropy reflects the property of being invariant under rotations of the spatial coordinates [7, 12]. Here we want to stress that, in cosmology, we refer to these two properties at a statistical level: we see indeed strong inhomogeneities in our Universe such as, for example, density fluctuations between the extra-galactic void and the core of a star. However, if we define galaxies as the fundamental blocks of the largest cosmological structures, namely clusters and filaments, we are then able to think about scales so large that single stars are not distinguishable any more. On those scales we can think the Universe as homogeneous and isotropic.

As we were saying before, today one of the best validations of the principle comes from the extreme isotropy of the CMB radiation temperature once cleared from the dipole anisotropy due to the Earth motion: a combination of its revolution around the centre of mass of the Solar System, superimposed with the movement of the Solar System itself around the centre of the Milky Way and the one of the Milky Way towards the Great Attractor of the Local Group. The superposition of all these effects corresponds to a solar dipole with an amplitude of $3362.08 \pm 0.99 [\mu K_{\text{CMB}}]$ [1]. In Figure 1.1 we report the latest measurement of the CMB radiation cleared by the solar dipole; each point in the picture represents the temperature deviation from the main value of the CMB, 2.7260 [K] [25], up to a maximum of 300 [μK] [1], with colder regions depicted in blue and hotter ones in red. Through the CMB radiation temperature we are able to support the concept of isotropy. This does not necessarily imply, however, statistical homogeneity without the additional assumption that the observer is not placed in a special place in the Universe: the *Copernican Principle*. In fact, one would be able to observe statistical isotropy in any spherical matter distribution only if they were in its centre. Therefore, observed isotropy implies homogeneity only when coupled with the Copernican Principle [22, 12].

The same reasoning could be applied for matter by looking at the galaxy density field, but it requires some more caution due to the well documented presence of *Cold Dark Matter* (CDM hereafter³), which we cannot directly observe as our detectors are photon sensitive. Consequently, without any further consideration, looking at the galaxy density field we can probe isotropy for luminous matter only, which constitutes the minority of it. We can overcome this problem by asserting that baryonic matter is not placed randomly in the Universe but it rather traces CDM with some sort of bias factor⁴, with galaxies forming more efficiently inside DM halos and filaments [64]. In addition to that, density fields present more severe excursions at small scales than the CMB and thus, in order to exploit the Cosmological Principle while dealing with galaxies, one should care about observing a "sufficiently large" sample (Figure 1.2) [51, 52].

Taken alone, the Cosmological Principle can help us retrieving information about the observable Universe, but then a profound question arises: how can we extend these results to its unseen, and perhaps infinite, part causally disconnected from us? To do so we require an additional condition of the observed field: *Ergodicity*. With the ergodic hypothesis we state that the ensemble average of a

²Note that the two possibilities are not necessarily mutually exclusive. Indeed, within inflation, homogeneity and isotropy come as a consequence of the re-evaluation of the cosmological horizon.

³Throughout the work the acronym CDM is often reported as just DM (Dark Matter), as today cold dark matter is our best candidate of dark matter.

⁴More detailed considerations on the bias will be done in Section 2.3.1.

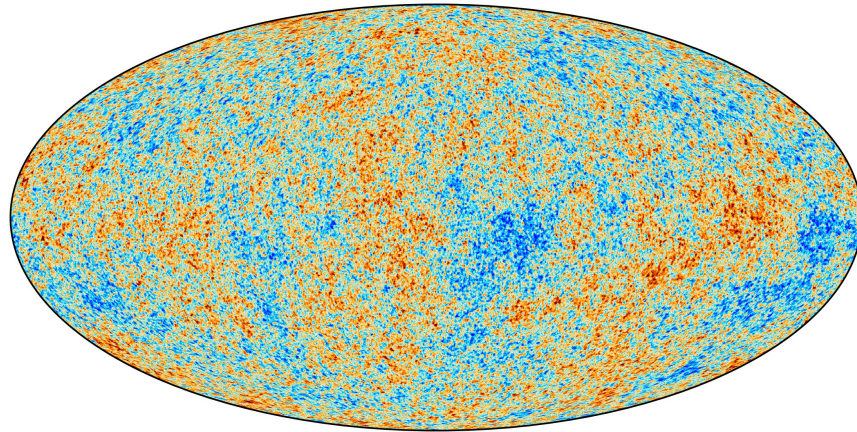


Figure 1.1: Full sky map of the CMB radiation temperature obtained from the Planck survey and presented in 2018. Zones colder than the mean value are depicted in blue while zones hotter than the mean value are depicted in red [1].

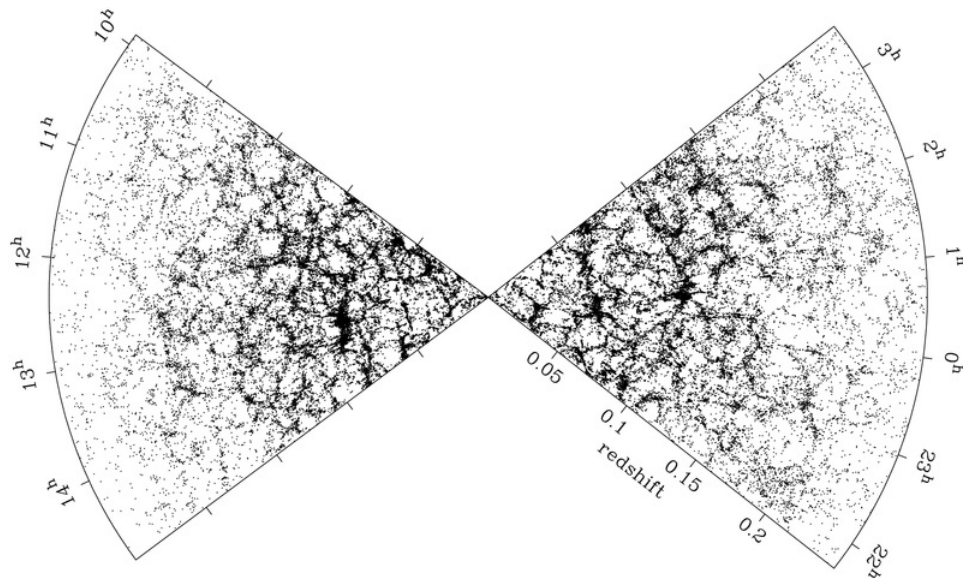


Figure 1.2: The figure illustrates the spatial distribution of the nearly 80000 galaxies included in the 2dFGRS survey, plotted in the redshift/right ascension plane. It is clearly visible that the galaxies are not randomly distributed, but grouped in clusters and filaments enclosing void regions. Figure taken from the 2dFGRS Image Gallery.

given field $f(\mathbf{x})$ is equal to the spatial average taken over one realization of the field itself, namely

$$\langle f(\mathbf{x}) \rangle = \int \mathcal{P}(f) df = \frac{1}{V} \int_V f(\mathbf{x}) d^3\mathbf{x}, \quad (1.1)$$

where $\mathcal{P}(f)$ represents the *Probability Distribution Function* (PDF) of $f(\mathbf{x})$ and V is the volume of the single realization [46]. In other words, if the spatial correlation $\langle f(\mathbf{x}) \rangle$ decays sufficiently fast with an increasing separation, then there will exist many statistical independent volumes in one single realization of the field.

Given the fact that the ergodic hypothesis is proven for Gaussian random fields, like the ones we expect coming from most inflation theories [7], we can pair it with the Cosmological Principle and extend our "local" results to the whole Universe.

To conclude this Section we want to highlight the fact that the assumptions of homogeneity and isotropy do not constitute a theoretical requirement: a strongly inhomogeneous and/or anisotropic universe would not be forbidden by the general theory of relativity. The strength of those assumptions comes from the extremely powerful considerations that can be derived from them and, ultimately, from their agreement with data [52].

1.2 Background Cosmology

Following assumptions of homogeneity and isotropy coming from the Cosmological Principle, it can be shown that we can define the so called *Friedmann-Lemaître-Robertson-Walker metric* (FLRW) as follows [22]

$$ds^2 = -c^2 dt^2 + a^2(t) dl^2 = -c^2 dt^2 + a^2(t) (dx^2 + f_K^2(x) [d\theta^2 + \sin^2(\theta) d\phi^2]), \quad (1.2)$$

with $a(t)$ being the (dimensionless) scale factor of the expanding Universe, c being the speed of light and dl representing the spatial part of the metric. The choice of a dimensionless scale factor is due to the fact that, in this way, we are able to choose freely the normalization of $a(t)$, with the common normalization fixing the today value⁵ of it being $a(t_0) := a_0 = 1$. With a dimensionless $a(t)$, it follows the comoving radial coordinate x to have the dimension of a length and K with dimension of $(\text{length})^{-2}$. The K parameter then gives information about the intrinsic curvature scale R_0 [22] according to

$$|K| = R_0^{-2} = (a_0 H_0 \sqrt{|\Omega_{K0}|})^{-2}, \quad (1.3)$$

with Ω_{K0} being the energy associated with the curvature at the present time; thus $K = 0$ describes a flat space, while $K < 0$ and $K > 0$ relate respectively to open (hyperbolic) and closed (spherical) ones.

The function $f_K(x)$ is the comoving angular diameter distance that depends on the curvature parameter of the Universe K ; this function takes the form [22]

$$f_K(x) = \begin{cases} \sinh(\sqrt{-K}x)/\sqrt{-K}, & \text{if } K < 0 \\ x, & \text{if } K = 0 \\ \sin(\sqrt{K}x)/\sqrt{K}, & \text{if } K > 0. \end{cases} \quad (1.4)$$

⁵Throughout this work, the today value of a given quantity will be labelled with a 0 as subscript.

From the latest cosmological observations, like for example [1], we have a value of K very close to zero⁶, which allows us to consider $f_K(x) = x$.

FLRW metric of equation (1.2) can be further simplified by the definition of the *Conformal Time* τ through the infinitesimal relation

$$d\tau := \frac{dt}{a(t)}; \quad (1.5)$$

with such a redefinition of the time coordinate, the FLRW metric takes the following form

$$ds^2 = a^2(\tau)[-c^2 d\tau^2 + dl^2]. \quad (1.6)$$

The FLRW metric presented above is an exact solution of the Einstein's field equations

$$G_{\mu\nu} + \Lambda g_{\mu\nu} = \frac{8\pi G}{c^4} T_{\mu\nu}, \quad (1.7)$$

where $G_{\mu\nu}$ is the Einstein tensor, Λ is the cosmological constant associated to the vacuum energy, $g_{\mu\nu}$ is the metric tensor, G is the Newton's gravitational constant and $T_{\mu\nu}$ is the stress-energy tensor. If we assume the cosmic fluid to be a perfect one, namely a fluid that can be completely described by just its rest frame mass density ρ and the isotropic pressure P , we can then insert the FLRW metric (1.2) inside the Einstein equations (1.7) to obtain the so called Friedmann equations

$$\begin{aligned} \frac{\ddot{a}}{a} &= -\frac{4\pi G}{3} \left(\rho + \frac{3P}{c^2} \right) + \frac{\Lambda}{3} \\ \left(\frac{\dot{a}}{a} \right)^2 &\equiv H^2 = \frac{8\pi G\rho}{3} - \frac{kc^2}{a^2} + \frac{\Lambda}{3}, \end{aligned} \quad (1.8)$$

where dots represent derivatives with respect to cosmic time. In the previous set of equations we have set $a \equiv a(t)$ in order to lighten the expression and we have defined the Hubble parameter, which gives information about the expansion rate of the Universe, as

$$H(t) := \frac{\dot{a}}{a}. \quad (1.9)$$

The today value of the Hubble parameter, H_0 , is often parametrized as $H_0 := 100h$ km/sMpc, where h is a dimensionless factor of order unity. From the second Friedmann equation we can define the critical density as [73]

$$\rho_{crit} := \frac{3H^2}{8\pi G} \sim 1.95 \times 10^{-29} h^2 \text{ [g/cm}^3\text{]} \quad (1.10)$$

once we have assumed $K = \Lambda = 0$. The critical density is useful because from that we can define the total density parameter

$$\Omega := \frac{\rho}{\rho_{crit}} \quad (1.11)$$

⁶It is important to say that we have not been able to exclude the possibility of a curved Universe yet: referring again to the results of the Planck collaboration [1], we can see they have retrieved a value for the curvature parameter $\Omega_K = 0.0007 \pm 0.0019$. That result is still compatible with anyone of the three scenarios, but since value is so close to zero, the assumption of a flat spacetime is reasonable.

and analogously the density parameters of each component of the Universe

$$\Omega_m := \frac{\rho_m}{\rho_{crit}}, \quad \Omega_r := \frac{\rho_r}{\rho_{crit}}, \quad \Omega_\Lambda := \frac{\rho_\Lambda}{\rho_{crit}}, \quad (1.12)$$

where the suffix m refers to the totality of matter, which is determined by the sum of baryons, labelled with b as a subscript, and CDM $\Omega_m = \Omega_b + \Omega_{\text{CDM}}$. It is important to highlight that with the label "baryons" we identify all the species which constitute ordinary matter, namely protons, neutrons and, despite the fact they are leptons, their associated electrons; this association comes from the fact that neutral atoms require electrons to be paired with the other baryonic particles and, therefore, their mass needs to be accounted for the computation of the density parameter of baryonic matter itself. The label r refers to radiation, which includes photons, labelled with γ , and neutrinos, with ν , $\Omega_r = \Omega_\gamma + \Omega_\nu$; this parameter accounts for the energy density of the relativistic particles of the early Universe and its contribution is negligible at the present day ($\Omega_r(t_0)h^2 \simeq 10^{-4}$) [18]. Finally, DE is labelled with Λ ; its presence comes from the fact that we expect a total density parameter very close to one, but at the same time the total mass density coming from matter is observed to be one third with respect to the critical one: this means that the remaining energy density must be, in absence of curvature, due to DE. The choice of this label rely on the fact that often DE is associated with the famous Einstein's cosmological constant Λ ; it is important to know however, that in full generality we do not have yet constrained properties of DE to be constant at all times [18].

Each one of the density parameters above give information about the relevance of a given species in the energy budget of the Universe. We can see it clearly by looking at the second Friedmann equation (1.8), where the energy density ρ includes contributions from both matter and radiation, if we divide by H^2 we get

$$1 + \frac{kc^2}{a^2H^2} = \Omega_m + \Omega_r + \Omega_\Lambda, \quad (1.13)$$

which is valid at any epoch. Once accounted for all the different species above, we can see from equation (1.13) that the energy density associated to the curvature, $\Omega_k := kc^2/a^2H^2$, can be obtained by subtracting all the other ones to unity.

The best possible present day values of the Ω parameters, retrieved from Planck data [1] coupled with BAOs, are reported in Table 1.1. They describe a Universe very close to flatness but not exactly flat, as predicted by inflationary models [22], with DE taking approximately 70% of the energy density inside it. With the present day energy density of radiation being of the order of 10^{-4} [22], the remaining 30% of the energy budget is due to matter, which is split in approximately 4% determined by baryons and, consequently, 26% due to CDM.

1.2.1 Cosmological Redshift

For each galaxy in a given survey, ideally we want pair up its right ascension and declination coordinates, which mark the direction in the sky to point at in order to observe the galaxy itself, with its radial distance from us; this, done for every galaxy in the survey, will allows us to retrieve a three dimensional map of the galaxy distribution. The point is that we do not have direct access to the radial distance, so we need to rely on different observables like for example the *Redshift* z : the shift toward the red part of the spectrum of a given electromagnetic radiation induced by the recession

Table 1.1: Summary of the present day values of the density parameters, with the subscript 0 referring to the today value of the quantity. Taken from [1].

Cosmological Parameter	Planck + BAOs
Hubble Constant $H(t_0)$	67.66 ± 0.42 [km/s/Mpc]
Baryon Density $\Omega_b(t_0)h^2$	0.02242 ± 0.00014
CDM Density $\Omega_{\text{CDM}}(t_0)h^2$	0.11933 ± 0.00091
DE Density $\Omega_\Lambda(t_0)$	0.6889 ± 0.0056
curvature Density, $\Omega_k(t_0)$	0.0007 ± 0.0019

velocity of the source, which is expanding with the Universe⁷.

In the specific case of an homogeneous and isotropic universe, to define the redshift we start from the FLRW metric of equation (1.2). Again, thanks to the symmetry properties of the line element we can consider photons as if they were travelling radially in their path between the source and the observer, with $d\phi = d\theta = 0$

$$c^2 dt^2 = a^2(t) dx^2. \quad (1.14)$$

Thus equation (1.14) can be integrated to obtain the radial coordinate of the photon as a function of the time of flight of the photons

$$x(t) = \int_t^{t_0} \frac{cdt'}{a(t')}, \quad (1.15)$$

where we have set $x(t_0) = 0$. Here it is important to note that $x(t)$ is a comoving coordinate and, therefore, it does not change due to the Universe expansion. It represents the distance travelled by the electromagnetic signal going from the source, at the time t of the emission, to the observer, at the present time t_0 when the signal is received.

Consider now the computation of the same quantity between the times $t' = t + \delta t_e$ and $t'_0 = t_0 + \delta t_0$, with the two infinitesimal times δt_e and δt_0 representing respectively the time interval between two points with the same phase, i.e. two maxima or two minima, in the wave function of the signal at the emission and at the reception. Since $x(t)$ is constant we can write

$$\int_{t+\delta t_e}^{t_0+\delta t_0} \frac{cdt'}{a(t')} = \int_t^{t_0} \frac{cdt'}{a(t')}, \quad (1.16)$$

which can be written, using the additivity property of integrals, as follows

$$\begin{aligned} \int_{t+\delta t_e}^{t_0} \frac{cdt'}{a(t')} + \int_{t_0}^{t_0+\delta t_0} \frac{cdt'}{a(t')} &= \int_t^{t+\delta t_e} \frac{cdt'}{a(t')} + \int_{t+\delta t_e}^{t_0} \frac{cdt'}{a(t')} \\ \implies \int_{t_0}^{t_0+\delta t_0} \frac{cdt'}{a(t')} &= \int_t^{t+\delta t_e} \frac{cdt'}{a(t')}. \end{aligned} \quad (1.17)$$

⁷In full generality we would have to consider also peculiar velocities of galaxies, this will be done in Section 2.1. For the moment, however, it is sufficient to consider galaxies as if their velocity were due to the expansion of the Universe only.

For an arbitrarily distant source, the time separation between two points with the same phase is much less than the time of flight of photons, hence we can assume $\delta t_e, \delta t_0 \rightarrow 0$ to obtain

$$\frac{\delta t_0}{a(t_0)} = \frac{\delta t}{a(t)} \implies \omega a(t) = \omega_0 a(t_0), \quad (1.18)$$

with the two infinitesimal δt_0 and δt_e that have been identified with the inverse of frequencies of the radiation ω_0 (as seen from the observer today) and $\omega(t)$ (as it was at the emission).

Recalling now the definition of redshift coming from the Doppler effect [12]

$$z := \frac{\omega - \omega_0}{\omega_0} \quad (1.19)$$

we can see that, as a result of the expansion of the Universe, photons travelling the comoving distance between source and observer will be redshifted by

$$1 + z = \frac{\omega}{\omega_0} = \frac{a(t_0)}{a(t)}, \quad (1.20)$$

which links the redshift measurement with the ratio between the scale factor at the time of observation with the one at the time of the emission, making all photons we observe to be redshifted by some amount depending on how far in the past the source emitted the signal. Here we highlight the fact that this reasoning can be done only for distant galaxies: in the nearby Universe the effects due to the cosmological expansion are minimal and, therefore, the redshift effect is dominated by the peculiar motion of the sources.

If the mutual velocity between source and observer is due to the Universe expansion only, then the ratio between the two scale factors inside equation (1.20) can be translated, at least at small redshifts, into a measure of the radial (physical) distance r through the well established Hubble-Lemaître law

$$z = \frac{a(t_0)}{a(t)} - 1 \simeq \frac{a(t_0)}{a(t_0) + \left. \frac{da(t)}{dt} \right|_{t=t_0} (t - t_0)} - 1 \simeq (t_0 - t)H_0, \quad (1.21)$$

where an expansion around the present time t_0 of the time-dependent scale factor has been done. The previous equation can then be recast into the usual form of the Hubble-Lemaître's law using $(t_0 - t) = r/c$, namely

$$z = \frac{r}{c}H_0 \implies cz \simeq w_{\parallel} = rH_0, \quad (1.22)$$

with w_{\parallel} being the radial component of the recession velocity. For larger redshifts this expression has to be replaced by a model-dependent relation.

1.3 On Matter Clustering

The Universe described in the previous Section through the FLRW metric, equation (1.2), is characterized by homogeneity and isotropy. However, with gravitation giving the major contribution for the building of cosmic structures we observe today, such galaxies and clusters of galaxies, a certain amount of small initial density perturbations is required, which need to be properly described. In this

Section we examine cosmological perturbations and their evolution in a regime where their magnitude is small. Given our interest in structures much smaller than the horizon size⁸ [46]

$$x(t) = \int_0^t \frac{cdt'}{a(t')} \quad (1.23)$$

here we will develop a Newtonian description of perturbation in linear regime.

As it is shown schematically below [18], after recombination⁹ matter perturbations, δ and v , depend only on the gravitational potential field Φ , which turns out to be completely independent from radiation at such later times [18]

$$\text{Gravitational Potential: } \Phi \longrightarrow \text{Matter Perturbations: } \delta, v. \quad (1.24)$$

Matter perturbations shown in the schematic representation above are the density contrast δ , which tells us how much the density field differs from its main value, and the peculiar velocity v , which gives information about how the velocity differs from the Hubble expansion. The idea describing matter perturbations, gravitational instability, turns out to be fairly easy to picture: as the cosmic time proceeds, the initial perturbation of the potential start attracting matter inducing a growth of δ and v fields. The other important quantity to correctly describe the growth of matter perturbations before recombination is the pressure, which acts against their growth. Hence, if pressure is low, δ grows exponentially while if it is large, δ presents an oscillating behaviour [18].

First of all, the considerations above are able to give an explanation on why collapse of baryonic matter could not start before recombination: at early times baryons were coupled with radiation and therefore they were affected by radiation pressure, which became stronger as they fell into the potential wells of Φ ; after recombination, when they decoupled from radiation, the pressure contribution vanish until extremely small scales, making baryons able to start their collapse to form galaxies. DM, on the other hand, is never coupled with radiation by definition and so it can start collapsing even before recombination. The oscillating behaviour of baryons in the early Universe is precisely what we call BAOs and their mark is detectable in the present day galaxy statistics. At this point it is clear that, given the dominance of DM over baryons, to characterise correctly matter perturbations one necessarily needs to incorporate DM behaviour.

Since our aim is describing those perturbations in a FLRW universe, it is useful to use comoving rather than physical coordinates; the two are related as follows

$$\mathbf{x}_{\text{phys}}(t) = a(t)\mathbf{x}. \quad (1.25)$$

Then we can identify the recession velocity of a given galaxy, $\mathbf{w}(t, \mathbf{x})$, placed at a comoving coordinate \mathbf{x} as

$$\begin{aligned} \mathbf{w}(t, \mathbf{x}) &= \dot{\mathbf{x}}_{\text{phys}} = \dot{a}(t)\mathbf{x} + a(t)\dot{\mathbf{x}} \\ &= a(t)H(t)\mathbf{x} + a(t)\dot{\mathbf{x}} \equiv \mathcal{H}(t)\mathbf{x} + \mathbf{v}(t, \mathbf{x}), \end{aligned} \quad (1.26)$$

⁸Note that the quantity here defined as the horizon corresponds to the distance travelled by a photon from the origin of the Universe until the given time t . This should not be surprising, since information can travel at most at the speed of light and, therefore, such a definition represents also the maximum radius within which causality holds.

⁹With "recombination" we refer to the epoch around, redshift $z \simeq 1080$, at which the temperature of the Universe reached a value that allowed the recombination of free electrons with the protons in the primordial plasma. The sudden disappearance of charged particles caused the decoupling between the radiation and the baryonic matter, leaving the latter able to cluster into galaxies.

where the dots represent derivatives with respect to time t , $\mathcal{H}(t) := a(t)H(t)$ refer to the conformal Hubble parameter and, finally, $\mathbf{v}(t, \mathbf{x}) := a(t)\mathbf{x}$ is the peculiar velocity describing the motion of the fluid element relative to a comoving observer at coordinate \mathbf{x} . For future convenience, here we define also the velocity divergence field as in [57]

$$\theta(\mathbf{x}) = -\frac{\nabla \cdot \mathbf{v}(t, \mathbf{x})}{aHf}, \quad (1.27)$$

where we have introduced the growth factor f , which is defined as the logarithmic derivative of the growing mode of perturbations $D^{(+)}(t)$ with respect to the scale factor

$$f := \frac{d \ln(D^{(+)})}{d \ln(a)} = \frac{a}{D^{(+)}} \frac{dD^{(+)}}{da} \quad (1.28)$$

and it can be shown that it is linked to the density parameter of the totality of matter as $f \simeq \Omega_m^{0.6}$ when we are in matter domination [7, 18]. The expression of δ can be retrieved from the equation describing the perturbed density field

$$\rho(t, \mathbf{x}) = \bar{\rho}(t)[1 + \delta(t, \mathbf{x})], \quad (1.29)$$

where $\rho(t, \mathbf{x})$ is the matter density in a given point in the sky and $\bar{\rho}(t)$ the average matter density at a given time. Inverting equation (1.29) we have

$$\delta(\mathbf{x}, \tau) = \frac{\rho(\mathbf{x}, \tau) - \bar{\rho}(\tau)}{\bar{\rho}(\tau)}. \quad (1.30)$$

This definition of δ is general, therefore the density contrast can be built for either DM, luminous matter (galaxies) or the sum of the two. For this initial part of the work, since we are trying to theoretically describe DM, we choose to leave quantities referred to it without labels while quantities referring to the total amount of matter and the ones referring to galaxies alone will be labelled respectively with m and g as subscripts.

1.3.1 Evolution of Perturbations

Even with the nature of DM being still unknown, the up to date most valid candidate for DM turns out to be CDM, which becomes non relativistic very early in the history of the Universe. The evolution of collisionless CDM particles can be described, as long as particle diffusion is negligible at the scales of interest, by a set of hydrodynamical equations derived from the collisionless Boltzmann equation, which will be reported below directly in comoving coordinates. The first moment of the Boltzmann equation leads to mass conservation

$$\frac{\partial \delta}{\partial t} + \frac{1}{a} \nabla \cdot [(1 + \delta)\mathbf{v}] = 0, \quad (1.31)$$

where $\nabla \equiv \nabla_{\mathbf{x}}$ and $\partial/\partial t$ is now for fixed \mathbf{x} [46]. Following the same notation, the second moment determines instead the momentum conservation

$$\frac{\partial \mathbf{v}}{\partial t} + H(t)\mathbf{v} + \frac{1}{a}(\mathbf{v} \cdot \nabla)\mathbf{v} = -\frac{1}{a}\nabla\Phi - \frac{1}{a\rho}\nabla P \quad (1.32)$$

with P being the pressure of the fluid, which in the most general case is dependent on both density ρ and entropy S through the equation of state

$$P = P(\rho, S). \quad (1.33)$$

To close the previous set, we need an equation linking the gravitational potential with the density perturbation: this is given by the Poisson equation

$$\nabla^2 \Phi = 4\pi G \bar{\rho} a^2 \delta. \quad (1.34)$$

It is important to notice that $\Phi(t, \mathbf{x})$ is the cosmological gravitational potential, which is related with the classic Newtonian potential $\phi(t, \mathbf{x})$ through [46]

$$\Phi = \phi + \frac{1}{2} a \ddot{a} x^2. \quad (1.35)$$

Now, differentiating once with respect to time the continuity equation (1.31) and using both the Euler (1.32) and the Poisson (1.34) ones, we are able to obtain the equation of motion for the density contrast field [46]

$$\frac{\partial^2 \delta}{\partial t^2} + 2H \frac{\partial \delta}{\partial t} = 4\pi G \bar{\rho} \delta - \frac{1}{a(1+\delta)} \frac{\nabla P}{\bar{\rho}}, \quad (1.36)$$

where the second term of the left hand side describes the Hubble drag contribution, which acts against the growth of perturbations due to the Universe expansion. The first term of the right hand side is the gravitational term which, as we were presenting before, acts in favour of perturbations via gravitational instability. Lastly, the second term in the right hand side is the pressure term, depending both on spatial variations of the fluid density and spatial variation of its specific entropy.

The fluid approximation discussed above is valid only if the mean free path of the particles is much smaller than the spatial scale of the perturbations we are considering. In the case when collisions between particles are much more rare and the resulting mean free path is large, the evolution of perturbations is retrieved from the particle distribution function $f(t, \mathbf{x}, \mathbf{p})$, which brings information about the number of particle per unit volume in phase space according to

$$dN = f(t, \mathbf{x}, \mathbf{p}) d^3 \mathbf{x} d^3 \mathbf{p}, \quad (1.37)$$

with $p_i := \partial \mathcal{L} / \partial \dot{x}^i$ being the canonical momentum conjugate to the comoving coordinates x^i [46]. Thus, to obtain \mathbf{p} we use the Lagrangian of a particle with mass m in an expanding universe

$$\mathcal{L} = \frac{1}{2} m a^2 \dot{x}^2 - m \Phi, \quad (1.38)$$

which gives

$$\mathbf{p}(t, \mathbf{x}) = m a \mathbf{v} \quad (1.39)$$

and an equation of motion

$$\frac{d\mathbf{p}}{dt} = -m \nabla \Phi. \quad (1.40)$$

Enforcing particle conservation in phase space we can write the Vlasov equation for $f(t, \mathbf{x}, \mathbf{p})$

$$\frac{\partial f}{\partial t} + \frac{1}{ma^2} \mathbf{p} \cdot \nabla f - m \nabla \Phi \cdot \frac{\partial f}{\partial \mathbf{p}} = 0. \quad (1.41)$$

Being a nonlinear partial differential equation, the Vlasov equation above turns out to be very difficult to solve, we can however deal with it by enforcing the *single stream approximation*¹⁰ and taking momentum moments of the spatial distribution. The zeroth order moment, for example, relates the phase space density to the density field of the local mass

$$\int d^3 \mathbf{p} f(t, \mathbf{x}, \mathbf{p}) = \rho \frac{a^3}{m} := n(\mathbf{x}) \quad (1.42)$$

and it can be identified with the comoving number density of the given particle¹¹ at the coordinate \mathbf{x} . The zeroth order moment of the Vlasov equation gives the continuity equation

$$\frac{\partial \delta}{\partial t} + \frac{1}{a} \sum_j \frac{\partial}{\partial x_j} [(1 + \delta) \langle v_j \rangle] = 0, \quad (1.43)$$

which is equivalent to the continuity equation (1.31), with the peculiar velocity of the particle substituted with the mean streaming motion $\langle \mathbf{v} \rangle$. From the first moment of (1.41), once we have subtracted $\langle \mathbf{v} \rangle$ times the continuity equation we are able to obtain the Euler equation in an expanding universe

$$\frac{\partial \langle v_i \rangle}{\partial t} + H \langle v_i \rangle + \frac{1}{a} \sum_j \langle v_j \rangle \frac{\partial \langle v_j \rangle}{\partial x_j} = -\frac{1}{a} \frac{\partial \Phi}{\partial x_i} - \frac{1}{a(1 + \delta)} \sum_j \frac{\partial}{\partial x_j} [(1 + \delta) \sigma_{ij}^2], \quad (1.44)$$

with $\sigma_{ij}^2 := \langle v_i v_j \rangle - \langle v_i \rangle \langle v_j \rangle$ [46, 7]. A quick comparison with equation (1.32) shows that the quantity $\rho \sigma_{ij}^2$ plays the role of pressure, such a quantity is called the stress tensor. It is important to note that equation (1.43) couples the zeroth order moment of the distribution, in the form of the density contrast, with the first order one, the mean streaming motion, as expected in full generality. One can note the same behaviour also in equation (1.44), which relates the first moment of the distribution with the stress tensor σ_{ij}^2 . Thus, in principle, one could keep building up higher and higher moments of the Vlasov equation; the hierarchy can be closed, however, if one makes some assumptions on the stress tensor like in the single stream approximation¹² [7]. With a negligible stress tensor the right hand side of equation (1.44) turns out to be dominated by the gravitational term and therefore, up to first order in δ , equations (1.43) and (1.44) can be combined to give [46]

$$\frac{\partial^2 \delta}{\partial t^2} + 2H \frac{\partial \delta}{\partial t} = 4\pi G \bar{\rho} \delta, \quad (1.45)$$

which is the equation of motion of perturbations. It shows the density contrast field δ behaves like an ideal fluid with zero pressure (1.36).

¹⁰By single stream approximation we refer to the fact that we are neglecting the stress tensor at large scales. This is because on such scales there are no deviations from the coherent flow of the fluid until later times, when structures have had a sufficient amount of time to collapse and virialize [7].

¹¹Here we are assuming the density of the Universe to be dominated by the selected collisionless species.

¹²Essentially, such an assumption on the stress tensor comes from the fact that data support a scenario in which structure formation is driven by matter with negligible velocity dispersion and zero pressure, like for example CDM.

At large scales, where we expect the Universe to become smooth, matter perturbation fields described in equations (1.26), (1.30) and (1.35) become negligible compared with the homogeneous solution. Hence we can linearize equations (1.31) and (1.32) [7]

$$\frac{\partial \delta}{\partial t} + \frac{1}{a} \nabla \cdot \mathbf{v} = 0 \quad (1.46)$$

$$\frac{\partial \mathbf{v}}{\partial t} + H \mathbf{v} = -\frac{1}{a} \nabla \Phi. \quad (1.47)$$

The solution for the equation of motion of the density contrast field (1.45) is then described by the sum of two independent solutions [7]

$$\delta(t, \mathbf{x}) := D^{(+)}(t)A(\mathbf{x}) + D^{(-)}(t)B(\mathbf{x}), \quad (1.48)$$

with $A(\mathbf{x})$ and $B(\mathbf{x})$ being two arbitrary functions describing the initial density field configuration and $D^{(+)}$ is the linear growth factor. For an Einstein-De Sitter universe with $\Omega_m = 1$ and $\Omega_\Lambda = 0$ the two solutions obey [7, 46]

$$\begin{aligned} D^{(+)} &= a \quad \& \quad D^{(-)} = a^{-3/2} \\ \implies f(\Omega_m, \Omega_\Lambda) &= 1, \end{aligned} \quad (1.49)$$

while for an open universe with $\Omega_m < 1$ and $\Omega_\Lambda = 0$ we have

$$\begin{aligned} D^{(+)} &= 1 + \frac{3}{x} + 3\sqrt{\frac{1+x}{x^3}} \ln(\sqrt{1+x} - \sqrt{x}) \quad \& \quad D^{(-)} = \sqrt{\frac{1+x}{x^3}} \\ f(\Omega_m, \Omega_\Lambda) &\sim \Omega_m^{0.6}, \end{aligned} \quad (1.50)$$

with $x := (\Omega_m^{-1} - 1)/(1 + z)$ and a scale factor normalized to one at the present day, $a_0 = 1$. Here it is important to stress that matter perturbations grow faster in a Einstein-De Sitter universe than in an open one: this is due to the fact that the latter scenario, as well as one with a non-zero cosmological constant Λ , determines a larger Hubble expansion rate and hence a larger drag term inside equation (1.45) [46]. The definition of the growth factor anticipated above, equation (1.28), depends exclusively on the growing mode of perturbations, this is because, as time proceeds, the decaying mode of perturbations becomes negligible and at early times the consideration of the growing mode only is well motivated by inflation [18].

1.4 On Galaxy Statistics

From the previous Section we can have an hint on how perturbations of matter evolve throughout the history of the Universe, now we have to find a way to link them with observations. Due to the elusiveness of DM we will never be able to have a comprehensive look on matter perturbations using photon based detectors. Thanks to insights coming from theory however, and confirmed by observations and projects like the *Millennium Simulation* [64], we know we can look at the baryonic component of matter which has clustered into galaxies to track the behaviour of the totality of matter. This quality of the galaxy field is pictured very well in Figure 1.3, where it is clear that baryonic matter

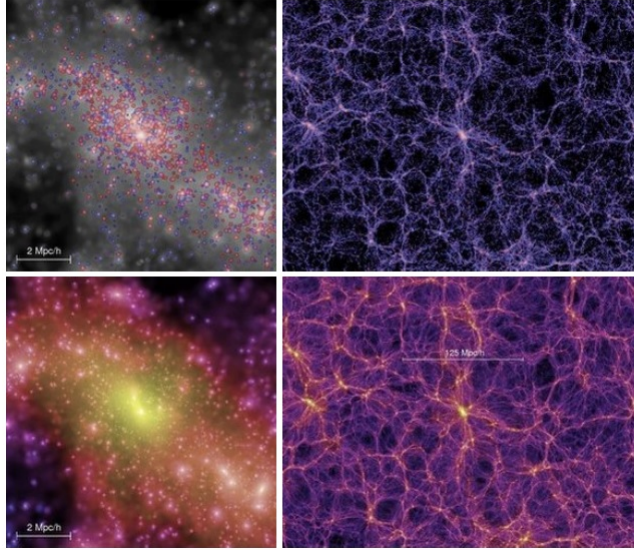


Figure 1.3: The top row shows the galaxy distribution in the Millennium Simulation, for both a single cluster (left) and the whole large scale structure around it (right). The images in the bottom row show the corresponding DM distribution. Figure taken from the Gerard Lemson & Virgo Consortium database.

tends to cluster inside DM halos and filaments. The statistical properties of the galaxy clustering can be described starting from a re-adaptation of the BBGKY hierarchy used in plasma physics [14, 51], which deals with the generalization of the n -point correlation functions to the joint distributions in position and peculiar velocity of galaxies.

From the definition of canonical momentum given in equation (1.39), we can write down the probability of finding a particle moving in the comoving volume element $d^3\mathbf{x}$ with conjugate momentum \mathbf{p} in the range $d^3\mathbf{p}$ as

$$dP := b(p, t) d^3\mathbf{x} d^3\mathbf{p}. \quad (1.51)$$

With the galaxy distribution assumed to be an homogeneous and isotropic random process, the 1-point correlation function $b(p, t)$ turns out to be independent of both the position \mathbf{x} and the direction $\hat{\mathbf{p}}$ given by the peculiar motion of the galaxies themselves. The normalization of $b(p, t)$ is then given by

$$\int d^3\mathbf{p} b(p, t) = n \equiv n_{\text{phys}} a^3, \quad (1.52)$$

where n is the comoving number density of galaxies, which is constant in time, and n_{phys} is the time dependent physical one. The probability defined in equation (1.51) can be generalized for two particles, labelled as 1 and 2, being in the comoving volumes $d\mathbf{x}_1$ and $d\mathbf{x}_2$ with respective momenta \mathbf{p}_1 and \mathbf{p}_2 inside $d\mathbf{p}_1$ and $d\mathbf{p}_2$, as follows

$$\begin{aligned} dP &= \rho_2(1, 2) d^3\mathbf{x}_1 d^3\mathbf{p}_1 d^3\mathbf{x}_2 d^3\mathbf{p}_2 \\ &= [b(1)b(2) + c(1, 2)] d^6\mathbf{x} d^6\mathbf{p}, \end{aligned} \quad (1.53)$$

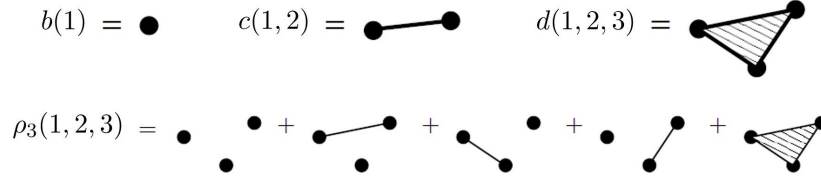


Figure 1.4: Graphical representation of the connected and unconnected correlation functions. Figure taken from [7]; labels have been modified to match our definitions.

where the function $c(1, 2)$ represents the connected part of the two-point function. For three particles we have

$$\begin{aligned}
 dP &= \rho_3(1, 2, 3) d^3 \mathbf{x}_1 d^3 \mathbf{p}_1 d^3 \mathbf{x}_2 d^3 \mathbf{p}_2 d^3 \mathbf{x}_3 d^3 \mathbf{p}_3 \\
 &= [b(1)b(2)b(3) + b(1)c(2, 3) + b(2)c(1, 3) + b(3)c(1, 2) + d(1, 2, 3)] d^9 \mathbf{x} d^9 \mathbf{p}.
 \end{aligned}
 \tag{1.54}$$

In the previous two equations, the functions $c(1, 2)$ and $d(1, 2, 3)$ are respectively the connected two and three point functions. The important property of connected correlation functions is that they vanish when one or more particles of the ensemble are separated by an infinite distance. In Figure 1.4 we show a visual representation of the connected correlation functions present in the three multi point probabilities (1.51), (1.53) and (1.54) and, as an example, their interaction inside (1.54). Integrating both of them over all momenta we are then able to find the usual spatial correlation functions [14]

$$\begin{aligned}
 \int d^3 \mathbf{p}_1 d^3 \mathbf{p}_2 c(1, 2) &= n^2 \xi(r, t), \\
 \int d^3 \mathbf{p}_1 d^3 \mathbf{p}_2 d^3 \mathbf{p}_3 d(1, 2, 3) &= n^3 \zeta(1, 2, 3),
 \end{aligned}
 \tag{1.55}$$

where in the first row r labels the separation between the two galaxies in comoving units, defined as $\mathbf{r} := \mathbf{x}_2 - \mathbf{x}_1$. The function $c(1, 2)$ has the following symmetry properties: [14, 51]

Homogeneity: in principle the correlation function would be dependent on all four variables. At the scales of our interest however, where we can describe the Universe using FLRW (1.2), homogeneity of space simplifies those dependencies. More precisely, with the galaxy-galaxy comoving separation defined as $\mathbf{r} = \mathbf{x}_2 - \mathbf{x}_1$ we have

$$c(\mathbf{x}_1, \mathbf{x}_2, \mathbf{p}_1, \mathbf{p}_2) = c(\mathbf{x}_1, \mathbf{x}_1 + \mathbf{r}, \mathbf{p}_1, \mathbf{p}_2).$$

If we are under FLRW, then a variation of the position of Galaxy 1 alone, \mathbf{x}_1 , should not make the correlation vary. Thus, what really determines a variation of the correlation function is the separation between the two

$$\implies c(\mathbf{x}_1, \mathbf{x}_2, \mathbf{p}_1, \mathbf{p}_2) = c(\mathbf{r}, \mathbf{p}_1, \mathbf{p}_2). \tag{1.56}$$

Exchange: this property comes from the fact that galaxies are indistinguishable particles and therefore we are able to freely exchange the labels $c(1, 2) = c(2, 1)$. Explicitly we obtain

$$\begin{aligned}
 c(\mathbf{x}_2 - \mathbf{x}_1, \mathbf{p}_1, \mathbf{p}_2) &= c(\mathbf{x}_1 - \mathbf{x}_2, \mathbf{p}_2, \mathbf{p}_1) \\
 \implies c(\mathbf{r}, \mathbf{p}_1, \mathbf{p}_2) &= c(-\mathbf{r}, \mathbf{p}_2, \mathbf{p}_1);
 \end{aligned}
 \tag{1.57}$$

Parity: this property follows from isotropy: since we expect galaxy clustering to behave the same in all directions, then the correlation function should not vary under a reflection of the coordinates

$$c(\mathbf{r}, \mathbf{p}_1, \mathbf{p}_2) = c(-\mathbf{r}, -\mathbf{p}_1, -\mathbf{p}_2).$$

To give this result in the same fashion of [51], we apply exchange symmetry to the previous equation

$$c(\mathbf{r}, \mathbf{p}_1, \mathbf{p}_2) = c(\mathbf{r}, -\mathbf{p}_2, -\mathbf{p}_1). \quad (1.58)$$

In full generality, we could keep building an infinite amount of higher multi-point correlation functions, each one involving more and more particles at the same time. For a Gaussian distribution however, we know that the only non vanishing connected correlation function is the 2 point one [7] and thus the statistical properties of any Gaussian field can be described in terms of combinations of the 2PCF of the field itself. This is the key aspect behind our following description ignoring the 3-point correlation and higher ones: we expect perturbations of galaxies, which can be traced back to inflation [7], to be very close to Gaussianity and, consequently, with most of the statistical information stored in the 2PCF.

1.4.1 Two Point Correlation Function and Power Spectrum

Following the conventions used in [57] and [68], we define the Fourier transform of a given function $f(\mathbf{x})$ as

$$f(\mathbf{k}) := \int d^3\mathbf{x} e^{i\mathbf{k}\cdot\mathbf{x}} f(\mathbf{x}), \quad (1.59)$$

while its inverse takes the form

$$f(\mathbf{x}) := \int \frac{d^3\mathbf{k}}{(2\pi)^3} e^{-i\mathbf{k}\cdot\mathbf{x}} f(\mathbf{k}). \quad (1.60)$$

Before proceeding further, it is useful to show some properties of the functions just defined: first of all, using the definition of the inverse Fourier transform stated above, in full generality we have $f(\mathbf{k})$ being a complex random variable, thus we can write

$$\begin{aligned} f(\mathbf{k}) &= \int d^3\mathbf{x} e^{i\mathbf{k}\cdot\mathbf{x}} f(\mathbf{x}), \\ f^*(\mathbf{k}) &= \int d^3\mathbf{x} e^{-i\mathbf{k}\cdot\mathbf{x}} f(\mathbf{x}). \end{aligned} \quad (1.61)$$

Since $f(\mathbf{x})$ is generally linked with observables, we want it to be real. With this constraint we are then able to retrieve the relation

$$f^*(\mathbf{k}) = f(-\mathbf{k}), \quad (1.62)$$

which is able to describe the complex conjugate of a Fourier space function as the function itself. This will be useful to write explicitly the redshift space PS.

The 2PCF inside (1.55) can be linked directly to the product of the density contrast fields, described in equation (1.30), of two different points in space separated by a distance $\mathbf{r} := \mathbf{x}' - \mathbf{x}$ [7]

$$\xi(r) := \langle \delta(\mathbf{x}) \delta(\mathbf{x} + \mathbf{r}) \rangle. \quad (1.63)$$

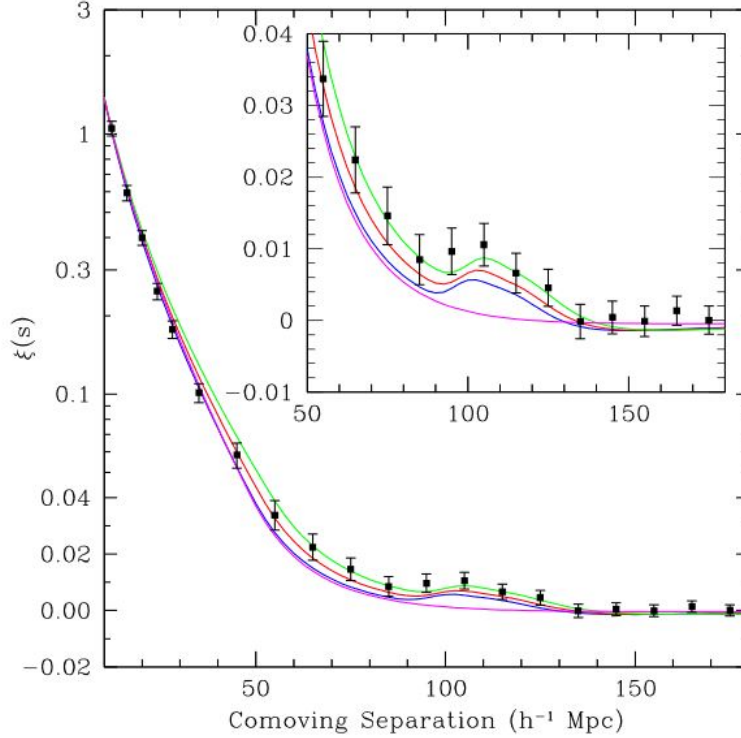


Figure 1.5: Large scale redshift space 2PCF of the SDSS LRG galaxy survey. The various lines represent different models with different cosmological parameters: $\Omega_m h^2 = 0.12$ (green), $\Omega_m h^2 = 0.13$ (red) and $\Omega_m h^2 = 0.14$ (blue). All the three models have $\Omega_b h^2 = 0.24$. the magenta line represent a pure CDM model with no baryons and $\Omega_m h^2 = 0.105$ without the acoustic peak. Note that the vertical axis mixes linear and logarithmic coordinates. Figure taken from [21].

Here we stress that the function presented above, thank to the properties (1.56)-(1.58), is dependent only on the modulus of the distance r and not on the vectorial quantity \mathbf{r} , nor on the individual galaxy coordinates \mathbf{x} and \mathbf{x}' separately. This is a direct consequence of the statistical homogeneity and isotropy of the Universe we have treated in Section 1.1.

In terms of the spatial 2PCF, equation (1.53) reads

$$dP = n^2[1 + \xi(r)]dV_1dV_2. \quad (1.64)$$

As stated in the Section above, the 2PCF gives information about the probability of finding two particles in the volume elements dV_1 and dV_2 , placed at a distance r from each other. From the expression above we are able to immediately grasp the meaning of the 2PCF: if the observed galaxies are more clustered than a random distribution, then $\xi(r) > 0$ and we have an enhanced probability of finding neighbours; if instead they are less clustered than a random distribution, $\xi(r) < 0$, the probability of finding neighbours is suppressed. In Figure 1.5 we show the form of the 2PCF function retrieved using data from the SDSS LRG galaxy survey.

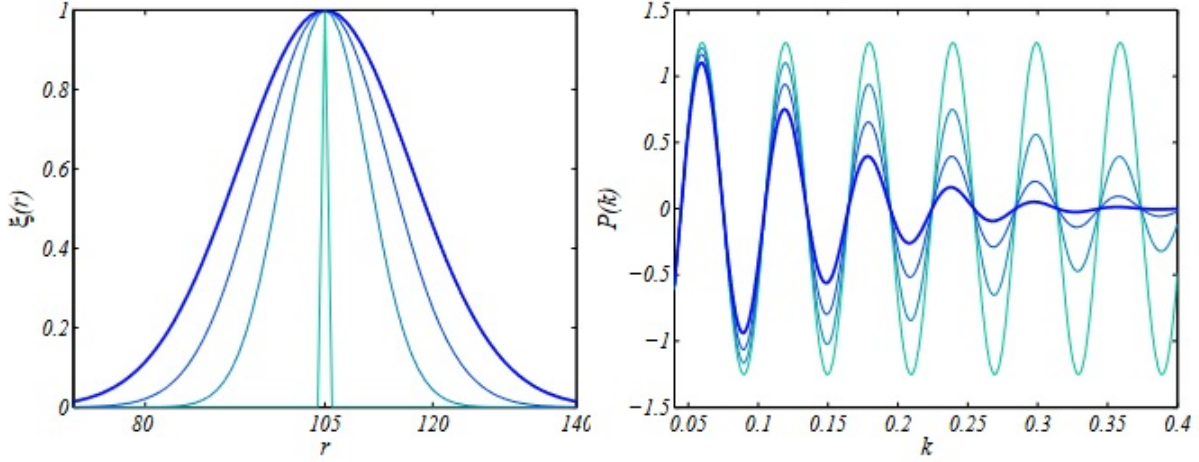


Figure 1.6: Schematic representation of the Fourier pairs $\xi(r)$ and $P(k)$. The lighter blue curve represents the mathematical relation, relating a δ function in real space to an infinite series of oscillations in Fourier space; the darker blue curve instead, shows a more physical situation in which we have just a δ -type function, like the baryon acoustic peak, translating into a series of damped oscillations. Figure taken from [6].

The Fourier counterpart of the 2PCF is the PS

$$P(k) := \int d^3\mathbf{r} e^{i\mathbf{k}\cdot\mathbf{r}}\xi(r); \quad (1.65)$$

with the two quantities being Fourier pairs, we have that any δ -type function at a characteristic scale in the 2PCF, as the baryon acoustic peak, translates into PS oscillations in Fourier space. The relation is represented schematically in Figure 1.6.

Using property (1.62) we are able to see explicitly why the 2PCF and PS are Fourier pairs; we have

$$\begin{aligned} \langle \delta(\mathbf{k})\delta(\mathbf{k}') \rangle &= \int d^3\mathbf{x} e^{i(\mathbf{k}+\mathbf{k}')\cdot\mathbf{x}} \int d^3\mathbf{r} e^{i\mathbf{k}\cdot\mathbf{r}} \langle \delta(\mathbf{x})\delta(\mathbf{x}+\mathbf{r}) \rangle \\ &= (2\pi)^3 \delta_D(\mathbf{k}+\mathbf{k}') \int d^3\mathbf{r} e^{i\mathbf{k}\cdot\mathbf{r}}\xi(r) \\ &= (2\pi)^3 \delta_D(\mathbf{k}+\mathbf{k}')P(k), \end{aligned} \quad (1.66)$$

where the $(2\pi)^3$ factor is due to the Dirac delta definition as both Fourier transform and anti transform of 1

$$\delta_D(\mathbf{x}+\mathbf{x}') := \int \frac{d^3\mathbf{k}}{(2\pi)^3} e^{-i\mathbf{k}\cdot(\mathbf{x}+\mathbf{x}')} \quad \& \quad \delta_D(\mathbf{k}+\mathbf{k}') := \int \frac{d^3\mathbf{x}}{(2\pi)^3} e^{i(\mathbf{k}+\mathbf{k}')\cdot\mathbf{x}}. \quad (1.67)$$

Regarding the relation between the Fourier space correlation function and the PS, in the passage from the first and the second line the integration along $d^3\mathbf{x}$ has been rewritten in the form of the Dirac delta. This approach, in full generality, should not be valid due to the \mathbf{x} dependence of the correlation

function. To overcome this one needs to assume, following the homogeneity of space, the correlation function $\langle \delta(\mathbf{x})\delta(\mathbf{x} + \mathbf{r}) \rangle$ is not really a function of the two coordinates \mathbf{x} and $\mathbf{x} + \mathbf{r}$ separately, but rather a function of the galaxy-galaxy separation \mathbf{r} .

Here it is important to highlight that the PS gives information about the galaxy distribution in the same way as the 2PCF above, with higher values of $P(k)$ referring to more clustered regions and lower values of $P(k)$ referring to less clustered ones instead. The huge advantage of the latter comes clear if we are interested in large scales: for sufficiently small values of k we have different Fourier modes evolving independently, while the amplitude of the 2PCF is always a superposition of different modes. This means that, at least for large scales, choosing to deal with the PS in Fourier space one is able avoid dealing with the highly nonlinear physics present at small scales [30, 46].

1.4.2 The Matter Power Spectrum

The shape of the matter PS can be, at first approximation, derived focusing on the evolution of DM only [18]. This approach is justified by observations, with the totality of matter representing roughly 30% of the energy budget of the Universe versus the more or less 4% of its luminous component [1]. Nonlinear contributions will be relevant only in the small scale part of the PS (high values of the wavenumber k) as clearly visible in Figure 1.7, which shows the matter PS at redshift $z = 0$ inferred from different cosmological models. It is important to note the fact that the nonlinear scale is directly linked with the growth factor of matter perturbation $f(t)$, defined in equation (1.28), which is an increasing function of time; hence, as far as we move to higher values of redshift the boundary between linear and nonlinear regime tends to move to smaller scales (higher values of k in the PS).

Referring again to Figure 1.7, we can clearly divide it into three main regions: the large scale one, at small values of k ; the region of the peak at intermediate scales, where the PS reaches its maximum value, and the small scale one at large values of k . We now proceed to highlight the main features of the PS in each of these regions. Recalling the scheme given in Section 1.3, at (1.24), we can see the behaviour of the matter perturbations, and consequently the PS one, is directly linked to the value of the potential during time. At large scales, the potential can be thought to be constant, with a late time value 10% lower than the initial one, set by inflation. This decrease is determined by the passage through matter/radiation equality [18].

Upon inverting the Poisson equation (1.34) to describe δ in terms of Φ , it is possible to express the large scales PS, which turns out to be proportional to the wavenumber k [18]. This part of the PS can then be used, thanks to the nearly null modification of the gravitational potential at low values of k , to define the primordial PS of matter

$$P(k) \propto k^n, \tag{1.68}$$

where n is the spectral index of the spectrum.

At small scales the behaviour of $\Phi(\mathbf{k})$ becomes less simple than before: once two regions enter in causal connection before matter/radiation equality, the potential associated to them starts decaying: this is due to the combined effect of the pressure forces in the plasma, which do not allow perturbations to grow, and the expansion of the Universe, which makes the density decrease. Once the decay is complete, $\Phi(\mathbf{k})$ starts oscillating as the baryon/photon plasma do with BAOs. Modes that enter in causal connection earlier in radiation dominated epoch undergo a more severe suppression of the potential, thus in this region the PS is a decreasing function of k .

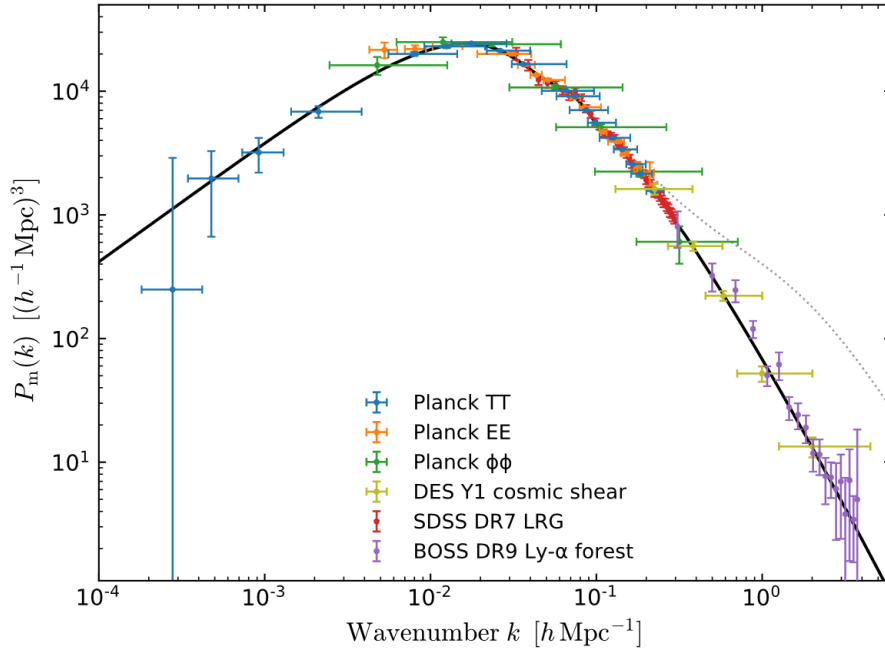


Figure 1.7: Reconstruction of the linear theory matter PS at $z = 0$ from different cosmological probes (solid line) versus the nonlinear theory at $z = 0$ (dotted line). The agreement between the theory and data points, which are spanning roughly 14 Gyr in time, shows the extreme power of the Λ CDM model of the Universe. Figure taken from [1].

The opposite behaviour in the two regimes delineates the presence of a peak in the middle, determined by those modes which enter in causal connection exactly during matter/radiation equality. Since the position of the peak is sensitive to the epoch of equality, it turns out to be an important characteristic for the determination of the underlying cosmology, with the peak moving to larger scales implying an equivalence epoch moving earlier in time [18].

1.5 On Baryon Acoustic Oscillations

BAOs was firstly identified as a potential effect on the CMB radiation in the late '60s and later extended to the late time matter PS. The presence of BAOs in both the spectra of radiation and matter is a direct consequence of the fact that they are a phenomenon which happened in the primordial plasma before the recombination epoch, were baryons and photons were coupled together. In fact, prior to recombination, the Universe was hot and dense enough that electrons were free moving in the plasma rather than bounded in neutral atoms; in this conditions they were able to provide enough cross-section to interact with photons via Thomson scattering while still connected with matter via Coulomb interaction.

In this regime the schematic representation (1.24) given in Section 1.3 can be rewritten considering

also photon perturbations

$$\text{Photon Perturbations: } \Theta_0, \Theta_1 \leftrightarrow \text{Gravitational Potential: } \Phi \rightarrow \text{Matter Perturbations: } \delta, v, \quad (1.69)$$

where the new perturbations are the monopole Θ_0 and the dipole Θ_1 of radiation¹³. In such an environment, the initial perturbations of both the potential and the photons determines the potential wells in which matter (CDM plus baryons) started to be attracted in. Even if CDM does not interact with photons, the same is not true for baryons: as far as they fell into the potential wells via gravitational instability, radiation pressure became larger and larger until it was sufficiently strong to overtake the gravitational attraction and started pushing away the plasma, with the net result that perturbations in the baryon-photon fluid oscillated as sound waves [72].

Mathematically we can observe this behaviour looking back to equation (1.36) and analyse it under some different approximations: first of all we consider now a fluid made of DM and baryons, with the mean density of the Universe dominated by DM ($\Omega_{\text{CDM}} \gg \Omega_b$) and where baryon perturbations are not self-gravitating, namely the potential for the gravitational source is given by CDM only; second of all, since the pressure felt by baryons is a key aspect for the description of BAOs we cannot neglect the pressure term in (1.36) any more. To deal with it we apply the first law of thermodynamics to a unit mass of an ideal monoatomic non relativistic gas

$$TdS = d\left(\frac{3P}{2\rho}\right) + Pd\left(\frac{1}{\rho}\right), \quad (1.70)$$

where T is the temperature, P the pressure and ρ the density. We can rewrite the temperature using $P = (\rho/\mu m_p)k_B T$ with μ mean molecular weight in units of the proton mass m_p and k_B Boltzmann constant and solve the equation

$$d\ln(P) = \frac{5}{3}d\ln(\rho) + \frac{2}{3}\frac{\mu m_p}{k_B}Sd\ln(S), \quad (1.71)$$

which gives [46]

$$P \propto \rho^{5/3} \exp\left\{\frac{2}{3}\frac{\mu m_p}{k_B}S\right\}. \quad (1.72)$$

From the equation of state (1.72) we then can write

$$\begin{aligned} \frac{\nabla P}{\bar{\rho}} &= \frac{1}{\bar{\rho}} \left[\left(\frac{\partial P}{\partial \rho} \right) \Big|_{S=\text{const.}} \nabla \rho + \left(\frac{P}{S} \right) \Big|_{\rho=\text{const.}} \nabla S \right] \\ &= c_s^2 \nabla \rho + \frac{2}{3}(1 + \delta)T \nabla S, \end{aligned} \quad (1.73)$$

where we have defined the *adiabatic speed of sound* as

$$c_s := \left(\frac{\partial P}{\partial \rho} \right) \Big|_{S=\text{const.}}^{1/2}, \quad (1.74)$$

¹³With considerations like the ones in Section 1.3.1, in full generality perturbations with higher order than the dipole should be present. Since we are dealing with photons before recombination however, the higher order moments are suppressed thanks to the tight coupling between photons and baryons [18].

which makes equation (1.36) become

$$\frac{\partial^2 \delta_b}{\partial t^2} + 2H \frac{\partial \delta_b}{\partial t} = -\frac{1}{a^2} \nabla^2 \Phi_{\text{CDM}} + \frac{c_s^2}{a^2} \nabla^2 \delta_b + \frac{2}{3} \frac{\bar{T}}{a^2} \nabla S \quad (1.75)$$

with \bar{T} the mean temperature of the fluid. At our scale of interest, the curvature of the Universe becomes negligible making us able to write the mode functions of baryon perturbations, $\delta_{b\mathbf{k}}$, as plane waves and perturbations themselves as their Fourier transform following (1.60) [46]

$$\delta_b(t, \mathbf{x}) = \sum_{\mathbf{k}} \delta_{b\mathbf{k}}(t) e^{i\mathbf{k}\cdot\mathbf{x}} \quad \& \quad \delta_{b\mathbf{k}}(t) = \frac{1}{V} \int_{-\infty}^{\infty} d^3\mathbf{x} \delta_b(t, \mathbf{x}) e^{-i\mathbf{k}\cdot\mathbf{x}}, \quad (1.76)$$

with V the volume over which the perturbation are assumed to be periodic. Once translated in Fourier space equation (1.75) becomes

$$\frac{d^2 \delta_{b\mathbf{k}}}{dt^2} + 2H \frac{d\delta_{b\mathbf{k}}}{dt} = -\frac{k^2}{a^2} \Phi_{\text{CDM}} - \frac{k^2 c_s^2}{a^2} \delta_{b\mathbf{k}} + \frac{2}{3} \frac{\bar{T}}{a^2} k^2 S_{\mathbf{k}}, \quad (1.77)$$

with $S_{\mathbf{k}}$ being entropy perturbations which are directly linked to perturbations in the curvature of the Universe. If the time scale of interest is much shorter than the Hubble time, we can neglect the universe expansion and thus (1.77) reads [46] (we drop the \mathbf{k} subscripts for clarity, but we are still in Fourier space)

$$\frac{d^2 \delta_b}{dt^2} + \frac{k^2 c_s^2}{a^2} \delta_b = -\frac{k^2}{a^2} \Phi_{\text{CDM}}, \quad (1.78)$$

which is the equation of a damped harmonic oscillator. If the gravitational potential remains constant over the time of interest, the solution written in terms of the conformal time τ reads [46]

$$\delta_b(\tau) = \left[\delta_b + \frac{\Phi_{\text{CDM}}}{c_s^2} \right] \cos(kc_s\tau) + \frac{1}{kc_s} \frac{d\delta_b}{d\tau}(0) \sin(kc_s\tau) - \frac{\Phi_{\text{CDM}}}{c_s^2}; \quad (1.79)$$

it oscillates around a zero point, $-\Phi_{\text{CDM}}/c_s$, with a frequency $\omega = kc_s$ and amplitude and phase set by initial conditions. By translating the Euler equation (1.32) in Fourier space, maintaining the same considerations, it is possible to retrieve the time evolution of the corresponding velocity perturbations

$$\mathbf{v}_b(\tau) = -\frac{ic_s \mathbf{k}}{k} \left[\delta_b(0) + \frac{\Phi_{\text{CDM}}}{c_s^2} \right] \sin(kc_s\tau) + \frac{i\mathbf{k}}{k} \frac{d\delta_b}{d\tau}(0) \cos(kc_s\tau), \quad (1.80)$$

which has a phase difference of $\pi/2$ with respect to the density perturbation as expected for longitudinal acoustic waves. Here it is important to stress that before recombination, for each mode, the oscillation frequency as well as the amplitude and the zero point all depend upon the ratio between baryons and photons through the adiabatic sound speed (1.74), which in such a condition¹⁴ can be written as [46]

$$c_s = \frac{c}{\sqrt{3}} \left[1 + \frac{3}{4} \frac{\bar{\rho}_b(z)}{\bar{\rho}_\gamma(z)} \right]^{-1/2}. \quad (1.81)$$

The behaviour of a single acoustic wave is reported schematically in Figure 1.8 following its evolution in time through the most relevant epochs

¹⁴Where the density and pressure of the plasma are given by $\rho_{\text{plasma}} = \rho_b + \rho_\gamma$ and $P_{\text{plasma}} \equiv P_r = \rho_\gamma c^2/3$.

Before Recombination ($z = 6824$ and $z = 1440$ panels) In this epoch photons and baryons are coupled in a single fluid. At first, CDM overdensities develop point-like perturbations; later on, with the generation of acoustic waves of plasma those point-like overdensities are brought to higher radial coordinates by the outgoing waves.

After Recombination ($z = 848$ and $z = 478$ panels) During recombination photons and baryons decouple, leaving the latter without the pressure forces that were pushing them away from the initial overdensity: the net result is a central overdensity of CDM, with a second one constituted by baryons in a spherical shell at a radius of 150 Mpc (note that in this case it is given in absolute units).

Later Times ($z = 79$ and $z = 10$ panels) With the pressure forces gone, the only interaction left is the gravitational one between CDM and baryons, which leads to a common final shape of perturbations. Galaxy clustering is expected to be enhanced around the central perturbation and the shell at 150 Mpc.

1.5.1 BAOs as a Statistical Standard Ruler

The great importance of BAOs for cosmology comes from the fact that they can be used as cosmological ruler: the acoustic scale can in fact be computed as the comoving distance that sound waves could travel from the Big Bang until recombination, labelled with a $*$ subscript here below, as a simple integral

$$r_s = \int_0^{t_*} dt \frac{c_s(t)}{a(t)} \equiv \int_{z_*}^{\infty} dz \frac{c_s(z)}{H(z)}, \quad (1.82)$$

where c_s is the adiabatic sound speed we have described in equation (1.81), which depends on the baryon-to-photon ratio and thus it is proportional to $\Omega_b h^2$. The behaviour of $H(z)$ depends, at least for simple cosmological models, on the ratio between the matter density and radiation density [72]. The acoustic scale is about 150 Mpc because primordial sound waves travel at a relativistic speed, which tops at about $c/\sqrt{3}$ during the earliest epochs where the baryon density was null compared to radiation density. This is a huge advantage: such a large scale is able to protect clustering features of galaxies from nonlinearities in the local universe, making the BAO peak a stable statistical feature of the galaxy density field and hence an extremely good standard ruler [72]. This stable characteristics of BAOs is reported schematically in Figure 1.9 (left panel) and compared with a more realistic scenario, where the BAO acoustic peak has been broadened by gravitational instability (right panel): it is clear that, in the second case, the BAO rings are not visible any more and therefore they must be recovered statistically. At small redshift, $z \lesssim 0.5$, BAO measurements are able to complement Supernovae Ia ones because they provide a strong connection to the CMB peaks and therefore a better absolute scale of distance, while Supernovae allow a more precise determination of the relative distance between objects. At high redshift, $z \gtrsim 0.5$, the large volumes accessible for observations, coupled with the direct access to $H(z)$ provided from BAOs, makes statistical analysis of galaxy clustering (and the CMB) an extremely useful tool to understand DE and the cosmic geometry of our Universe [72].

With the BAO method it is possible to relate redshift separation between galaxies, Δz , with the Hubble parameter, $H(z)$, while angular separations, $\Delta\theta$, are related with the angular diameter

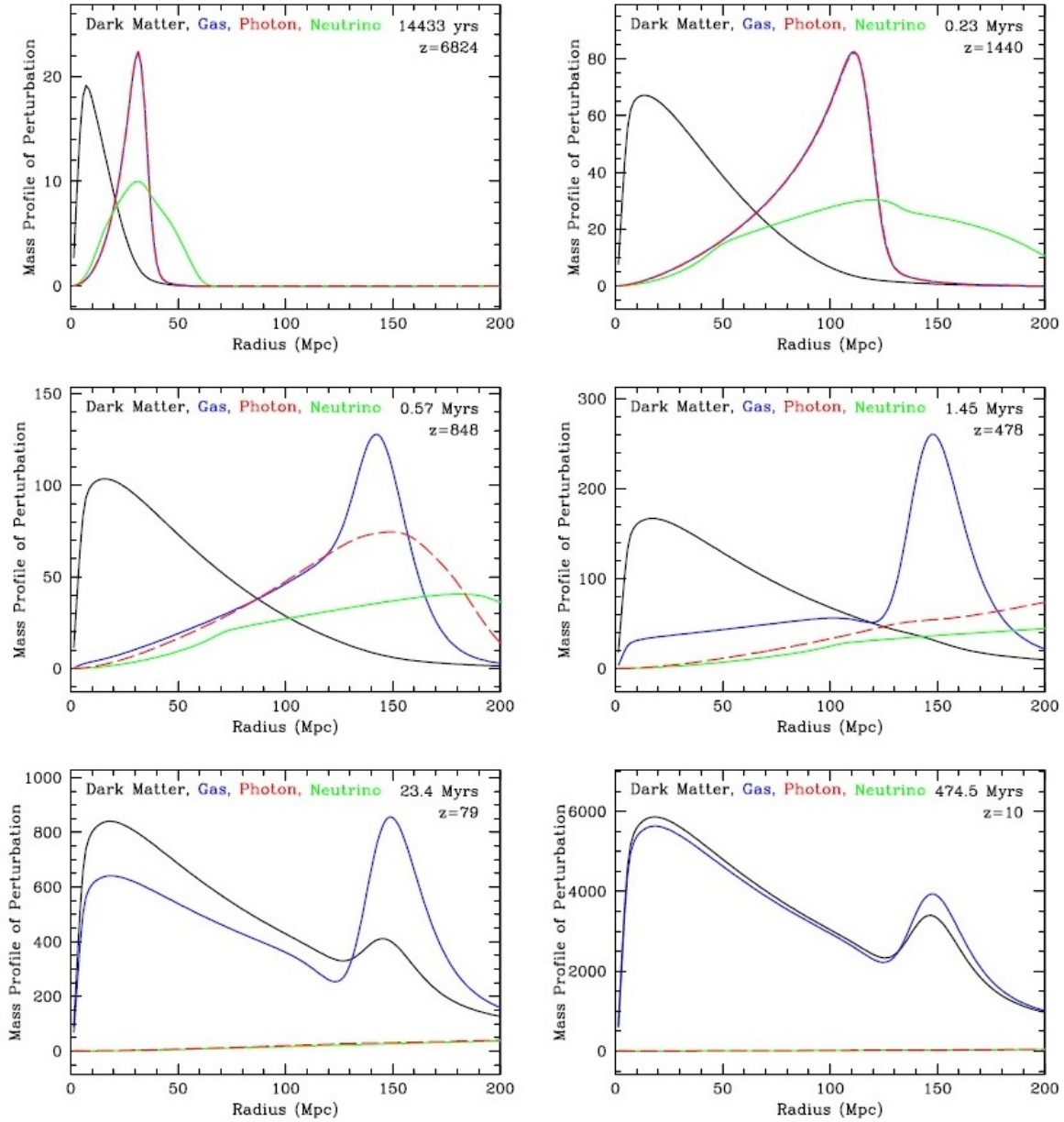


Figure 1.8: Generation of the BAO peak via the linear theory response to a point-like initial overdensity and the acoustic pressure wave. Each panel shows the radial profile of (fractional) mass perturbations for the four species: CDM (black), baryons (blue), photons (red) and neutrinos (green). The redshift and the time after the big bang are given in each panel. Note that the radial profile has been multiplied by the square of the radial coordinate in order to yield the mass profile. Figure taken from [20].

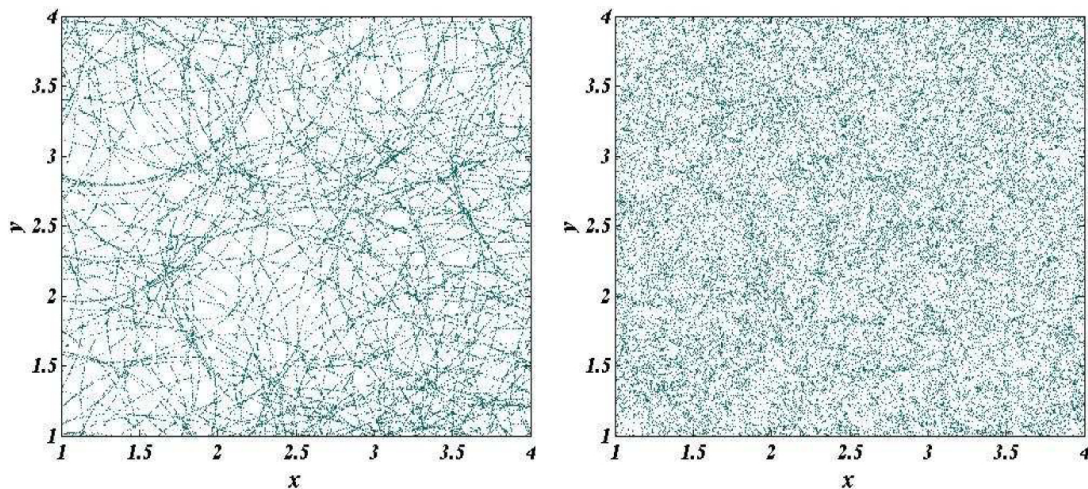


Figure 1.9: Schematic representation of BAO acoustic rings. The two panels contain the same number of points; the left one represents the case of a sharp BAO peak in the mass profile of perturbations, while the right one shows a more realistic scenario where the peak has been broadened (i.e.: due to gravitational instability), but is still present. Figure taken from [6].

distance, $D_A(z)$, as follows [6]

$$\begin{aligned}
 H(z) &= \frac{c\Delta z}{s_{\parallel}(z)} \\
 D_A(z) &= \frac{s_{\perp}}{\Delta\theta(1+z)},
 \end{aligned}
 \tag{1.83}$$

where $s_{\parallel}(z)$ and s_{\perp} are respectively the separations between galaxies in redshift space (they will be defined in detail in Section 2.2). This means that, since the acoustic scale is set by the sound horizon at decoupling (equation (1.82)), they can be turned into a calibrated Alcock-Paczynski test [2]. Since the monopole of the correlation function in redshift space is still isotropic, the measurement of the two parameters from the Alcock-Paczynski test is not independent but rather it measures the product $H(z) \times D_A(z)$. The same happens with the determination of DE parameters, which needs measurements of both $H(z)$ and $D_A(z)$ to be effectively improved by BAOs [6]. Thanks to the fact that the monopole is sensitive to the quantity $D_V(z) := [cz(1+z)^2 D_A(z)^2 / H(z)]^{1/3}$ while the quadrupole is sensitive to $D_A(z)H(z)$ [34]. In this context redshift distortions become a fundamental tool: as higher order multipoles become anisotropic, then a deep understanding of their behaviour helps us disentangle the two parameters.

1.5.2 Retrieving Cosmological Information From BAOs

With their capability of determine the Hubble expansion parameter and angular diameter distance as functions of redshift, BAOs have been exploited to probe DE and its equation of state. Even if in

general DE does not need to obey an equation of state, it is always possible to define a function like

$$\omega(z) := \frac{\bar{p}_\Lambda(z)}{\bar{\rho}_\Lambda(z)} \quad (1.84)$$

which, if DE behaves like a cosmological constant, corresponds to $\omega(z) = -1$. Equation (1.84) can then be parametrized by the value $\Omega_\Lambda := \rho_\Lambda/\rho_{\text{crit}}$ today, which is linked to other density parameters through $\Omega_\Lambda = 1 - \Omega_m - \Omega_k$. If the assumption of having perfectly uncorrelated data from observations holds, it is possible to reconstruct $\omega(z)$ without assuming a specific parametrization [32].

To see how it is possible to retrieve $\omega(z)$ from the observables (1.83), it is useful to define the dimensionless, transverse, comoving distance [32]

$$D(z) := \frac{1}{\sqrt{-\Omega_k}} \sin \left(\sqrt{-\Omega_k} \int_0^z dz' \frac{H_0}{H(z')} \right), \quad (1.85)$$

which is related to the angular diameter distance as

$$D(z) = \frac{c}{H_0} (1+z) D_A(z). \quad (1.86)$$

The Hubble parameter in equation (1.85) can be computed from the Friedmann equation and it reads

$$H^2(z) = H_0^2 [\Omega_m (1+z)^3 + \Omega_k (1+z)^2 + \Omega_\Lambda f(z)], \quad (1.87)$$

where $f(z)$ is the dimensionless DE density

$$f(z) := \frac{\rho_\Lambda(z)}{\rho_\Lambda(z=0)} = \exp \left\{ 3 \int_0^z dz' \frac{1 + \omega(z')}{1 + z'} \right\}. \quad (1.88)$$

It is then possible to find $\omega(z)$ using the Hubble parameter by inverting equation (1.87) [32]

$$\omega(z) = -\frac{1}{3} \frac{\Omega_k H_0^2 (1+z)^2 + 2(1+z) H H' - 3H^2}{H_0^2 (1+z)^2 [\Omega_m (1+z) + \Omega_k] - H^2}, \quad (1.89)$$

where ' denote derivatives with respect to the redshift z . At the same time we can accomplish the same result using $D(z)$ if we invert equation (1.85) [32]

$$\omega(z) = \frac{2(1+z)(D^2 \Omega_k + 1)D'' - D'[\Omega_k (1+z)^2 D'^2 + 2\Omega_k D(1+z)D' - 3 - 3D^2 \Omega_k]}{3D' \{[\Omega_k + \Omega_m (1+z)](1+z)^2 D'^2 - D^2 \Omega_k - 1\}}. \quad (1.90)$$

Here it is important to notice that both of the two reconstruction of the DE equation of state presented above are effective only if we previously know Ω_m and Ω_k .

In addition to that, by inverting equation (1.85) it is possible to give a determination of the cosmological curvature of the Universe, as well as hints on the validity of FLRW, independently from other parameters and/or DE models. Explicitly we have [32]

$$\Omega_k = \frac{[H(z)D'(z)]^2 - H_0^2}{[H_0 D(z)]^2}, \quad (1.91)$$

which gives the value of the curvature parameter *at the present day* as a function of measurements done at any redshift. This has an important implication: since the definition of $D(z)$ given in equation (1.85) is valid in any FLRW universe and the curvature parameter is a single number, then the right hand side of equation (1.91) should have the same value at any given redshift if we are in a FLRW background; if instead it turns out to have a redshift dependence this would mean that the assumption of a FLRW metric is wrong [6].

2. Theoretical Models of Redshift Space Distortions

In this Chapter we proceed describing *Redshift Space Distortions* (RSD from now on) and their up to date theoretical description.

- In Section 2.1, starting from the redshift definition (1.20), we define the coordinate of redshift space and give an overview of the RSD phenomenon caused by the real-to-redshift map.
- In Section 2.2 we describe the plane-parallel approximation, which is a useful tool to simplify theoretical calculations, as well as the conditions in which it can be enforced and, lastly, its implications for the models.
- With Section 2.3 we intend to show the derivation of the first result proposed by N. Kaiser [36] by applying dynamical considerations we have made in Section 1.3 and 1.4. In Section 2.3.1 we focus on the bias problem, which is affecting the measurements of density and velocity fields, and state what assumptions have been made in our treatment of RSDs.
- In Section 2.4 we summarize the first attempts to build a model having a more large range of validity by incorporating the Kaiser result at large scales with a phenomenological damping factor able to explain the Finger of God effect at small ones.
- With Section 2.5 we report the work by R. Scoccimarro [58] on the streaming model, which is able to give a more general description of the redshift space behaviour of the 2PCF and PS. In Section 2.5.1 we define the various relations between correlations and pairwise velocity moments, while in Sections 2.5.2 and 2.5.3 we respectively summarize the large scale limit of the streaming model and the PS we are able to obtain from it.
- In Section 2.6 we report the multipole expansion of the 2PCF and PS in order to quantify the magnitude of the correction needed on those quantities to explain RSDs.
- We proceed with Section 2.7, in which we summarize the attempt to improve the streaming model done by A. Taruya, T. Nishimichi and S. Saito (TNS) including density-velocity correlations. The TNS model exploits a large scale expansion of the problem we have reported as follows: the zeroth order contributions in Section 2.7.1, the first order ones in Section 2.7.2 and the second order one in Section 2.7.3.
- Lastly, with Section 2.8 we compare the two models presented in the Chapter and demonstrate they are equivalent, while in Section 2.8.1 we give an alternative definition of the pairwise velocity generating function, which allows a more direct comparison between models.

2.1 On Redshift Space Distortions

In galaxy surveys the access to the third dimension cannot be obtained probing directly the radial distance from the observer, but rather it is provided by a redshift measurement. The Hubble-Lemaître law tells that the recession velocity of an object is proportional to its distance from us as shown in (1.22). As we can see from the definition of the recession velocity of a galaxy, equation (1.26), it is dependent not only on the radial distance from the observer, but also on its peculiar velocity \mathbf{v} (more precisely, on its radial component v_{\parallel}), which is generated due to the dynamics of galaxy clustering and, therefore, unrelated to the expansion of the Universe. We express the redshift coordinate, in velocity units, as follows [30]

$$S := cz, \quad (2.1)$$

with c being the speed of light and z the cosmological redshift (1.20). These considerations allow us to deal with the approximation done in equation (1.22) by accounting peculiar velocity perturbations in the recession velocity description

$$S = aHx_{\parallel} + v_{\parallel}, \quad (2.2)$$

where, differently from (1.22), the physical distance $x_{\parallel, \text{phys}}$ has been written in terms of the comoving (radial) distance, x_{\parallel} , times the product between scale factor a and the Hubble parameter H . The two quantities $x_{\parallel} := \mathbf{x} \cdot \hat{\mathbf{z}}$ and $\mathbf{v}_{\parallel} := \mathbf{v} \cdot \hat{\mathbf{z}}$ are radial components of, respectively, the comoving coordinate of the target and its peculiar velocity, with the radial direction labelled as $\hat{\mathbf{z}}$. Thus the redshift space position of galaxies gets distorted by their peculiar velocities, resulting in a distortion of their redshift space clustering properties: this distortions behave differently at different scales and they are precisely what we call RSDs. They are visualized in Figure 2.1, where on the left is depicted a thin slice of a cosmological simulation and on the right side it is possible to see the same slice after the real-to-redshift space mapping has been applied.

At large scales RSD are dominated by the coherent motion of galaxies towards the centre of clusters: galaxies between us and the cluster have their infall velocities added to the Hubble flow and thus they appear further away in redshift space; at the same time, galaxies beyond the cluster have their infall velocities subtracted to the Hubble flow and thus they appear closer to us than in real space. As a consequence, the effect of RSD at large scales is a "squash" along the *Line of Sight*¹ (LOS hereafter). At small scales (smaller than the typical cluster size) the main effect of peculiar velocity is due to the velocity dispersion from virialization, which causes an elongation along the LOS: this is the so called *Finger of God* (FOG from now on) effect.

To better compare our work with the references, it is useful to report the real-to-redshift map defined above, equation (2.2), using quantities expressed in units of length [58, 68, 77]

$$\mathbf{s} = \mathbf{x} + f \frac{v_{\parallel}(\mathbf{x})}{aHf} \hat{\mathbf{z}} = \mathbf{x} - fu_{\parallel}(\mathbf{x}) \hat{\mathbf{z}}, \quad (2.3)$$

with f being the growth function defined in (1.28). The vectorial formulation of the previous equation has to be intended as two dimensional, with one component parallel to the LOS, s_{\parallel} , and the other

¹Since with redshift space mappings we deal with lots of targets, with LOS we refer to the average direction we are pointing at. This concept will become clear once we enforce the distant observer/plane-parallel approximation depicted in the next Section.

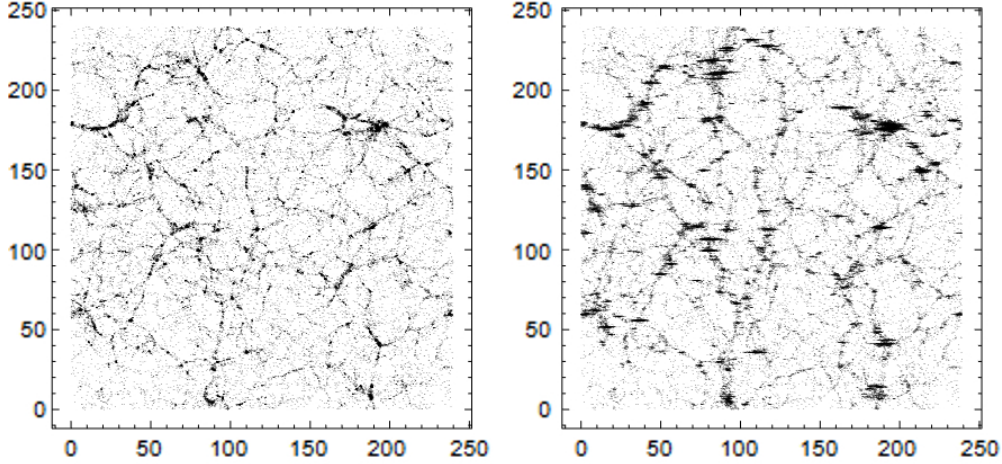


Figure 2.1: Distribution of DM particles from LCDM240, with the horizontal axis corresponding to the radial coordinate. The two panels show the same slice of $1 h^{-1}\text{Mpc}$: in the left one particles are disposed according to their real space coordinates, while in the right one they are disposed according to their redshift space coordinates. The right panel reproduces the distribution as seen from Earth. Figure taken from [26]

perpendicular to it, \mathbf{s}_\perp . By looking at the explicit form of the velocity fields in equation (2.3), in both spatial $v_{\parallel} := \mathbf{v} \cdot \hat{\mathbf{x}}$ and velocity units $u_{\parallel} := \mathbf{u} \cdot \hat{\mathbf{x}}$, it is then clear that the perpendicular component of the redshift coordinate

$$\mathbf{s}_\perp = \mathbf{x}_\perp + f \frac{\mathbf{v}_\perp \cdot \hat{\mathbf{x}}}{aHf} \hat{\mathbf{z}} = \mathbf{x}_\perp - f(\mathbf{u}_\perp \cdot \hat{\mathbf{x}}) \hat{\mathbf{z}}, \quad (2.4)$$

is equal to the real space one $\mathbf{s}_\perp = \mathbf{x}_\perp$ thanks to $\mathbf{v}_\perp \cdot \hat{\mathbf{x}} = 0$ (and $\mathbf{u}_\perp \cdot \hat{\mathbf{x}} = 0$). As a consequence of equation (2.3), the redshift separation between two galaxies $\tilde{\mathbf{s}} := \mathbf{s} - \mathbf{s}'$, which in real space are respectively at coordinates \mathbf{x} and $\mathbf{x}' := \mathbf{x} + \mathbf{r}$, can be retrieved from the real-to-redshift map

$$\tilde{\mathbf{s}} = \mathbf{r} + f \frac{\Delta v_{\parallel}(\mathbf{r})}{aHf} \hat{\mathbf{z}} = \mathbf{r} - f \Delta u_{\parallel}(\mathbf{r}) \hat{\mathbf{z}}, \quad (2.5)$$

where the galaxy displacement along the LOS direction, denoted with $\hat{\mathbf{z}}$, has been defined as

$$\begin{aligned} \Delta u_{\parallel}(\mathbf{r}) &:= u_{\parallel}(\mathbf{x}') - u_{\parallel}(\mathbf{x}), \\ \Delta v_{\parallel}(\mathbf{r}) &:= v_{\parallel}(\mathbf{x}') - v_{\parallel}(\mathbf{x}) \end{aligned} \quad (2.6)$$

in units of length and velocity respectively. The two are related to each other through $\mathbf{u}(\mathbf{r}) \equiv -\mathbf{v}(\mathbf{r})/aHf$, as stated in [68, 77].

2.2 Plane-Parallel Approximation

Using the real-to-redshift map we have defined in equation (2.3), it is possible to derive quantities in redshift space starting from their counterparts in real space; the only assumption made to describe the

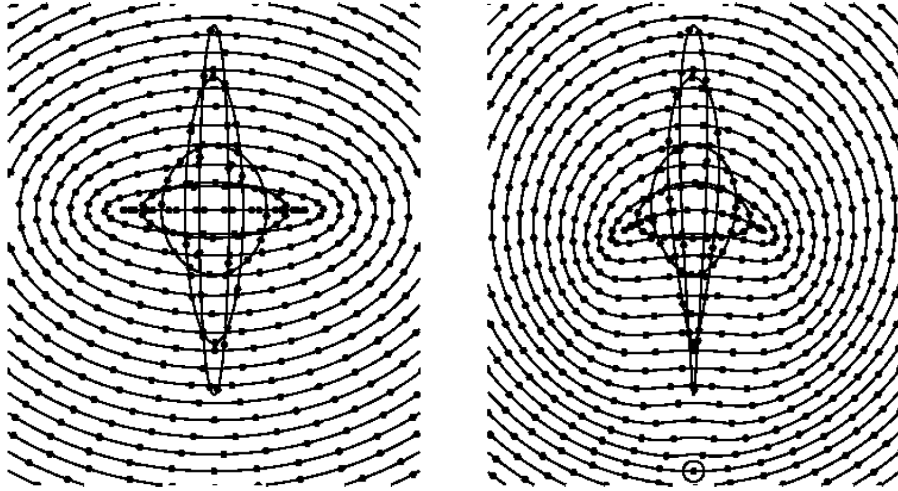


Figure 2.2: Representation of a spherical overdensity distorted by peculiar velocities. The left panel shows in the plane-parallel approximation, with the observer placed at great distance; the right panel represents a situation in which the observer (the bigger circle in the bottom part of the picture) is near the target galaxies, making large scale distortions kidney-shaped and FOG effect like it is pointing to the observer. Figure taken from [30].

map is the *plane-parallel approximation*. With plane-parallel approximation we refer to the simplification we enforce to avoid spherical distortions while dealing with galaxy surveys: it tells us that if we are observing two sufficiently distant targets we can consider the LOS as fixed in a single direction, called $\hat{\mathbf{x}}_{pp}$, instead of computing the projection along the coordinate direction $\hat{\mathbf{x}}$ for each target. A schematic visualization of what we are trying to do is given in Figure 2.2, where RSDs are represented with and without this assumption. Once the LOS is fixed, we can treat the direction of the survey as common among all the targets; the *directional cosine* becomes

$$\mathbf{k} \cdot \hat{\mathbf{x}} = \mathbf{k} \cdot \hat{\mathbf{x}}' \equiv \mathbf{k} \cdot \hat{\mathbf{x}}_{pp}, \quad (2.7)$$

where we treated $\mathbf{x} = x\hat{\mathbf{x}}$ as the radial coordinate of each target in full generality and $\mathbf{x}_{pp} = x\hat{\mathbf{x}}_{pp}$ the with the fixed LOS thanks to the plane-parallel approximation. Without the assumption of the plane-parallel approximation the velocity field in the real-to-redshift map would have been projected along different directions instead of along the LOS

$$\begin{aligned} u_{||}(\mathbf{x}) &\longrightarrow \mathbf{u}(\mathbf{x}) \cdot \hat{\mathbf{x}} \\ u_{||}(\mathbf{x}') &\longrightarrow \mathbf{u}(\mathbf{x}') \cdot \hat{\mathbf{x}}', \end{aligned} \quad (2.8)$$

making the computation between fields located at different real space coordinates more complicated to calculate [58]. It is important to note that in some references [57, 68, 66, 77] the directional cosine has been defined as $\mu := \hat{\mathbf{k}} \cdot \hat{\mathbf{x}}_{pp}$ which is controlled by the angle between the fixed LOS and the vector \mathbf{k} ; the direction cosine is related to $k_{||}$, or k_z [57, 58, 68, 77], through the relation $k_{||} \equiv k_z = \mathbf{k} \cdot \hat{\mathbf{x}}_{pp} = k\hat{\mathbf{k}} \cdot \hat{\mathbf{x}}_{pp} = k\mu$.

We refer to what we have stated before as the *global* plane-parallel approximation, which is a powerful tool but breaks down for extreme large-scale modes. So, thinking about modern large-angle surveys, in some cases it could be appropriate to refine the approximation above by making it *local* [57] as we show below

$$\mathbf{k} \cdot \hat{\mathbf{x}}_1 \simeq \mathbf{k} \cdot \hat{\mathbf{x}}_2 \simeq \mathbf{k} \cdot \hat{\mathbf{x}}_h, \quad (2.9)$$

with $\hat{\mathbf{x}}_1$ and $\hat{\mathbf{x}}_2$ mark the directions of the two galaxies and $\hat{\mathbf{x}}_h := (\hat{\mathbf{x}}_1 + \hat{\mathbf{x}}_2)/2$ the middle point between them on the celestial sphere.

2.3 Derivation of the Kaiser Formula

We now discuss how the effect of RSDs applies on the clustering statistics and, furthermore, is able to reproduce the Kaiser results of 1987 [36]. For distant galaxies, the radial distance \mathbf{x} in is mapped in redshift space as (2.3). As mentioned above, we restrict ourselves to the plane-parallel approximation so that the LOS is taken as a fixed direction for all the galaxies considered, denoted by $\hat{\mathbf{z}}$. Plane-parallel distortions maintain statistical homogeneity, so Fourier modes are still the natural basis in redshift space. However, statistical isotropy breaks down because the real-to-redshift mapping of equation (2.3) defines a preferred direction, denoted by the LOS itself, along which the clustering statistics is different from the one in each of the other possible directions [30].

As a consequence of number conservation between real and redshift space, it is possible to apply the real-to-redshift map (2.3) to the mass density

$$\rho_s d^3 \mathbf{s} = \rho d^3 \mathbf{x}, \quad (2.10)$$

where ρ_s is the redshift space density field associated with ρ ; by expanding the equation using (1.29) we obtain

$$\bar{\rho}_s (1 + \delta_s) d^3 \mathbf{s} = \bar{\rho} (1 + \delta) d^3 \mathbf{x}. \quad (2.11)$$

Since the average density cannot be different between the two spaces, the equation deriving from number conservation reads

$$(1 + \delta_s) d^3 \mathbf{s} = (1 + \delta) d^3 \mathbf{x}, \quad (2.12)$$

which is able to relate the redshift perturbation of the density field in redshift space with the real space one [18, 36, 55, 57, 58, 68]. The Jacobian of the real-to-redshift transformation is defined as

$$J(\mathbf{x}) = \left| \frac{d^3 \mathbf{s}}{d^3 \mathbf{x}} \right|; \quad (2.13)$$

its computation follows directly from the real-to-redshift map we have defined in equation (2.3) [36, 57]

$$\begin{aligned} J(\mathbf{x}) &= \left| \frac{d^3 \mathbf{s}}{d^3 \mathbf{x}} \right| = \left| \frac{s^2 ds}{x^2 dx} \right| = \left| \frac{1}{x^2} \left(x^2 + 2f \frac{1}{aHf} x v_{||}(\mathbf{x}) + f^2 \frac{1}{(aHf)^2} v_{||}^2(\mathbf{x}) \right) \left(1 + f \frac{1}{aHf} \frac{\partial v_{||}(\mathbf{x})}{\partial x} \right) \right| \\ &= \left| \left(1 + 2f \frac{1}{aHf} \frac{v_{||}(\mathbf{x})}{x} + f^2 \frac{1}{(aHf)^2} \frac{v_{||}^2(\mathbf{x})}{x^2} \right) \left(1 + f \frac{1}{aHf} \frac{\partial v_{||}(\mathbf{x})}{\partial x} \right) \right| \\ &\equiv \left| \left(1 - 2f \frac{u_{||}(\mathbf{x})}{x} + f^2 \frac{u_{||}^2(\mathbf{x})}{x^2} \right) \left(1 - f \frac{\partial u_{||}(\mathbf{x})}{\partial x} \right) \right| \end{aligned} \quad (2.14)$$

and from it it is possible to see that the Jacobian is composed by two factors: the first one containing the square of the ratio between the redshift and the real coordinates and the second one containing the term involving the gradient of the LOS component of the peculiar velocity. With equation (2.14) written explicitly, we can now quantify exactly the "sufficiently distant targets" condition stated above: the two velocity dependent terms inside the first factor can be dropped out if the peculiar velocities $v_{\parallel}(\mathbf{x})$ (or equivalently $u_{\parallel}(\mathbf{x})$ in unit of length) are much smaller than the radial distance x at which structures are being observed [31], namely

$$\frac{v_{\parallel}(\mathbf{x})}{x} \ll 1. \quad (2.15)$$

When the condition above is met, the first term inside equation (2.14) becomes very close to unity; thus we can exploit the distant target condition and simplify the Jacobian (2.14) as follows [10, 36, 57]

$$J(\mathbf{x}) \simeq \left(1 + f \nabla_{\parallel} \frac{v_{\parallel}(\mathbf{x})}{aHf} \right) \equiv (1 - f \nabla_{\parallel} u_{\parallel}(\mathbf{x})), \quad (2.16)$$

where with $\nabla_{\parallel} f(\mathbf{x}) := \partial f(\mathbf{x}) / \partial x$ we denote the directional derivative along the LOS.

The same approximation can be done taking pairs of galaxies, by deriving the Jacobian from (2.5) rather than (2.3), to obtain

$$J(r) \simeq (1 - f \nabla_{\parallel} \Delta u_{\parallel}(\mathbf{r})). \quad (2.17)$$

In linear theory this treatment is justified because one can reasonably expect peculiar velocities of galaxies along the LOS, $v_{\parallel}(\mathbf{x})$, to be much smaller than the expansion rate of the Universe, H ; as a consequence the real-to-redshift separation coming from the map defined in (2.3) will tend to zero making the Jacobian, in both the forms (2.16) and (2.17), approaching unity.

The original derivation by N. Kaiser [36], as well as most of the work based on it [10, 30, 68, 57, 77], starts from number conservation (2.12) and derives the redshift space description of the mass perturbation by isolating the redshift space density contrast field $\delta_s(\mathbf{s})$, rather than the one of the total mass $(1 + \delta_s(\mathbf{s}))$

$$\delta_s(\mathbf{s}) = \frac{1 + \delta(\mathbf{x})}{J(\mathbf{x})} - 1. \quad (2.18)$$

Inserting the form of the Jacobian coming from linear theory (2.16), the redshift space mass perturbation becomes

$$\begin{aligned} \delta_s(\mathbf{s}) &= [1 + \delta(\mathbf{x})] J^{-1}(\mathbf{x}) - 1 \simeq [1 + \delta(\mathbf{x})][1 + f \nabla_{\parallel} u_{\parallel}(\mathbf{x})] - 1 \\ &= \delta(\mathbf{x}) + f \nabla_{\parallel} u_{\parallel}(\mathbf{x}) + \delta(\mathbf{x}) f \nabla_{\parallel} u_{\parallel}(\mathbf{x}) \\ &\simeq \delta(\mathbf{x}) + f \nabla_{\parallel} u_{\parallel}(\mathbf{x}). \end{aligned} \quad (2.19)$$

Here we notice that the form of the redshift space density contrast field given above can be reached only assuming $\nabla_{\parallel} u_{\parallel}(\mathbf{x}) \ll 1$ to further expand the Jacobian of equation (2.16). Taking equation (2.19) to Fourier space with definition (1.59) we obtain

$$\begin{aligned} \delta_s(\mathbf{k}) &= \int d^3 \mathbf{s} e^{i\mathbf{k} \cdot \mathbf{s}} \delta_s(\mathbf{s}) \\ &= \int d^3 \mathbf{x} e^{i\mathbf{k} \cdot \mathbf{x}} e^{-ik_{\parallel} f u_{\parallel}(\mathbf{x})} [\delta(\mathbf{x}) + f \nabla_{\parallel} u_{\parallel}(\mathbf{x})]. \end{aligned} \quad (2.20)$$

It is important to notice that, in the computation of (2.20), we have enforced the linear theory only for the transformation of the mass perturbation $\delta_s(\mathbf{s})$: to retrieve the Kaiser formula one needs to apply linear theory also to the transformation itself, which enters in (2.20) via the exponential of the Fourier transform [57]. By expanding the exponential involving the velocity field $u_{\parallel}(\mathbf{x})$ around $u_{\parallel}(\mathbf{x}) = 0$, one can obtain

$$\begin{aligned}
\delta_s(\mathbf{k}) &\simeq \int d^3\mathbf{x} e^{i\mathbf{k}\cdot\mathbf{x}} [\delta(\mathbf{x}) + f\nabla_{\parallel}u_{\parallel}(\mathbf{x})] \\
&= \delta(\mathbf{k}) + f \int d^3\mathbf{x} e^{i\mathbf{k}\cdot\mathbf{x}} \nabla_{\parallel}u_{\parallel}(\mathbf{x}) \\
&= \delta(\mathbf{k}) + f \int d^3\mathbf{x} e^{i\mathbf{k}\cdot\mathbf{x}} \nabla_{\parallel} \int \frac{d^3\mathbf{p}}{(2\pi)^3} e^{-i\mathbf{p}\cdot\mathbf{x}} u_{\parallel}(\mathbf{p}) \\
&= \delta(\mathbf{k}) - if \int \frac{d^3\mathbf{p}d^3\mathbf{x}}{(2\pi)^3} e^{i(\mathbf{k}-\mathbf{p})\cdot\mathbf{x}} p_{\parallel}u_{\parallel}(\mathbf{p}) \\
&= \delta(\mathbf{k}) + \frac{i}{aH} \int d^3\mathbf{p} \delta_D(\mathbf{k}-\mathbf{p}) p_{\parallel}v_{\parallel}(\mathbf{p}) \\
&= \delta(\mathbf{k}) + \frac{i}{aH} k_{\parallel}v_{\parallel}(\mathbf{k}),
\end{aligned} \tag{2.21}$$

where, going from the third to the fourth line, we have used the definition of the Dirac delta function given in equation (1.67).

Thus, the expression of the redshift space density contrast field in Fourier space is directly linked to the velocity field in the same domain; to derive it we start by applying the Fourier transform to the velocity divergence field (1.27)

$$\theta(\mathbf{k}) = \int d^3\mathbf{x} e^{i\mathbf{k}\cdot\mathbf{x}} \left[-\frac{\nabla \cdot \mathbf{v}(\mathbf{x})}{aHf} \right]. \tag{2.22}$$

In order to deal with the gradient inside (2.22), we look at the velocity field in real space as if it were its Fourier counterpart, on which we then apply the anti-transform

$$\begin{aligned}
aHf\theta(\mathbf{k}) &= \int d^3\mathbf{x} e^{i\mathbf{k}\cdot\mathbf{x}} \left[-\nabla \cdot \int \frac{d^3\mathbf{p}}{(2\pi)^3} e^{-i\mathbf{p}\cdot\mathbf{x}} \mathbf{v}(\mathbf{p}) \right] \\
&= \int d^3\mathbf{x} e^{i\mathbf{k}\cdot\mathbf{x}} \left[-\int \frac{d^3\mathbf{p}}{(2\pi)^3} e^{-i\mathbf{p}\cdot\mathbf{x}} (-i\mathbf{p} \cdot \mathbf{v}(\mathbf{p})) \right] \\
&= i \int \frac{d^3\mathbf{k}d^3\mathbf{x}}{(2\pi)^3} e^{i(\mathbf{k}-\mathbf{p})\cdot\mathbf{x}} [\mathbf{p} \cdot \mathbf{v}(\mathbf{p})] \\
&= i \int \frac{d^3\mathbf{p}}{(2\pi)^3} \delta_D(\mathbf{k}-\mathbf{p}) [\mathbf{p} \cdot \mathbf{v}(\mathbf{p})] \\
&= i\mathbf{k} \cdot \mathbf{v}(\mathbf{k}),
\end{aligned} \tag{2.23}$$

where once again we have used the definition of Dirac delta given in equation (1.67) passing from the third to the fourth line. Inverting the equation we can now express the peculiar velocity field in Fourier space as a function of its divergence

$$\mathbf{v}(\mathbf{k}) = -iaHf \frac{\mathbf{k}}{k^2} \theta(\mathbf{k}). \tag{2.24}$$

To link the velocity field (2.24) with the density contrast (2.21), we make use of the linearized continuity equation (1.46). We start by applying the Fourier transform to it

$$\begin{aligned}\frac{\partial\delta(\mathbf{k})}{\partial t} + \frac{1}{a} \int d^3\mathbf{x} e^{i\mathbf{k}\cdot\mathbf{x}} \nabla \cdot \mathbf{v}(\mathbf{x}) &= 0 \\ \frac{\partial\delta(\mathbf{k})}{\partial t} + \frac{1}{a} \int d^3\mathbf{x} e^{i\mathbf{k}\cdot\mathbf{x}} \nabla \cdot \int \frac{d^3\mathbf{p}}{(2\pi)^3} e^{-i\mathbf{p}\cdot\mathbf{x}} \mathbf{v}(\mathbf{p}) &= 0,\end{aligned}\tag{2.25}$$

which exploiting the same procedure of (2.23) to deal with the gradient, becomes [46]

$$\begin{aligned}\frac{\partial\delta(\mathbf{k})}{\partial t} - \frac{1}{a} i\mathbf{k} \cdot \mathbf{v}(\mathbf{k}) &= 0 \\ \implies \mathbf{v}(\mathbf{k}) &= -ia \frac{\mathbf{k}}{k^2} \frac{\partial\delta(\mathbf{k})}{\partial t}.\end{aligned}\tag{2.26}$$

The derivative of the density perturbation can be computed by noticing that $\delta \propto D^{(+)}$ and then proceeding as follows

$$\frac{\partial\delta}{\partial t} \simeq \frac{\partial D^{(+)}}{\partial t} = \frac{D^{(+)}}{a} \frac{a}{D^{(+)}} \frac{\partial a}{\partial t} \frac{\partial D^{(+)}}{\partial a} \simeq \delta H f,\tag{2.27}$$

where for the last equality we have used the definitions of the Hubble parameter (1.9) and linear growth factor (1.28). Thus, the linearized continuity equation in Fourier space becomes [46]

$$\mathbf{v}(\mathbf{k}) = -iaHf \frac{\mathbf{k}}{k^2} \delta(\mathbf{k}),\tag{2.28}$$

which provides, after a comparison between (2.28) and (2.24), the relation linking density and velocity perturbations in linear dynamics

$$\delta = \theta.\tag{2.29}$$

Inserting equation (2.24) into (2.21) and exploiting (2.29), we are able to write

$$\delta_s(\mathbf{k}) = \delta(\mathbf{k}) + f \frac{k_n^2}{k^2} \theta(\mathbf{k}) = \delta(\mathbf{k}) + f\mu^2 \theta(\mathbf{k}) = (1 + f\mu^2) \delta_L(\mathbf{k}),\tag{2.30}$$

with $\delta_L(\mathbf{k})$ being the linear dynamics density contrast field. With this description of the redshift space density contrast, it is possible now to build the PS of matter perturbations through (1.63) and (1.65) we have

$$P_s(\mathbf{k}) = (1 + f\mu^2)^2 P_L(k).\tag{2.31}$$

The important thing to keep in mind here is that equation (2.31) is describing the PS of DM perturbations, while through observations coming from photon based detectors we are capable to observe only its luminous counterpart. As we have previously seen, in Section 1.4, galaxies can be used as tracers of the underlying DM distribution; this approach comes, however, with some important caveat: in principle galaxies could be a *biased* tracer of the totality of matter, both in their velocity and density fields. Below we give the form of the galaxy PS under the assumption of a linear bias for the density field, $\delta_g = b\delta$ with b as linear bias factor, and no bias for the velocity field, $v_g = v$,

$$P_{s,g}(\mathbf{k}) = b^2(1 + \beta\mu^2)^2 P_L(k), \quad \beta := \frac{f}{b} \simeq \frac{\Omega_m^{0.6}}{b}.\tag{2.32}$$

Through the bias factor, the equation above is able to link the observed galaxy PS to the underlying DM one (solid line in Figure 1.7). It is important to notice that β is not a cosmological parameter in full generality, like Ω_m for example, because it is defined only in this context of a linear bias approximation. Under this assumptions, however, it is still a useful quantity thanks to the fact that it is able to relate the velocity field with the density contrast one [76].

Before proceeding with the next Sections, it is important to keep track of the assumptions made to retrieve the Kaiser results [10]

1. Linear evolution of DM, in order to utilize equations (1.46) and (1.47) for DM and, consequently, of galaxies (at least at large scales).
2. $\sigma_{ij} \ll 1$, in order to close the hierarchy of the Vlasov equation moments and recover the ideal pressureless fluid treatment of DM.
3. Number conservation of sources between real and redshift space, in order to relate the real density contrast field with its redshift space counterpart.
4. Plane-parallel/Distant observer approximation, namely $\mathbf{x} \simeq \mathbf{x}_{pp} = x\hat{\mathbf{x}}_{pp}$, to avoid spherical distortions and set $u_{,i}(\mathbf{x})/x \ll 1$ to describe the Jacobian as proposed in equation (2.16).
5. $d\Delta u_{,i}(\mathbf{r})/dr \ll 1$, so that the Jacobian can be expanded as in equation (2.19).

As we will show during the following of this Chapter, although this result works for the largest scales, this model can be refined further by reducing the amount of assumptions; in such a way we can hope to extend its regime of validity even at smaller scales where nonlinear effects become important.

2.3.1 On the Bias Factor

The linear bias model mentioned in the previous Section was originally motivated by the threshold biasing model of galaxy formation, in which galaxy formation results to be amplified in those regions where the density field of matter exceed a certain value [35], and the peak biasing model, in which galaxies are supposed to form only at the peaks of matter density [5].

Regarding the linear bias model, $\delta_g = b\delta$, it is important to note that it must break down in the highly nonlinear regime, namely when $b > 1$: if not regions without matter, where $\delta = -1$, would have a negative galaxy density, which is obviously impossible [30]. In addition to that, if a linear bias $b(t_i)$ is established at some initial time t_i so that the relation

$$\delta_g(\mathbf{r}, t_i) = b(t_i)\delta(\mathbf{r}, t_i) \quad (2.33)$$

holds and after which the continuity equation of galaxy is fulfilled (no more formation or destruction of galaxies starting from t_i), we have an evolution of the bias factor $b(t > t_i) = \delta_g(t > t_i)/\delta(t > t_i)$. During linear growth, the matter density perturbation remains small and their evolution can be described by the linear growth solution $D^{(+)}(t)$ expressed in equation (1.48) as

$$\frac{\delta(t)}{\delta(t_i)} = \frac{D^{(+)}(t)}{D^{(+)}(t_i)}. \quad (2.34)$$

Hence the bias evolution turns out to be decrease its magnitude in time, while it remains constant in space [30]

$$b(t) - 1 = (b(t_i) - 1) \frac{D^{(+)}(t_i)}{D^{(+)}(t)}; \quad (2.35)$$

this tells us that the bias factor tends to reach unity as fluctuations grow.

If the continuity condition of galaxies persists into the nonlinear regime, then the bias becomes a function of the position [30]

$$b(\mathbf{r}, t) - 1 = \delta(\mathbf{r}, t_i) \left(\frac{1}{\delta(\mathbf{r}, t)} + 1 \right) (b(t_i) - 1) \quad (2.36)$$

which has limit values $b = 1$ in zero density regions, $\delta(\mathbf{r}, t) \rightarrow -1$, and $b = 1 + \delta(\mathbf{r}, t)(b(t_i) - 1)$ in regions of high density, $\delta(\mathbf{r}, t) \rightarrow \infty$. As the conditions becomes more and more nonlinear, streams with different initial coordinates may end up in the same final point, so it is important to say that in principle equation (2.36) should be averaged over streams.

In the linear bias model of the previous Section, the velocity field is an unbiased field, $\mathbf{v}_g(t) = \mathbf{v}(t)$, as long as one has a good description of the density contrast field of the biased tracer. Nevertheless, it is not necessarily true that the velocity bias is always negligible, as stated in [57, 68, 77].

The model presented briefly in this Section is a simplified one: the point in showing that is, as times goes and the continuity condition for galaxies holds, the bias factor $b(t)$ tends to become closer and closer to unity making galaxies a progressively less biased tracer of DM. Obviously non linear bias model have been theorized, but they turn out to be beyond the goal of this work; if the reader is interested, they could look at [17, 44] and references therein for some examples.

2.4 RSDs: a Phenomenological Description

Although the Kaiser formula given in equation (2.32) is able to reproduce the redshift behaviour of the PS at large scales, it fails to reproduce it at small scales where nonlinear effects start to become relevant, inducing the FOG effect we have mentioned before. The FOG effect can be reproduced by multiplying the linear distortion term of Kaiser by a damping factor which treats the distortion as a convolution with an incoherent velocity component [4]

$$P_s(k, \mu) = D_{FOG}(k\mu f_{\sigma_{v, \text{eff}}}) P_{Kaiser}(k, \mu), \quad (2.37)$$

where $P_{Kaiser}(k, \mu)$ represents the Kaiser effect squashing the PS at large scales, equation (2.32), and the $\sigma_{v, \text{eff}}$ function is the effective velocity dispersion, which is treated as a free parameter.

The FOG damping factor is directly dependent on the pairwise velocity distribution function, historically [4, 11, 43, 49] it has been assumed to have an exponential form

$$f(v_{12}) = \frac{1}{\sqrt{2\sigma_{v, \text{eff}}^2}} \exp \left\{ -\frac{\sqrt{2}|v_{12}|}{\sigma_{v, \text{eff}}} \right\} \quad (2.38)$$

for the treatment of nonlinear scales; alternatively, also a Gaussian form has been proposed

$$f(v_{12}) = \frac{1}{\sqrt{2\sigma_{v, \text{eff}}^2}} \exp \left\{ -\frac{v_{12}^2}{2\sigma_{v, \text{eff}}^2} \right\} \quad (2.39)$$

in the case where the density field can be thought to be a pure random field. Once brought in Fourier space, the two descriptions of the pairwise velocity distribution function presented above determine exactly $D_{FOG}(k\mu f\sigma_{v,\text{eff}})$. Respectively we have [4]

$$D_{FOG}(k\mu f\sigma_{v,\text{eff}}) = \begin{cases} (1 + k^2\mu^2 f^2\sigma_{v,\text{eff}}^2/2)^{-1} \\ \exp\left\{-\frac{k^2\mu^2 f^2\sigma_{v,\text{eff}}^2}{2}\right\}. \end{cases} \quad (2.40)$$

Despite the differences between the two pairwise velocity models, it turns out that they determine very little variations once inserted in (2.37) until the damping factor reaches values $D_{FOG}(k\mu f\sigma_{v,\text{eff}}) \gtrsim 2$ [4]. Since the FOG effect is thought to be a completely nonlinear effect [68, 58], an analytic description of the velocity dispersion inside $D_{FOG}(k\mu f\sigma_{v,\text{eff}})$ cannot be written in terms of the linear theory: this is the reason behind the choice of treating it as a free parameter.

In linear theory, the Kaiser effect in equation (2.37) can be described using the result we presented in Section 2.3 with equation (2.31), which was proposed for the first time by N. Kaiser in [36]. The $P_{Kaiser}(k, \mu)$ term inside (2.37) can be improved further if one does not enforce linear dynamics between the density and velocity fields through equation (2.29), and defines three new power spectra: $P_{\delta\delta}(k)$, $P_{\theta\theta}(k)$ and $P_{\delta\theta}(k)$, which are respectively the auto power spectra of the density and velocity field and their cross PS. Following the definition given in equation (1.66), we can write [41, 60]

$$\begin{aligned} \langle \delta(\mathbf{k})\delta(\mathbf{k}') \rangle &= (2\pi)^3 \delta_D(\mathbf{k} + \mathbf{k}') P_{\delta\delta}(k), \\ \langle \delta(\mathbf{k})\theta(\mathbf{k}') \rangle &= (2\pi)^3 \delta_D(\mathbf{k} + \mathbf{k}') P_{\delta\theta}(k), \\ \langle \theta(\mathbf{k})\theta(\mathbf{k}') \rangle &= (2\pi)^3 \delta_D(\mathbf{k} + \mathbf{k}') P_{\theta\theta}(k). \end{aligned} \quad (2.41)$$

Then from equation (2.30) it is possible to retrieve the nonlinear PS in redshift space using (2.41), which gives² [53, 58]

$$\begin{aligned} \langle \delta_s(\mathbf{k})\delta_s(\mathbf{k}') \rangle &= \langle [\delta(\mathbf{k}) + f\mu^2\theta(\mathbf{k})][\delta(\mathbf{k}') + f\mu^2\theta(\mathbf{k}')] \rangle \\ &= \langle \delta(\mathbf{k})\delta(\mathbf{k}') + f\mu^2\delta(\mathbf{k})\theta(\mathbf{k}') + f\mu^2\theta(\mathbf{k})\delta(\mathbf{k}') + f^2\mu^4\theta(\mathbf{k})\theta(\mathbf{k}') \rangle \\ &= \langle \delta(\mathbf{k})\delta(\mathbf{k}') \rangle + f\mu^2 \langle \delta(\mathbf{k})\theta(\mathbf{k}') \rangle + f\mu^2 \langle \theta(\mathbf{k})\delta(\mathbf{k}') \rangle + f^2\mu^4 \langle \theta(\mathbf{k})\theta(\mathbf{k}') \rangle \\ &\implies P_s(\mathbf{k}) = P_{\delta\delta}(k) + 2f\mu^2 P_{\delta\theta}(k) + f^2\mu^4 P_{\theta\theta}(k). \end{aligned} \quad (2.42)$$

Thus the two descriptions of the Kaiser effect given by the phenomenological are

$$P_{Kaiser}(k, \mu) = \begin{cases} (1 + f\mu^2)^2 P_L(k), & \text{Linear} \\ P_{\delta\delta}(k) + 2f\mu^2 P_{\delta\theta}(k) + f^2\mu^4 P_{\theta\theta}(k), & \text{non-Linear.} \end{cases} \quad (2.43)$$

In Figure 2.3 we report a comparison³ between various combinations of terms inside (2.40) and (2.43), once inserted inside equation (2.37), with the N-body simulation results from `wmap5` [67] at

²Note that the last equality in equation (2.30) implies (2.31), while here we are using $\delta_s(\mathbf{k}) = \delta(\mathbf{k}) + f\mu^2\theta(\mathbf{k})$; this is done to take into account nonlinear dynamics in the galaxy statistics, which is ignored if we enforce the last equivalence, $\delta = \theta$, to retrieve the Kaiser formula (2.31).

³Note that the comparison is given for both the monopole (left panel) and the quadrupole (right panel) components of the PS, which will be described in detail in Section 2.6

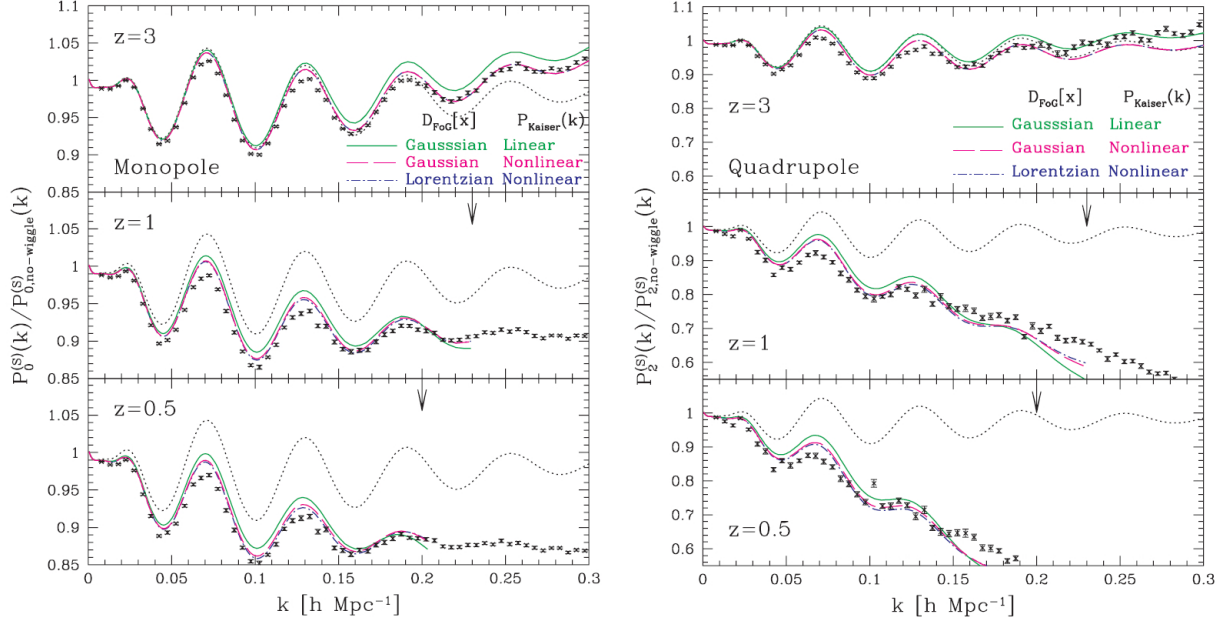


Figure 2.3: Comparison between the dispersion model of equation (2.37) and N-body simulation results from `wmap5` [67] at different redshifts. The dotted line depicts the linear behaviour of the PS, while the three coloured lines are various combinations of the phenomenological description terms. The three coloured lines are: Gaussian velocity distribution coupled with a linear description of the PS (solid green line), Gaussian velocity distribution and nonlinear description of the PS (dashed magenta) and Lorentzian velocity distribution coupled with nonlinear description of the PS (dash-dotted blue). The reference PS is calculated from [19]. Figure taken from [57].

various redshifts. Here we stress again that in all the cases shown the one-dimensional velocity dispersion $\sigma_{v,\text{eff}}^2$ was determined by a fitting procedure to the N-body simulation, rather than predicted from theory. The reference spectrum, $P_{no-Wiggle}^{(S)}(k)$, is the redshift space PS determined from the no-wiggle approximation of the linear transfer function [19] coupled with the linear theory of the Kaiser effect (2.31) and reported as a dotted line. From Figure 2.3 we can clearly see why the FOG factor was needed to give a proper characterization of the redshift PS: indeed the linear description from (2.31) strongly deviates from simulation results as far as we go to higher value of k (smaller scales), while the introduction of the FOG suppression term is able to better reproduce the expected behaviour.

2.5 The Streaming Model

In this Section we present the theoretical model known as the *Streaming Model* proposed by P. J. E. Peebles in his book *The Large Scale Structure of the Universe* [51] using the later approach depicted by R. Scoccimarro in [58], which is able to give a full characterization of RSDs (still remaining in the plane-parallel approximation though) while reducing the number of assumptions required to recover

the Kaiser results of [36]. It aims to describe the real and redshift power spectra with the pairwise velocity PDF and its Fourier transform. The pairwise velocity PDF needs then to be modelled as function of the linear matter PS and cosmological parameters [58].

Starting from the number conservation of sources between real and redshift space of equation (2.12) and recalling the real-to-redshift map (2.3), it is possible to describe the redshift space behaviour of matter perturbations by applying the Fourier transform (1.59) to the real space density contrast as follows

$$\begin{aligned} (2\pi)^3 \delta_D(\mathbf{k}) + \delta_s(\mathbf{k}) &= \int d^3\mathbf{s} e^{i\mathbf{k}\cdot\mathbf{s}} [1 + \delta_s(\mathbf{s})] \\ &= \int d^3\mathbf{x} e^{i\mathbf{k}\cdot\mathbf{x}} e^{-ifk_{\parallel}u_{\parallel}(\mathbf{x})} [1 + \delta(\mathbf{x})], \end{aligned} \quad (2.44)$$

where the only approximation made is the plane-parallel one and no additional dynamical information has been used in the derivation of equation (2.44); moreover, since there is no dependence on the Jacobian inside equation (2.44), it is valid also in regions where there is multi streaming [7, 58, 68]. As a summary, below we list all the assumptions made by R. Scoccimarro in [58] to implement the model

1. Number conservation of sources between real and redshift space, in order to relate the real density contrast field with its redshift space counterpart.
2. Plane-parallel/Distant observer approximation, namely $\mathbf{x} \simeq \mathbf{x}_{pp} = x\hat{\mathbf{x}}_{pp}$, to avoid spherical distortions.

These assumptions are the reason behind the strength of the streaming model proposed by R. Scoccimarro: once compared with the Kaiser derivation, the description of the redshift space density field itself, in the form of $(2\pi)^3 \delta_D(\mathbf{k}) + \delta_s(\mathbf{k})$, rather than perturbations alone made possible to drop all the dynamical assumptions that were made in Section 2.3 to describe the linearized Jacobian of the transformation.

Starting from equation (2.44), it is possible to describe the redshift space PS of the totality of matter. To do so we start by isolating the density contrast field

$$\delta_s(\mathbf{k}) = \left(\int d^3\mathbf{x} e^{i\mathbf{k}\cdot\mathbf{x}} e^{-ifk_{\parallel}u_{\parallel}(\mathbf{x})} \right) - (2\pi)^3 \delta_D(\mathbf{k}), \quad (2.45)$$

where to lighten the equation we have set $u_{\parallel} := u_{\parallel}(\mathbf{x})$; for future reference we use the same conventions setting $u'_{\parallel} := u_{\parallel}(\mathbf{x}')$, $\delta := \delta(\mathbf{x})$ and $\delta' := \delta(\mathbf{x}')$. Defining now the redshift space PS of matter perturbations analogously to equation (1.66)⁴

$$\langle \delta_s(\mathbf{k}) \delta_s(\mathbf{k}') \rangle = (2\pi)^3 \delta_D(\mathbf{k} + \mathbf{k}') P_s(\mathbf{k}, \mathbf{k}') \quad (2.46)$$

we can look at the correlator between the two redshift space density contrasts: we insert equation

⁴Notice that here, since we are dealing with Fourier transforms of redshift space quantities, we cannot write the PS as a function of the magnitude of k only but rather, in full generality, a function of both \mathbf{k} and \mathbf{k}' .

(2.45) inside (2.46) to get

$$\begin{aligned}
(2\pi)^3 \delta_D(\mathbf{k} + \mathbf{k}') P_s(\mathbf{k}, \mathbf{k}') &= \\
&= \left\langle \left[\int d^3 \mathbf{x} e^{i\mathbf{k} \cdot \mathbf{x}} e^{-ifk_{\parallel} u_{\parallel}} (1 + \delta) - (2\pi)^3 \delta_D(\mathbf{k}) \right] \left[\int d^3 \mathbf{x}' e^{i\mathbf{k}' \cdot \mathbf{x}'} e^{-ifk'_{\parallel} u'_{\parallel}} (1 + \delta) - (2\pi)^3 \delta_D(\mathbf{k}') \right] \right\rangle \\
&= \int d^3 \mathbf{x} d^3 \mathbf{x}' e^{i\mathbf{k} \cdot \mathbf{x}} e^{i\mathbf{k}' \cdot \mathbf{x}'} \left\langle e^{-if(k_{\parallel} u_{\parallel} + k'_{\parallel} u'_{\parallel})} (1 + \delta)(1 + \delta') \right\rangle + \\
&\quad - (2\pi)^3 \delta_D(\mathbf{k}) \int d^3 \mathbf{x}' e^{i\mathbf{k}' \cdot \mathbf{x}'} \left\langle e^{-ifk'_{\parallel} u'_{\parallel}} (1 + \delta') \right\rangle + \\
&\quad - (2\pi)^3 \delta_D(\mathbf{k}') \int d^3 \mathbf{x} e^{i\mathbf{k} \cdot \mathbf{x}} \left\langle e^{-ifk_{\parallel} u_{\parallel}} (1 + \delta) \right\rangle + (2\pi)^6 \delta_D(\mathbf{k}) \delta_D(\mathbf{k}').
\end{aligned} \tag{2.47}$$

Equation (2.47) can then be further simplified dealing with the two integrals involving one point correlations, namely the ones of the second and third addenda. It is possible to notice that, for Gaussian fields at least, the velocity and density fields evaluated at the same coordinate are uncorrelated [24], giving

$$\left\langle e^{-ifk'_{\parallel} u'_{\parallel}} \delta' \right\rangle = \left\langle e^{ifk_{\parallel} u_{\parallel}} \delta \right\rangle = 0. \tag{2.48}$$

The two remaining integrals in the second and third addenda of equation (2.47) are thus

$$\begin{aligned}
\int d^3 \mathbf{x}' e^{i\mathbf{k}' \cdot \mathbf{x}'} \left\langle e^{-ifk'_{\parallel} u'_{\parallel}} \right\rangle &= \int d^3 \mathbf{x}' e^{i\mathbf{k}' \cdot \mathbf{x}'} e^{-ifk'_{\parallel} \langle u'_{\parallel} \rangle} = \int d^3 \mathbf{x}' e^{i\mathbf{k}' \cdot \mathbf{x}'} = (2\pi)^3 \delta_D(\mathbf{k}') \\
\int d^3 \mathbf{x} e^{i\mathbf{k} \cdot \mathbf{x}} \left\langle e^{-ifk_{\parallel} u_{\parallel}} \right\rangle &= \int d^3 \mathbf{x} e^{i\mathbf{k} \cdot \mathbf{x}} e^{-ifk_{\parallel} \langle u_{\parallel} \rangle} = \int d^3 \mathbf{x} e^{i\mathbf{k} \cdot \mathbf{x}} = (2\pi)^3 \delta_D(\mathbf{k})
\end{aligned} \tag{2.49}$$

thanks to the isotropy of the velocity field. Hence equation (2.47) becomes

$$\begin{aligned}
(2\pi)^3 \delta_D(\mathbf{k} + \mathbf{k}') P_s(\mathbf{k}, \mathbf{k}') &= \int d^3 \mathbf{x} d^3 \mathbf{x}' e^{i\mathbf{k} \cdot \mathbf{x}} e^{i\mathbf{k}' \cdot \mathbf{x}'} \left\langle e^{-if(k_{\parallel} u_{\parallel} + k'_{\parallel} u'_{\parallel})} (1 + \delta)(1 + \delta') \right\rangle + \\
&\quad - (2\pi)^6 \delta_D(\mathbf{k}) \delta_D(\mathbf{k}') - (2\pi)^6 \delta_D(\mathbf{k}') \delta_D(\mathbf{k}) + (2\pi)^6 \delta_D(\mathbf{k}) \delta_D(\mathbf{k}') \\
&= \int d^3 \mathbf{x} d^3 \mathbf{x}' e^{i\mathbf{k} \cdot \mathbf{x}} e^{i\mathbf{k}' \cdot \mathbf{x}'} \left\langle e^{-if(k_{\parallel} u_{\parallel} + k'_{\parallel} u'_{\parallel})} (1 + \delta)(1 + \delta') \right\rangle + \\
&\quad - (2\pi)^6 \delta_D(\mathbf{k}) \delta_D(\mathbf{k}')
\end{aligned} \tag{2.50}$$

and, recalling the correlation inside (2.50) depends only on the galaxy-galaxy separation \mathbf{r} (thanks to the considerations we made to define the PS in equation (1.66)), we can write

$$\begin{aligned}
(2\pi)^3 \delta_D(\mathbf{k} + \mathbf{k}') P_s(\mathbf{k}, \mathbf{k}') &= (2\pi)^3 \delta_D(\mathbf{k} + \mathbf{k}') \int d^3 \mathbf{r} e^{i\mathbf{k}' \cdot \mathbf{r}} \left\langle e^{-ifk'_{\parallel} \Delta u_{\parallel}} (1 + \delta)(1 + \delta') \right\rangle + \\
&\quad - (2\pi)^6 \delta_D(\mathbf{k}) \delta_D(\mathbf{k}'),
\end{aligned} \tag{2.51}$$

with the velocity difference defined as before $\Delta u_{\parallel}(\mathbf{r}) := u'_{\parallel} - u_{\parallel}$.

The PS of matter, denoted below with a bold character, is then

$$\begin{aligned}
\mathbf{P}_s(\tilde{\mathbf{k}}) &= \int d^3\tilde{\mathbf{s}} e^{i\tilde{\mathbf{k}}\cdot\tilde{\mathbf{s}}} \langle \rho_s(\mathbf{s})\rho_s(\mathbf{s}') \rangle \\
&= \bar{\rho}_s^2 \int d^3\tilde{\mathbf{s}} e^{i\tilde{\mathbf{k}}\cdot\tilde{\mathbf{s}}} \langle (1 + \delta_s(\mathbf{s}))(1 + \delta_s(\mathbf{s}')) \rangle \\
&= \bar{\rho}_s^2 \int d^3\tilde{\mathbf{s}} e^{i\tilde{\mathbf{k}}\cdot\tilde{\mathbf{s}}} [1 + \langle \delta_s(\mathbf{s})\delta_s(\mathbf{s}') \rangle],
\end{aligned} \tag{2.52}$$

where the quantity $\tilde{\mathbf{s}} := \mathbf{s}' - \mathbf{s}$ is the redshift space correspondent of the galaxy-galaxy separation $\mathbf{r} = \mathbf{x}' - \mathbf{x}$ previously defined in real space coordinates. We can rearrange equation (2.52), which follows directly from (1.65), in order to be able to exploit the Fourier space correlation of redshift space contrast fields inside it (through equation (1.66))

$$\begin{aligned}
\mathbf{P}_s(\tilde{\mathbf{k}}) &= \bar{\rho}_s^2 \int d^3\tilde{\mathbf{s}} e^{i\tilde{\mathbf{k}}\cdot\tilde{\mathbf{s}}} \left[1 + \int \frac{d^3\mathbf{k}}{(2\pi)^3} e^{-i\mathbf{k}\cdot\mathbf{s}} \int \frac{d^3\mathbf{k}'}{(2\pi)^3} e^{-i\mathbf{k}'\cdot\mathbf{s}'} \langle \delta_s(\mathbf{k})\delta_s(\mathbf{k}') \rangle \right] \\
&= \bar{\rho}_s^2 \int d^3\tilde{\mathbf{s}} e^{i\tilde{\mathbf{k}}\cdot\tilde{\mathbf{s}}} \left[1 + \int \frac{d^3\mathbf{k}}{(2\pi)^3} e^{-i\mathbf{k}\cdot\mathbf{s}} \int \frac{d^3\mathbf{k}'}{(2\pi)^3} e^{-i\mathbf{k}'\cdot\mathbf{s}'} (2\pi)^3 \delta_D(\mathbf{k} + \mathbf{k}') P_s(\mathbf{k}, \mathbf{k}') \right].
\end{aligned} \tag{2.53}$$

We can now use equation (2.51) to write

$$\begin{aligned}
\mathbf{P}_s(\tilde{\mathbf{k}}) &= \bar{\rho}_s^2 \int d^3\tilde{\mathbf{s}} e^{i\tilde{\mathbf{k}}\cdot\tilde{\mathbf{s}}} \left[1 + \int \frac{d^3\mathbf{k}}{(2\pi)^3} e^{-i\mathbf{k}\cdot\mathbf{s}} \int \frac{d^3\mathbf{k}'}{(2\pi)^3} e^{-i\mathbf{k}'\cdot\mathbf{s}'} (2\pi)^3 \delta_D(\mathbf{k} + \mathbf{k}') P_s(\mathbf{k}, \mathbf{k}') \right] \\
&= \bar{\rho}_s^2 \int d^3\tilde{\mathbf{s}} e^{i\tilde{\mathbf{k}}\cdot\tilde{\mathbf{s}}} \left[1 + \int \frac{d^3\mathbf{k}}{(2\pi)^3} e^{-i\mathbf{k}\cdot\mathbf{s}} \int \frac{d^3\mathbf{k}'}{(2\pi)^3} e^{-i\mathbf{k}'\cdot\mathbf{s}'} (2\pi)^3 \delta_D(\mathbf{k} + \mathbf{k}') \times \right. \\
&\quad \times \int d^3\mathbf{r} e^{i\mathbf{k}'\cdot\mathbf{r}} \langle e^{-ifk_{||}\Delta u_{||}} (1 + \delta)(1 + \delta') \rangle + \\
&\quad \left. - \int \frac{d^3\mathbf{k}}{(2\pi)^3} e^{-i\mathbf{k}\cdot\mathbf{s}} \int \frac{d^3\mathbf{k}'}{(2\pi)^3} e^{-i\mathbf{k}'\cdot\mathbf{s}'} (2\pi)^6 \delta_D(\mathbf{k})\delta_D(\mathbf{k}') \right],
\end{aligned} \tag{2.54}$$

where the inverse Fourier transforms of the two Dirac delta functions give a -1 which simplifies with the one at the beginning. To deal with the only remaining term we can integrate over $d^3\mathbf{k}'$ and obtain

$$\begin{aligned}
\mathbf{P}_s(\tilde{\mathbf{k}}) &= \bar{\rho}_s^2 \int d^3\tilde{\mathbf{s}} e^{i\tilde{\mathbf{k}}\cdot\tilde{\mathbf{s}}} \int \frac{d^3\mathbf{k}}{(2\pi)^3} e^{-i\mathbf{k}\cdot\mathbf{s}} e^{i\mathbf{k}\cdot\mathbf{s}'} \int d^3\mathbf{r} e^{-i\mathbf{k}\cdot\mathbf{r}} \langle e^{ifk_{||}\Delta u_{||}} (1 + \delta)(1 + \delta') \rangle \\
&= \bar{\rho}_s^2 \int d^3\tilde{\mathbf{s}} e^{i\tilde{\mathbf{k}}\cdot\tilde{\mathbf{s}}} \int \frac{d^3\mathbf{k}}{(2\pi)^3} e^{i\mathbf{k}\cdot\tilde{\mathbf{s}}} \int d^3\mathbf{r} e^{-i\mathbf{k}\cdot\mathbf{r}} \langle e^{ifk_{||}\Delta u_{||}} (1 + \delta)(1 + \delta') \rangle \\
&= \bar{\rho}_s^2 \int \frac{d^3\tilde{\mathbf{s}} d^3\mathbf{k}}{(2\pi)^3} e^{i(\tilde{\mathbf{k}}+\mathbf{k})\cdot\tilde{\mathbf{s}}} \int d^3\mathbf{r} e^{-i\mathbf{k}\cdot\mathbf{r}} \langle e^{ifk_{||}\Delta u_{||}} (1 + \delta)(1 + \delta') \rangle \\
&= \bar{\rho}_s^2 \int d^3\mathbf{k} \delta_D(\tilde{\mathbf{k}} + \mathbf{k}) \int d^3\mathbf{r} e^{-i\mathbf{k}\cdot\mathbf{r}} \langle e^{ifk_{||}\Delta u_{||}} (1 + \delta)(1 + \delta') \rangle \\
&= \bar{\rho}_s^2 \int d^3\mathbf{r} e^{i\tilde{\mathbf{k}}\cdot\mathbf{r}} \langle e^{-if\tilde{k}_{||}\Delta u_{||}} (1 + \delta)(1 + \delta') \rangle.
\end{aligned} \tag{2.55}$$

By looking at the construction of the total matter PS, we can see that equation (5) of [58] is valid: the demonstration is straightforward if we go back to equation (2.53) and integrate over $d^3\mathbf{k}'$ before substituting (2.51). By doing so we obtain

$$\begin{aligned} \mathbf{P}_s(\tilde{\mathbf{k}}) &= \bar{\rho}_s^2 \int d^3\tilde{\mathbf{s}} e^{i\tilde{\mathbf{k}}\cdot\tilde{\mathbf{s}}} \left[1 + \int \frac{d^3\mathbf{k}}{(2\pi)^3} e^{-i\mathbf{k}\cdot\mathbf{s}} e^{i\mathbf{k}\cdot\mathbf{s}'} P_s(\mathbf{k}) \right] \\ &= \bar{\rho}_s^2 \int d^3\tilde{\mathbf{s}} e^{i\tilde{\mathbf{k}}\cdot\tilde{\mathbf{s}}} \left[1 + \int \frac{d^3\mathbf{k}}{(2\pi)^3} e^{i\mathbf{k}\cdot\tilde{\mathbf{s}}} P_s(\mathbf{k}) \right], \end{aligned} \quad (2.56)$$

which obeys (2.55) only if

$$(2\pi)^3 \delta_D(\mathbf{k}) + P_s(k) = \int d^3\mathbf{r} e^{i\mathbf{k}\cdot\mathbf{r}} \left\langle e^{-ifk_{\parallel}\Delta u_{\parallel}} (1 + \delta)(1 + \delta') \right\rangle. \quad (2.57)$$

The only difference of (2.57) with respect to its counterpart in [58] is the $(2\pi)^3$ factor before the Dirac delta: it comes from our different normalization convention on the Dirac delta definition itself (1.67) with respect to [58]. The power spectrum presented in equation (2.57) is related to the average of real space quantities in a very complicated way but it turns out to be, qualitatively speaking at least, easy to understand: the two effects in play here are the compression at large scales, the well known Kaiser effect [36], and the FOG. The Kaiser effect comes from the combination of the brackets in the right hand side and the Dirac delta in the left hand one [68] and represents the coherent distortion due to the peculiar velocity along the LOS; in linear theory it is controlled by the growth factor f and hence can give information about the growth of structure as we mentioned in Section 1.5.2. The FOG effect comes from the exponential factor inside the ensemble average of equation (2.57) and it provides a damping of the power spectrum due to the random peculiar velocities. Unfortunately the two effects cannot be treated separately and a mixture of them is expected to be relevant in the trans-linear regime, where the velocity and density fields are still correlated [68].

Now it is possible to describe the redshift space 2PCF by applying an inverse Fourier transform (1.60) to equation (2.57)

$$\int \frac{d^3\mathbf{k}}{(2\pi)^3} e^{-i\mathbf{k}\cdot\mathbf{s}} [(2\pi)^3 \delta_D(\mathbf{k}) + P_s(k)] = 1 + \xi_s(\mathbf{s}) \equiv 1 + \xi_s(s_{\perp}, s_{\parallel}), \quad (2.58)$$

in which the redshift coordinate parallel to the LOS is linked with the real one through equation (2.3), while for the perpendicular one we have $\mathbf{s}_{\perp} = \mathbf{r}_{\perp}$. Thus we can write [58]

$$\begin{aligned} 1 + \xi_s(s_{\perp}, s_{\parallel}) &= \int \frac{d^3\mathbf{k}}{(2\pi)^3} e^{-i\mathbf{k}\cdot\mathbf{s}} \int d^3\mathbf{r} e^{i\mathbf{k}\cdot\mathbf{r}} \left\langle e^{ifk_{\parallel}\Delta u_{\parallel}} (1 + \delta)(1 + \delta') \right\rangle \\ &= \int \frac{d^2\mathbf{k}_{\perp}}{(2\pi)^2} \frac{dk_{\parallel}}{2\pi} e^{-ik_{\perp}s_{\perp}} e^{-ik_{\parallel}s_{\parallel}} \int \frac{d^2\mathbf{r}_{\perp}}{(2\pi)^2} \frac{dr_{\parallel}}{2\pi} e^{ik_{\perp}r_{\perp}} e^{ik_{\parallel}r_{\parallel}} \times \\ &\quad \times \left\langle e^{ifk_{\parallel}\Delta u_{\parallel}} (1 + \delta)(1 + \delta') \right\rangle \\ &= \int \frac{dr_{\parallel} d\gamma}{2\pi} e^{i\gamma(r_{\parallel} - s_{\parallel})} \left\langle e^{\lambda\Delta u_{\parallel}} (1 + \delta)(1 + \delta') \right\rangle, \end{aligned} \quad (2.59)$$

where for the last row we have defined the quantity $\lambda := -ifk_{\parallel}$ in Fourier space, which is equivalent to $\lambda := -if\gamma$ in configuration space [57, 58]. From the redshift space 2PCF expressed as above we

are then able to define the *Pairwise Velocity Generating Function* $\mathcal{M}(\lambda, \mathbf{r})$ as follows

$$\mathcal{M}(\lambda, \mathbf{r}) := \frac{\langle e^{\lambda \Delta u_{\parallel}} [1 + \delta][1 + \delta'] \rangle}{[1 + \xi(r)]}. \quad (2.60)$$

At this point we can write equation (2.59) in a more compact way [58]

$$1 + \xi_s(s_{\perp}, s_{\parallel}) = \int \frac{dr_{\parallel} d\gamma}{2\pi} e^{i\gamma(r_{\parallel} - s_{\parallel})} [1 + \xi(r)] \mathcal{M}(\lambda, \mathbf{r}). \quad (2.61)$$

Before proceeding in our presentation of the streaming model it is useful, in order to avoid carrying around the $1/aH$ factor needed to describe the peculiar velocity of galaxies with units of length, to define a new quantity: the real-to-redshift separation

$$y := s_{\parallel} - r_{\parallel}. \quad (2.62)$$

Then the PDF of the pairwise velocity can be defined as the inverse Fourier transform (1.60) of the pairwise velocity generating function

$$\mathcal{P}(y, \mathbf{r}) := \int \frac{d\gamma}{2\pi} e^{-i\gamma y} \mathcal{M}(\lambda, \mathbf{r}), \quad (2.63)$$

from which we can see it links the radial coordinate in real space r_{\parallel} with the redshift one s_{\parallel} through the relative velocity between the two galaxies $s_{\parallel} - r_{\parallel} = \Delta v_{\parallel}/\mathcal{H} \equiv y$. The common normalization of (2.63) for a scale independent generating function reads

$$\int dy \mathcal{P}(y) = 1. \quad (2.64)$$

Here we highlight the fact that the condition above is no longer valid in the case of a scale dependent generating function, which is the case we expect for a realistic scenario [58]: it is possible to see it by inverting equation (2.63) to retrieve the pairwise velocity generating function

$$\mathcal{M}(\lambda, \mathbf{r}) = \int dy e^{\lambda y(\mathbf{r})/f} \mathcal{P}(y; \mathbf{r}); \quad (2.65)$$

from equation (2.60) we have

$$\mathcal{M}(\lambda, \mathbf{r}) = \frac{\langle e^{\lambda y(\mathbf{r})} [1 + \delta][1 + \delta'] \rangle}{[1 + \xi(r)]}, \quad (2.66)$$

which is not necessarily equal to one if the real-to-redshift velocity field $y(\mathbf{r})$ is scale dependent.

It is now possible now to recast equation (2.59) in its most common formulation [23, 24, 51, 58],

$$1 + \xi_s(s_{\perp}, s_{\parallel}) = \int dy [1 + \xi(r)] \mathcal{P}(y; \mathbf{r}). \quad (2.67)$$

Here it is important to notice that both equation (2.63) and (2.65) determine the scale dependence of the pairwise velocity PDF through the \mathbf{r} dependence of $\mathcal{M}(\lambda, \mathbf{r})$. If the PDF turns out to be scale independent, $\mathcal{P}(v)$, then the formulation of the redshift space correlation given in terms of perturbations alone presented in the previous Sections would be equivalent to the one presented here in terms of $1 + \xi$; if instead the PDF has a scale dependence, the first contribution inside the integral defining $\mathcal{P}(v, \mathbf{r})$ (2.63) would be different from one, making the formulation of (2.67) the correct one [58].

2.5.1 Pairwise Velocity Moments

The utility of the pairwise velocity generating function (2.60) is not limited with the simplification it implies in the description of the correlation (and the spectrum) of matter density, it allows also a useful description of velocity auto and cross correlation functions. To see that, from equation (2.60) it is useful to define the velocity moments as follows⁵

$$\begin{aligned} v_{12}(\mathbf{r}) &:= \left(\frac{\partial \mathcal{M}}{\partial \lambda} \right) \Big|_{\lambda=0} = \frac{\langle \Delta u_{\parallel}(\mathbf{r}) [1 + \delta(\mathbf{x})] [1 + \delta(\mathbf{x}')] \rangle}{[1 + \xi(r)]}, \\ \sigma_{12}^2(\mathbf{r}) &:= \left(\frac{\partial^2 \mathcal{M}}{\partial \lambda^2} \right) \Big|_{\lambda=0} = \frac{\langle \Delta u_{\parallel}^2(\mathbf{r}) [1 + \delta(\mathbf{x})] [1 + \delta(\mathbf{x}')] \rangle}{[1 + \xi(r)]}. \end{aligned} \quad (2.68)$$

The moments thus defined can then be related with the pairwise velocity PDF using equation (2.65)

$$\begin{aligned} \int dv \mathcal{P}(v, \mathbf{r}) v(\mathbf{r}) &= f v_{12}(\mathbf{r}), \\ \int dv \mathcal{P}(v, \mathbf{r}) v^2(\mathbf{r}) &= f^2 \sigma_{12}^2(\mathbf{r}). \end{aligned} \quad (2.69)$$

Below we show as an example the derivation for the first relation of (2.69) using the definition of the pairwise velocity moments (2.68) and equation (2.65)

$$\begin{aligned} v_{12}(\mathbf{r}) &= \left(\frac{\partial \mathcal{M}}{\partial \lambda} \right) \Big|_{\lambda=0} = \int dv \frac{\partial}{\partial \lambda} e^{\lambda v/f} \mathcal{P}(v; \mathbf{r}) \Big|_{\lambda=0} \\ &= \int dv \frac{v(\mathbf{r})}{f} \mathcal{P}(v; \mathbf{r}) \\ \implies f v_{12}(\mathbf{r}) &= \int dv v(\mathbf{r}) \mathcal{P}(v; \mathbf{r}); \end{aligned} \quad (2.70)$$

for the second relation it is sufficient to carry out the same procedure, but applied to the definition of the pairwise velocity dispersion inside (2.68).

The pairwise velocity auto correlation can then be written, using symmetry considerations, in the following form (equation (72.3) of [51])

$$\langle u_i(\mathbf{x}) u_j(\mathbf{x} + \mathbf{r}) \rangle = \psi_{\perp} \delta_{ij} + [\psi_{\parallel} - \psi_{\perp}] \frac{r_i r_j}{r^2} \quad (2.71)$$

where ψ_{\parallel} and ψ_{\perp} are respectively the velocity correlation functions parallel and perpendicular to the LOS. The two correlation functions can be defined starting from the velocity divergence PS and by assuming a potential flow [28], namely $\psi_{\parallel}(r) = d(r\psi_{\perp})/dr$ and $\psi_{\perp}(r) \leq \psi_{\parallel}(r)$, obtaining

$$\begin{aligned} \psi_{\perp} &:= \int \frac{d^3 \mathbf{k}}{(2\pi)^3} \frac{P_{\theta\theta}(k)}{k^2} \frac{j_1(kr)}{kr} \\ \psi_{\parallel} &:= \int \frac{d^3 \mathbf{k}}{(2\pi)^3} \frac{P_{\theta\theta}(k)}{k^2} \left[j_0(kr) - 2 \frac{j_1(kr)}{kr} \right], \end{aligned} \quad (2.72)$$

⁵Also in this case, like we did for the moments of the Vlasov equation in Section 1.3.1, it is possible to keep defining moments of higher order without an upper limit. Like we did with the Vlasov equation however, with this work we stop our description at the second order moment: the velocity dispersion.

with the functions $j_l(x)$ being spherical Bessel functions. The difference between the two potentials can then be written as [58]

$$\Delta\psi := \psi_{\perp}(r) - \psi_{\parallel}(r) = \int \frac{d^3\mathbf{k}}{(2\pi)^3} \frac{P_{\theta\theta}(k)}{k^2} j_2(kr), \quad (2.73)$$

which coupled with the one dimensional velocity dispersion given by linear dynamics [58]

$$\sigma_v^2 := \frac{1}{3} \int \frac{d^3\mathbf{k}}{(2\pi)^3} \frac{P_{\theta\theta}(k)}{k^2} \quad (2.74)$$

allows us to describe the variance of the velocity field as

$$\begin{aligned} \langle \Delta u_{\parallel}^2 \rangle &= \langle (u_{\parallel})^2 \rangle + \langle (u'_{\parallel})^2 \rangle - 2 \langle u_{\parallel} u'_{\parallel} \rangle \\ &= \langle (u_{\parallel})^2 \rangle + \langle (u'_{\parallel})^2 \rangle + 2 \left(-\psi_{\perp}(r) - [\psi_{\parallel}(r) - \psi_{\perp}(r)] \frac{r_{\parallel}^2}{r^2} \right) \\ &= 2 \left(\sigma_v^2 - \psi_{\perp}(r) + \frac{r_{\parallel}^2}{r^2} \Delta\psi(r) \right). \end{aligned} \quad (2.75)$$

It is important to note that when $r \rightarrow 0$ we have $\psi_{\perp}(r) = \psi_{\parallel}(r) = \sigma_v^2$ and therefore $\langle \Delta u_{\parallel}^2 \rangle \rightarrow 0$; in the opposite regime, when $r \rightarrow +\infty$, we have $\psi_{\perp}(r), \psi_{\parallel}(r) \rightarrow 0$, making $\langle \Delta u_{\parallel}^2 \rangle \rightarrow \sigma_v^2$. An other important thing to notice is that, differently from what was done for the phenomenological description in Section 2.4, here the one dimensional velocity dispersion is not a free parameter but rather it is dependent on the velocity auto PS.

To describe the density-velocity correlation function it is possible to use the definition of the pairwise velocity moments of equation (2.68)

$$\langle \Delta u_{\parallel} [1 + \delta] [1 + \delta'] \rangle = v_{12}(\mathbf{r})(1 + \xi), \quad (2.76)$$

which once expanded gives

$$\langle \Delta u_{\parallel} [1 + \delta + \delta' + \delta\delta'] \rangle = v_{12}(\mathbf{r})(1 + \xi). \quad (2.77)$$

The first term, $\langle \Delta u_{\parallel} \rangle$, is equal to zero for symmetry reasons [24, 57, 58], therefore we have to deal with just the terms where the velocity field is coupled with the density one

$$\langle \Delta u_{\parallel} [\delta + \delta'] \rangle + \langle \Delta u_{\parallel} \delta\delta' \rangle = v_{12}(\mathbf{r})(1 + \xi). \quad (2.78)$$

At linear order, the $\langle \Delta u_{\parallel} \delta\delta' \rangle$ term can be dropped [24], hence the only remaining quantities to evaluate are $\langle \Delta u_{\parallel} \delta \rangle$ and $\langle \Delta u_{\parallel} \delta' \rangle$. We know that Gaussian fields have the property that the density and velocity, evaluated at the same coordinate, are not correlated [24], namely $\langle u_{\parallel} \delta \rangle = \langle u'_{\parallel} \delta' \rangle = 0$; this implies that $\langle \Delta u_{\parallel} \delta \rangle = \langle u'_{\parallel} \delta \rangle$ and $\langle \Delta u_{\parallel} \delta' \rangle = -\langle u_{\parallel} \delta' \rangle$. Furthermore, for symmetry reasons the two contributions should be the same. Consequently the correlations above read

$$\langle u_{\parallel} \delta' \rangle = \int \frac{d^3\mathbf{k}}{(2\pi)^3} e^{-i\mathbf{k}\cdot\mathbf{x}'} \langle u_{\parallel} \delta(\mathbf{k}) \rangle = \int \frac{d^3\mathbf{k}}{(2\pi)^3} e^{-i\mathbf{k}\cdot\mathbf{x}'} \int \frac{d^3\mathbf{p}}{(2\pi)^3} e^{-i\mathbf{p}\cdot\mathbf{x}} \langle u_{\parallel}(\mathbf{p}) \delta(\mathbf{k}) \rangle, \quad (2.79)$$

which can be simplified if we transform the galaxy separation in distance units u_{\parallel} back into the separation in velocity units v_{\parallel} using equation (2.24) and exploiting the definition of the density/velocity cross-PS (2.41). Implementing all of that we get

$$\begin{aligned}
\langle v_{\parallel} \delta' \rangle &= \int \frac{d^3 \mathbf{k}}{(2\pi)^3} e^{-i\mathbf{k} \cdot \mathbf{x}'} \int \frac{d^3 \mathbf{p}}{(2\pi)^3} e^{-i\mathbf{p} \cdot \mathbf{x}} \left[-iaHf \frac{\mathbf{p}}{p^2} \langle \theta(\mathbf{p}) \delta(\mathbf{k}) \rangle \right] \\
&= \int \frac{d^3 \mathbf{k}}{(2\pi)^3} e^{-i\mathbf{k} \cdot \mathbf{x}'} \int \frac{d^3 \mathbf{p}}{(2\pi)^3} e^{-i\mathbf{p} \cdot \mathbf{x}} \left[-iaHf \frac{\mathbf{p}}{p^2} (2\pi)^3 \delta_D(\mathbf{k} + \mathbf{p}) P_{\delta\theta}(k) \right] \\
&= - \int \frac{d^3 \mathbf{k}}{(2\pi)^3} e^{-i\mathbf{k} \cdot (\mathbf{x}' - \mathbf{x})} \left[iaHf \frac{\mathbf{k}}{k^2} P_{\delta\theta}(k) \right] \\
&= - \int \frac{dk d\Omega_{\mathbf{k}}}{(2\pi)^3} k^2 e^{-i\mathbf{k} \cdot (\mathbf{x}' - \mathbf{x})} iaHf \frac{\hat{\mathbf{k}}}{k} P_{\delta\theta}(k) \\
&= - \hat{\mathbf{r}} aHf \int_0^{\infty} \frac{dk}{2\pi^2} k P_{\delta\theta}(k) j_1(kr),
\end{aligned} \tag{2.80}$$

where we have used the relation

$$\int \frac{d\Omega_{\mathbf{k}}}{4\pi} e^{-i\mathbf{k} \cdot \mathbf{r}} \hat{\mathbf{k}} = i\hat{\mathbf{r}} j_1(kr). \tag{2.81}$$

From equation (2.80) is immediate to retrieve the linear relation, where $P_{\delta\theta}(k) = P(k)$, given in equation (10) of the paper by Fisher [24]

$$\langle v \delta' \rangle = -\hat{\mathbf{r}} aH\beta \int_0^{\infty} \frac{dk}{2\pi^2} k P_g(k) j_1(kr). \tag{2.82}$$

Applying all these considerations on equation (2.76) gets us

$$\begin{aligned}
\langle \Delta u_{\parallel} [\delta + \delta'] \rangle &= v_{12}(\mathbf{r})(1 + \xi) = 2 \frac{r_{\parallel}}{r} \int \frac{d^3 \mathbf{k}}{(2\pi)^3} \frac{P_{\delta\theta}(k)}{k} j_1(kr) \\
\implies \langle \Delta u_{\parallel} \delta \rangle &= \langle \Delta u_{\parallel} \delta' \rangle = \frac{1}{2} v_{12}(1 + \xi).
\end{aligned} \tag{2.83}$$

For the second order term we have

$$\begin{aligned}
\sigma_{12}^2(\mathbf{r})(1 + \xi) &= \langle \Delta u_{\parallel}^2 [1 + \delta][1 + \delta'] \rangle \\
&= \langle \Delta u_{\parallel}^2 \rangle + \langle \Delta u_{\parallel}^2 (\delta + \delta') \rangle + \langle \Delta u_{\parallel}^2 \delta \delta' \rangle \\
&= \langle \Delta u_{\parallel}^2 \rangle + \langle \Delta u_{\parallel}^2 (\delta + \delta') \rangle + \langle \Delta u_{\parallel}^2 \delta \delta' \rangle_c - 2 \langle \Delta u_{\parallel}^2 \rangle \langle \delta \rangle \langle \delta' \rangle + \\
&\quad + \{ \langle \Delta u_{\parallel}^2 \rangle \langle \delta \delta' \rangle + \langle \delta \rangle \langle \Delta u_{\parallel}^2 \delta' \rangle + \langle \delta' \rangle \langle \Delta u_{\parallel}^2 \delta \rangle \}.
\end{aligned} \tag{2.84}$$

The equation above can then be simplified further once we get rid of the terms which involve $\langle \delta \rangle$ or $\langle \delta' \rangle$, if we do so we obtain the form shown in [58]

$$\begin{aligned}
\sigma_{12}^2(\mathbf{r})(1 + \xi) &= \langle \Delta u_{\parallel}^2 \rangle (1 + \xi) + \langle \Delta u_{\parallel}^2 (\delta + \delta') \rangle + \langle \Delta u_{\parallel}^2 \delta \delta' \rangle_c \\
&= \langle \Delta u_{\parallel}^2 \rangle (1 + \xi) + \sigma_{12}^{2,c}.
\end{aligned} \tag{2.85}$$

If we were interested in linear dynamics only, the Gaussianity condition would make the last two terms of equation (2.85) vanish. In a more realistic scenario however, non-Gaussian corrections remains in

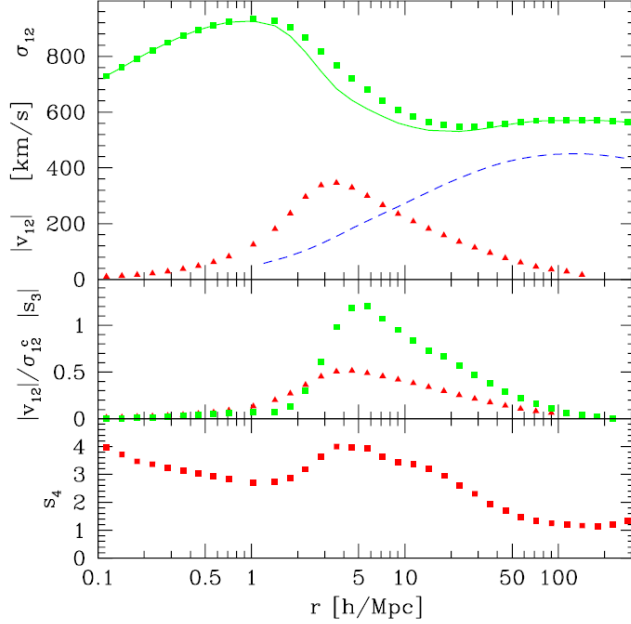


Figure 2.4: Moments of pairwise velocity parallel to the LOS as function of scale. *Top:* σ_{12}^2 as function of scale (green squares) from N-body simulations, its connected part (green solid line) and the linear dynamic prediction (blue dashed line). The mean velocity v_{12} from N-body simulations is reported with red triangles. *Middle:* computation of the dimensionless measure of the infall $|v_{12}|/\sigma_{12}^{2,c}$ (red triangles) and the skewness of the PDF (green squares). *Bottom:* kurtosis of the PDF.

the σ_{12}^2 description up to fourth moment, giving a constant contribution even at large scales. The complete behaviour of the velocity dispersion is depicted in Figure 2.4 as a function of scale: the top panel shows $\sigma_{12}^2(\mathbf{r})$ as computed with different methods, while the middle and the bottom panels show respectively the skewness and kurtosis of the pairwise velocity PDF. From Figure 2.4 it is possible to notice that, at least in the linear case, the velocity dispersion has an opposite behaviour with respect to the mean, with $\sigma_{12}^2(\mathbf{r})$ becoming close to zero at small scales while approaching a finite, non-zero value when $r \rightarrow \infty$. The linear order inversion is due to the higher correlation of the velocity field which makes $\langle \Delta u_i^2 \rangle$ smaller and, furthermore, no correlation between density and velocity is accounted for the linear theory computation. On the other hand, the constant value of the velocity dispersion at large scales is present for both linear and nonlinear treatment: this comes from the fact that we are dealing with velocity differences and thus, at large separations, the individual velocities of galaxies are uncorrelated; this then reflects into the pairwise velocity generating function, which factorizes into a product of individual particles ones. These single particle generating functions are susceptible to nonlinearities because we are in a situation in which we basically cannot define the "large scale limit" of the problem [58]. By looking at the middle and bottom panel one can easily understand why a Gaussian approximation of the velocity dispersion is never a good one: for reference, a Gaussian distribution has zero skewness and kurtosis $s_4 = 3$.

For our purposes, however, we can identify the second pairwise velocity moment with simply $\langle \Delta u_{\parallel}^2 \rangle$, as proposed by [55], which thanks to equation (2.75) reads

$$\sigma_{12}^2(\mathbf{r})(1 + \xi) \simeq \langle \Delta u_{\parallel}^2 \rangle = 2 (\sigma_v^2 - \Psi_{\perp}(r)(1 - \mu^2) - \Psi_{\parallel}(r)\mu^2), \quad (2.86)$$

where, differently from equation (2.75), we have utilized the relation $r_{\parallel}/r = \mu$ and decomposed $\Delta\Psi$ in terms of the difference between $\Psi_{\perp}(r)$ and $\Psi_{\parallel}(r)$. This description of the pairwise velocity moments in terms of integrals of the PS will be very useful later on, during Chapter 3, to describe the redshift space 2PCF as a function of its real space radial multipoles, defined in equation (2.106).

2.5.2 The Large Scale Limit

Recovering the Kaiser formula from the streaming model formulation, equation (2.67), turns out to be very complicated due to the fact one has to perform two integrations: one along the LOS and the other over different PDFs, due to their anisotropy and scale dependence. However, at large scales, one can recover equation (2.32) by expressing the redshift 2PCF in terms of velocity moments [58].

First of all we have to define a little bit more rigorously the "large scales" condition cited above because, even if ξ and v_{12} vanish in the large scale limit, the same is not for σ_{12}^2 and therefore, in full generality, we are not allowed to perform a small amplitude expansion. At the same time, if we are dealing with galaxies having high redshift coordinate separations, it is possible to meet the condition $s_{\parallel}^2 \gg f^2\sigma_{12}^2$, which makes the integration over r_{\parallel} to be sharply peaked around $s_{\parallel} = r_{\parallel}$. This sharp peak is due to the fact that, at such high redshift separations, the shape of the PDF forces s_{\parallel} (which is linked to the real space coordinate through (2.5)) to be described with much higher probability by a large value of r_{\parallel} rather than an high pairwise velocity v_{\parallel} ; this is equivalent to set $y = 0$, making us able to expand real space about redshift space as follows [58]

$$\mathcal{P}(y; r_{\parallel}) \simeq \mathcal{P}(y; s_{\parallel}) + y \frac{d\mathcal{P}(y; s_{\parallel})}{ds_{\parallel}} + \frac{1}{2}y^2 \frac{d^2\mathcal{P}(y; s_{\parallel})}{ds_{\parallel}^2} + \mathcal{O}(y^2). \quad (2.87)$$

Equation (2.87) is then able to convert the integration over an infinite number of PDFs we have in the streaming model (2.67) into a single one and its derivatives. It is important to highlight the fact that the expansion presented here can be done for any PDF, not only for the one determined by linear dynamics, making results retrieved from (2.87) completely general and hence they can be applied also in the fully nonlinear case [58]. The same expansion can be implemented for the real space 2PCF inside (2.67)

$$1 + \xi(r) \simeq 1 + \xi(s_{\parallel}) + y \frac{d\xi(s_{\parallel})}{ds_{\parallel}} + \frac{1}{2}y^2 \frac{d^2\xi(s_{\parallel})}{ds_{\parallel}^2} + \mathcal{O}(y^2). \quad (2.88)$$

Thus the product of the two expanded quantities reads

$$\begin{aligned} (1 + \xi)\mathcal{P}(y, \mathbf{r}) \simeq & [1 + \xi(s_{\parallel})] \left(\mathcal{P}(y; s_{\perp}, s_{\parallel}) + y\mathcal{P}'(y; s_{\perp}, s_{\parallel}) + \frac{1}{2}y^2\mathcal{P}''(y; s_{\perp}, s_{\parallel}) \right) + \\ & + y\xi'(s_{\parallel})\mathcal{P}(y, s_{\perp}, s_{\parallel}) + y^2\xi'(s_{\parallel})\mathcal{P}'(y, s_{\perp}, s_{\parallel}) + \frac{1}{2}y^2\xi''(s_{\parallel})\mathcal{P}(y, s_{\perp}, s_{\parallel}) + \mathcal{O}(y^2), \end{aligned} \quad (2.89)$$

where for clarity we wrote derivatives with respect to y (which are equal to the one with respect to s_{\parallel} thanks to the chain rule of derivatives) using prime signs and omitted the r dependence of the real

space 2PCF. The integration of (2.67) can then be performed by exchanging the order of integrals and derivatives over the PDF⁶, after which it is possible to integrate term by term exploiting the fact that $r_{\parallel} = s_{\parallel}$ alongside the properties of the PDF given in equation (2.69) [58]

$$\begin{aligned}
1 + \xi_s(s_{\perp}, s_{\parallel}) &= \int dy (1 + \xi) \mathcal{P}(y; \mathbf{r}) \\
&\simeq (1 + \xi) \int dy \left(\mathcal{P}(y; s_{\perp}, s_{\parallel}) + y \mathcal{P}'(y; s_{\perp}, s_{\parallel}) + \frac{1}{2} y^2 \mathcal{P}''(y; s_{\perp}, s_{\parallel}) + \mathcal{O}(y^2) \right) + \\
&+ \xi' \int dy (y \mathcal{P}(y; s_{\perp}, s_{\parallel}) + y^2 \mathcal{P}'(y; s_{\perp}, s_{\parallel})) + \xi'' \int dy y^2 \mathcal{P}(y; s_{\perp}, s_{\parallel}) + \mathcal{O}(y^2) \quad (2.90) \\
&= (1 + \xi) \left(1 + f v'_{12} + \frac{1}{2} f^2 \sigma_{12}^2{}'' + \mathcal{O}(y^2) \right) + \\
&+ \xi' \left(f v_{12} + f^2 \sigma_{12}^2{}' \right) + \xi'' f^2 \sigma_{12}^2 + \mathcal{O}(y^2),
\end{aligned}$$

where we called s_{\perp} and s_{\parallel} the redshift components of the separation between the two galaxies, respectively perpendicular and parallel to the LOS. Note that the scale dependence of the pairwise velocity moments have been dropped when they are evaluated in real space. Recall that from equation (2.5) we have $s_{\perp} = r_{\perp}$. Moreover all the quantities in the right hand side, with the exception of the linear growth factor f , are functions of $\mathbf{s} = \{s_{\perp}, s_{\parallel}\}$ and are evaluated at large scales $y = r_{\parallel} - s_{\parallel} = 0$ due to the Taylor expansion procedure.

Keeping only terms linear in quantities that vanish in the large scale limit, namely ξ , ξ' , ξ'' , v_{12} and v'_{12} , we have [58]

$$\xi_s(s_{\perp}, s_{\parallel}) \sim \xi + f v'_{12} + \frac{1}{2} (1 + \xi) f^2 \sigma_{12}^2{}'' + \xi' f^2 \sigma_{12}^2{}' + \xi'' f^2 \sigma_{12}^2. \quad (2.91)$$

As mentioned in Section 2.5.1, the velocity dispersion is non vanishing at large scales and hence still remains in the description of the redshift space 2PCF. However, from Figure 2.4, R. Scoccimarro claimed in [58] it tends to a constant value when $r \rightarrow \infty$; we can call that limit, which is composed by the sum of the linear velocity dispersion with the connected contributions, $\sigma_{12}^2|_{\infty}$. These considerations imply also that the derivatives of σ_{12}^2 , once computed in the large scale limit, tend to zero simplifying the equation above as follows [58]

$$\xi_s(s_{\perp}, s_{\parallel}) \sim \xi + f v'_{12} + \frac{1}{2} f^2 \sigma_{12}^2{}'' + \xi'' \sigma_{12}^2|_{\infty}. \quad (2.92)$$

In Fourier space equation (2.92) reads

$$P_s(\mathbf{k}) \sim P_{\delta\delta}(k) \left(1 - \frac{1}{2} f^2 k_{\parallel}^2 \sigma_{12}^2|_{\infty} \right) + i f k_{\parallel} v_{12}(\mathbf{k}) - \frac{1}{2} f^2 k_{\parallel}^2 \sigma_{12}^2(\mathbf{k}). \quad (2.93)$$

Expanding real space about redshift space should work well when the derivatives in equation (2.92) are small, namely when we are considering waves with \mathbf{k} that has a small component with respect to

⁶Note that such a procedure it is not strictly valid on a mathematical level since equation (2.87) does not converge uniformly [58].

the LOS. We have the large scale limit of v_{12} is given by linear theory, $v_{12}(\mathbf{k}) = -2ik_{\parallel}P_{\delta\theta}(k)/k^2$, while for $\sigma_{12}^2|_{\infty}$ and $\sigma_{12}^2(\mathbf{k})$ both Gaussian and non-Gaussian terms contribute. Referring again to Section 2.5.1, in the computation of the large scale limit $\sigma_{12}^2|_{\infty}$ the difference of pairwise velocities decouple into a sum of one-point ones. Thus the gap between the linear estimation and the nonlinear one in Figure 2.4 comes from $A_{\sigma} := \langle (u_{\parallel})^2 \delta \rangle$ contribution, making us able to write [58]

$$\sigma_{12}^2|_{\infty} = 2(\sigma_v^2 + A_{\sigma}), \quad (2.94)$$

where the 2 factor of the nonlinear contribution comes from the usual symmetry consideration for the velocity field $\langle (u_{\parallel})^2 \delta \rangle = \langle (u'_{\parallel})^2 \delta' \rangle$. For the computation of the Fourier space of velocity dispersion, all the non Gaussian terms of equation (2.85) are involved, nonetheless we can collect the whole nonlinear contribution by defining [58]

$$B_{\sigma}(\mathbf{k}) = \int d^3\mathbf{s} e^{i\mathbf{k}\cdot\mathbf{s}} \langle \Delta u_{\parallel}^2 [\delta + \delta' + \delta\delta'] \rangle. \quad (2.95)$$

Now, equation (2.93) can be rewritten incorporating (2.94) and (2.95)

$$P_s(\mathbf{k}) \sim P_{\delta\delta}(k) \left(1 - \frac{1}{2} f^2 k_{\parallel}^2 (\sigma_v^2 - A_{\sigma}) \right) + 2f \frac{k_{\parallel}^2}{k^2} P_{\delta\theta}(k) + f^2 \frac{k_{\parallel}^4}{k^4} P_{\theta\theta}(k) - \frac{1}{2} f^2 k_{\parallel}^2 B_{\sigma}(\mathbf{k}). \quad (2.96)$$

The Kaiser result, equation (2.31), can then be recovered from equation (2.96) by investigating its $k_{\parallel}^2 f^2 \sigma_v^2 \ll 1$ limit. Moreover, in [58] R. Scoccimarro assumes a Λ CDM model with $\sigma_v^2 \sim 40 h^{-2} \text{Mpc}^2$ and $f(z=0) \sim 0.5$, making the large scale condition above equal to $k_{\parallel} \equiv k\mu \ll 0.2 h \text{Mpc}^{-1}$ and finding

$$P_s(\mathbf{k}) = P_{\delta\delta}(k) + 2f\mu^2 P_{\delta\theta}(k) + f^2\mu^4 P_{\theta\theta}(k). \quad (2.97)$$

The equation above tells us that the nonlinear effects of velocity dispersion A_{σ} and B_{σ} can be neglected only if one considers modes nearly perpendicular to the LOS ($\mu \sim 0$), otherwise they should be considered also for smaller scales [58].

The expansion in equation (2.87) works at its best when the scale dependence of the PDF is small. Therefore this approach is going to be less safer as s_{\perp} becomes smaller due to the fact that, at large s_{\perp} , variations in r_{\parallel} enter only in quadrature ($s^2 = r_{\parallel}^2 + s_{\perp}^2$) as one integrates, while at small s_{\perp} they enter linearly into s (which is the analogous situation of having k_{\parallel} not small in Fourier space) determining the large deviations from the exact Gaussian result depicted in Figure 2.5; those $\mu \sim 1$ deviations are due exactly to the effect of A_{σ} and B_{σ} terms that have been ignored in the $k_{\parallel} \ll 0.2$ limit to retrieve equation (2.97) [58].

2.5.3 The Power Spectrum in the Streaming Model

Equation (2.97) reproduces correctly the Kaiser effect of the PS in the large scale limit; as it was mentioned already in [58], however, it fails to reproduce nonlinearities of the velocity dispersion for separations oriented closely to the parallel direction. To improve the model it has been proposed, following the approach of the phenomenological model of Section 2.4, to insert a suppression factor which is a function of the Gaussian velocity dispersion σ_v

$$P_s(\mathbf{k}) = \exp \{ -f^2 k_{\parallel}^2 \sigma_v^2 \} (P_{\delta\delta}(k) + 2f\mu^2 P_{\delta\theta}(k) + f^2\mu^4 P_{\theta\theta}(k)). \quad (2.98)$$

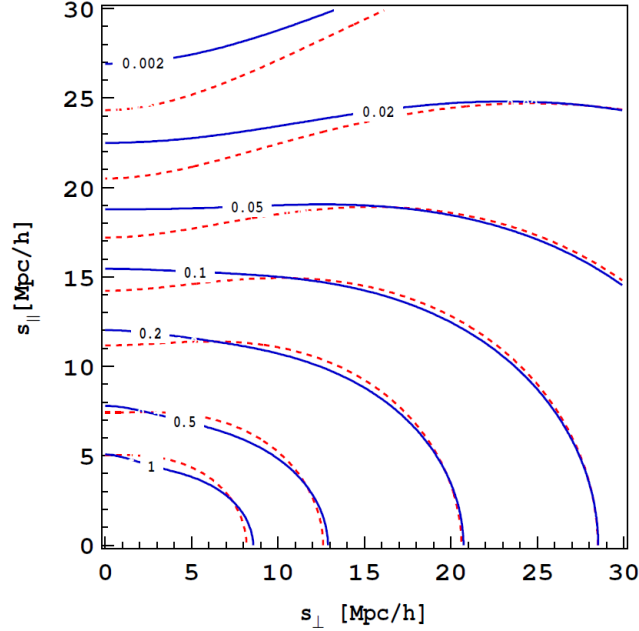


Figure 2.5: Comparison between contours of the redshift space 2PCF $\xi_s(s_\perp, s_\parallel)$ in the Gaussian limit (solid blue line) and in the Kaiser limit (dashed red lines) for a flat Λ CDM cosmological model with $\Omega_m = 0.26$, $\sigma_8 = 0.9$, $\Omega_b = 0.04$, $h = 0.7$ and linear bias $b = 1$. Figure taken from [58].

In this way the streaming model is able to mimic the effect of non the Gaussian terms A_σ and B_σ , but it has been pointed out by R. Scoccimarro himself in [58] that this is an oversimplification. Even if equation (2.98) seems very similar to the phenomenological model description coming from the combination of a Gaussian description of the suppression factor, equation (2.40), and a nonlinear treatment for the PS, equation (2.43), it turns out to be quite different: here we don't fit for a velocity dispersion factor $\sigma_{v,\text{eff}}^2$, but rather σ_v^2 is predicted by linear dynamics according to equation (2.74). In Figure 2.6 it is presented a comparison of equation (2.98) (blue dashed line) against numerical simulations (red solid) and the Kaiser formulation we derived in Section 2.3 (green dashed): it is clear that the equation predicted by the streaming model is able to better mimic numerical results but, even if the improvement it brings is good for the extrema of the direction cosine, it fails to reproduce them in at intermediate angles due to the approximated treatment of (2.96).

2.6 Multipole Expansion of the Redshift Power Spectrum

The Kaiser formula presented in equation (2.31), as well as the ones coming from the phenomenological approach (2.37) and the streaming model (2.98), once the bias factors are accounted makes us able to relate the PS of matter in real space with its redshift counterpart. We can do so by introducing a correction dependent on the bias we assume galaxies have as tracers of matter and the directional cosine with respect to the LOS. To understand how important this correction could be, we can expand

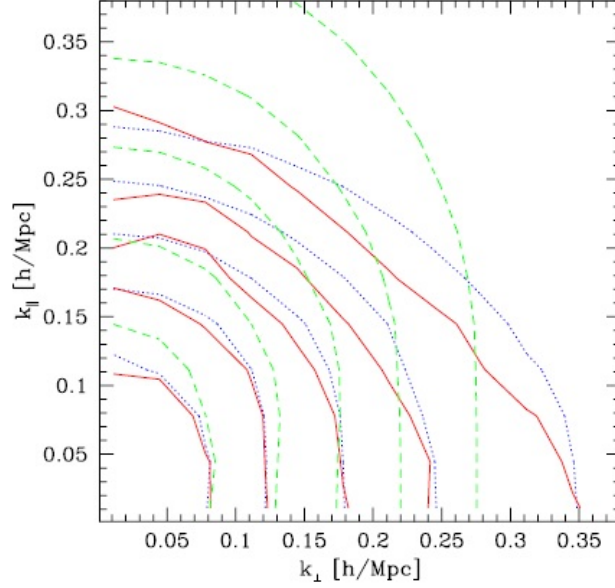


Figure 2.6: Representation of the redshift power spectrum at $z = 0$. The solid red lines correspond to results of numerical simulations, the dashed green lines show the expected shape according to the Kaiser formula (equation (2.31)) and dotted blue lines represent the expected results according to the large scales expansion of the streaming model (equation (2.98)). Figure taken from [58].

the redshift space PS using Legendre polynomials $\mathcal{L}_i(\mu)$

$$\begin{aligned}
 P_s(k, \mu) &= \sum_l P_{s,l}(k) \mathcal{L}_l(\mu), \\
 &= P_{s,0}(k) + P_{s,1}(k)\mu + P_{s,2}(k) \frac{1}{2}(3\mu^2 - 1) + \\
 &\quad + P_{s,3}(k) \frac{1}{2}(5\mu^3 - 3\mu) + P_{s,4}(k) \frac{1}{8}(35\mu^4 - 30\mu^2 + 3) + \mathcal{O}(l \geq 5),
 \end{aligned} \tag{2.99}$$

where the four polynomials reported above are $\mathcal{L}_0(\mu) = 1$, $\mathcal{L}_2(\mu) = (3\mu^2 - 1)/2$, $\mathcal{L}_3(\mu) = (5\mu^3 - 3\mu)/2$ and $\mathcal{L}_4(\mu) = (35\mu^4 - 30\mu^2 + 3)/8$. If we now impose the expansion above to be equal to the Kaiser formula of (2.32), (2.43) and/or (2.98), knowing that at the end we should have only terms dependent on even powers of μ , we can immediately exclude $l = 1$, $l = 3$, $l = 5$ and $l \geq 5$ contributions. Hence we are left with the monopole ($l = 0$), quadrupole ($l = 2$) and hexadecapole ($l = 4$) parts of the PS, which we can write explicitly using the inverse relation [10, 24, 30, 57]

$$P_{s,l}(k) = \frac{2l+1}{2} \int_{-1}^1 d\mu P_s(k, \mu) \mathcal{L}_l(\mu). \tag{2.100}$$

Separating the contributions of the three different multipoles for an easier understanding we obtain the following

$$\begin{aligned}
P_{s,l=0}(k, \mu) &= P(k)b^2 \left(1 + \frac{2}{3}\beta + \frac{1}{5}\beta^2 \right), \\
P_{s,l=2}(k, \mu) &= P(k)b^2 \left(\frac{4}{3}\beta + \frac{4}{7}\beta^2 \right), \\
P_{s,l=4}(k, \mu) &= P(k)b^2 \left(\frac{8}{35}\beta^2 \right).
\end{aligned} \tag{2.101}$$

Below we present the explicit derivation for the monopole contribution (where $\mathcal{L}_{l=0} = 1$) starting from the Kaiser formula (2.32)

$$\begin{aligned}
P_{s,l=0}(k) &= \frac{1}{2} \int_{-1}^1 d\mu P_s(k, \mu) \\
&= \frac{1}{2} b^2 P(k) \int_{-1}^1 d\mu (1 + 2\beta\mu^2 + \beta^2\mu^4) \\
&= \frac{1}{2} b^2 P(k) \left[\mu + \frac{2}{3}\beta\mu^3 + \frac{1}{5}\beta^2\mu^5 \right] \Big|_{\mu=-1}^{\mu=1} \\
&= b^2 P(k) \left[1 + \frac{2}{3}\beta + \frac{1}{5}\beta^2 \right].
\end{aligned} \tag{2.102}$$

For the other moments it is sufficient to change the numerical factor accordingly and accounting for more complex forms of the Legendre polynomials of higher order.

Obviously we can apply the same concepts for the redshift space 2PCF, which also can be expanded using Legendre polynomials

$$\begin{aligned}
\xi_g(s, \mu) &= \sum_{l \text{ even}} \xi_{gl}(s) \mathcal{L}_l(\mu) \\
&= \xi_{g0}(s) \mathcal{L}_0(\mu) + \xi_{g2}(s) \mathcal{L}_2(\mu) + \xi_{g4}(s) \mathcal{L}_4(\mu) + \mathcal{O}(l \geq 5),
\end{aligned} \tag{2.103}$$

where the odd harmonics vanish due to exchange symmetry. Again we stop at $l = 4$ because at linear order we want to agree with the Kaiser formula (2.32). The link between the 2PCF and the PS, and consequently the agreement with (2.32), (2.43) and/or (2.98), is given by [30]

$$\xi_{gl}(s) = i^{-l} 4\pi \int_0^\infty \frac{dk k^2}{(2\pi)^3} P_{s,l}(k, \mu) j_l(kr). \tag{2.104}$$

Hence, exploiting (2.101), we are able to find out the explicit contribution of the 2PCF multipoles. Once again we give an explicit derivation for the monopole only

$$\begin{aligned}
\xi_{g0}(s) &= \int_0^\infty \frac{dk k^2}{2\pi^2} P(k) b^2 \left(1 + \frac{2}{3}\beta + \frac{1}{5}\beta^2 \right) j_0(kr) \\
&= b^2 \left(1 + \frac{2}{3}\beta + \frac{1}{5}\beta^2 \right) \int_0^\infty \frac{dk k^2}{2\pi^2} P(k) j_0(kr),
\end{aligned} \tag{2.105}$$

where the only radial dependence is inside the integral of the spherical-Bessel-weighted PS, which is equivalent to the more general expression [34]

$$\xi_n^m(r) = \int_0^\infty \frac{dk k^2}{2\pi^2} P(k) \frac{j_n(kr)}{(kr)^m} \quad (2.106)$$

when we have $m = 0$. The value of m can be set to zero without losing generality thanks to the general property of spherical Bessel functions (the explicit calculation will be carried in Appendices A and B)

$$j_{l+1} + j_{l-1} = \frac{2l+1}{x} j_l(x). \quad (2.107)$$

Thus equation (2.103) can be written as

$$\begin{aligned} \xi_g(s, \mu) = & \left(1 + \frac{2}{3}\beta + \frac{1}{5}\beta^2\right) \xi_{g0}^0(r) \mathcal{L}_0(\mu) - \left(\frac{4}{3}\beta + \frac{4}{7}\beta^2\right) \xi_{g2}^0(r) \mathcal{L}_2(\mu) + \\ & + \frac{8}{35}\beta^2 \xi_{g4}^0(r) \mathcal{L}_4(\mu), \end{aligned} \quad (2.108)$$

where we highlight the minus sign in the quadrupole component is due to the i^l factor in equation (2.104): it implies that the large scale squashing of the 2PCF corresponds to a stretching of the redshift PS along the line of sight [30].

2.7 The TNS Model

One improvement of the streaming model of Section 2.5 was proposed by Taruya, Nishimichi and Saito (TNS) in 2010 [68], which was then implemented further by Zheng and Song in 2016 [77]. Its construction starts following the first works on the subject [10, 30, 36] and tries to improve it by incorporating the additional considerations done by R. Scoccimarro [58] we have reported in Section 2.5. To see that we start once more from the redshift space description of the density contrast field (2.18) and apply to that a Fourier transform

$$\begin{aligned} \delta_s(\mathbf{k}) &= \int d^3\mathbf{s} e^{i\mathbf{k}\cdot\mathbf{s}} \delta_s(\mathbf{s}) \\ &= \int d^3\mathbf{s}(\mathbf{x}) J(\mathbf{x}) e^{i\mathbf{k}\cdot[\mathbf{x}-f u_{||}(\mathbf{x})\hat{\mathbf{z}}]} \left[\frac{1 + \delta(\mathbf{x}) - J(\mathbf{x})}{J(\mathbf{x})} \right] \\ &= \int d^3\mathbf{x} e^{i\mathbf{k}\cdot\mathbf{x}} e^{-ifk_{||}u_{||}(\mathbf{x})} [1 + \delta(\mathbf{x}) - J(\mathbf{x})]. \end{aligned} \quad (2.109)$$

Here it is important to highlight a crucial difference between the streaming model of Section 2.5 and the one coming from the TNS approach: in the latter we are isolating the redshift space density contrast field, rather than applying number conservation through a direct application of equation (2.12). By doing so, equation (2.109) has now a dependence on the Jacobian of the transformation (2.14), which is the generic one, and therefore its regime of validity is smaller compared with the more general model of Section 2.5. In this approach we still make use of the plane-parallel/distant observe approximation: as we have shown before we make use of it in the exponential coming from

the Fourier transform; at the same time it is useful to retrieve an expression involving the Jacobian of the transformation in its most general form and hence, we will insert the plane-parallel approximation for it, equation (2.16), in a couple of passages. More precisely, our need to keep track of the Jacobian comes from the fact that it makes the model to be viable only at scales larger than the ones described by [58], where it is possible to assume the single streaming approximation [63, 77].

These differences with the treatment of Section 2.5 turn out to be very important: they show that, again, it is possible to retrieve a Fourier description of the redshift space density contrast field analogous to equation (2.20) even without enforcing the $\nabla_{\parallel} u_{\parallel}(\mathbf{x})/x \ll 1$ condition (which was required to describe the Jacobian of the transformation $J(\mathbf{x})$ at linear order). It is now possible to describe the redshift space PS of density perturbations as follows

$$\begin{aligned} (2\pi)^3 \delta_D(\mathbf{k} + \mathbf{k}') P_s(k, k') &= \langle \delta_s(\mathbf{k}) \delta_s(\mathbf{k}') \rangle \\ &= \int d^3 \mathbf{x}' e^{i\mathbf{k}' \cdot \mathbf{x}'} \int d^3 \mathbf{x} e^{i\mathbf{k} \cdot \mathbf{x}} \left\langle e^{-if(-k_{\parallel} u_{\parallel} + k'_{\parallel} u'_{\parallel})} (1 + \delta - J)(1 + \delta' - J') \right\rangle \\ &= \int d^3 \mathbf{r} e^{i\mathbf{k}' \cdot \mathbf{r}} \int d^3 \mathbf{x} e^{i(\mathbf{k}' + \mathbf{k}) \cdot \mathbf{x}} \left\langle e^{-if(-k_{\parallel} u_{\parallel} + k'_{\parallel} u'_{\parallel})} (1 + \delta - J)(1 + \delta' - J') \right\rangle. \end{aligned} \quad (2.110)$$

Recalling once more that the correlation inside equation (2.110) is not a function of real space coordinates \mathbf{x} and \mathbf{x}' separately, but rather a function on the galaxy-galaxy distance \mathbf{r} alone⁷, we can write

$$\begin{aligned} (2\pi)^3 \delta_D(\mathbf{k} + \mathbf{k}') P_s(k) &= \int d^3 \mathbf{x} e^{i\mathbf{k} \cdot \mathbf{x}} \int d^3 \mathbf{x}' e^{i\mathbf{k}' \cdot \mathbf{x}'} \left\langle e^{-if(k_{\parallel} u_{\parallel} + k'_{\parallel} u'_{\parallel})} (1 + \delta - J)(1 + \delta' - J') \right\rangle \\ &= (2\pi)^3 \delta_D(\mathbf{k} + \mathbf{k}') \int d^3 \mathbf{r} e^{i\mathbf{k} \cdot \mathbf{r}} \left\langle e^{-ifk_{\parallel} \Delta u_{\parallel}} (1 + \delta - J)(1 + \delta' - J') \right\rangle \end{aligned} \quad (2.111)$$

and consequently a form of the PS of matter perturbations analogous to the one presented in both [57, 68, 77]

$$P_s(k) = \int d^3 \mathbf{r} e^{i\mathbf{k} \cdot \mathbf{r}} \left\langle e^{-ifk_{\parallel} \Delta u_{\parallel}} (1 + \delta - J)(1 + \delta' - J') \right\rangle. \quad (2.112)$$

By substituting the explicit form of the plane-parallel description of J and J' , equation (2.16), we have [57, 68, 77]

$$P_s(k) = \int d^3 \mathbf{r} e^{i\mathbf{k} \cdot \mathbf{r}} \left\langle e^{-ifk_{\parallel} \Delta u_{\parallel}(\mathbf{r})} [\delta + f \nabla_{\parallel} u_{\parallel}] [\delta' + f \nabla_{\parallel} u'_{\parallel}] \right\rangle, \quad (2.113)$$

which has the same role of equation (2.57) for the streaming model of Section 2.5. As it was for the derivation done in the Section above, the form of equation (2.113) has been retrieved with no dynamical assumptions for the density or velocity fields and thus it is an exact expression for the redshift space PS [57, 68]; the only assumption made were

1. Plane-parallel/Distant observer approximation, namely $\mathbf{x} \simeq \mathbf{x}_{pp} = x \hat{\mathbf{z}}$, to avoid spherical distortions and being able to write the Jacobian as in equation (2.16).
2. Single streaming approximation, in order to improve the streaming model of Section 2.5 by treating explicitly the Jacobian of the transformation.

⁷Again, this is the same reasoning we adopted to retrieve equation (1.66) in Section 1.4.1.

Again, it is important to highlight the consequences determined by differences we have with respect to the PS from the streaming model by R. Scoccimarro [58]; by a simple comparison between equation (2.57) and (2.113) we can easily see the former equation is containing just δ_s , while in the latter also LOS derivatives of the velocity fields are present. This difference comes from the fact that for the building of the TNS model researchers had to consider, following earlier works on the subject [10, 24, 23, 36], the Jacobian of the real-to-redshift transformation explicitly (equation (2.16) in its plane-parallel approximation) due to the fact they were calculating the form of the redshift space perturbation δ_s alone. With the approach proposed by R. Scoccimarro instead, the same calculation is applied to find the total field $1 + \delta_s$ and hence he was able to avoid the description of the Jacobian by using number conservation in its form (2.12).

Before diving into the analysis of equation (2.113) it is useful to re-define the variables inside the ensemble average to make the next calculations easier to control

$$\begin{aligned} j_1 &:= -ik_{||}f \\ A_1 &:= \Delta u_{||} = u'_{||} - u_{||} \\ A_2 &:= \delta + f\nabla_{||}u_{||} \\ A_3 &:= \delta' + f\nabla_{||}u'_{||}. \end{aligned} \tag{2.114}$$

Despite the differences between the two models, which at this level determine modifications in the definitions of the various A_i quantities, the procedure using the cumulant expansion is completely general and thus it can be carried out equally in the two approaches. Thus equation (2.113) itself can be rewritten in a more compact form as

$$P_s(k) = \int d^3\mathbf{r} e^{i\mathbf{k}\cdot\mathbf{r}} \langle e^{j_1 A_1} A_2 A_3 \rangle. \tag{2.115}$$

Now we can proceed simplifying the ensemble average terms inside the integral using the cumulant expansion theorem [57]

$$\langle e^{\mathbf{j}\cdot\mathbf{A}} \rangle = \exp \left\{ \langle e^{\mathbf{j}\cdot\mathbf{A}} \rangle_c \right\} \tag{2.116}$$

where we have collected the quantities j_i and A_j into the generic vector notation $\mathbf{j} := \{j_1, j_2, j_3\}$ and $\mathbf{A} := \{A_1, A_2, A_3\}$, with $j_2 = j_3 = 0$. The subscript c in the previous expression refers to the connected part of the ensemble average which, for a product of fields, is defined as below (for a more complete description of the cumulant expansion method we suggest to look at [38])

$$\begin{aligned} \langle X_i X_j \rangle_c &= \langle X_i X_j \rangle - \langle X_i \rangle \langle X_j \rangle \\ \langle X_i X_j X_l \rangle_c &= \langle X_i X_j X_l \rangle + 2 \langle X_i \rangle \langle X_j \rangle \langle X_l \rangle - \{ \langle X_i \rangle \langle X_j X_l \rangle + \langle X_j \rangle \langle X_l X_i \rangle + \langle X_l \rangle \langle X_i X_j \rangle \}. \end{aligned} \tag{2.117}$$

Noticing that the following relations hold

$$\begin{aligned} \langle e^{j_1 A_1} A_2 \rangle &= \left. \frac{\partial \langle e^{\mathbf{j}\cdot\mathbf{A}} \rangle}{\partial j_2} \right|_{j_2=j_3=0} \\ \langle e^{j_1 A_1} A_3 \rangle &= \left. \frac{\partial \langle e^{\mathbf{j}\cdot\mathbf{A}} \rangle}{\partial j_3} \right|_{j_2=j_3=0} \\ \langle e^{j_1 A_1} A_2 A_3 \rangle &= \left. \frac{\partial^2 \langle e^{\mathbf{j}\cdot\mathbf{A}} \rangle}{\partial j_2 \partial j_3} \right|_{j_2=j_3=0} \end{aligned} \tag{2.118}$$

we have just to apply the cumulant expansion theorem and evaluate the derivatives of the connected parts, expressed in the forms given in equations (2.117). Implementing the calculations we find [57, 58, 68, 77]

$$\begin{aligned}
\langle e^{j_1 A_1} A_2 \rangle &= \left. \frac{\partial \exp \{ \langle e^{\mathbf{j} \cdot \mathbf{A}} \rangle_c \}}{\partial j_2} \right|_{j_2=j_3=0} \\
&= \exp \left\{ \langle e^{\mathbf{j} \cdot \mathbf{A}} \rangle_c \right\} \left. \frac{\partial \langle e^{\mathbf{j} \cdot \mathbf{A}} \rangle_c}{\partial j_2} \right|_{j_2=j_3=0} \\
&= \exp \left\{ \langle e^{\mathbf{j} \cdot \mathbf{A}} \rangle_c \right\} \langle e^{\mathbf{j} \cdot \mathbf{A}} A_2 \rangle_c \Big|_{j_2=j_3=0} \\
&= \exp \{ \langle e^{j_1 A_1} \rangle_c \} \langle e^{j_1 A_1} A_2 \rangle_c.
\end{aligned} \tag{2.119}$$

Clearly, the second expression of (2.118) can be evaluated from the previous equation by substituting each index 2 with 3. For the third equation of (2.118) we have [57, 58, 68, 77]

$$\begin{aligned}
\langle e^{j_1 A_1} A_2 A_3 \rangle &= \left. \frac{\partial^2 \exp \{ \langle e^{\mathbf{j} \cdot \mathbf{A}} \rangle_c \}}{\partial j_2 \partial j_3} \right|_{j_2=j_3=0} \\
&= \frac{\partial}{\partial j_2} \left[\exp \left\{ \langle e^{\mathbf{j} \cdot \mathbf{A}} \rangle_c \right\} \left. \frac{\partial \langle e^{\mathbf{j} \cdot \mathbf{A}} \rangle_c}{\partial j_3} \right|_{j_2=j_3=0} \right] \\
&= \exp \left\{ \langle e^{\mathbf{j} \cdot \mathbf{A}} \rangle_c \right\} \left[\left. \frac{\partial \langle e^{\mathbf{j} \cdot \mathbf{A}} \rangle_c}{\partial j_2} \frac{\partial \langle e^{\mathbf{j} \cdot \mathbf{A}} \rangle_c}{\partial j_3} + \frac{\partial^2 \langle e^{\mathbf{j} \cdot \mathbf{A}} \rangle_c}{\partial j_2 \partial j_3} \right|_{j_2=j_3=0} \right] \\
&= \exp \{ \langle e^{j_1 A_1} \rangle_c \} [\langle e^{j_1 A_1} A_2 \rangle_c \langle e^{j_1 A_1} A_3 \rangle_c + \langle e^{j_1 A_1} A_2 A_3 \rangle_c].
\end{aligned} \tag{2.120}$$

At this point it is possible to evaluate the PS of perturbations retrieved in equation (2.115), it reads

$$P_s(k) = \int d^3 \mathbf{r} e^{i \mathbf{k} \cdot \mathbf{r}} \exp \{ \langle e^{j_1 A_1} \rangle_c \} [\langle e^{j_1 A_1} A_2 \rangle_c \langle e^{j_1 A_1} A_3 \rangle_c + \langle e^{j_1 A_1} A_2 A_3 \rangle_c]. \tag{2.121}$$

So far we have made no dynamical approximations and therefore equation (2.121) is still an exact expression. The implementation of the TNS model comes from a perturbative treatment of (2.121), where k_{\parallel} and, as a consequence, j_1 tend to zero. This reasoning is justified because the various modifications determined by the model within the Kaiser term are expected to be small at scales relevant for BAOs [68]. It is important to stress, however, that the usual perturbation theory cannot be applied due to the nonlinearity of the velocity field: more explicitly we Taylor expand around $j_1 = 0$ the terms inside the brackets, while we keep $j_1 \neq 0$ in the FOG factor [68, 77]. From a mathematical point of view, not expanding the FOG factor in equation (2.121) would mean that it is independent of the galaxy separation \mathbf{r} , which is clearly not the case given the definition of A_1 presented in (2.114). As reported in the next couple of pages, this approach is still mathematically justified from the fact that the FOG factor can be split in two parts: the first one, which will be called D_{1pt}^{FOG} , describing the velocity cumulants of single points and the second one, $D_{corr.}^{FOG}$, where all the dependence on \mathbf{r} is

gathered [77]

$$\begin{aligned}
\exp \left\{ \langle e^{j_1 A_1} \rangle_c \right\} &= \exp \left\{ \sum_{n=1}^{\infty} j_1^n \frac{\langle A_1^n \rangle_c}{n!} \right\} = \exp \left\{ \sum_{n=1}^{\infty} j_1^{2n} \frac{\langle (u'_1 - u_{11})^{2n} \rangle_c}{(2n)!} \right\} \\
&= \exp \left\{ \sum_{n=1}^{\infty} j_1^{2n} \frac{\langle (u'_1 - u_{11})^{2n} \rangle_c + \langle (u'_{11})^{2n} \rangle_c - \langle (u_{11})^{2n} \rangle_c}{(2n)!} \right\} \\
&= \exp \left\{ \sum_{n=1}^{\infty} j_1^{2n} \frac{2 \langle (u'_{11})^{2n} \rangle_c}{(2n)!} \right\} \exp \left\{ \sum_{n=1}^{\infty} j_1^{2n} \frac{\langle (u'_1 - u_{11})^{2n} \rangle_c - \langle (u'_{11})^{2n} \rangle_c - \langle (u_{11})^{2n} \rangle_c}{(2n)!} \right\} \\
&:= D_{1pt}^{\text{FOG}}(k\mu) \times D_{\text{corr.}}^{\text{FOG}}(k\mu, \mathbf{r}).
\end{aligned} \tag{2.122}$$

It is also worth noticing that the terms inside the series are all even: this is because odd power terms are nullified due to the symmetry property of the velocity field [77]. As we mentioned earlier, this approach to the FOG effect allows us to isolate the FOG term determined by the one-point velocity distribution function and remove it from the integration. The multipoint FOG term remains inside the integration and it will be expanded in terms of higher-order polynomials of density-velocity correlations.

First we focus on the Taylor expansion of the one-point function, which can be simplified once one notices it is described by $2 \langle (u'_{11})^{2n} \rangle_c$: following the reasoning behind the large-scale description of equation (2.86), it is possible to equate the one-point term we have with an effective one-dimensional velocity dispersion $\sigma_{v,\text{eff}}^2$. Hence, for any generic even number n we can write [57, 68, 77]

$$\langle \Delta u_{11}^n \rangle_c \simeq 2 \langle (u'_{11})^n \rangle_c \equiv 2 \langle (u_{11})^n \rangle_c = 2c_n \sigma_{v,\text{eff}}^n, \tag{2.123}$$

where the velocity dispersion $\sigma_{v,\text{eff}}^2$ here reported is not the one defined in equation (2.74) any more, but rather it is treated as a free parameter: this is due because this term becomes important at small scales and therefore we cannot describe $\langle \Delta u_{11}^2 \rangle_c$ with its large scale limit σ_v^2 alone. As already mentioned by the authors behind this model [57, 68, 77], this constitutes the major disadvantage of the TNS model. In addition to that, with the aim to recover the Gaussian/Lorentzian form of the PS given from the FOG effect which was inserted in the phenomenological description of the RSD phenomenon, it is possible to assume the following condition of the c_n coefficients [68]

$$\begin{cases} c_2 = 1 \\ c_{2n} = (2n - 1)! \\ c_{2n-1} = 0. \end{cases} \tag{2.124}$$

Given the considerations above the one-point function reads

$$\begin{aligned}
D_{1pt}^{\text{FOG}}(k\mu) &= \exp \left\{ \sum_{n=1}^{\infty} j_1^{2n} \frac{2 \langle (u'_{11})^{2n} \rangle_c}{(2n)!} \right\} \\
&= \exp \left\{ j_1^2 \sigma_{v,\text{eff}}^2 + \sum_{n=2}^{\infty} j_1^{2n} \frac{2 \langle (u'_{11})^{2n} \rangle_c}{(2n)!} \right\} \simeq \exp \left\{ -k^2 \mu^2 f^2 \sigma_{v,\text{eff}}^2 \right\},
\end{aligned} \tag{2.125}$$

where the last approximation comes from the fact that our large scale expansion will be performed up to the second order of j_1 , making $\exp\{j_1^2\sigma_{v,\text{eff}}^2\}$ the only term to be computed explicitly. Regarding the multi-point FOG factor, we divide further the expansion series in two parts [77]

$$D_{\text{corr.}}^{\text{FOG}}(k\mu, \mathbf{r}) = \exp \left\{ -j_1^2 \langle u_{\parallel} u'_{\parallel} \rangle_c + \sum_{n=2}^{\infty} j_1^{2n} \frac{\langle (u'_{\parallel} - u_{\parallel})^{2n} \rangle_c - \langle (u'_{\parallel})^{2n} \rangle_c - \langle (u_{\parallel})^{2n} \rangle_c}{(2n)!} \right\} : \quad (2.126)$$

this is done because the first term of the series, with $n = 1$, is already of order j_1^2 and therefore it will be the only relevant one once we will multiply $D_{\text{corr.}}^{\text{FOG}}$ with the Kaiser term.

The large scale expansion of the Kaiser terms, equation (2.121), gives the following results

$$\begin{aligned} \langle e^{j_1 A_1} A_2 \rangle_c \langle e^{j_1 A_1} A_3 \rangle_c + \langle e^{j_1 A_1} A_2 A_3 \rangle_c &\simeq \langle A_2 A_3 \rangle_c + j_1 \langle A_1 A_2 A_3 \rangle_c + \\ &+ j_1^2 \left\{ \frac{1}{2} \langle A_1^2 A_2 A_3 \rangle_c + \langle A_1 A_2 \rangle_c \langle A_1 A_3 \rangle_c \right\} + \mathcal{O}(j_1^3), \end{aligned} \quad (2.127)$$

with

$$\langle e^{j_1 A_1} A_2 \rangle_c \simeq \langle A_2 \rangle_c + j_1 \langle A_1 A_2 \rangle_c + \frac{j_1^2}{2} \langle A_1^2 A_2 \rangle_c + \mathcal{O}(j_1^3). \quad (2.128)$$

Thus the product between the large scale expansions of the multi-point FOG factor (2.126) and the Kaiser contribution, with (2.127) and (2.128), gives

$$\begin{aligned} D_{\text{corr.}}^{\text{FOG}}(k\mu, \mathbf{r}) [\langle e^{j_1 A_1} A_2 \rangle_c \langle e^{j_1 A_1} A_3 \rangle_c + \langle e^{j_1 A_1} A_2 A_3 \rangle_c] &\simeq \langle A_2 A_3 \rangle_c + j_1 \langle A_1 A_2 A_3 \rangle_c + \\ &+ j_1^2 \left\{ \frac{1}{2} \langle A_1^2 A_2 A_3 \rangle_c + \langle A_1 A_2 \rangle_c \langle A_1 A_3 \rangle_c - \langle u_{\parallel} u'_{\parallel} \rangle_c \langle A_2 A_3 \rangle_c \right\} + \mathcal{O}(j_1^3). \end{aligned} \quad (2.129)$$

The first term of equation (2.127) turns out to be equal to the Kaiser effect described by the streaming model of R. Scoccimarro [58], and hence, for the time being, we borrow it from equation (2.98); its explicit derivation will be shown in detail later, through Section 2.7.1. To deal with higher order terms we follow again [57, 68, 77] by defining them as follows

$$\begin{aligned} A(k, \mu) &:= j_1 \int d^3 \mathbf{r} e^{i\mathbf{k}\cdot\mathbf{r}} \langle A_1 A_2 A_3 \rangle_c \\ B(k, \mu) &:= j_1^2 \int d^3 \mathbf{r} e^{i\mathbf{k}\cdot\mathbf{r}} \langle A_1 A_2 \rangle_c \langle A_1 A_3 \rangle_c \\ T(k, \mu) &:= \frac{1}{2} j_1^2 \int d^3 \mathbf{r} e^{i\mathbf{k}\cdot\mathbf{r}} \langle A_1^2 A_2 A_3 \rangle_c \\ F(k, \mu) &:= -j_1^2 \int d^3 \mathbf{r} e^{i\mathbf{k}\cdot\mathbf{r}} \langle u_{\parallel} u'_{\parallel} \rangle_c \langle A_2 A_3 \rangle_c. \end{aligned} \quad (2.130)$$

Finally, we are now able to derive the RSD model in coherent expansion of $k\mu$ as it was first derived by Taruya, Nishimichi and Saito in their paper [68] and, then, implemented further by Zheng and Song in [77] accounting for $T(k, \mu)$ and $F(k, \mu)$ terms

$$\begin{aligned} P_s(k, \mu) &= \exp \left\{ -k^2 \mu^2 f^2 \sigma_v^2 \right\} [P_{\delta\delta}(k) + 2f\mu^2 P_{\delta\theta}(k) + f^2 \mu^4 P_{\theta\theta}(k) + \\ &+ A(k, \mu) + B(k, \mu) + T(k, \mu) + F(k, \mu)]. \end{aligned} \quad (2.131)$$

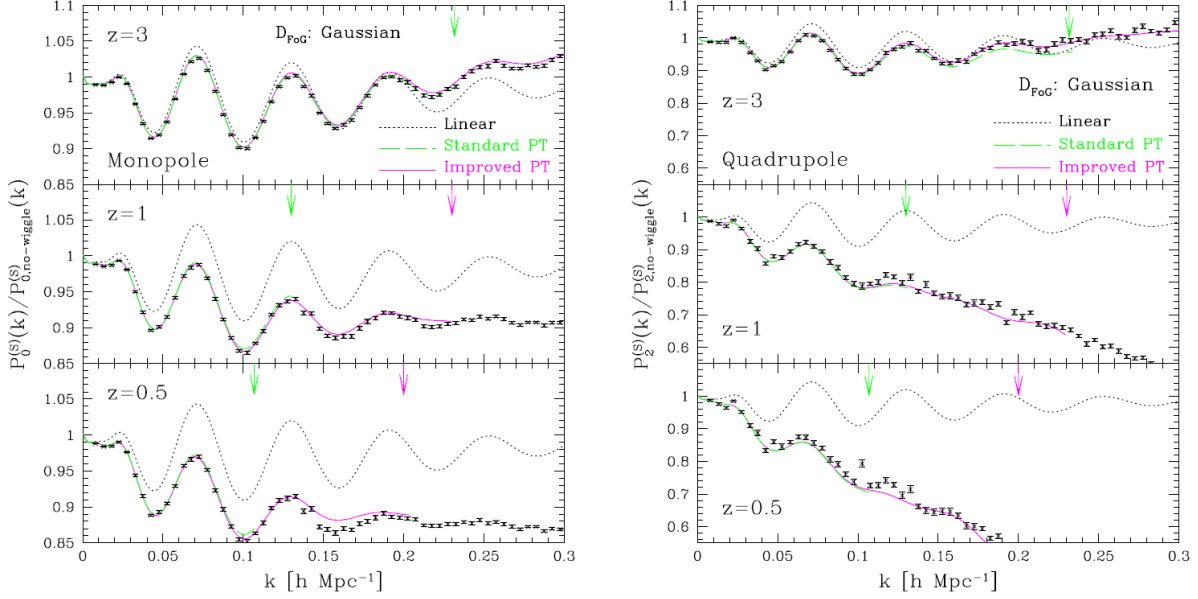


Figure 2.7: Plot analogous to the one given in Figure 2.3, with the only difference being the adoption of the TNS model here. Figure taken from [57].

In Figure 2.7 the evaluation of the redshift PS according to the TNS model is reported analogously to the one given for the dispersion model in Figure 2.3. From a comparison between the two it is clear the TNS model works better generally, even if its performance becomes worse when we reach large values of $k_{||}$, namely when we are investigating small scales. In the following Sections each term inside equation (2.131) is presented alone, in order to give a better understanding of their meaning.

2.7.1 Zeroth Order Power Spectra

To see the equivalence between the zeroth order PS of the TNS and the streaming model of Section 2.5 we cited before, we first write it back in terms of density contrasts and velocities using (2.114) and the fact that, for two fields, the connected and unconnected parts of the ensemble average are the same

$$\begin{aligned} \langle A_2 A_3 \rangle_c &\equiv \langle A_2 A_3 \rangle = \langle [\delta + f \nabla_{||} u_{||}] [\delta' + f \nabla_{||} u'_{||}] \rangle \\ &= \langle \delta \delta' + f \delta \nabla u'_{||} + f \delta' \nabla_{||} u_{||} + f^2 \nabla_{||} u_{||} \nabla_{||} u'_{||} \rangle. \end{aligned} \quad (2.132)$$

From equation (2.115) we can describe the zeroth order of the perturbation as

$$P_s^{(0)}(k) = \int d^3 \mathbf{r} e^{i \mathbf{k} \cdot \mathbf{r}} \langle \delta \delta' + f \delta \nabla u'_{||} + f \delta' \nabla_{||} u_{||} + f^2 \nabla_{||} u_{||} \nabla_{||} u'_{||} \rangle. \quad (2.133)$$

Exploiting the additive property of integrals, thanks to equation (1.1) we can now split the ensemble average of the sum into a sum of ensemble averages; this allows us to treat each addendum inside

(2.132) separately. From the definition of the PS given in equation (1.65), once adapted for the nonlinear power spectra, we have

$$\int d^3\mathbf{r} e^{i\mathbf{k}\cdot\mathbf{r}} \langle \delta\delta' \rangle = P_{\delta\delta}(k); \quad (2.134)$$

for the derivation of terms involving velocities we have to recall also equation (2.24) to retrieve

$$\begin{aligned} \int d^3\mathbf{r} e^{i\mathbf{k}\cdot\mathbf{r}} \langle f\delta\nabla_{\parallel}u'_{\parallel} \rangle &= f \int d^3\mathbf{r} e^{i\mathbf{k}\cdot\mathbf{r}} \left\langle \delta\nabla_{\parallel} \int \frac{d^3\mathbf{k}}{(2\pi)^3} e^{-i\mathbf{k}\cdot\mathbf{x}'} u_{\parallel}(\mathbf{k}) \right\rangle \\ &= -ik_{\parallel}f \int d^3\mathbf{r} e^{i\mathbf{k}\cdot\mathbf{r}} \left\langle \delta \int \frac{d^3\mathbf{k}}{(2\pi)^3} e^{-i\mathbf{k}\cdot\mathbf{x}'} i\frac{k_{\parallel}}{k^2} \theta(\mathbf{k}) \right\rangle \\ &= f\mu^2 \int d^3\mathbf{r} e^{i\mathbf{k}\cdot\mathbf{r}} \langle \delta\theta' \rangle = f\mu^2 P_{\delta\theta}(k) \equiv f\mu^2 P_{\theta\delta}(k), \end{aligned} \quad (2.135)$$

where the equivalence $f\mu^2 P_{\delta\theta}(k) \equiv f\mu^2 P_{\theta\delta}(k)$ come from symmetry between $\langle f\delta\nabla_{\parallel}u'_{\parallel} \rangle = \langle f\delta'\nabla_{\parallel}u_{\parallel} \rangle$ terms, and

$$\begin{aligned} \int d^3\mathbf{r} e^{i\mathbf{k}\cdot\mathbf{r}} \langle f^2\nabla_{\parallel}u_{\parallel}\nabla_{\parallel}u'_{\parallel} \rangle &= f^2 \int d^3\mathbf{r} e^{i\mathbf{k}\cdot\mathbf{r}} \left\langle \nabla_{\parallel} \int \frac{d^3\mathbf{k}}{(2\pi)^3} e^{-i\mathbf{k}\cdot\mathbf{x}} u_{\parallel}(\mathbf{k}) \nabla_{\parallel} \int \frac{d^3\mathbf{k}}{(2\pi)^3} e^{-i\mathbf{k}\cdot\mathbf{x}'} u_{\parallel}(\mathbf{k}) \right\rangle \\ &= f^2\mu^4 \int d^3\mathbf{r} e^{i\mathbf{k}\cdot\mathbf{r}} \langle \theta\theta' \rangle = f^2\mu^4 P_{\theta\theta}(k). \end{aligned} \quad (2.136)$$

Summing back together all the zeroth order components we have

$$P_s^{(0)}(k) = P_{\delta\delta}(k) + 2f\mu^2 P_{\delta\theta}(k) + f^2\mu^4 P_{\theta\theta}(k), \quad (2.137)$$

which gives exactly equation (2.97) of the Kaiser PS determined from the streaming model.

The zeroth order PS has been calculated by Zheng and Song in their 2016 paper [77] using perturbation theory, which was then regularized to improve the UV behaviour of the model (they refer to it as **RegPT**). Their **RegPT** theory was presented in [65] and it is based on a multi-point propagator expansion for both the density and velocity fields. The model results were tested against N-body simulations and it is possible to see from Figure 2.8 that they start to fail when the UV behaviour becomes dominant ($k \gtrsim 0.1 h\text{Mpc}^{-1}$): this is a direct consequence of the single stream approximation which is no longer fulfilled once we hit the small scale regime⁸.

⁸For a direct comparison, the large scale limit of the more generic streaming model presented in Section 2.5.2 is valid in the regime of $k_{\parallel} \lesssim 0.2 h\text{Mpc}^{-1}$, making it able to describe smaller scales compared with the TNS model.

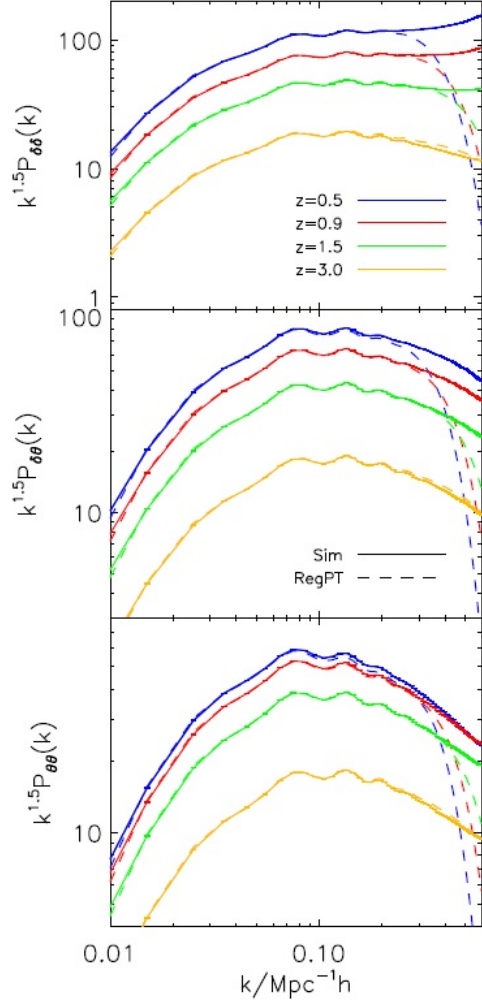


Figure 2.8: Comparison between theoretical prediction of the Kaiser effect done using `RegPT` [65] (dashed lines) and numerical simulations (continuous lines). The simulation lines are mean values out of 100 simulations, with the small error bars on the curves being the standard errors for the mean, $\sigma_{mean} = \sigma/\sqrt{N}$, where σ corresponds to the standard deviation and N is the number of simulations. Figure taken from [77].

2.7.2 First Order Power Spectra

The $A(k, \mu)$ is the leading contribution at first order in j_1 , it comes from the non linear mapping of density-velocity cross-correlation. Following [68], we describe it as

$$\begin{aligned}
A(k, \mu) &= j_1 \int d^3 \mathbf{r} e^{i\mathbf{k}\cdot\mathbf{r}} \langle A_1 A_2 A_3 \rangle_c \\
&= j_1 \int d^3 \mathbf{r} e^{i\mathbf{k}\cdot\mathbf{r}} \langle \Delta u_{\parallel} [\delta + \nabla_{\parallel} u_{\parallel}] [\delta' + \nabla_{\parallel} u'_{\parallel}] \rangle_c \\
&= k\mu \int \frac{d^3 \mathbf{p}}{(2\pi)^3} \frac{p_{\parallel}}{p^2} \{ B_{\sigma}(\mathbf{p}, \mathbf{k} - \mathbf{p}, -\mathbf{k}) - B_{\sigma}(\mathbf{p}, \mathbf{k}, -\mathbf{k}, -\mathbf{p}) \},
\end{aligned} \tag{2.138}$$

with function B_{σ} being a bispectrum; it is defined as follows

$$\left\langle \theta(\mathbf{k}_1) \left\{ \delta(\mathbf{k}_2) + \frac{k_{2\parallel}^2}{k_2^2} \theta(\mathbf{k}_2) \right\} \left\{ \delta(\mathbf{k}_3) + \frac{k_{3\parallel}^2}{k_3^2} \theta(\mathbf{k}_3) \right\} \right\rangle = (2\pi)^3 \delta_D(\mathbf{k}_1 + \mathbf{k}_2 + \mathbf{k}_3) B_{\sigma}(\mathbf{k}_1, \mathbf{k}_2, \mathbf{k}_3). \tag{2.139}$$

The theoretical solution for $A(k, \mu)$ has been calculated using the RegPT algorithm, with the theoretical prediction derived integrating bispectra in Fourier space from numerical simulations according to the last row of equation (2.138); for the numerical prediction they exploited the second row of equation (2.138): they measured separately all the perturbative fields to, then, combine them at two different points under the assumption of a fiducial Λ CDM model. Explicitly we have [63]

$$\begin{aligned}
A(k, \mu) &= j_1 \int d^3 \mathbf{r} e^{i\mathbf{k}\cdot\mathbf{r}} \langle \Delta u_{\parallel} [\delta + \nabla_{\parallel} u_{\parallel}] [\delta' + \nabla_{\parallel} u'_{\parallel}] \rangle_c = \sum_{n=1}^6 \mathcal{A}_n, \\
\mathcal{A}_1 &:= 2j_1 \int d^3 \mathbf{r} e^{i\mathbf{k}\cdot\mathbf{r}} \langle u_{\parallel} \delta \delta' \rangle_c \\
\mathcal{A}_2 &:= j_1 \int d^3 \mathbf{r} e^{i\mathbf{k}\cdot\mathbf{r}} \langle u_{\parallel} \delta \nabla_{\parallel} u'_{\parallel} \rangle_c \\
\mathcal{A}_3 &:= j_1 \int d^3 \mathbf{r} e^{i\mathbf{k}\cdot\mathbf{r}} \langle u_{\parallel} \nabla_{\parallel} u_{\parallel} \delta' \rangle_c \\
\mathcal{A}_4 &:= 2j_1 \int d^3 \mathbf{r} e^{i\mathbf{k}\cdot\mathbf{r}} \langle u_{\parallel} \nabla_{\parallel} u_{\parallel} \nabla_{\parallel} u'_{\parallel} \rangle_c \\
\mathcal{A}_5 &:= j_1 \int d^3 \mathbf{r} e^{i\mathbf{k}\cdot\mathbf{r}} \langle -\delta u'_{\parallel} \nabla_{\parallel} u'_{\parallel} \rangle_c \\
\mathcal{A}_6 &:= j_1 \int d^3 \mathbf{r} e^{i\mathbf{k}\cdot\mathbf{r}} \langle -\nabla_{\parallel} u_{\parallel} u'_{\parallel} \delta' \rangle_c.
\end{aligned} \tag{2.140}$$

The terms are then cross-correlated appropriately and the configuration space pairs are mapped into Fourier space. These results are presented in Figure 2.9 for various redshifts. Both theoretical calculations and predictions from N-body simulations agree for small values of μ (along the perpendicular direction) but deviate from each other at $\mu \rightarrow 1$, with the first order correction to the PS determining an enhancement for modes having a low value of k and a suppression for ones having high values of k (recall from (2.114) that j_1 is negative). This behaviour of the $A(k, \mu)$ term at high values of μ could be due to the fact that both numerical and theoretical predictions truncate the perturbation expansion at the leading order, ignoring higher order levels of the bispectrum [77].

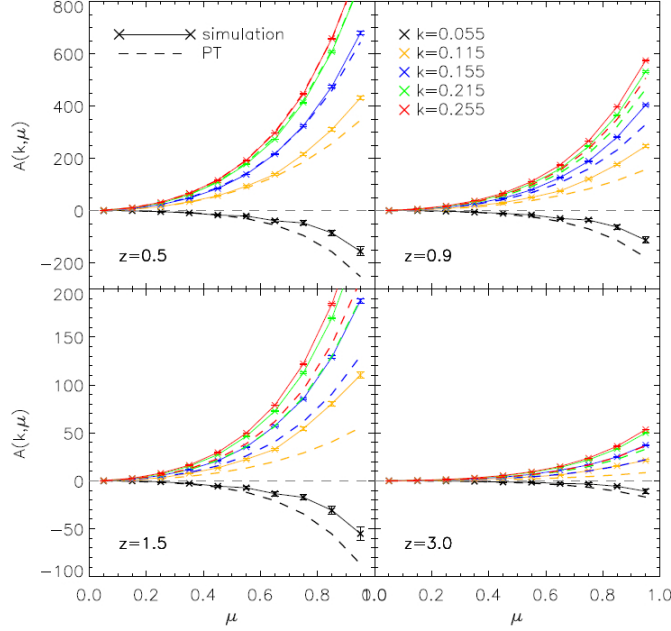


Figure 2.9: $A(k, \mu)$ term measured from 100 N-body simulations at redshift $z = 0.5, 0.9, 1.5$ and 3.0 . Different colours represent different k bins as summarized in the legend. Solid lines are the mean value averaged over the 100 simulations, the dashed lines show predictions from the standard perturbation theory. It is important to note that the scale of the vertical axis varies between top and bottom panels. Figure taken from [77].

2.7.3 Second Order Power Spectra

The three terms $B(k, \mu)$, $T(k, \mu)$ and $F(k, \mu)$ consist in the complete j_1^2 expansion. $B(k, \mu)$ and $T(k, \mu)$ are provided from density-velocity cross-correlations, while $F(k, \mu)$ comes from velocity auto-correlation pairs which are generated by the FOG effect. For each one of them, the theoretical predictions are shown against N-body simulations as done for $A(k, \mu)$.

Following again [68], $B(k, \mu)$ is written as

$$\begin{aligned}
 B(k, \mu) &= j_1^2 \int d^3 \mathbf{r} e^{i\mathbf{k} \cdot \mathbf{r}} \langle A_1 A_2 \rangle_c \langle A_1 A_3 \rangle_c \\
 &= j_1^2 \int d^3 \mathbf{r} e^{i\mathbf{k} \cdot \mathbf{r}} \langle \Delta u_{\parallel} [\delta + \nabla_{\parallel} u_{\parallel}] \rangle_c \langle \Delta u_{\parallel} [\delta' + \nabla_{\parallel} u'_{\parallel}] \rangle_c
 \end{aligned} \tag{2.141}$$

which can be also expressed in Fourier space as

$$\begin{aligned}
 B(k, \mu) &= (k\mu f)^2 \int \frac{d^3 \mathbf{p}}{(2\pi)^3} F(\mathbf{p}) F(\mathbf{k} - \mathbf{p}), \\
 F(\mathbf{p}) &:= \frac{p_{\parallel}}{p^2} \left\{ P_{\delta\theta}(p) + f \frac{p_{\parallel}^2}{p^2} P_{\theta\theta}(p) \right\}.
 \end{aligned} \tag{2.142}$$

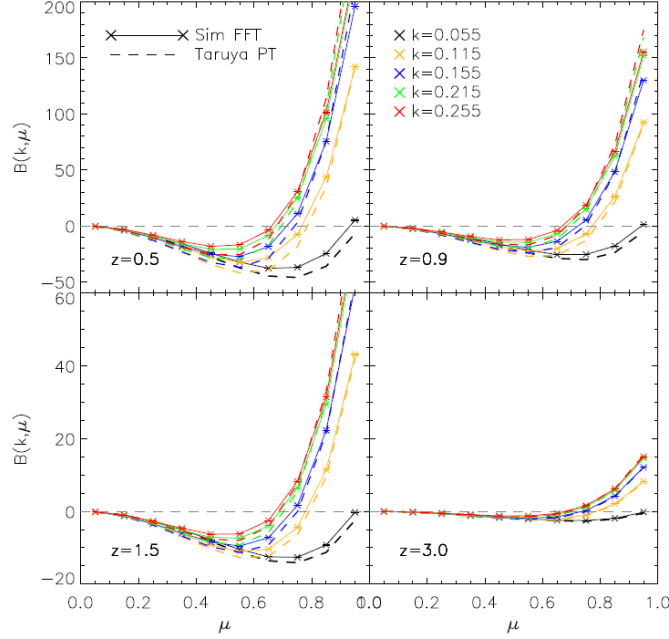


Figure 2.10: The figure reports the results for $B(k, \mu)$, with the same conventions used in Figure 2.9. Figure taken from [77].

Results from the two previous equations are presented in Figure 2.10, where in this case they appear to be consistent with each other for every value of μ .

Referring again to the relations given in equation (2.117), the expression of $T(k, \mu)$ is given by

$$\begin{aligned}
 T(k, \mu) &= \frac{1}{2} j_1^2 \int d^3 \mathbf{r} e^{i\mathbf{k} \cdot \mathbf{r}} \langle A_1^2 A_2 A_3 \rangle_c \\
 &= \frac{1}{2} j_1^2 \int d^3 \mathbf{r} e^{i\mathbf{k} \cdot \mathbf{r}} \{ \langle A_1^2 A_2 A_3 \rangle - \langle A_1^2 \rangle \langle A_2 A_3 \rangle - 2 \langle A_1 A_2 \rangle \langle A_1 A_3 \rangle \} \\
 &= \frac{1}{2} j_1^2 \int d^3 \mathbf{r} e^{i\mathbf{k} \cdot \mathbf{r}} \{ \langle \Delta u_{||}^2 [\delta + \nabla_{||} u_{||}] [\delta' + \nabla_{||} u'_{||}] \rangle - \langle A_1^2 \rangle \langle A_2 A_3 \rangle - 2 \langle A_1 A_2 \rangle \langle A_1 A_3 \rangle \}
 \end{aligned} \tag{2.143}$$

We see from Figure 2.11 that $T(k, \mu)$ suppresses the PS at all scales and pair orientations and its magnitude is comparable to the one of terms $A(k, \mu)$ and $B(k, \mu)$ [77]. Since $T(k, \mu)$ determines a suppression of the PS, it might come to mind to insert it in the FOG description, by doing that however the FOG effect will lose its scale independence: recall that the improvement of the TNS model proposed in [77] is based upon the assumption that the FOG factor can be split in two factors as shown in (2.122), one scale independent which remains in the final FOG description, equation (2.125), and the other scale dependent which can be evaluated in the computation of the Kaiser effect, equation (2.126). Here we highlight that the $T(k, \mu)$ term of equation (2.143) is of the order of $O(P_L^3)$ and hence its contribution is often omitted in the computation of the second order PS [57, 68].

The $F(k, \mu)$ term comes from the local FOG effect, which contains higher order velocity correlations

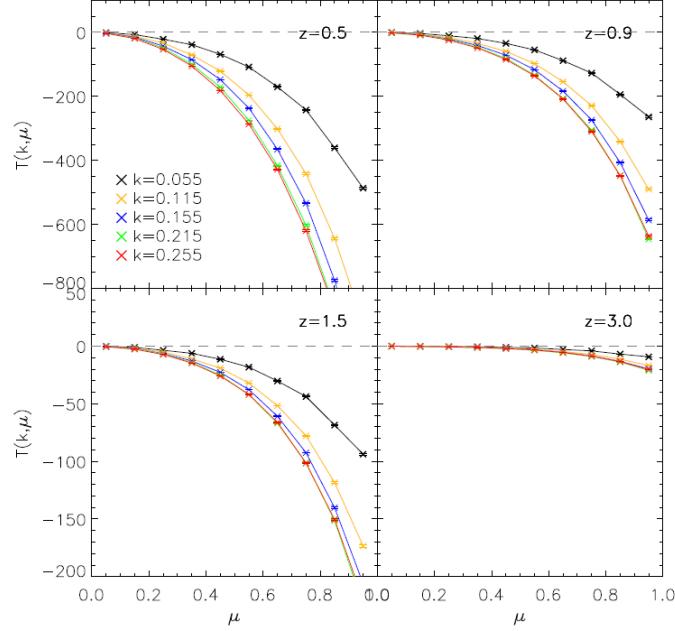


Figure 2.11: The figure reports the results for $T(k, \mu)$, with the same conventions used in Figure 2.9. Figure taken from [77].

depending on the separation of two points. The term reads

$$\begin{aligned}
 F(k, \mu) &= -j_1^2 \int d^3 \mathbf{r} e^{i\mathbf{k} \cdot \mathbf{r}} \langle u_{\parallel} u'_{\parallel} \rangle_c \langle A_2 A_3 \rangle_c \\
 &= -j_1^2 \int d^3 \mathbf{r} e^{i\mathbf{k} \cdot \mathbf{r}} \langle u_{\parallel} u'_{\parallel} \rangle_c \langle [\delta + \nabla_{\parallel} u_{\parallel}] [\delta' + \nabla_{\parallel} u'_{\parallel}] \rangle_c.
 \end{aligned} \tag{2.144}$$

This equation is evaluated from simulations as $B(k, \mu)$ was. Its form in Fourier space is given by

$$\begin{aligned}
 F(k, \mu) &= (k\mu f)^2 \int \frac{d^3 \mathbf{p} d^3 \mathbf{q}}{(2\pi)^3} \delta_D(\mathbf{k} - \mathbf{p} - \mathbf{q}) \frac{\mu_p^2}{p^2} P_{\theta\theta}(p) \{ P_{\delta\delta}(q) + 2f\mu_q^2 P_{\delta\theta}(q) + f^2 \mu_q^4 P_{\theta\theta}(q) \} \\
 &\simeq (k\mu f)^2 \int \frac{d^3 \mathbf{p} d^3 \mathbf{q}}{(2\pi)^3} \delta_D(\mathbf{k} - \mathbf{p} - \mathbf{q}) \frac{\mu_p^2}{p^2} (1 + f\mu_q^2)^2 P_L(p) P_L(q)
 \end{aligned} \tag{2.145}$$

where in the last row the linear approximation of the PS has been enforced, making $P_L(p)$ and $P_L(q)$ the linear power spectra in Fourier space. Again, results coming from the previous two equations are consistent with each other for each value of the direction cosine. In Figure 2.12 theoretical prediction of $T(k, \mu)$, determined from (2.144) (solid curves), are compared with predictions coming from the linear approximation of (2.145) (dashed curves) against N-body simulations. Both formulations agrees with simulation results. Here it is important to note that the contribution coming from $F(k, \mu)$ to the PS turns out to be comparable in magnitude with the one determined by $T(k, \mu)$ but with the opposite sign: therefore the combined effect of the two terms on the observed spectrum can be smaller resulting

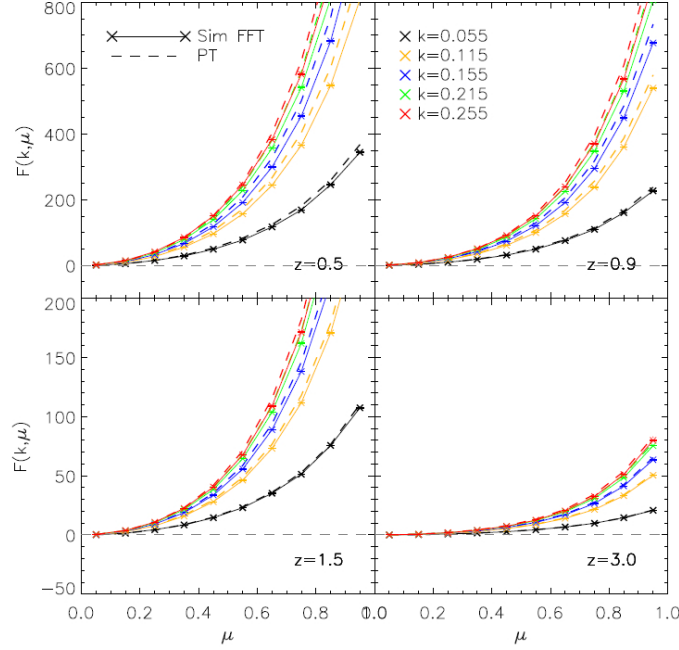


Figure 2.12: The figure reports the results for $F(k, \mu)$, with the same conventions used in Figure 2.9. Figure taken from [77].

in a minor improvement on the original model. Indeed their corrections turn out to be subdominant for both the monopole and quadrupole contributions [57, 68]; this is the reason behind the fact they were ignored in later numerical simulations such [63].

2.8 Comparison Between Different Models

The cumulant expansion theorem used in Section 2.7 can be applied to different models, here as an example, we give its implementation for the streaming model [58] of Section 2.5: an expansion correspondent to the one presented in equations (2.125), (2.127) and (2.129) can be implemented also for equation (2.57). This however requires different definitions for the A_2 and A_3 quantities, while A_1 and j_1 remain the same as in (2.114), respectively we have

$$\begin{aligned} A_2 &:= \delta, \\ A_3 &:= \delta, \end{aligned} \tag{2.146}$$

which gives

$$\begin{aligned} (2\pi)^3 \delta_D(\mathbf{k}) + P_s(k) &= \int d^3\mathbf{r} e^{i\mathbf{k}\cdot\mathbf{r}} \langle e^{j_1 A_1} [1 + A_2][1 + A_3] \rangle \\ &\simeq \int d^3\mathbf{r} e^{i\mathbf{k}\cdot\mathbf{r}} \exp \{ \langle e^{j_1 A_1} \rangle_c \} [1 + \langle e^{j_1 A_1} A_2 \rangle_c + \langle e^{j_1 A_1} A_3 \rangle_c + \\ &\quad + \langle e^{j_1 A_1} A_2 \rangle_c \langle e^{j_1 A_1} A_3 \rangle_c + \langle e^{j_1 A_1} A_2 A_3 \rangle_c]. \end{aligned} \tag{2.147}$$

On a first look, these different definitions seem to lead into a different form of the matter perturbation PS between the models of Scoccimarro and TNS once the explicit values of A_i s and j_1 are substituted back, with the latter containing mixed products of density contrast and gradient of LOS velocities in the right hand side (equation (2.129)). Nonetheless, it is possible to show that the two descriptions are identical, with all the "extra terms" coming from the TNS description folding back into a $-(2\pi)^3\delta_D(\mathbf{k})$.

To develop such a demonstration we start reporting the two descriptions before the application of the cumulant expansion theorem, respectively equations (2.57) and (2.111),

$$\begin{aligned} (2\pi)^3\delta_D(\mathbf{k}) + P_s(k) &= \int d^3\mathbf{r} e^{i\mathbf{k}\cdot\mathbf{r}} \left\langle e^{-ifk_{||}\Delta u_{||}} (1 + \delta)(1 + \delta') \right\rangle \\ (2\pi)^3\delta_D(\mathbf{k} + \mathbf{k}')P_s(k) &= (2\pi)^3\delta_D(\mathbf{k} + \mathbf{k}') \int d^3\mathbf{r} e^{i\mathbf{k}\cdot\mathbf{r}} \left\langle e^{-ifk_{||}\Delta u_{||}} (1 + \delta - J)(1 + \delta' - J') \right\rangle. \end{aligned} \quad (2.148)$$

The TNS expression can then be rearranged as

$$\begin{aligned} (2\pi)^3\delta_D(\mathbf{k} + \mathbf{k}')P_s(k) &= (2\pi)^3\delta_D(\mathbf{k} + \mathbf{k}') \int d^3\mathbf{r} e^{i\mathbf{k}\cdot\mathbf{r}} \left\langle e^{-ifk_{||}\Delta u_{||}} (1 + \delta)(1 + \delta') \right\rangle + \\ &+ (2\pi)^3\delta_D(\mathbf{k} + \mathbf{k}') \int d^3\mathbf{r} e^{i\mathbf{k}\cdot\mathbf{r}} \left\langle e^{-ifk_{||}\Delta u_{||}} [-J(1 + \delta') - J'(1 + \delta) + JJ'] \right\rangle, \end{aligned} \quad (2.149)$$

which makes us able to focus only on the second row, with the aim of finding a way to deal with the TNS contributions

$$(2\pi)^3\delta_D(\mathbf{k} + \mathbf{k}') \int d^3\mathbf{r} e^{i\mathbf{k}\cdot\mathbf{r}} \left\langle e^{-ifk_{||}\Delta u_{||}} [-J(1 + \delta') - J'(1 + \delta) + JJ'] \right\rangle. \quad (2.150)$$

In order to be completely general, let us deal with equation (2.150) before the enforcement of spatial homogeneity we implemented in Section 2.7

$$\int d^3\mathbf{x} e^{i\mathbf{k}\cdot\mathbf{x}} \int d^3\mathbf{x}' e^{i\mathbf{k}'\cdot\mathbf{x}'} \left\langle e^{-if(k_{||}u_{||} + k'_{||}u'_{||})} [-J(1 + \delta') - J'(1 + \delta) + JJ'] \right\rangle; \quad (2.151)$$

with this expression in hands, we exploit now the definition of ensemble average of equation (1.1) to express it as an integral over the galaxy-galaxy distance⁹ \mathbf{r}

$$\int d^3\mathbf{x} d^3\mathbf{x}' \frac{d^3\mathbf{r}}{V_{\mathbf{r}}} e^{i\mathbf{k}\cdot\mathbf{x}} e^{i\mathbf{k}'\cdot\mathbf{x}'} e^{-if(k_{||}u_{||} + k'_{||}u'_{||})} [-J(1 + \delta') - J'(1 + \delta) + JJ'] \quad (2.152)$$

and start dealing with each of the three terms in the sum inside the square brackets singularly. Using the definition of the Jacobian of transformation given in equation (2.13) and the results of equations

⁹As we mentioned various times throughout the work, we are under the assumption that all the ensemble average we are dealing with are not function of the two different coordinates at the same time, but rather functions of only \mathbf{r} .

(2.48) and (2.49), for the first term we have

$$\begin{aligned}
- \int d^3\mathbf{x}d^3\mathbf{x}' \frac{d^3\mathbf{r}}{V_{\mathbf{r}}} e^{i\mathbf{k}\cdot\mathbf{x}} e^{i\mathbf{k}'\cdot\mathbf{x}'} e^{-if(k_{\parallel}u_{\parallel}+k'_{\parallel}u'_{\parallel})} J(1+\delta') &= - \int d^3\mathbf{s}d^3\mathbf{x}' \frac{d^3\mathbf{r}}{V_{\mathbf{r}}} e^{i\mathbf{k}\cdot\mathbf{s}} e^{i\mathbf{k}'\cdot\mathbf{x}'} e^{-ifk'_{\parallel}u'_{\parallel}} (1+\delta') \\
&= - \int d^3\mathbf{s}d^3\mathbf{x}' e^{i\mathbf{k}\cdot\mathbf{s}} e^{i\mathbf{k}'\cdot\mathbf{x}'} \left\langle e^{-ifk'_{\parallel}u'_{\parallel}} (1+\delta') \right\rangle \\
&= - \int d^3\mathbf{s}d^3\mathbf{x}' e^{i\mathbf{k}\cdot\mathbf{s}} e^{i\mathbf{k}'\cdot\mathbf{x}'} \\
&= - (2\pi)^6 \delta_D(\mathbf{k}) \delta_D(\mathbf{k}');
\end{aligned} \tag{2.153}$$

the same result can then be obtained for the second addendum just exchanging primed with unprimed quantities

$$\begin{aligned}
- \int d^3\mathbf{x}d^3\mathbf{x}' \frac{d^3\mathbf{r}}{V_{\mathbf{r}}} e^{i\mathbf{k}\cdot\mathbf{x}} e^{i\mathbf{k}'\cdot\mathbf{x}'} e^{-if(k_{\parallel}u_{\parallel}+k'_{\parallel}u'_{\parallel})} J'(1+\delta) &= - \int d^3\mathbf{x}d^3\mathbf{s}' \frac{d^3\mathbf{r}}{V_{\mathbf{r}}} e^{i\mathbf{k}\cdot\mathbf{x}} e^{i\mathbf{k}'\cdot\mathbf{s}'} e^{-ifk_{\parallel}u_{\parallel}} (1+\delta) \\
&= - \int d^3\mathbf{x}d^3\mathbf{s}' e^{i\mathbf{k}\cdot\mathbf{x}} e^{i\mathbf{k}'\cdot\mathbf{s}'} \left\langle e^{-ifk_{\parallel}u_{\parallel}} (1+\delta) \right\rangle \\
&= - \int d^3\mathbf{x}d^3\mathbf{s}' e^{i\mathbf{k}\cdot\mathbf{x}} e^{i\mathbf{k}'\cdot\mathbf{s}'} \\
&= - (2\pi)^6 \delta_D(\mathbf{k}) \delta_D(\mathbf{k}').
\end{aligned} \tag{2.154}$$

The third term reads

$$\int d^3\mathbf{x}d^3\mathbf{x}' \frac{d^3\mathbf{r}}{V_{\mathbf{r}}} e^{i\mathbf{k}\cdot\mathbf{x}} e^{i\mathbf{k}'\cdot\mathbf{x}'} e^{-if(k_{\parallel}u_{\parallel}+k'_{\parallel}u'_{\parallel})} J J' = \int d^3\mathbf{s}d^3\mathbf{s}' e^{i\mathbf{k}\cdot\mathbf{s}} e^{i\mathbf{k}'\cdot\mathbf{s}'} = (2\pi)^6 \delta_D(\mathbf{k}) \delta_D(\mathbf{k}'), \tag{2.155}$$

making the total expression of the TNS contribution

$$\begin{aligned}
(2\pi)^3 \delta_D(\mathbf{k} + \mathbf{k}') P_s(\mathbf{k}, \mathbf{k}') &= (2\pi)^3 \delta_D(\mathbf{k} + \mathbf{k}') \int d^3\mathbf{r} e^{i\mathbf{k}\cdot\mathbf{r}} \left\langle e^{-ifk_{\parallel}\Delta u_{\parallel}} (1+\delta)(1+\delta') \right\rangle + \\
&\quad - (2\pi)^6 \delta_D(\mathbf{k}) \delta_D(\mathbf{k}').
\end{aligned} \tag{2.156}$$

Here it is important to stress that even if, in full generality, the product of two Dirac delta functions is not well defined, in this case it turns out to be harmless. To see that we can recall the demonstration done in Section 2.5 to explicit the form of the total matter PS: we need to think of equation (2.156) as inserted in (2.53), where it is preceded by two inverse Fourier transforms. By making use of the one which integrates over $d^3\mathbf{k}'$ as we did for equation (2.56), equation (2.156) then becomes

$$P_s(k) = \int d^3\mathbf{r} e^{i\mathbf{k}\cdot\mathbf{r}} \left\langle e^{-ifk_{\parallel}\Delta u_{\parallel}} (1+\delta)(1+\delta') \right\rangle - (2\pi)^3 \delta_D(\mathbf{k}), \tag{2.157}$$

showing that it satisfies equation (2.53) and the two models are equivalent.

2.8.1 A New Definition for the Generating Function

To better grasp the difference between the various models, it is useful to redefine the pairwise velocity generating function (2.60) in the following way

$$\mathcal{Z}(\lambda, \mathbf{r}) := (1 + \xi)\mathcal{M}(\lambda, \mathbf{r}) = \left\langle e^{\lambda\Delta u_{\parallel}}(1 + \delta)(1 + \delta') \right\rangle, \quad (2.158)$$

which is very useful for the comparison between different models [57]. Then the form of the generating function for the streaming model of Section 2.5 is obtained from equation (2.147) [57, 58]

$$\begin{aligned} \mathcal{Z}(\lambda, \mathbf{r}) = \exp \left\{ \left\langle e^{\lambda\Delta u_{\parallel}} \right\rangle_c \right\} & \left[1 + \left\langle e^{\lambda\Delta u_{\parallel}} \delta \right\rangle_c + \left\langle e^{\lambda\Delta u_{\parallel}} \delta' \right\rangle_c + \right. \\ & \left. + \left\langle e^{\lambda\Delta u_{\parallel}} \delta \right\rangle_c \left\langle e^{\lambda\Delta u_{\parallel}} \delta' \right\rangle_c + \left\langle e^{\lambda\Delta u_{\parallel}} \delta \delta' \right\rangle_c \right]. \end{aligned} \quad (2.159)$$

With the previous definition we can compare different models by looking at how the form of (2.158) can be expressed under different assumptions; as an example, below we report its form for an exact Gaussian field [58]

$$\mathcal{Z}^G(\lambda, \mathbf{r}) = \exp \left\{ \frac{\lambda^2}{2} \langle \Delta u_{\parallel}^2 \rangle \right\} [1 + \xi(r) + \lambda \langle \Delta u_{\parallel}(\delta + \delta') \rangle + \lambda^2 \langle \Delta u_{\parallel} \delta \rangle \langle \Delta u_{\parallel} \delta' \rangle], \quad (2.160)$$

for which both the FOG exponential and the Kaiser term in the square brackets have been expanded around $\lambda = 0$ and the contributions of pairwise velocity terms different from the second one have been neglected according to the considerations given in Section 2.5.1 [58]. The derivation of equation (2.160) from (2.159) implies also linear dynamics, making the velocity proportional to the density contrast according to equation (2.29).

The two can then be compared with the one derived using the TNS model assumptions [57]; to retrieve it we exploit the equivalence between the streaming and the TNS model we have demonstrated in Section 2.8. Before proceeding, we take advantage of the negligible result coming from the interaction of the corrective terms of Section 2.7.3 [57, 77], $T(k, \mu)$ and $F(k, \mu)$, by using the TNS model expressed in its original derivation without them [68]. We start our derivation by applying the TNS approach to the *exact* equation (2.159), namely we perturbatively expand the Kaiser term for $\lambda = 0$

$$\begin{aligned} \mathcal{Z}^{\text{TNS}}(\lambda, \mathbf{r}) = \exp \left\{ \left\langle e^{\lambda\Delta u_{\parallel}} \right\rangle_c \right\} & \left[1 + \langle \delta \rangle_c + \lambda \langle \Delta u_{\parallel} \delta \rangle_c + \frac{\lambda^2}{2} \langle \Delta u_{\parallel}^2 \delta \rangle_c + \langle \delta' \rangle_c + \lambda \langle \Delta u_{\parallel} \delta' \rangle_c + \right. \\ & + \frac{\lambda^2}{2} \langle \Delta u_{\parallel}^2 \delta' \rangle_c + \langle \delta \rangle_c \langle \delta' \rangle_c + \lambda (\langle \delta \rangle_c \langle \Delta u_{\parallel} \delta' \rangle_c + \langle \Delta u_{\parallel} \delta \rangle_c \langle \delta' \rangle_c) + \\ & \left. + \lambda^2 \langle \Delta u_{\parallel} \delta \rangle_c \langle \Delta u_{\parallel} \delta' \rangle_c + \langle \delta \delta' \rangle_c + \lambda \langle \Delta u_{\parallel} \delta \delta' \rangle_c + \frac{\lambda^2}{2} \langle \Delta u_{\parallel}^2 \delta \delta' \rangle_c \right] \end{aligned} \quad (2.161)$$

and use the fact that δ and δ' are perturbations to get rid of the vanishing terms involving $\langle \delta \rangle_c = \langle \delta' \rangle_c = 0$

$$\begin{aligned} \mathcal{Z}^{\text{TNS}}(\lambda, \mathbf{r}) = \exp \left\{ \left\langle e^{\lambda\Delta u_{\parallel}} \right\rangle_c \right\} & \left[1 + \lambda \langle \Delta u_{\parallel} \delta \rangle_c + \frac{\lambda^2}{2} \langle \Delta u_{\parallel}^2 \delta \rangle_c + \lambda \langle \Delta u_{\parallel} \delta' \rangle_c + \frac{\lambda^2}{2} \langle \Delta u_{\parallel}^2 \delta' \rangle_c + \right. \\ & \left. + \lambda^2 \langle \Delta u_{\parallel} \delta \rangle_c \langle \Delta u_{\parallel} \delta' \rangle_c + \langle \delta \delta' \rangle_c + \lambda \langle \Delta u_{\parallel} \delta \delta' \rangle_c + \frac{\lambda^2}{2} \langle \Delta u_{\parallel}^2 \delta \delta' \rangle_c \right]. \end{aligned} \quad (2.162)$$

To convert the various ensemble averages into their unconnected counterparts we use equation (2.117) for products of two and three fields, while for products involving four fields we apply [38]

$$\begin{aligned}
\langle X_j X_k X_l X_m \rangle_c &= \langle X_j X_k X_l X_m \rangle - \{ \langle X_j \rangle \langle X_k X_l X_m \rangle + \text{cycl.} \} + \\
&\quad - \{ \langle X_j X_k \rangle \langle X_l X_m \rangle + \langle X_j X_l \rangle \langle X_k X_m \rangle + \langle X_j X_m \rangle \langle X_k X_l \rangle \} + \\
&\quad + 2 \{ \langle X_j \rangle \langle X_k \rangle \langle X_l X_m \rangle + \langle X_j \rangle \langle X_l \rangle \langle X_k X_m \rangle + \langle X_j X_m \rangle \langle X_k X_l \rangle \} + \\
&\quad + \langle X_j X_k \rangle \langle X_l \rangle \langle X_m \rangle + \langle X_j X_l \rangle \langle X_k \rangle \langle X_m \rangle + \langle X_j X_m \rangle \langle X_k \rangle \langle X_l \rangle \} + \\
&\quad - 6 \langle X_j \rangle \langle X_k \rangle \langle X_l \rangle \langle X_m \rangle ;
\end{aligned} \tag{2.163}$$

with that we have

$$\langle \delta \delta' \rangle_c = \langle \delta \delta' \rangle - \langle \delta \rangle \langle \delta' \rangle \equiv \langle \delta \delta' \rangle \tag{2.164}$$

$$\langle \Delta u_{ii} \delta \rangle_c = \langle \Delta u_{ii} \delta \rangle - \langle \Delta u_{ii} \rangle \langle \delta \rangle \equiv \langle \Delta u_{ii} \delta \rangle \tag{2.165}$$

$$\begin{aligned}
\langle \Delta u_{ii}^2 \delta \rangle_c &= \langle \Delta u_{ii}^2 \delta \rangle + 2 \langle \Delta u_{ii} \rangle \langle \Delta u_{ii} \rangle \langle \delta \rangle - 2 \langle \Delta u_{ii} \rangle \langle \Delta u_{ii} \delta \rangle - \langle \delta \rangle \langle \Delta u_{ii}^2 \rangle \equiv \langle \Delta u_{ii}^2 \delta \rangle \\
&\implies \langle \Delta u_{ii}^2 \delta' \rangle_c = \langle \Delta u_{ii}^2 \delta' \rangle
\end{aligned} \tag{2.166}$$

$$\begin{aligned}
\langle \Delta u_{ii} \delta \delta' \rangle_c &= \langle \Delta u_{ii} \delta \delta' \rangle + 2 \langle \Delta u_{ii} \rangle \langle \delta \rangle \langle \delta' \rangle - \langle \Delta u_{ii} \rangle \langle \delta \delta' \rangle - \langle \delta \rangle \langle \Delta u_{ii} \delta' \rangle - \langle \delta' \rangle \langle \Delta u_{ii} \delta \rangle \equiv \\
&\equiv \langle \Delta u_{ii} \delta \delta' \rangle
\end{aligned} \tag{2.167}$$

$$\begin{aligned}
\langle \Delta u_{ii}^2 \delta \delta' \rangle_c &= \langle \Delta u_{ii}^2 \delta \delta' \rangle - \{ \langle \Delta u_{ii} \rangle \langle \Delta u_{ii} \delta \delta' \rangle + \text{cycl.} \} - \{ \langle \Delta u_{ii}^2 \rangle \langle \delta \delta' \rangle + 2 \langle \Delta u_{ii} \delta \rangle \langle \Delta u_{ii} \delta' \rangle \} + \\
&\quad + 2 \{ \langle \Delta u_{ii} \rangle \langle \Delta u_{ii} \rangle \langle \delta \delta' \rangle + \text{cycl.} \} - 6 \langle \Delta u_{ii} \rangle \langle \Delta u_{ii} \rangle \langle \delta \rangle \langle \delta' \rangle \equiv \\
&\equiv \langle \Delta u_{ii}^2 \delta \delta' \rangle - \langle \Delta u_{ii}^2 \rangle \langle \delta \delta' \rangle - 2 \langle \Delta u_{ii} \delta \rangle \langle \Delta u_{ii} \delta' \rangle ,
\end{aligned} \tag{2.168}$$

where the quantities on the right of the equivalence symbols are the remaining ones after enforcing symmetry considerations. Once inserted into (2.162) and grouped by powers of λ , the equations above give

$$\begin{aligned}
\mathcal{Z}^{\text{TNS}}(\lambda, \mathbf{r}) &= \exp \left\{ \left\langle e^{\lambda \Delta u_{ii}} \right\rangle_c \right\} \left[1 + \xi + \lambda \langle \Delta u_{ii} (\delta + \delta' + \delta \delta') \rangle + \right. \\
&\quad \left. + \frac{\lambda^2}{2} \{ \langle \Delta u_{ii}^2 (\delta + \delta' + \delta \delta') \rangle - \langle \Delta u_{ii}^2 \rangle \xi \} \right] .
\end{aligned} \tag{2.169}$$

Taking advantage of the fact that $\langle \Delta u_{ii} \rangle = 0$ due to symmetry, we can add it to the $O(\lambda)$ term without consequences while, on the other hand, we have to keep in mind $\langle \Delta u_{ii}^2 \rangle \neq 0$ for the $O(\lambda^2)$ contribution. Thus, from the definition of the real space 2PCF (1.63) we can write

$$\begin{aligned}
\mathcal{Z}^{\text{TNS}}(\lambda, \mathbf{r}) &= \exp \left\{ \left\langle e^{\lambda \Delta u_{ii}} \right\rangle_c \right\} \left[\langle (1 + \delta)(1 + \delta') \rangle + \lambda \langle \Delta u_{ii} (1 + \delta)(1 + \delta') \rangle + \right. \\
&\quad \left. + \frac{\lambda^2}{2} \{ \langle \Delta u_{ii}^2 (1 + \delta)(1 + \delta') \rangle - \langle \Delta u_{ii}^2 \rangle (1 + \xi) \} \right] .
\end{aligned} \tag{2.170}$$

Recalling now the definition of the pairwise velocity dispersion (2.68), as well as equation (2.85), we can express the $O(\lambda^2)$ term as [58]

$$\langle \Delta u_{ii}^2 (1 + \delta)(1 + \delta') \rangle - \langle \Delta u_{ii}^2 \rangle (1 + \xi) = \langle \Delta u_{ii}^2 (\delta + \delta') \rangle + \langle \Delta u_{ii}^2 \delta \delta' \rangle_c , \tag{2.171}$$

where $\langle \Delta u_{\parallel}^2 \delta \delta' \rangle_c$ corresponds to the $O(\lambda^3)$ contribution $\langle A_1^2 A_2 A_3 \rangle_c$ of Section 2.7.3 if one substitutes (2.146) rather than (2.114). Therefore it is not considered in the TNS approach [57, 68, 77] (see the final comment on equation (2.143)). Here we stress once more that this substitution can be performed with such an ease thanks to the equivalence between the two models we have demonstrated in Section 2.8; for what concerns the expansion of the Kaiser term, one has just to have in mind that (2.146) comes from a J -independent model, which could be extended in multi-streaming regions, while (2.114) arises from a model that maintain an explicit J dependence. From those considerations we finally arrive to the final expression of the TNS pairwise velocity generating function

$$\mathcal{Z}^{\text{TNS}}(\lambda, \mathbf{r}) = \exp \left\{ \left\langle e^{\lambda \Delta u_{\parallel}} \right\rangle_c \right\} \left[\langle (1 + \delta)(1 + \delta') \rangle + \lambda \langle \Delta u_{\parallel} (1 + \delta)(1 + \delta') \rangle + \frac{\lambda^2}{2} \langle \Delta u_{\parallel}^2 (\delta + \delta') \rangle \right], \quad (2.172)$$

which gets rid of (possible) typos in equation (64) of [57]. By comparing (2.172) with the generating function resulting from Gaussianity, (2.160), one can see that differences arise in both the FOG term and the $O(\lambda^2)$ one of the Kaiser contribution, with the Gaussian approach resulting in a much more simplified expression of the exponential prefactor and a Kaiser term expressed by simpler statistical quantities.

From the demonstration above we have also given an explanation of why the TNS method ends up with no explicit dependence upon v_{12}^2 as the Gaussian streaming model does: even if it is derived from the exact relation (2.159), the perturbative treatment of the Kaiser term makes the contribution coming from $\langle e^{\lambda \Delta u_{\parallel} \delta} \rangle_c \langle e^{\lambda \Delta u_{\parallel} \delta'} \rangle_c$, which obviously is still present, to be incorporated into the $O(\lambda^2)$ terms that ends up being equal to $\langle \Delta u_{\parallel}^2 (\delta + \delta') \rangle$.

3. Nonlinear Description of the Redshift Space 2PCF

With this third Chapter we want to write the redshift space behaviour of the 2PCF as done in [34] but exploiting the TNS description of RSDs, as well as various models present in the current scientific debate. The main goal is to obtain a description of the redshift space 2PCF accounting for the nonlinear terms, from which it will be possible to expand and improve the derivation given in [34] and retrieve information about cosmological parameters as illustrated in Section 1.5.2. To do so, we use formalisms we have summarized in Chapter 2, throughout Sections 2.5 and 2.7. We proceed as follows

- In Section 3.1 we give a brief summary of the results presented in [34], with the intent of rebuilding their large scale expansion of the redshift space 2PCF following our nomenclature.
- Through Section 3.2 we arrive at a description of the pairwise velocity PDF following the TNS approach and examine it against the one obtained assuming Gaussianity in [58], which is the one determining the results of [34], while in Section 3.2.1 we convert the Fourier space description of RSDs coming from the TNS approach into configuration space so that they become directly comparable with outcomes from [34].
- In Section 3.3 we report a third approach proposed by B. Reid and M. White in 2011 [55] which agrees with both of the previous two at linear order. Going beyond linear order, we show it is able to recover [34], but also TNS if one matches the different way of reasoning given in [68].
- In Section 3.4 we go back to the more general procedure to obtain the large-scale expansion proposed by R. Scoccimarro in [58], trying to understand how it can improve results coming from [34] if one accounts for nonlinear contributions; with Sections 3.4.1 we revise the multipole expansion (2.108) considering nonlinearities.
- Finally, in Section 3.5 we look at how a nonlinear description of the redshift space 2PCF affects the BAO acoustic peak and, from that, our ability to probe DE and cosmological parameters.

3.1 On the D. Jeong et al. Description of the Redshift Space 2PCF

In this Section we intend to briefly summarize the results present in [34] in order to have a coherent notation throughout the entire thesis and, therefore, to better understand the differences coming from the addition of nonlinear terms we will do in Section 3.4. To do so, we start from the pairwise velocity generating function obtained under the assumption of Gaussianity of perturbations presented

in equation (2.160) and here given with the Kaiser contribution, collected inside the square brackets, written in terms of powers of the mean pairwise velocity (expressed as in equations (2.78) and (2.83))

$$\mathcal{Z}^G(\lambda, \mathbf{r}) = \exp \left\{ \frac{\lambda^2}{2} \langle \Delta u_{ii}^2 \rangle \right\} (1 + \xi) \left[1 + \lambda v_{12} + \frac{\lambda^2}{4} v_{12}^2 (1 + \xi) \right]. \quad (3.1)$$

Following the procedure proposed by R. Scoccimarro in [58], if one is interested in linear theory it is possible to expand the Gaussian generating function of equation (2.160) for large scales, namely for $\lambda = 0$ (recall that $\lambda = -ifk_{ii} \equiv -if\gamma$ in Fourier and configuration space respectively [57, 58])

$$\mathcal{Z}^G(\lambda, \mathbf{r}) \simeq \mathcal{Z}^G(\lambda = 0, \mathbf{r}) + \left. \frac{d\mathcal{Z}^G(\lambda, \mathbf{r})}{d\lambda} \right|_{\lambda=0} \lambda + \left. \frac{d^2\mathcal{Z}^G(\lambda, \mathbf{r})}{d\lambda^2} \right|_{\lambda=0} \frac{\lambda^2}{2} + \mathcal{O}(\lambda^2). \quad (3.2)$$

In order to have a simple derivation, let us rename the Kaiser term inside (3.1) as $A(\lambda, \mathbf{r}) := 1 + \lambda v_{12} + \lambda^2 [v_{12}^2 (1 + \xi)]/4$, which makes (3.1)

$$\mathcal{Z}^G(\lambda, \mathbf{r}) = \exp \left\{ \frac{\lambda^2}{2} \langle \Delta u_{ii}^2 \rangle \right\} (1 + \xi) A(\lambda, \mathbf{r}). \quad (3.3)$$

Thus the derivatives inside the expansion (3.2) read

$$\begin{aligned} \mathcal{Z}^G(0, \mathbf{r}) &= 1 + \xi, \\ \left. \frac{d\mathcal{Z}^G(\lambda, \mathbf{r})}{d\lambda} \right|_{\lambda=0} &= (1 + \xi) \left[v_{12} + \frac{\lambda}{2} v_{12}^2 (1 + \xi) \right] \exp \left\{ \frac{\lambda^2}{2} \langle \Delta u_{ii}^2 \rangle \right\} \Big|_{\lambda=0} + \\ &\quad + (1 + \xi) A(\lambda, \mathbf{r}) \exp \left\{ \frac{\lambda^2}{2} \langle \Delta u_{ii}^2 \rangle \right\} \lambda \langle \Delta u_{ii}^2 \rangle \Big|_{\lambda=0} \\ &= v_{12} (1 + \xi) \end{aligned} \quad (3.4)$$

and

$$\begin{aligned} \left. \frac{d^2\mathcal{Z}^G(\lambda, \mathbf{r})}{d\lambda^2} \right|_{\lambda=0} &= \frac{1}{2} (1 + \xi)^2 v_{12}^2(\mathbf{r}) \exp \left\{ \frac{\lambda^2}{2} \langle \Delta u_{ii}^2 \rangle \right\} \Big|_{\lambda=0} + \\ &\quad + 2(1 + \xi) \left[v_{12} + \frac{\lambda}{2} v_{12}^2 (1 + \xi) \right] \exp \left\{ \frac{\lambda^2}{2} \langle \Delta u_{ii}^2 \rangle \right\} \lambda \langle \Delta u_{ii}^2 \rangle \Big|_{\lambda=0} + \\ &\quad + (1 + \xi) A(\lambda, \mathbf{r}) \exp \left\{ \frac{\lambda^2}{2} \langle \Delta u_{ii}^2 \rangle \right\} \lambda^2 \langle \Delta u_{ii}^2 \rangle^2 \Big|_{\lambda=0} + \\ &\quad + (1 + \xi) A(\lambda, \mathbf{r}) \exp \left\{ \frac{\lambda^2}{2} \langle \Delta u_{ii}^2 \rangle \right\} \langle \Delta u_{ii}^2 \rangle \Big|_{\lambda=0} \\ &= \frac{1}{2} (1 + \xi)^2 v_{12}^2 + (1 + \xi) \langle \Delta u_{ii}^2 \rangle, \end{aligned} \quad (3.5)$$

which once coupled together give

$$\mathcal{Z}^G(\lambda, \mathbf{r}) \simeq 1 + \xi + \lambda(1 + \xi)v_{12} + \frac{\lambda^2}{2}(1 + \xi) \langle \Delta u_{ii}^2 \rangle + \frac{\lambda^2}{4}(1 + \xi)^2 v_{12}^2 + \mathcal{O}(\lambda^2). \quad (3.6)$$

By placing ourselves in the limit where both the real space 2PCF and the pairwise velocity are small quantities, $\xi \ll 1$ and $v_{12} \ll 1$, we are now able to simplify further (3.2) (equation (59) of [58])

$$\mathcal{Z}^G(\lambda, \mathbf{r}) \simeq 1 + \xi + \lambda v_{12} + \frac{\lambda^2}{2} \langle \Delta u_{\parallel}^2 \rangle + \mathcal{O}(\lambda^2). \quad (3.7)$$

From (3.6), it is then possible to retrieve the pairwise velocity PDF using equation (2.63) (equation (60) of [58])

$$\mathcal{P}^G(y, \mathbf{r}) \simeq \left(1 + f v_{12} \frac{d}{dy} + \frac{f^2}{2} \langle \Delta u_{\parallel}^2 \rangle \frac{d^2}{dy^2} + \mathcal{O}(y^2) \right) \delta_D(y). \quad (3.8)$$

The equation above can be easily computed by exploiting the fact that the pairwise velocity PDF has been defined as the inverse Fourier transform of the generating function (in either its $\mathcal{M}(\lambda, \mathbf{r})$ or $\mathcal{Z}(\lambda, \mathbf{r})$ form), coupled with the following property of the Fourier transform [3]

$$\mathcal{F}[\gamma^n f(\gamma)](y) = i^{-n} \frac{d^n}{dy^n} F(y), \quad (3.9)$$

with $\mathcal{F}[\cdot](y)$ representing the Fourier transform from the γ domain to the y one and $F(y)$ being the Fourier pair of the function $f(\gamma)$. Explicitly we have (recall that in configuration space $\lambda = -if\gamma$)

$$\begin{aligned} \mathcal{P}^G(y, \mathbf{r}) &\simeq \int \frac{d\gamma}{2\pi} e^{-i\gamma y} \frac{1}{1 + \xi} \mathcal{Z}^G(\lambda, \mathbf{r}) \\ &= \int \frac{d\gamma}{2\pi} e^{-i\gamma y} \left(1 + \lambda v_{12} + \frac{\lambda^2}{2} \langle \Delta u_{\parallel}^2 \rangle + \mathcal{O}(y^2) \right) \\ &= \left(1 + f v_{12} \frac{d}{dy} + \frac{f^2}{2} \langle \Delta u_{\parallel}^2 \rangle \frac{d^2}{dy^2} + \mathcal{O}(y^2) \right) \delta_D(y), \end{aligned} \quad (3.10)$$

where for the one dimensional Dirac delta we have used the same convention of (1.67). Here it is important to highlight the fact that the sign difference between equation (3.8) and the correspondent equation in [58] comes from the fact that our definition of the real-to-redshift separation, $y := s_{\parallel} - r_{\parallel} \equiv \Delta v_{\parallel}/\mathcal{H}$ and theirs, $v := r_{\parallel} - s_{\parallel}$ are one the opposite of the other, making the minus sign at the first order term being absorbed in the derivative

$$y = -v \implies \frac{df}{dy} = -\frac{df}{dv}, \quad \frac{d^2 f}{dy^2} = \frac{d^2 f}{dv^2}. \quad (3.11)$$

Also, from our definition of y we have that

$$y := s_{\parallel} - r_{\parallel} \quad \& \quad y = 0 \implies \frac{df}{dy} = \frac{df}{ds_{\parallel}} = -\frac{df}{dr_{\parallel}}. \quad (3.12)$$

From that, it is possible to insert the large scale PDF (3.8) into the streaming model (2.67) to obtain

$$1 + \xi_s(s_{\perp}, s_{\parallel}) = \int dy (1 + \xi) \left(1 + f v_{12} \frac{d}{dy} + \frac{1}{2} f^2 \langle \Delta u_{\parallel}^2 \rangle \frac{d^2}{dy^2} \right) \delta_D(y). \quad (3.13)$$

Before integrating however, it is necessary to explicit the y -dependence of the real space 2PCF using the definition of y we have given above, coupled with the real-to-redshift map of equation (2.5), inside the description of the magnitude of r

$$\begin{aligned}
r &= \sqrt{r_{\perp}^2 + r_{\parallel}^2} = \sqrt{s_{\perp}^2 + (s_{\parallel} - y)^2} \\
&= \sqrt{s_{\perp}^2 + s_{\parallel}^2 + y^2 - 2s_{\parallel}y} \\
&= \sqrt{\tilde{s}^2 + y^2 - 2s_{\parallel}y},
\end{aligned} \tag{3.14}$$

where we have used $r_{\perp} = s_{\perp}$. Also, as defined in Section 2.1, \tilde{s} represents the redshift separation between two galaxies. With that in mind the real space 2PCF reads

$$1 + \xi(r) = 1 + \xi \left(\sqrt{\tilde{s}^2 + y^2 - 2s_{\parallel}y} \right). \tag{3.15}$$

Then, the integration of equation (3.13) can be performed easily thanks to the defining property of the Dirac delta function [56], namely

$$\int f(y)\delta(y - a) = f(a), \quad a \in \mathbb{R}. \tag{3.16}$$

Hence we can write

$$1 + \xi_s(s_{\perp}, s_{\parallel}) = 1 + \xi(r) - f \frac{dv_{12}}{dr_{\parallel}} + \frac{1}{2} f^2 \frac{d^2 \langle \Delta u_{\parallel}^2 \rangle}{dr_{\parallel}^2} + \mathcal{O}(\xi^2), \tag{3.17}$$

where it was possible to set $r_{\parallel} = s_{\parallel}$ thanks to the $y = 0$ condition. Here it is important to stress some differences between the nomenclature used in this work and the one present in [34]: although we have defined the real to redshift separation $y := s_{\parallel} - r_{\parallel}$ in the same way as [34], what they call $\langle y \rangle$, $\langle y^2 \rangle$ and $\mathbf{v}_{12}(\mathbf{r})$ differs from our notation. We have reported a map collecting all the different definitions between the two works in Table 3.1. Recalling now that the last term in (3.17) coincides with the linear dynamics description of the second pairwise velocity moment, we can see that the result given by D. Jeong et al. in [34] uses the large scale description of the general pairwise velocity first moment while, see equation (2.85), the pairwise velocity dispersion enters only with its linear description we have called $\sigma_{12}^{2,LD}$

$$1 + \xi_s(s_{\perp}, s_{\parallel}) = 1 + \xi(r) - f \frac{dv_{12}}{dr_{\parallel}} + \frac{1}{2} f^2 \frac{d^2 \sigma_{12}^{2,LD}}{dr_{\parallel}^2} + \mathcal{O}(\xi^2). \tag{3.18}$$

By looking at Table 3.1, we want too highlight the fact that the quantity equivalent to $\langle y \rangle$ is not v_{12} but rather the product between the first cumulant with the 2PCF of matter, $v_{12}(1 + \xi)$, making the exact equivalence the one reported in the Table. However, one needs to recall equation (3.18) has been retrieved after a large scale expansion and, therefore, in a regime where the condition $\xi \ll 1$ holds: this allows to set the equivalence of Table 3.1 as

$$v_{12}(1 + \xi) \simeq v_{12} \equiv \langle y \rangle. \tag{3.19}$$

Table 3.1: Summary of the different definitions between the present work and [34]. For each quantity, the first line of the "Notation" column reports our definition while the second one the symbols used in the paper by D. Jeong et al.; if only one line is present the two definitions coincide. Note that we have never defined the pairwise velocity before, but only its mean value. However one can retrieve it by multiplying (2.6) with $(1 + \delta)(1 + \delta')$ as explained in [24].

	Reference Equation	Notation
Real-to-Redshift Displacement:	(2.62)	$y := s_{\parallel} - r_{\parallel}$
Pairwise Velocity:	(2.6)	$\Delta u_{\parallel}(1 + \delta)(1 + \delta')$ $\mathcal{H}\mathbf{v}_{12}(\mathbf{r}) \cdot \hat{\mathbf{z}}$
1 st Pairwise Velocity Moment:	(2.68)	$f v_{12}(1 + \xi) := \langle \Delta u_{\parallel}(1 + \delta)(1 + \delta') \rangle$ $\langle y \rangle \equiv \langle \mathbf{v}_{12,\parallel}(\mathbf{r}) \rangle / \mathcal{H}$
Mean of the Squared Pairwise Velocity:	(2.86)	$f^2 \langle \Delta u_{\parallel}^2(1 + \delta)^2(1 + \delta')^2 \rangle$ $\langle y^2 \rangle \equiv \langle \mathbf{v}_{12}^2(\mathbf{r}) \rangle / \mathcal{H}^2$

Following the same reasoning, the linear dynamics second cumulant reads

$$\sigma_{12}^{2\text{LD}} \equiv \langle \Delta u_{\parallel}^2 \rangle \equiv \langle y^2 \rangle \quad (3.20)$$

and hence, by enforcing the equivalences above we can now easily see that equation (3.18) is exactly equation (17) of [34].

3.2 Toward a Configuration Space Description of the TNS Model

Through Chapter 2 we have illustrated how it is possible to describe nonlinear features present in galaxy clustering using general properties, such homogeneity and isotropy of perturbations, as well as symmetries of galaxy density and velocity fields. Furthermore, staying within a Newtonian treatment and plane-parallel approximation, we have shown and emphasized that the streaming model of Section 2.5 is the most general way to describe the clustering phenomenon at nonlinear scales, while the TNS model of Section 2.7 is, yes, able to expand and improve the description of the same concepts at the BAO scale, but it needs the introduction of some more caveats. The other difference between the two presented works is the fact that the former gives a description of the clustering phenomenon in configuration space while the latter focuses on Fourier space, making the confrontation between the two complicated.

In this Section we want to convert the equations of the TNS model back in configuration space; by doing that we will be able to compare them with the results proposed by R. Scoccimarro [58] in 2004. First of all we report the expression of the pairwise velocity generating function $\mathcal{Z}(\lambda, \mathbf{r})$ following the assumptions of the TNS model, equation (2.172)

$$\mathcal{Z}^{\text{TNS}}(\lambda, \mathbf{r}) = \exp \left\{ \left\langle e^{\lambda \Delta u_{\parallel}} \right\rangle_c \right\} \left[\langle (1 + \delta)(1 + \delta') \rangle + \lambda \langle \Delta u_{\parallel}(1 + \delta)(1 + \delta') \rangle + \frac{\lambda^2}{2} \langle \Delta u_{\parallel}^2(\delta + \delta') \rangle \right], \quad (3.21)$$

which can be written in a more useful way using the definitions of the real space 2PCF (1.63) and mean pairwise velocity (2.68), as well as the configuration space description of the scale parameter $\lambda = -if\gamma$

$$\begin{aligned} \mathcal{Z}^{\text{TNS}}(-if\gamma, \mathbf{r}) &= \exp \left\{ \left\langle e^{-if\gamma\Delta u_{\parallel}} \right\rangle_c \right\} \times \\ &\times \left[1 + \xi - if\gamma v_{12}(1 + \xi) - \frac{f^2\gamma^2}{2} \langle \Delta u_{\parallel}^2(\delta + \delta') \rangle \right]. \end{aligned} \quad (3.22)$$

We can now insert it in the PDF description of equation (2.63) through the definition of \mathcal{Z} given in equation (2.158). Before writing the PDF, let us recall the definition of the real-to-redshift galaxy separation we have given in Section 2.5: $s_{\parallel} - r_{\parallel} = \Delta v_{\parallel}/\mathcal{H} := y$; the PDF then reads¹

$$\begin{aligned} \mathcal{P}(y, \mathbf{r}) &= \int \frac{d\gamma}{2\pi} e^{-i\gamma y} \frac{1}{1 + \xi} \exp \left\{ \left\langle e^{-if\gamma\Delta u_{\parallel}} \right\rangle_c \right\} \times \\ &\times \left[1 + \xi - if\gamma v_{12}(1 + \xi) - \frac{f^2\gamma^2}{2} \langle \Delta u_{\parallel}^2(\delta + \delta') \rangle \right]. \end{aligned} \quad (3.23)$$

With this expression of the PDF in mind, after simplifying the common factor $1 + \xi$ of the Kaiser term with the one outside, the next thing to address is the exponential prefactor describing the FOG effect: to do so we exploit the reasoning we have illustrated in Section 2.7, with equation (2.125),² as an exponential function dependent on the velocity dispersion of the virialized objects, $\sigma_{v, \text{eff}}^2$. This allows us to write

$$\begin{aligned} \mathcal{P}(y, \mathbf{r}) &= \int \frac{d\gamma}{2\pi} \exp \left\{ -i\gamma y - f^2\gamma^2 \sigma_{v, \text{eff}}^2 \right\} \times \\ &\times \left[1 - if\gamma v_{12} - \frac{f^2\gamma^2}{2} \frac{\langle \Delta u_{\parallel}^2(\delta + \delta') \rangle}{1 + \xi} \right]. \end{aligned} \quad (3.24)$$

Since we are trying to describe the form of the redshift space 2PCF, the integral formulation of the pairwise velocity PDF is not very useful, forcing us to find a way to carry on the integration: we can do that if we notice equation (3.24) is constituted by a sum of functions that can be traced back to generic Gaussian ones. With that in mind, we can now divide the PDF above into a sum of three integrals thanks to their additive property, making our show of the computation a little bit cleaner. We start with the first term, which we call $\mathcal{P}^{(1)}(v, \mathbf{r})$, and proceed by noticing that the integration is of the type

$$\int_{-\infty}^{+\infty} dx a \exp \{-bx^2 + cx + d\} = a \sqrt{\frac{\pi}{b}} \exp \left\{ \frac{c^2}{4b} + d \right\}, \quad (3.25)$$

¹The definition of the y quantity allows us to carry on the various derivations without worrying about the $1/\mathcal{H}$ factors to make the velocities in units of length. Notice that we are calling the real-to-redshift separation y following [34], while in the previous works of R. Scoccimarro and the review by S. Saito they call the velocity in units of length v : we have chosen the former way in order to facilitate the final comparison between our results and the ones given in [34].

²Here it is important to recall that now we are working in configuration space and, hence, we need to substitute k_{\parallel}^2 with γ^2 to adapt the FOG description to the configuration space domain.

where in the actual resolution of equation (3.24) we substitute the generic terms with $a = 1/2\pi$, $b = f^2\sigma_{v,\text{eff}}^2$, $c = -iv$ and $d = 0$ obtaining

$$\begin{aligned}\mathcal{P}^{(1)}(y, \mathbf{r}) &= \int \frac{d\gamma}{2\pi} \exp \{-i\gamma y - f^2\gamma^2\sigma_{v,\text{eff}}^2\} = \frac{1}{2\pi} \sqrt{\frac{\pi}{f^2\sigma_{v,\text{eff}}^2}} \exp \left\{ -\frac{y^2}{4f^2\sigma_{v,\text{eff}}^2} \right\} \\ &= \frac{1}{f\sqrt{2\pi}(2\sigma_{v,\text{eff}}^2)^{1/2}} \exp \left\{ -\frac{y^2}{4f^2\sigma_{v,\text{eff}}^2} \right\}.\end{aligned}\quad (3.26)$$

Thus the first term of equation (3.24) turns out to be an exact Gaussian centred at $v = 0$ with $\sigma = f(2\sigma_{v,\text{eff}}^2)^{1/2}$. For the second term, the one involving the first moment, v_{12} , we can see that the integration is of the type

$$\int_{-\infty}^{+\infty} dx cx \exp \{-a(x-b)^2\} = cb\sqrt{\frac{\pi}{a}} \quad (3.27)$$

if we complete the square in the exponential term. Explicitly it reads

$$\begin{aligned}\mathcal{P}^{(2)}(y, \mathbf{r}) &= -ifv_{12} \int \frac{d\gamma}{2\pi} \gamma \exp \{-i\gamma y - f^2\gamma^2\sigma_{v,\text{eff}}^2\} \\ &= -ifv_{12} \int \frac{d\gamma}{2\pi} \gamma \exp \left\{ -i\gamma y - f^2\gamma^2\sigma_{v,\text{eff}}^2 + \frac{i^2y^2}{4f^2\sigma_{v,\text{eff}}^2} - \frac{i^2y^2}{4f^2\sigma_{v,\text{eff}}^2} \right\} \\ &= -ifv_{12} \int \frac{d\gamma}{2\pi} \gamma \exp \left\{ -f^2\sigma_{v,\text{eff}}^2 \left(\gamma^2 + \frac{i\gamma y}{f^2\sigma_{v,\text{eff}}^2} + \frac{i^2y^2}{4f^4(\sigma_{v,\text{eff}}^2)^2} \right) + \frac{i^2y^2}{4f^2\sigma_{v,\text{eff}}^2} \right\} \\ &= -ifv_{12} \int \frac{d\gamma}{2\pi} \gamma \exp \left\{ -f^2\sigma_{v,\text{eff}}^2 \left(\gamma + \frac{i\gamma y}{2f^2\sigma_{v,\text{eff}}^2} \right)^2 \right\} \exp \left\{ \frac{i^2y^2}{4f^2\sigma_{v,\text{eff}}^2} \right\}\end{aligned}\quad (3.28)$$

with, referring to the generic integration of equation (3.27), $a = f^2\sigma_{v,\text{eff}}^2$, $b = -iy/2f^2\sigma_{v,\text{eff}}^2$ and $c = -ifv_{12}(\mathbf{r}) \exp \{i^2v^2/4f^2\sigma_{v,\text{eff}}^2\}/2\pi$. Implementing all the substitutions we have

$$\begin{aligned}\mathcal{P}^{(2)}(y, \mathbf{r}) &= \frac{ifv_{12}}{2\pi} \exp \left\{ -\frac{y^2}{4f^2\sigma_{v,\text{eff}}^2} \right\} \frac{iy}{2f^2\sigma_{v,\text{eff}}^2} \sqrt{\frac{\pi}{f^2\sigma_{v,\text{eff}}^2}} \\ &= -\frac{1}{f\sqrt{2\pi}(2\sigma_{v,\text{eff}}^2)^{1/2}} \exp \left\{ -\frac{y^2}{4f^2\sigma_{v,\text{eff}}^2} \right\} \frac{yv_{12}}{2f\sigma_{v,\text{eff}}^2}.\end{aligned}\quad (3.29)$$

With the general Gaussian integrals of equations (3.25) and (3.27), the computation of the third term inside equation (3.24) comes almost free along the way: indeed what we have to do is completing the square once again

$$\begin{aligned}\mathcal{P}^{(3)}(y, \mathbf{r}) &= -\frac{f^2 \langle \Delta u_{ii}^2(\delta + \delta') \rangle}{2(1 + \xi)} \exp \left\{ -\frac{y^2}{4f^2\sigma_{v,\text{eff}}^2} \right\} \times \\ &\quad \times \int \frac{d\gamma}{2\pi} \gamma^2 \exp \left\{ -f^2\sigma_{v,\text{eff}}^2 \left(\gamma + \frac{i\gamma y}{2f^2\sigma_{v,\text{eff}}^2} \right)^2 \right\}\end{aligned}\quad (3.30)$$

and then perform the following change of the integration variable

$$\eta := \gamma + \frac{iy}{2f^2\sigma_{v,\text{eff}}^2}, \quad d\gamma = d\eta. \quad (3.31)$$

Thus equation (3.30) becomes (we will call the η -independent factor outside the integral of (3.30) " $B(y; \mathbf{r})$ " to lighten the following passages)

$$\begin{aligned} \mathcal{P}^{(3)}(y, \mathbf{r}) &= B(y; \mathbf{r}) \int \frac{d\eta}{2\pi} \left(\eta - \frac{iy}{2f^2\sigma_{v,\text{eff}}^2} \right)^2 \exp \left\{ -f^2\sigma_{v,\text{eff}}^2\eta^2 \right\} \\ &= B(y; \mathbf{r}) \int \frac{d\eta}{2\pi} \left(\eta^2 - \frac{y^2}{4f^4(\sigma_{v,\text{eff}}^2)^2} - \frac{iy\eta}{f^2\sigma_{v,\text{eff}}^2} \right) \exp \left\{ -f^2\sigma_{v,\text{eff}}^2\eta^2 \right\}, \\ B(y; \mathbf{r}) &:= -\frac{f^2 \langle \Delta u_{ii}^2(\delta + \delta') \rangle}{2(1 + \xi)} \exp \left\{ -\frac{y^2}{4f^2\sigma_{v,\text{eff}}^2} \right\}, \end{aligned} \quad (3.32)$$

with which we can exploit once more the additive property of integration to split the sum inside the brackets, making the second and third addenda solvable using equations (3.25) and (3.27) respectively. The first term is now of the type

$$\int_{-\infty}^{+\infty} dx x^2 e^{-ax^2} = \frac{1}{2} \sqrt{\frac{\pi}{a^3}}, \quad (3.33)$$

with $a = f^2\sigma_{v,\text{eff}}^2$. Hence the whole expression for the third integration reads

$$\begin{aligned} \mathcal{P}^{(3)}(y, \mathbf{r}) &= B(y; \mathbf{r}) \left[\frac{1}{4\pi} \sqrt{\frac{\pi}{f^6(\sigma_{v,\text{eff}}^2)^3}} - \frac{y^2}{8\pi f^4(\sigma_{v,\text{eff}}^2)^2} \sqrt{\frac{\pi}{f^2\sigma_{v,\text{eff}}^2}} \right] \\ &= B(y; \mathbf{r}) \left[\frac{1}{f^3\sqrt{2\pi}(2\sigma_{v,\text{eff}}^2)^{3/2}} - \frac{y^2}{f^5\sqrt{2\pi}(2\sigma_{v,\text{eff}}^2)^{5/2}} \right], \end{aligned} \quad (3.34)$$

where we have implemented the appropriate substitutions; in particular we have $c = d = 0$ in (3.25) and $b = 0$ in (3.27). Summing back together the three equations (3.26), (3.29) and (3.34), the PDF determined by the TNS model reads

$$\begin{aligned} \mathcal{P}(y, \mathbf{r}) &= \mathcal{P}^{(1)}(y, \mathbf{r}) + \mathcal{P}^{(2)}(y, \mathbf{r}) + \mathcal{P}^{(3)}(y, \mathbf{r}) \\ &= \frac{1}{f\sqrt{2\pi}(2\sigma_{v,\text{eff}}^2)^{1/2}} \exp \left\{ -\frac{y^2}{4f^2\sigma_{v,\text{eff}}^2} \right\} \left[1 - \frac{yv_{12}}{2f\sigma_{v,\text{eff}}^2} + \right. \\ &\quad \left. - \frac{f^2 \langle \Delta u_{ii}^2(\delta + \delta') \rangle}{2(1 + \xi)} \left(\frac{1}{2f^2\sigma_{v,\text{eff}}^2} - \frac{y^2}{f^4(2\sigma_{v,\text{eff}}^2)^2} \right) \right] \\ &= \frac{1}{f\sqrt{2\pi}(2\sigma_{v,\text{eff}}^2)^{1/2}} \exp \left\{ -\frac{y^2}{4f^2\sigma_{v,\text{eff}}^2} \right\} \left[1 - \frac{yv_{12}}{2f\sigma_{v,\text{eff}}^2} + \right. \\ &\quad \left. + \frac{1}{4} \frac{\langle \Delta u_{ii}^2(\delta + \delta') \rangle}{\sigma_{v,\text{eff}}^2(1 + \xi)} \left(\frac{y^2}{f^2 2\sigma_{v,\text{eff}}^2} - 1 \right) \right], \end{aligned} \quad (3.35)$$

which has to be compared with the PDF coming from the Gaussianity assumption presented in equation (44) of [58] that has been taken, after a large scale ($\lambda = 0$) expansion, as the starting point for [34].

Before comparing equation (3.35) with the results given for a Gaussian field by R. Scoccimarro, it is useful to track down the different notation between the two works, as well as the terms coming from different assumptions. First of all we highlight that our real-to-redshift separation y is related to the one in [58], called v , as $y = s_{\parallel} - r_{\parallel} = \Delta v_{\parallel}/\mathcal{H} \equiv -v$; additionally, we have to take into account also the fundamental assumptions done in the TNS model which made us able to describe the FOG term itself: in Section 2.7, with equation (2.123), we have identified the ensemble average of pairwise velocity powers inside the (unexpanded) FOG term as $\langle A_1^n \rangle_c = \langle \Delta u_{\parallel}^n \rangle_c \simeq 2c_n \sigma_{v,\text{eff}}^n$, with the particular case of our interest $c_2 = 1$. This made us able to write $\langle \Delta u_{\parallel}^2 \rangle \simeq 2\sigma_{v,\text{eff}}^2$ and, ultimately, distinguish factors derived from the FOG exponential, described using the virialized effective velocity dispersion, from the ones describing the second pairwise velocity moment that were originally in the Kaiser term. With that in mind we can now compare the two pairwise velocity PDFs coming respectively from equation (3.35) and equation (44) of [58]

$$\begin{aligned}
\mathcal{P}^{\text{TNS}}(v, \mathbf{r}) &= \frac{1}{f\sqrt{2\pi}(2\sigma_{v,\text{eff}}^2)^{1/2}} \exp\left\{-\frac{v^2}{2f^2(2\sigma_{v,\text{eff}}^2)}\right\} \times \\
&\times \left[1 + \frac{vv_{12}}{f(2\sigma_{v,\text{eff}}^2)} + \frac{1}{2} \frac{\langle \Delta u_{\parallel}^2(\delta + \delta') \rangle}{(2\sigma_{v,\text{eff}}^2)(1 + \xi)} \left(\frac{v^2}{f^2(2\sigma_{v,\text{eff}}^2)} - 1\right)\right] \\
\mathcal{P}^{\text{G}}(v, \mathbf{r}) &= \frac{1}{f\sqrt{2\pi} \langle \Delta u_{\parallel}^2 \rangle^{1/2}} \exp\left\{-\frac{v^2}{2f^2 \langle \Delta u_{\parallel}^2 \rangle}\right\} \times \\
&\times \left[1 + \frac{vv_{12}}{f \langle \Delta u_{\parallel}^2 \rangle} + \frac{1}{4} \frac{v_{12}^2}{\langle \Delta u_{\parallel}^2 \rangle} (1 + \xi) \left(\frac{v^2}{f^2 \langle \Delta u_{\parallel}^2 \rangle} - 1\right)\right].
\end{aligned} \tag{3.36}$$

It is clearly visible that the two equations are very similar, with the only two differences being the presence of $2\sigma_{v,\text{eff}}^2$ in the denominators of the former, coming from the assumption on the FOG factor, and the pairwise velocity moment used for the description of the third addendum inside the square parenthesis.

From equation (3.20) we can see that, for the PDF assuming Gaussianity, the second pairwise velocity moment enters only with its linear contribution. Indeed we notice that the Gaussianity assumption allows a description of the PDF using only the linear description of the first two pairwise velocity moments and their powers, while the TNS approach ends up determining a more complete one, involving nonlinear terms of the second one and, also, accounting for small scales nonlinear effects with the effective velocity dispersion. To better compare the third addendum inside the Kaiser term, we recall equation (2.83) and write

$$\frac{1}{4}v_{12}^2(1 + \xi) = \frac{\langle \Delta u_{\parallel} \delta \rangle \langle \Delta u_{\parallel} \delta' \rangle}{1 + \xi}. \tag{3.37}$$

Thus the two Kaiser terms become

$$\begin{aligned}\mathcal{P}_{\text{Kaiser}}^{\text{TNS}}(v, \mathbf{r}) &= 1 + \frac{vv_{12}}{f(2\sigma_{v, \text{eff}}^2)} + \frac{1}{2} \frac{\langle \Delta u_{\parallel}^2(\delta + \delta') \rangle}{(2\sigma_{v, \text{eff}}^2)(1 + \xi)} \left(\frac{v^2}{f^2(2\sigma_{v, \text{eff}}^2)} - 1 \right) \\ \mathcal{P}_{\text{Kaiser}}^{\text{G}}(v, \mathbf{r}) &= 1 + \frac{vv_{12}}{f\sigma_{12}^{\text{LD}}} + \frac{\langle \Delta u_{\parallel} \delta \rangle \langle \Delta u_{\parallel} \delta' \rangle}{\sigma_{12}^{\text{LD}}(1 + \xi)} \left(\frac{v^2}{f^2\sigma_{12}^{\text{LD}}} - 1 \right).\end{aligned}\tag{3.38}$$

Although the Gaussianity assumption allows a simpler description of the pairwise velocity PDF, already [58] highlighted it cannot properly describe the second order moment, and consequently higher order ones, due to the fact that in realistic scenarios nonlinear contributions to the velocity dispersion are never vanishing. This simplified treatment is clearly visible in (3.38), where the description of the Gaussian PDF completely ignores those nonlinear contributions of the velocity dispersion, $\langle \Delta u_{\parallel}^2(\delta + \delta') \rangle$ and $\langle \Delta u_{\parallel}^2 \delta \delta' \rangle_c$, while the TNS approach is capable to incorporate at least the first one of them (Recall it ignores $\langle \Delta u_{\parallel} \delta \delta' \rangle_c$ since it is of higher order in perturbation theory). Moreover, the TNS model allows us to separate and distinguish large and small scales velocity dispersions thanks to the parametrization of the FOG exponential (2.123).

The other important difference between the two models is the pairwise velocity moment used to describe the third addendum in the Kaiser term: while the Gaussian approximation still uses the mean squared, the TNS model calculations determine the presence of the nonlinear velocity dispersion. As seen in Section 2.8.1 this difference can be traced back to the perturbative expansion of the Kaiser contribution, which allows simplify $\langle \Delta u_{\parallel} \delta \rangle_c \langle \Delta u_{\parallel} \delta' \rangle_c$ with part of the unconnected relations coming from $\langle \Delta u_{\parallel}^2 \delta \delta' \rangle_c$ and obtain $\langle \Delta u_{\parallel}^2(\delta + \delta') \rangle$ (equations (2.161) to (2.172)).

As a final observation, we highlight the fact that the two equations in (3.38) remain quite different from each other even if one adds nonlinear dynamics contributions in the Gaussian moment description: indeed, the differences those terms will imply would not change the third addendum of the Kaiser term except for a more complete description of the velocity dispersions at the denominators which, in any case, would differ from the effective dispersion of the TNS model.

3.2.1 The Redshift Space 2PCF from the TNS Model

As shown earlier, the starting point of the treatment proposed in [34] is equation (3.7) (equivalent to equation (59) of [58]) and it is what determines the final form of the redshift space 2PCF, equation (3.18). Therefore it is immediate to see the redshift space 2PCF determined by the TNS model will be obtained inserting equation (3.35) inside (2.67)

$$1 + \xi_s^{\text{TNS}}(s_{\perp}, s_{\parallel}) = \int dy (1 + \xi) \mathcal{P}^{\text{TNS}}(y, \mathbf{r}).\tag{3.39}$$

The point is that, although equation (3.35) is useful to study the problem in redshift space, the same is not true for configuration space analysis: this is due to the scale dependence present in the FOG factor, which makes the integration inside (3.39) much more complicated³. Therefore, in order to compare the TNS model with the results from [34], we place ourselves in the same regime where the

³Recall that the r -dependence of ξ has to be translated into a y -dependence according to (3.14).

linear theory approximation made to obtain their equation (17) could be enforced, namely at large scales. To do so we expand the pairwise velocity PDF (3.22)

$$\begin{aligned} \mathcal{Z}^{\text{TNS}}(\lambda, \mathbf{r}) &= \exp \left\{ \left\langle e^{\lambda \Delta u_{ii}} \right\rangle_c \right\} \times \\ &\times \left[1 + \xi + \lambda v_{12}(1 + \xi) + \frac{\lambda^2}{2} \langle \Delta u_{ii}^2(\delta + \delta') \rangle \right] \end{aligned} \quad (3.40)$$

for $\lambda = 0$ expansion (recall that $\lambda = -if\gamma$ in configuration space)

$$\mathcal{Z}^{\text{TNS}}(\lambda, \mathbf{r}) \simeq \mathcal{Z}^{\text{TNS}}(\lambda = 0, \mathbf{r}) + \left. \frac{d\mathcal{Z}^{\text{TNS}}(\lambda, \mathbf{r})}{d\lambda} \right|_{\lambda=0} \lambda + \left. \frac{d^2\mathcal{Z}^{\text{TNS}}(\lambda, \mathbf{r})}{d\lambda^2} \right|_{\lambda=0} \frac{\lambda^2}{2} + \mathcal{O}(\lambda^2), \quad (3.41)$$

where the derivatives of the generating function are equal to⁴

$$\begin{aligned} \left. \frac{d\mathcal{Z}^{\text{TNS}}(\lambda, \mathbf{r})}{d\lambda} \right|_{\lambda=0} &= \exp \{ \lambda^2 \sigma_{v,\text{eff}}^2 \} 2\lambda \sigma_{v,\text{eff}}^2 C(\lambda, \mathbf{r}) \Big|_{\lambda=0} + \\ &+ \exp \{ \lambda^2 \sigma_{v,\text{eff}}^2 \} [v_{12}(1 + \xi) + \lambda \langle \Delta u_{ii}^2(\delta + \delta') \rangle] \Big|_{\lambda=0} \\ &= v_{12}(1 + \xi), \end{aligned} \quad (3.42)$$

$$C(\lambda, \mathbf{r}) := \left[1 + \xi(r) + \lambda v_{12}(1 + \xi(r)) + \frac{\lambda^2}{2} \langle \Delta u_{ii}^2(\delta + \delta') \rangle \right]$$

and

$$\begin{aligned} \left. \frac{d^2\mathcal{Z}^{\text{TNS}}(\lambda, \mathbf{r})}{d\lambda^2} \right|_{\lambda=0} &= \exp \{ \lambda^2 \sigma_{v,\text{eff}}^2 \} 4\lambda^2 (\sigma_{v,\text{eff}}^2)^2 C(\lambda, \mathbf{r}) \Big|_{\lambda=0} + \exp \{ \lambda^2 \sigma_{v,\text{eff}}^2 \} 2\sigma_{v,\text{eff}}^2 C(\lambda, \mathbf{r}) \Big|_{\lambda=0} + \\ &+ \exp \{ \lambda^2 \sigma_{v,\text{eff}}^2 \} 2\lambda (\sigma_{v,\text{eff}}^2)^2 [v_{12}(1 + \xi) + \lambda \langle \Delta u_{ii}^2(\delta + \delta') \rangle] \Big|_{\lambda=0} + \\ &+ \exp \{ \lambda^2 \sigma_{v,\text{eff}}^2 \} 2\lambda (\sigma_{v,\text{eff}}^2)^2 [v_{12}(1 + \xi) + \lambda \langle \Delta u_{ii}^2(\delta + \delta') \rangle] \Big|_{\lambda=0} + \\ &+ \exp \{ \lambda^2 \sigma_{v,\text{eff}}^2 \} \langle \Delta u_{ii}^2(1 + \delta + \delta') \rangle \Big|_{\lambda=0} = 2\sigma_{v,\text{eff}}^2(1 + \xi) + \langle \Delta u_{ii}^2(\delta + \delta') \rangle. \end{aligned} \quad (3.43)$$

Thus equation (3.41) reads

$$\begin{aligned} \mathcal{Z}^{\text{TNS}}(\lambda = 0, \mathbf{r}) &\simeq 1 + \xi + \lambda v_{12}(1 + \xi) + \frac{\lambda^2}{2} 2\sigma_{v,\text{eff}}^2(1 + \xi) + \frac{\lambda^2}{2} \langle \Delta u_{ii}^2(\delta + \delta') \rangle + \mathcal{O}(\lambda^2) \\ &= \langle (1 + \delta)(1 + \delta') \rangle + \lambda \langle \Delta u_{ii}(1 + \delta)(1 + \delta') \rangle + \\ &+ \frac{\lambda^2}{2} 2\sigma_{v,\text{eff}}^2(1 + \xi) + \frac{\lambda^2}{2} \langle \Delta u_{ii}^2(\delta + \delta') \rangle + \mathcal{O}(\lambda^2), \end{aligned} \quad (3.44)$$

where the second expression has been written using (1.63) and (2.68) for future reference.

⁴The exponential can be expressed as follows from (2.122) and (2.123)

$$\exp \left\{ \left\langle e^{j_1 \Delta u_{ii}} \right\rangle_c \right\} = \exp \left\{ \sum_{n=1}^{\infty} \lambda^n \frac{\langle \Delta u_{ii}^n \rangle_c}{n!} \right\} \simeq \exp \{ \lambda^2 \sigma_{v,\text{eff}}^2 \}, \quad \lambda \equiv j_1.$$

Also, with the same motivations of Section 3.1 we rename the Kaiser contribution in (3.40) as $C(\lambda, \mathbf{r})$.

It is now possible to insert the large scale expansion of the pairwise velocity generating function inside (2.63). Exploiting the fact that the PDF is defined as the inverse Fourier transform of the generating function (2.63), we can use the property (3.9) as in Section 3.1 and write

$$\mathcal{P}^{\text{TNS}}(y, \mathbf{r}) \simeq \left(1 + f v_{12} \frac{d}{dy} + \frac{1}{2} f^2 2\sigma_{v, \text{eff}}^2 \frac{d^2}{dy^2} + \frac{1}{2} f^2 \frac{\langle \Delta u_{\parallel}^2(\delta + \delta') \rangle}{1 + \xi} \frac{d^2}{dy^2} + \mathcal{O}(y^2) \right) \delta_D(y). \quad (3.45)$$

Analogously to what we did in Section 3.1, we can insert the large scale PDF (3.45) into equation (3.39) to obtain the redshift space description of the 2PCF. To do so, we use the integration property of the Dirac delta function of equation (3.16) to write⁵

$$1 + \xi_s^{\text{TNS}}(s_{\perp}, s_{\parallel}) \simeq (1 + \xi) \left(1 - f \frac{dv_{12}}{dr_{\parallel}} + \frac{f^2}{2} \frac{d^2 2\sigma_{v, \text{eff}}^2}{dr_{\parallel}^2} \right) + \frac{1}{2} f^2 \frac{d^2 \langle \Delta u_{\parallel}^2(\delta + \delta') \rangle}{dr_{\parallel}^2} + \mathcal{O}(\xi^2), \quad (3.46)$$

which is the equation we need to compare with (3.18) found out by [34]. Thus, in the regime where $\xi \ll 1$ we can exploit the additive property of both integrals and derivatives to obtain

$$1 + \xi_s^{\text{TNS}}(s_{\perp}, s_{\parallel}) \simeq 1 + \xi - f \frac{dv_{12}}{dr_{\parallel}} + \frac{1}{2} f^2 \frac{d^2 2\sigma_{v, \text{eff}}^2}{dr_{\parallel}^2} + \frac{1}{2} f^2 \frac{d^2 \langle \Delta u_{\parallel}^2(\delta + \delta') \rangle}{dr_{\parallel}^2} + \mathcal{O}(\xi^2). \quad (3.47)$$

With the term of equation (3.47) arranged as above, it is immediate to see that it has some similarities with (3.18), but it is still quite different. Below we analyse each term beyond $1 + \xi$:

- First among them is the derivative of the mean pairwise velocity, which is exactly the one obtained in (3.18) by [34]. This should not come as a surprise since already R. Scoccimarro [58], and S. Bharadwaj [8] before, have pointed out that the large scale mean pairwise velocity is well described from linear theory.
- Following the line we find

$$\frac{1}{2} f^2 \frac{d^2 2\sigma_{v, \text{eff}}^2}{dr_{\parallel}^2}.$$

To understand its meaning we recall once more the TNS model parametrization of the FOG factor given in equation (2.123), namely $\langle \Delta u_{\parallel}^2 \rangle \simeq 2\sigma_{v, \text{eff}}^2$, which makes this term dependent on the fitting parameter $\sigma_{v, \text{eff}}^2$. As the effective velocity dispersion thus expressed suggests, this term is directly linked to the derivatives of the FOG factor which have survived the $\lambda = 0$ expansion in (3.43). It was not present in the derivations of Section 3.1 because there we made no additional assumptions on the FOG factor and hence we had no way to distinguish the velocity dispersion therein with the one in the Kaiser term, with FOG contributions surviving the large scale expansion ended up being described as

$$\frac{1}{2} f^2 \frac{d^2 \sigma_{12}^{\text{LD}}}{dr_{\parallel}^2}.$$

Nonetheless, if one accepts that at least at large scales this parametrization can be described as the sum between the linear dynamics description of the pairwise velocity dispersion and the

⁵Recall that, if $y = 0$ then $r = s$.

one expressing *only* nonlinear effects from the virialized objects $2\sigma_{v,\text{eff}}^2 = \sigma_{12}^{\text{LD}} + \sigma_{12}^{\text{virialized}}$ in a similar fashion of (2.85), it is then possible to recast it as

$$\frac{1}{2}f^2 \frac{d^2 \sigma_{12}^{\text{LD}}}{dr_{\parallel}^2} + \frac{1}{2}f^2 \frac{d^2 \sigma_{12}^{\text{virialized}}}{dr_{\parallel}^2} \quad (3.48)$$

and recover the last term we miss from (3.18) plus the one linked with nonlinearities of the FOG factor.

- The last term of the second line is

$$\frac{1}{2}f^2 \frac{d^2 \langle \Delta u_{\parallel}^2(\delta + \delta') \rangle}{dr_{\parallel}^2}.$$

Since Gaussianity has not been assumed through the entire Section 3.2.1, it should not surprise we recover this contribution in equation (3.47). Indeed the fact that we will find it also in Section 3.4, equation (3.70), but not in (3.18) tells us it must be equal to zero if Gaussianity holds [58]. Looking back at the second order term in the expansion of the Gaussian generating function (3.5), we can see that the new term of both treatments (the TNS one here and the one we will perform in Section 3.4) has the same role of

$$\frac{1}{2}(1 + \xi)^2 v_{12}^2.$$

Thanks to the TNS approach we can understand why the square of the mean pairwise velocity turns into the pairwise velocity dispersion when one drops the assumption of Gaussianity and deals with the Kaiser term perturbatively: as we were already mentioning in the previous Section, with the comment on equation (3.38), the term involving v_{12}^2 comes as a result of the product $\langle \Delta u_{\parallel} \delta \rangle \langle \Delta u_{\parallel} \delta' \rangle$ in the Gaussian generating function (2.160); this term is exactly the one which gets associated with the other non vanishing second order terms of the TNS approach and directly determines $\langle \Delta u_{\parallel}^2(\delta + \delta') \rangle$. All the calculations showing the interaction between $\langle \Delta u_{\parallel} \delta \rangle \langle \Delta u_{\parallel} \delta' \rangle$ and the rest of the Kaiser contribution have been already covered in Section 2.8.1, between equations (2.161) and (2.172).

- The last thing to analyse is the absence of the term

$$\frac{1}{2}f^2 \frac{d^2 \langle \Delta u_{\parallel}^2 \delta \delta' \rangle_c}{dr_{\parallel}^2}$$

with respect to (3.70) of Section 3.4: this is due to the fact that, as mentioned already in [68], this term is of order $O(\xi^3)$ and hence it can be stored inside the remainder $\mathcal{O}(\xi^2)$ after the large scale expansion of the TNS model.

Following the considerations above the large scale redshift space 2PCF coming from the TNS model reads

$$\begin{aligned} 1 + \xi_s^{\text{TNS}}(s_{\perp}, s_{\parallel}) \simeq & 1 + \xi - f \frac{dv_{12}}{dr_{\parallel}} + \frac{1}{2}f^2 \frac{d^2 \sigma_{12}^{\text{LD}}}{dr_{\parallel}^2} + \\ & + \frac{1}{2}f^2 \frac{d^2 \sigma_{12}^{\text{virialized}}}{dr_{\parallel}^2} + \frac{1}{2}f^2 \frac{d^2 \langle \Delta u_{\parallel}^2(\delta + \delta') \rangle}{dr_{\parallel}^2} + \mathcal{O}(\xi^2), \end{aligned} \quad (3.49)$$

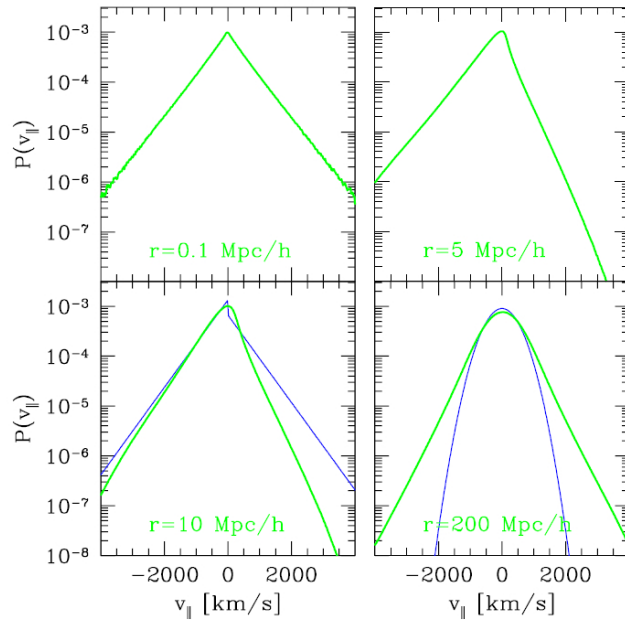


Figure 3.1: Pairwise velocity PDF relative to the LOS velocity for fixed real space separation (labelled in green inside each panel in units of $h^{-1}\text{Mpc}$) at redshift $z = 0$ for N-body simulations (green lines). The two blue lines in the third and fourth panel represent respectively the distribution given by the dispersion model and linear dynamics. The four panels show how the PDF changes with the increase of the real space separation. From the first three panels, scale separations of $r = 0.1, 5, 10 [h^{-1}\text{Mpc}]$, it is possible to see the skewness of the distribution, which tend to be mitigated once we larger scales are reached. Figure taken from [58].

which is exactly equation (3.18) (first line) with the addition of nonlinear contributions of the of the pairwise velocity dispersion from either the virialized motion of mass around halos and from the Kaiser contribution (second line).

3.3 The Reid & White Approach: A Bridge Between Streaming and TNS Models

In this Section we explore a different third approach, which can be compatible with both of the previous treatments before, namely the one proposed by B. A. Reid and M. White in [55]. They have proposed re-summing the Kaiser term, or part of it if we try to apply the same concept to the TNS pairwise PDF, inside the exponential FOG factor by exploiting the zero mean value of the PDF itself; this characteristic of the pairwise velocity PDF is reported in Figure 3.1 using N-body simulations (green lines). This procedure was possible starting from the Gaussian result of (3.36), once inserted

in the streaming model (2.67)

$$\begin{aligned}
1 + \xi_s(s_\perp, s_\parallel) &= \int dy (1 + \xi) \frac{1}{f\sqrt{2\pi}\langle\Delta u_\parallel^2\rangle^{1/2}} \exp\left\{-\frac{y^2}{2f^2\langle\Delta u_\parallel^2\rangle}\right\} \times \\
&\times \left[1 - \frac{yv_{12}}{f\langle\Delta u_\parallel^2\rangle} + \frac{1}{4}\frac{v_{12}^2}{\langle\Delta u_\parallel^2\rangle}(1 + \xi) \left(\frac{y^2}{f^2\langle\Delta u_\parallel^2\rangle} - 1\right)\right], \tag{3.50}
\end{aligned}$$

after noticing that the Kaiser term corresponds to the linear order $v_{12} = 0$ expansion of

$$\begin{aligned}
\exp\left\{-\frac{f^2v_{12}^2 - 2yfv_{12}}{2f^2\sigma_{12}^{\text{LD}}}\right\} &\simeq 1 + \exp\left\{-\frac{f^2v_{12}^2 - 2yfv_{12}}{2f^2\sigma_{12}^{\text{LD}}}\right\} \times \\
&\times \left.\frac{2f^2v_{12} - 2yf}{2f^2\sigma_{12}^{\text{LD}}}\right|_{v_{12}=0} v_{12} + \mathcal{O}(v_{12}) \tag{3.51} \\
&= 1 - \frac{yv_{12}}{f\sigma_{12}^{\text{LD}}} + \mathcal{O}(v_{12}).
\end{aligned}$$

With such an expansion, the v_{12}^2 term in (3.36) can be stored into the $\mathcal{O}(v_{12})$ and thus the whole Kaiser contribution of the pairwise velocity PDF can be expressed as the exponential in (3.51), making them able to complete the square in the exponential and write the linear order Gaussian streaming model as⁶ [55]

$$1 + \xi_s(s_\perp, s_\parallel) = \int dy (1 + \xi) \frac{1}{f\sqrt{2\pi}(\sigma_{12}^{\text{LD}})^{1/2}} \exp\left\{-\frac{(y - fv_{12})^2}{2f^2\sigma_{12}^{\text{LD}}}\right\}. \tag{3.52}$$

Being linear order, the equation above is expected to improve significantly its precision as far as we move to larger scales ($r \gtrsim 10 [h^{-1}\text{Mpc}]$).

As pointed out by [57], the re-summation above ends up describing a pairwise velocity PDF equal to

$$\mathcal{P}^{\text{RW}}(y, \mathbf{r}) = \frac{1}{f\sqrt{2\pi}(\sigma_{12}^{\text{LD}})^{1/2}} \exp\left\{-\frac{(y - fv_{12})^2}{2f^2\sigma_{12}^{\text{LD}}}\right\}, \tag{3.53}$$

which in turn determines a generating function; we can write it by applying the Fourier transform from y to the λ domain according to equation (2.65)

$$\mathcal{M}^{\text{RW}}(\lambda, \mathbf{r}) = \int dy e^{\lambda y/f} \frac{1}{f\sqrt{2\pi}(\sigma_{12}^{\text{LD}})^{1/2}} \exp\left\{-\frac{(y - fv_{12})^2}{2f^2\sigma_{12}^{\text{LD}}}\right\}. \tag{3.54}$$

⁶Recall that at linear order we have $\langle\Delta u_\parallel^2\rangle \equiv \sigma_{12}^{\text{LD}}$.

The derivation can be then carried out using the general Gaussian integral (3.25)

$$\begin{aligned}
\mathcal{M}^{\text{RW}}(\lambda, \mathbf{r}) &= \int dy \frac{1}{f\sqrt{2\pi}(\sigma_{12}^{\text{2LD}})^{1/2}} \exp \left\{ \frac{\lambda y}{f} - \frac{y^2 + f^2 v_{12}^2 - 2y f v_{12}}{2f^2 \sigma_{12}^{\text{2LD}}} \right\} \\
&= \int dy \frac{1}{f\sqrt{2\pi}(\sigma_{12}^{\text{2LD}})^{1/2}} \exp \left\{ -\frac{y^2}{2f^2 \sigma_{12}^{\text{2LD}}} + y \left(\frac{\lambda}{f} + \frac{v_{12}}{f\sigma_{12}^{\text{2LD}}} \right) - \frac{v_{12}^2}{2\sigma_{12}^{\text{2LD}}} \right\} \\
&= \frac{1}{f\sqrt{2\pi}(\sigma_{12}^{\text{2LD}})^{1/2}} \sqrt{\pi 2f^2 \sigma_{12}^{\text{2LD}}} \exp \left\{ \frac{1}{4} 2f^2 \sigma_{12}^{\text{2LD}} \left(\frac{\lambda}{f} + \frac{v_{12}}{f\sigma_{12}^{\text{2LD}}} \right)^2 - \frac{v_{12}^2}{2\sigma_{12}^{\text{2LD}}} \right\} \quad (3.55) \\
&= \exp \left\{ \frac{1}{4} 2f^2 \sigma_{12}^{\text{2LD}} \left(\frac{\lambda^2}{f^2} + \frac{v_{12}^2}{f^2(\sigma_{12}^{\text{2LD}})^2} + \frac{2\lambda v_{12}}{f\sigma_{12}^{\text{2LD}}} \right) - \frac{v_{12}^2}{2\sigma_{12}^{\text{2LD}}} \right\} \\
&= \exp \left\{ \frac{\lambda^2}{2} \sigma_{12}^{\text{2LD}} + \frac{v_{12}^2}{2\sigma_{12}^{\text{2LD}}} + \lambda v_{12} - \frac{v_{12}^2}{2\sigma_{12}^{\text{2LD}}} \right\} = \exp \left\{ \lambda v_{12} + \frac{\lambda^2}{2} \sigma_{12}^{\text{2LD}} \right\},
\end{aligned}$$

giving a \mathcal{Z} function of the type

$$\mathcal{Z}^{\text{RW}}(\lambda, \mathbf{r}) = (1 + \xi) \exp \left\{ \lambda v_{12} + \frac{\lambda^2}{2} \sigma_{12}^{\text{2LD}} \right\}. \quad (3.56)$$

It has been shown [8], that using linear perturbation theory it is possible to rewrite the general pairwise velocity dispersion in terms of a sum between its linear dynamics description and the square of the mean pairwise velocity, namely

$$\sigma_{12}^2 \simeq \sigma_{12}^{\text{2LD}} + \frac{1}{2} v_{12}^2. \quad (3.57)$$

By applying to (3.56) the large scale expansion around $\lambda = 0$ as in the previous Sections we have

$$\mathcal{Z}^{\text{RW}}(\lambda, \mathbf{r}) \simeq \mathcal{Z}^{\text{RW}}(\lambda = 0, \mathbf{r}) + \left. \frac{d\mathcal{Z}^{\text{RW}}(\lambda, \mathbf{r})}{d\lambda} \right|_{\lambda=0} \lambda + \left. \frac{d^2 \mathcal{Z}^{\text{RW}}(\lambda, \mathbf{r})}{d\lambda^2} \right|_{\lambda=0} \frac{\lambda^2}{2} + \mathcal{O}(\lambda^2), \quad (3.58)$$

where the generating function and its derivatives at $\lambda = 0$ read

$$\begin{aligned}
\mathcal{Z}^{\text{RW}}(\lambda = 0, \mathbf{r}) &= (1 + \xi) \\
\left. \frac{d\mathcal{Z}^{\text{RW}}(\lambda, \mathbf{r})}{d\lambda} \right|_{\lambda=0} &= (1 + \xi) \exp \left\{ \lambda v_{12} + \frac{\lambda^2}{2} \sigma_{12}^{\text{2LD}} \right\} (v_{12} + \lambda \sigma_{12}^{\text{2LD}}) \Big|_{\lambda=0} \\
&= \lambda(1 + \xi) v_{12} \\
\left. \frac{d^2 \mathcal{Z}^{\text{RW}}(\lambda, \mathbf{r})}{d\lambda^2} \right|_{\lambda=0} &= (1 + \xi) \exp \left\{ \lambda v_{12} + \frac{\lambda^2}{2} \sigma_{12}^{\text{2LD}} \right\} (v_{12} + \lambda \sigma_{12}^{\text{2LD}})^2 \Big|_{\lambda=0} \frac{\lambda^2}{2} + \quad (3.59) \\
&\quad + (1 + \xi) \exp \left\{ \lambda v_{12} + \frac{\lambda^2}{2} \sigma_{12}^{\text{2LD}} \right\} \sigma_{12}^{\text{2LD}} \Big|_{\lambda=0} \frac{\lambda^2}{2} \\
&= \frac{\lambda^2}{2} (1 + \xi) v_{12}^2 + \frac{\lambda^2}{2} (1 + \xi) \sigma_{12}^{\text{2LD}}
\end{aligned}$$

where, given the Gaussian framework we are working with, we can ignore the $(1 + \xi) v_{12}^2$ contribution

$$\mathcal{Z}^{\text{RW}}(\lambda, \mathbf{r}) \simeq (1 + \xi) + \lambda(1 + \xi) v_{12} + \frac{\lambda^2}{2} (1 + \xi) \sigma_{12}^{\text{2LD}} + \mathcal{O}(\lambda^2); \quad (3.60)$$

exploiting now the definition of velocity moments given in equation (2.68), we are able to obtain

$$\mathcal{Z}^{\text{RW}}(\lambda, \mathbf{r}) \simeq \langle (1 + \delta)(1 + \delta') \rangle + \lambda \langle \Delta u_{\parallel} (1 + \delta)(1 + \delta') \rangle + \frac{\lambda^2}{2} \langle \Delta u_{\parallel}^2 \rangle + \mathcal{O}(\lambda^2). \quad (3.61)$$

This shows that the B. A. Reid and M. White approach agrees at linear order with both the Gaussian case⁷ of Section 3.1 (equation (3.7)) [55] and with the TNS one (equation (3.44)). Looking beyond linear order we can see that, sticking to a non perturbative description this third approach is consistent with the large scale approximation of Gaussian results while it differentiates from the TNS ones; once more, these differences are due to the missing approximation of Gaussianity in the latter model, which makes us unable to set $\langle \Delta u_{\parallel}^2 (\delta + \delta') \rangle = 0$ for the second moment description, coupled with the peculiar treatment of the FOG factor that ends up describing a generating function dependent on two different velocity dispersions: the one considering nonlinear virialized motion $\sigma_{v, \text{eff}}^2$, as well as the intermediate/large scales one, σ_{12}^2 .

If one instead accepts to treat perturbatively the pairwise velocity dispersion, which differently from the mean is not well described by linear dynamics even at large scales, it is then possible to substitute equation (3.57) into the second derivative of the expansion (3.59) and see the two v_{12}^2 contributions leave us with a large scale expansion (we have described the square of the mean velocity as (2.83))

$$\begin{aligned} \mathcal{Z}^{\text{RW}}(\lambda, \mathbf{r}) \simeq & \langle (1 + \delta)(1 + \delta') \rangle + \lambda \langle \Delta u_{\parallel} (1 + \delta)(1 + \delta') \rangle + \frac{\lambda^2}{2} \langle \Delta u_{\parallel}^2 (1 + \delta)(1 + \delta') \rangle + \\ & + \frac{\lambda^2}{2} 2 \langle \Delta u_{\parallel} \delta \rangle \langle \Delta u_{\parallel} \delta' \rangle + \mathcal{O}(\lambda^2), \end{aligned} \quad (3.62)$$

which is much more similar to the one coming from the TNS approach. To see that, below we report the large scale expansion (3.44) after applying the considerations on $\sigma_{v, \text{eff}}^2$ that gave (3.49) inside Section 3.2.1 (recall the definition of the linear dynamics pairwise velocity dispersion (3.20) and the large scale limit of the 2PCF $\xi \ll 1$)

$$\begin{aligned} \mathcal{Z}^{\text{TNS}}(\lambda = 0, \mathbf{r}) \simeq & \langle (1 + \delta)(1 + \delta') \rangle + \lambda \langle \Delta u_{\parallel} (1 + \delta)(1 + \delta') \rangle + \frac{\lambda^2}{2} \langle \Delta u_{\parallel}^2 (1 + \delta + \delta') \rangle + \\ & + \frac{\lambda^2}{2} \sigma_{12}^2 \text{virialized} + \mathcal{O}(\lambda^2). \end{aligned} \quad (3.63)$$

This behaviour of the B. Reid & M. White model should not come as a surprise: indeed, one of the major characteristic of the TNS model is the perturbative treatment of the Kaiser term of the generating function (2.159) before its evaluation inside (2.121).

As pointed out by [70], deviations from Gaussianity quickly decline as a function of the real space pair separation when $r > 10 [h^{-1} \text{Mpc}]$, making results coming from equation (3.52) increase their accuracy as far as we move to larger separations. However, given the real-to-redshift space mapping described from (3.52), it has been pointed out in [55] (with their Figure 4) the redshift space 2PCF is still substantially different from the Kaiser one at quasi-linear scales ($\sim 30 : 80 [h^{-1} \text{Mpc}]$), even if one uses linear theory predictions for ξ , v_{12} and σ_{12}^2 . Inside [55] they also compare their model

⁷As we mentioned in Section 3.1, if we are dealing with large scales we can consider $v_{12} \simeq v_{12}(1 + \xi)$.

against N-body simulations, finding out it is able to accurately describe the monopole ξ_0 down to $s \sim 10 [h^{-1}\text{Mpc}]$; for the quadrupole ξ_2 , a 1-2% level accuracy has been obtained for redshift space separations $s \gtrsim 25 [h^{-1}\text{Mpc}]$ while the quadruple ξ_4 description deviated from the linear theory by $O(1)$ for $s < 80 [h^{-1}\text{Mpc}]$.

3.4 Improving the Derivation Accounting for Nonlinear terms

With the derivation of Section 3.1, D. Jeong et al. have been able to determine the large scale behaviour of the 2PCF using the large scale description of the Gaussian pairwise velocity generating function, as well as the linear description of pairwise velocity moments. We now want to show it is possible to arrive at the same result following the fully general approach of Section 2.5.2, with the only use of the large scale expansions of the pairwise velocity PDF (2.87) and 2PCF (2.88), both applied to the streaming model equation (2.67). We start reporting the large scale ($y = 0$) expansion of (2.67)⁸

$$\begin{aligned}
1 + \xi_s(s_\perp, s_\parallel) &\simeq \int dy \left(1 + \xi(s_\perp, s_\parallel) + y\xi'(s_\parallel) + \frac{1}{2}y^2\xi''(s_\parallel) + \mathcal{O}(y^2) \right) \times \\
&\times \left(\mathcal{P}(y; s_\parallel) + y\mathcal{P}'(y; s_\parallel) + \frac{1}{2}y^2\mathcal{P}''(y; s_\parallel) + \mathcal{O}(y^2) \right) \\
&= (1 + \xi) \left(1 + fv'_{12} + \frac{1}{2}f^2\sigma_{12}^2'' + \mathcal{O}(\xi^2) \right) + \\
&+ \int dy \xi'(s) (y\mathcal{P}(y; s_\parallel) + y^2\mathcal{P}'(y; s_\parallel) + \mathcal{O}(y^2)) + \\
&+ \int dy \frac{1}{2}\xi''(s) (y^2\mathcal{P}(y; s_\parallel) + \mathcal{O}(y^2));
\end{aligned} \tag{3.64}$$

as we were mentioning in Section 2.5.2, this can be done if the redshift space galaxy-galaxy separation satisfies $s_\parallel^2 \gg f^2\sigma_{12}^2$, condition which makes the PDF sharply peaked at $r_\parallel = s_\parallel$ [58].

With the equation above it would be possible to extract from the integral the various derivatives of $\xi(\mathbf{s})$ and thus obtain (2.90) (equation (53) inside [58]); however, we would end up with derivatives of the real space 2PCF which would require some parametrization of the function to be computed. To deal with it, we use integration by parts on the second and third rows of the equation above to get

$$\begin{aligned}
1 + \xi_s(s_\perp, s_\parallel) &\simeq (1 + \xi) \left(1 + fv'_{12} + \frac{1}{2}f^2\sigma_{12}^2'' + \mathcal{O}(\xi^2) \right) + \\
&+ \xi (y\mathcal{P}(y; s_\parallel) + y^2\mathcal{P}'(y; s_\parallel) + \mathcal{O}(y^2)) \Big|_{y=0}^{+\infty} + \\
&- \int dy \xi (\mathcal{P}(y; s_\parallel) + y\mathcal{P}'(y; s_\parallel) + 2y\mathcal{P}''(y; s_\parallel) + y^2\mathcal{P}'''(y; s_\parallel) + \mathcal{O}(y^2)) + \\
&+ \frac{1}{2}\xi' (y^2\mathcal{P}(y; s_\parallel)) \Big|_{y=0}^{+\infty} - \frac{1}{2} \int dy \xi'(s_\parallel) (2y\mathcal{P}(y; s_\parallel) + y^2\mathcal{P}'(y; s_\parallel) + \mathcal{O}(y^2)).
\end{aligned} \tag{3.65}$$

Both of the first terms coming from the integration by parts are null, killed by y powers in the $y = 0$ extrema of the integration and by the exponential tails of the pairwise velocity PDF in the $y \rightarrow +\infty$

⁸To lighten the equation we have dropped the various dependencies of the real space functions and, following the notation of Chapter 2, we have depicted y derivatives with a ' symbol.

limit⁹. Thus, swapping the order of integral and derivatives and exploiting the properties of the PDF (equation (2.69)) as done in the first row, we arrive to the expression

$$\begin{aligned}
1 + \xi_s(s_{\perp}, s_{\parallel}) &\simeq (1 + \xi) \left(1 + f v'_{12} + \frac{1}{2} f^2 \sigma_{12}^2{}'' + \mathcal{O}(\xi^2) \right) - \xi \left(1 + 3f v'_{12} + f^2 \sigma_{12}^2{}'' + \mathcal{O}(\xi^2) \right) + \\
&\quad - \frac{1}{2} \xi \left(2y \mathcal{P}(y; s_{\parallel}) + y^2 \mathcal{P}'(y; s_{\parallel}) + \mathcal{O}(y^2) \right) \Big|_{y=0}^{+\infty} + \\
&\quad + \frac{1}{2} \int dy \xi \left(2\mathcal{P}(y; s_{\parallel}) + 2y \mathcal{P}'(y; s_{\parallel}) + 2y \mathcal{P}''(y; s_{\parallel}) + y^2 \mathcal{P}'''(y; s_{\parallel}) + \mathcal{O}(y^2) \right) \quad (3.66) \\
&= (1 + \xi) \left(1 + f v'_{12} + \frac{1}{2} f^2 \sigma_{12}^2{}'' + \mathcal{O}(\xi^2) \right) - \xi \left(1 + 3f v'_{12} + f^2 \sigma_{12}^2{}'' + \mathcal{O}(\xi^2) \right) + \\
&\quad + \frac{1}{2} \xi \left(2 + 4f v'_{12} + f^2 \sigma_{12}^2{}'' + \mathcal{O}(\xi^2) \right)
\end{aligned}$$

which, once we have grouped the terms coming from the integration of ξ , becomes

$$\begin{aligned}
1 + \xi_s(s_{\perp}, s_{\parallel}) &\simeq (1 + \xi) \left(1 + f v'_{12} + \frac{1}{2} f^2 \sigma_{12}^2{}'' + \mathcal{O}(y^2) \right) + \\
&\quad + \xi \left(-f v'_{12} - \frac{1}{2} f^2 \sigma_{12}^2{}'' + \mathcal{O}(y^2) \right) \quad (3.67) \\
&= 1 + \xi + f v'_{12} + \frac{1}{2} f^2 \sigma_{12}^2{}'' + \mathcal{O}(\xi^2).
\end{aligned}$$

Once the derivatives with respect to y have been translated into r_{\parallel} derivatives according to equation (3.12) it is already visible the similarity with the Jeong et al. [34] result

$$1 + \xi_s(s_{\perp}, s_{\parallel}) \simeq 1 + \xi - f \frac{dv_{12}}{dr_{\parallel}} + \frac{1}{2} f^2 \frac{d^2 \sigma_{12}^2}{dr_{\parallel}^2} + \mathcal{O}(\xi^2). \quad (3.68)$$

The main difference with respect to (3.18) is the description of pairwise velocity moments: indeed the latter, coming from the most general derivation, is able to describe the redshift space 2PCF using their *exact* descriptions, while the former derivation of Jeong et al. involves only some of their components. Moreover, we arrive to an equation analogous to (3.18) without the additional assumptions of having vanishingly small ξ , ξ' , ξ'' and v_{12} .

In the attempt of giving an even better comparison with (3.18), we rewrite the pairwise velocity moments accounting for the nonlinear contributions we reported in Section 2.5.1; to do so we introduce back the assumption on the large scale behaviour of the real space 2PCF, $\xi \ll 1$, and write

$$\begin{aligned}
\sigma_{12}^2 &\simeq \sigma_{12}^2(1 + \xi) = \langle \Delta u_{\parallel}^2 \rangle (1 + \xi) + \langle \Delta u_{\parallel}^2 (\delta + \delta') \rangle + \langle \Delta u_{\parallel} \delta \delta' \rangle_c \\
&\simeq \langle \Delta u_{\parallel}^2 \rangle + \langle \Delta u_{\parallel}^2 (\delta + \delta') \rangle + \langle \Delta u_{\parallel}^2 \delta \delta' \rangle_c, \quad (3.69)
\end{aligned}$$

⁹It is important to keep in mind that we have not yet been able to describe the pairwise velocity PDF in the most general case; it is clear however that it should be peaked around zero due to symmetry and have exponentially decaying tails [39], making the consideration on the $y \rightarrow +\infty$ limit a valid one.

which are able to make equation (3.68)

$$\begin{aligned}
1 + \xi_s(s_\perp, s_\parallel) \simeq & 1 + \xi - f \frac{dv_{12}}{dr_\parallel} + \frac{1}{2} f^2 \frac{d^2 \sigma_{12}^{2\text{LD}}}{dr_\parallel^2} + \\
& + \frac{1}{2} f^2 \frac{d^2 \langle \Delta u_\parallel^2 (\delta + \delta') \rangle}{dr_\parallel^2} + \frac{1}{2} f^2 \frac{d^2 \langle \Delta u_\parallel^2 \delta \delta' \rangle_c}{dr_\parallel^2} + \mathcal{O}(\xi^2).
\end{aligned} \tag{3.70}$$

With the pairwise velocity dispersion thus expanded it is clear to see that the first row is exactly equal to (3.18), while in the second row contains all the nonlinear terms of the second moment.

Here we want to stress the fact that equation (3.70) comes as a result of a completely general procedure; the only external assumption we have inserted in the derivation above is the large scale condition of having a 2PCF $\xi \ll 1$, which is a reasonable one given the current way of describing the real space galaxy-galaxy correlation [12]. If one now assumes the Gaussianity condition, as did intrinsically in [34], the two extra term in the second line of the previous equation will vanish [58], making the general result equal to the one of (3.18). As already mentioned in the R. Scoccimarro's paper [58], Gaussianity is never a good approximation for the description of the pairwise velocity dispersion so, in principle, the terms in the second line of equation (3.70) should always be considered.

From equation (3.70) it is also possible to recover the redshift space 2PCF (3.49) coming from the TNS approach if one substitutes the linear dynamics pairwise velocity dispersion with its effective counterpart, expressed like $2\sigma_{v,\text{eff}}^2 = \sigma_{12}^{2\text{LD}} + \sigma_{12}^{2\text{virialized}}$ following (2.85), like we did in Section 3.2.1.

3.4.1 Multipole Decomposition Accounting for Nonlinear Terms

With their work [34], D. Jeong, L. Dai, M. Kamionkowski and A. S. Szalay are able to to give a description of the redshift space 2PCF in terms of real space multipoles ξ_n^m defined in equation (2.106) and Legendre polynomials $\mathcal{L}_i(\mu)$. In this Section we want to present the same description for the 2PCF coming from the more general derivation expressed above. To do so, our starting point will be equation (3.64), where ξ derivatives have been taken out of the integration implying equation (2.90) of Section 2.5.2

$$\begin{aligned}
1 + \xi_s(s_\perp, s_\parallel) = & (1 + \xi) \left(1 + f v'_{12} + \frac{1}{2} f^2 \sigma_{12}^{2''} + \mathcal{O}(y^2) \right) + \\
& + \xi' \left(f v_{12} + f^2 \sigma_{12}^{2'} \right) + \xi'' f^2 \sigma_{12}^2 + \mathcal{O}(y^2).
\end{aligned} \tag{3.71}$$

Once more, the first line corresponds to the results of D. Jeong et al. we have discussed in Section 3.1. To present this Section with more clarity, the explicit derivation of (2.108) from (3.18) has been moved to Appendices A and B; hence we have just to evaluate the two nonlinear terms of the second line. Here we borrow some of the results from the two Appendix A, namely the multipole description of the mean pairwise velocity (A.4), the velocity dispersion (A.13) and its first derivative (A.18). Below

we report them in their large scale limit¹⁰

$$\begin{aligned}
fv_{12} &= -2r_{\parallel}\beta\xi_1^1 \\
f^2\sigma_{12}^2{}^{\text{LD}} &= 2[\sigma_v^2 - \beta^2r^2(\xi_1^3 - \mu^2\xi_2^2)] \\
\frac{d}{dy}f^2\sigma_{12}^2{}^{\text{LD}} &= 2\beta^2[2r\mu(\xi_1^3 - \mu^2\xi_2^2) - r\mu(2\xi_1^3 + \xi_2^2) - 2r\mu(1 - \mu^2)\xi_2^2 + r\mu^3\xi_3^1] \\
&= 2\beta^2(-3r\mu\xi_2^2 + r\mu^3\xi_3^1).
\end{aligned} \tag{3.72}$$

Here, the usage of the linear description of the pairwise velocity dispersion comes from equation (2.85): we can divide the various contributions to the pairwise velocity dispersion as follows [55]

- The first contribution is given from the correlation of velocity fields, which can be described using linear dynamics only.
- The second contribution comes from $\langle\Delta u_{\parallel}^2(\delta + \delta')\rangle$; to deal with it we exploit it is a three point function and, therefore, it gives a vanishing result inside the multipole expansion due to the fact that it cannot be expanded in terms of 2PCFs. Indeed [55] shows that it is composed by constant contribution, coming from $\langle u_{\parallel}^2\delta\rangle$ that was already mentioned by R. Scoccimarro in [58] and a second more complex one, that can be evaluated using perturbation theory on density and velocity fields, which is dependent on the bispectrum $B_{\delta\theta\theta}$. Since giving a perturbative description of δ and u_{\parallel} is beyond the aim of this work, we do not consider those contributions; however we stress that they are evaluated explicitly in the Appendix A2 of [55] and in principle they should be included in the derivation.
- The final term to account for is then $\langle\Delta u_{\parallel}^2\delta\delta'\rangle_c$: as we stated many times so far, this terms turns out to be of order $O(\xi^3)$ and thus can be ignored in our second order description of the redshift space 2PCF [57, 68].

Considerations above are able to justify our choice to describe nonlinear terms of (3.71) using (3.72).

Derivatives of ξ can be performed from (B.35) using the property (A.6) of spherical Bessel functions, namely

$$\begin{aligned}
\frac{d\xi_0^0}{dy} &= -\frac{d\xi_0^0}{dr_{\parallel}} = -\mu\frac{d\xi_0^0}{dr} \\
&= -\mu\int\frac{dk}{2\pi^2}k^2P(k)k\frac{d}{dkr}j_0(kr) \\
&= -\mu\int\frac{dk}{2\pi^2}k^2P(k)k(-j_1(kr)) = -\mu\frac{1}{r}\xi_1^{-1}
\end{aligned} \tag{3.73}$$

for the first one; to deal with the second derivative we take advantage of the following recurrence relation of spherical Bessel functions [3]

$$(2l+1)\frac{dj_l(x)}{dx} = lf_{l-1}(x) - (l+1)f_{l+1} \tag{3.74}$$

¹⁰In this Section, as it can be noticed by the various $\beta := f/b$ powers present in the equations, we are dealing with galaxy power spectra rather than with total matter ones. Following the notation given in Section 2.6, we would have to label each quantity with g superscripts; to avoid their proliferation and increase the clarity of the equations we have chosen to drop them.

to write

$$\begin{aligned}
\frac{d^2\xi_0^0}{dy^2} &= \frac{d^2\xi_0^0}{dr_{\parallel}^2} = \frac{d}{dr_{\parallel}} \left(-\mu \frac{1}{r} \xi_1^{-1} \right) \\
&= - \left(\frac{1}{r} (1 - \mu^2) \right) \frac{1}{r} \xi_1^{-1} - \mu \left(-\frac{1}{r^2} \mu \right) \xi_1^{-1} - \mu \frac{1}{r} \left(\mu \int \frac{dk}{2\pi^2} k^2 P(k) k \frac{d}{dkr} (kr j_1(kr)) \right) \\
&= -\frac{1}{r^2} (1 - \mu^2) \xi_1^{-1} - \frac{1}{r^2} \mu^2 \xi_1^{-1} - \mu^2 \frac{1}{r^2} \int \frac{dk}{2\pi^2} k^2 P(k) kr \frac{d}{dkr} \left[j_1(kr) + kr \frac{1}{3} (j_0(kr) - 2j_2(kr)) \right] \\
&= -\frac{1}{r^2} \xi_1^{-1} - \mu^2 \frac{1}{r^2} \left(\xi_1^{-1} + \frac{1}{3} \xi_0^{-2} - \frac{2}{3} \xi_2^{-2} \right) = \frac{1}{r^2} (\mu^2 \xi_2^{-2} - \xi_1^{-1}),
\end{aligned} \tag{3.75}$$

where for the last equivalence we have exploited the fact that

$$\xi_1^{-1} = \frac{1}{3} (\xi_0^{-2} + \xi_2^{-2}) \tag{3.76}$$

from (A.24). We can see that these results are very similar to the ones computed using the 2-FAST algorithm in [27]: the only differences with respect to the ones presented in the 2018 paper are the μ and μ^2 factors we got in the two expressions above. This differences can be traced back to the fact that in [27] they computed derivatives with respect to r while we are trying to give a description using r_{\parallel} derivatives to be consistent with the calculations in Appendices. Their results completely equivalent to ours thanks to the chain rule of derivatives.

At this point we have collected all what we need to compute the nonlinear part of equation (3.71). We start with

$$\begin{aligned}
\xi' \left(f v_{12} + f^2 \sigma_{12}^{2\text{LD}'} \right) &= -\mu \frac{1}{r} \xi_1^{-1} \left[-2r_{\parallel} \beta \xi_1^1 + 2\beta^2 (-3r\mu\xi_2^2 + r\mu^3\xi_3^1) \right] \\
&= -\mu \xi_1^{-1} \left[-2\mu\beta\xi_1^1 + 2\beta^2 (-3\mu\xi_2^2 + \mu^3\xi_3^1) \right] \\
&= 2\beta\mu^2\xi_1^{-1}\xi_1^1 + 6\beta^2\mu^2\xi_1^{-1}\xi_2^2 - 2\beta^2\mu^4\xi_1^{-1}\xi_3^1;
\end{aligned} \tag{3.77}$$

then the last nonlinear term reads

$$\begin{aligned}
\xi'' f^2 \sigma_{12}^{2\text{LD}} &= \frac{1}{r^2} (\mu^2 \xi_2^{-2} - \xi_1^{-1}) 2[\sigma_v^2 - \beta^2 r^2 (\xi_1^3 - \mu^2 \xi_2^2)] \\
&= 2 \frac{\sigma_v^2}{r^2} (\mu^2 \xi_2^{-2} - \xi_1^{-1}) - 2\beta^2 (\mu^2 \xi_2^{-2} - \xi_1^{-1}) (\xi_1^3 - \mu^2 \xi_2^2) \\
&= 2 \frac{\sigma_v^2}{r^2} (\mu^2 \xi_2^{-2} - \xi_1^{-1}) - 2\beta^2 \mu^2 \xi_2^{-2} \xi_1^3 + 2\beta^2 \mu^4 \xi_2^{-2} \xi_2^2 + 2\beta^2 \xi_1^{-1} \xi_1^3 - 2\beta^2 \mu^2 \xi_1^{-1} \xi_2^2.
\end{aligned} \tag{3.78}$$

Here we stress that the expected value of the one dimensional velocity dispersion is $\sigma_{12}^2 \approx 9 [h^2 \text{Mpc}^{-2}]$ [62], making the first term of the equation above negligible in the large scale limit. Thus, nonlinearities in equation (3.71) sum to

$$\begin{aligned}
\xi' \left(f v_{12} + f^2 \sigma_{12}^{2\text{LD}'} \right) + \xi'' f^2 \sigma_{12}^{2\text{LD}} &= 2\beta\mu\xi_1^{-1}\xi_1^1 + 6\beta^2\mu^2\xi_1^{-1}\xi_2^2 - 2\beta^2\mu^4\xi_1^{-1}\xi_3^1 + \\
&\quad - 2\beta^2\mu^2\xi_2^{-2}\xi_1^3 + 2\beta^2\mu^4\xi_2^{-2}\xi_2^2 + 2\beta^2\xi_1^{-1}\xi_1^3 - 2\beta^2\mu^2\xi_1^{-1}\xi_2^2 \\
&= 2\beta\mu^2\xi_1^{-1}\xi_1^1 + 2\beta^2\xi_1^{-1}\xi_1^3 + 4\beta^2\mu^2\xi_1^{-1}\xi_2^2 + \\
&\quad - 2\beta^2\mu^4\xi_1^{-1}\xi_3^1 - 2\beta^2\mu^2\xi_2^{-2}\xi_1^3 + 2\beta^2\mu^4\xi_2^{-2}\xi_2^2.
\end{aligned} \tag{3.79}$$

In order to add our derivation into the multipole expansion (2.108), we need to write the polynomials of μ in terms of Legendre ones $\mathcal{L}_l(\mu)$. Since we have just even powers of μ , below we report the first three even ones [3]

$$\mathcal{L}_0(\mu) = 1, \quad \mathcal{L}_2(\mu) = \frac{1}{2}(3\mu^2 - 1), \quad \mathcal{L}_4(\mu) = \frac{1}{8}(35\mu^4 - 30\mu^2 + 3). \quad (3.80)$$

Thus, referring to (3.79), we get

$$\begin{aligned} \pm 2\beta\mu^2 &= \pm \frac{4}{3}\beta \frac{1}{2}(3\mu^2 - 1 + 1) = \pm \frac{4}{3}\beta \mathcal{L}_2(\mu) \pm \frac{2}{3}\beta \mathcal{L}_0(\mu) \\ 2\beta^2 &= 2\beta^2 \mathcal{L}_0(\mu) \\ 4\beta^2\mu^2 &= \frac{8}{3}\beta^2 \mathcal{L}_2(\mu) + \frac{4}{3}\beta^2 \mathcal{L}_0(\mu) \\ \pm 2\beta^2\mu^4 &= \pm \frac{16}{35}\beta^2 \frac{1}{8}(35\mu^4 - 30\mu^2 + 3 + 30\mu^2 - 3) \\ &= \pm \frac{16}{35}\beta^2 \mathcal{L}_4(\mu) \pm \frac{40}{35}\beta^2 \frac{1}{2}(3\mu^3 - 1) \pm \frac{14}{35}\beta^2 \\ &= \pm \frac{16}{35}\beta^2 \mathcal{L}_4(\mu) \pm \frac{40}{35}\beta^2 \mathcal{L}_2(\mu) \pm \frac{14}{35}\beta^2 \mathcal{L}_0(\mu). \end{aligned} \quad (3.81)$$

Before proceeding further let us recollect all nonlinear terms factoring out their angular dependence

$$\begin{aligned} &\xi' \left(f v_{12} + f^2 \sigma_{12}^{2\text{LD}'} \right) + \xi'' f^2 \sigma_{12}^{2\text{LD}} = \\ &= \left\{ \frac{2}{3}(\beta \xi_1^{-1} \xi_1^1 - \beta^2 \xi_2^{-2} \xi_1^3) + 2\beta^2 \xi_1^{-1} \xi_1^3 + \frac{4}{3}\beta^2 \xi_1^{-1} \xi_2^2 + \frac{2}{5}\beta^2 (\xi_2^{-2} \xi_2^2 - \xi_1^{-1} \xi_3^1) \right\} \mathcal{L}_0(\mu) + \\ &+ \left\{ \frac{4}{3}(\beta \xi_1^{-1} \xi_1^1 - \beta^2 \xi_2^{-2} \xi_1^3) + \frac{8}{3}\beta^2 \xi_1^{-1} \xi_2^2 + \frac{8}{7}\beta^2 (\xi_2^{-2} \xi_2^2 - \xi_1^{-1} \xi_3^1) \right\} \mathcal{L}_2(\mu) + \\ &+ \left\{ \frac{16}{35}\beta^2 (\xi_2^{-2} \xi_2^2 - \xi_1^{-1} \xi_3^1) \right\} \mathcal{L}_4(\mu). \end{aligned} \quad (3.82)$$

With equation (3.82) thus expressed we are finally able to generalize the multipole expansion of Section 2.6 accounting for large scales nonlinear terms. By defining the coefficients $G_l(\beta)$ and $N_{l,n_1,n_2}^{m_1,m_2}(\beta)$ we can write

$$1 + \xi_s(s_\perp, s_{||}, \mu) = \sum_{l=0}^4 G_l(\beta) \xi_l^0(s) \mathcal{L}_l(\mu) + \sum_{\substack{l,n_1,n_2, \\ m_1,m_2=0}}^4 N_{l,n_1,n_2}^{m_1,m_2}(\beta) \xi_{n_1}^{m_1} \xi_{n_2}^{m_2} \mathcal{L}_l(\mu), \quad (3.83)$$

where all non-vanishing $G_l(\beta)$ and $N_{n_1,n_2}^{l,m}(\beta)$ are the ones reported in Table 3.2. From (3.83) we can see that, if nonlinearities can be ignored, then all $N_{l,n_1,n_2}^{m_1,m_2}(\beta)$ terms vanish making it equal to the expansion (2.108). On the other hand, once the various quantities of Table 3.2 are inserted in the

Table 3.2: Non-vanishing coefficients $G_l(\beta)$ and $N_{l,n_1,n_2}^{m_1,m_2}(\beta)$ to be inserted in equation (3.83)

$G_l(\beta)$	$N_{l,n_1,n_2}^{m_1,m_2}(\beta)$		
$G_0(\beta) = \left(1 + \frac{2}{3}\beta + \frac{1}{5}\beta^2\right)$	$N_{0,1,1}^{-1,1}(\beta) = \frac{2}{3}\beta$	$N_{0,2,1}^{-2,3}(\beta) = -\frac{2}{3}\beta^2$	$N_{0,1,1}^{-1,3}(\beta) = 2\beta^2$
	$N_{0,1,2}^{-1,2}(\beta) = \frac{4}{3}\beta^2$	$N_{0,2,2}^{-2,2}(\beta) = \frac{2}{5}\beta^2$	$N_{0,1,3}^{-1,1}(\beta) = \frac{2}{5}\beta^2$
$G_2(\beta) = -\left(\frac{4}{3}\beta + \frac{4}{7}\beta^2\right)$	$N_{2,1,1}^{-1,1}(\beta) = \frac{4}{3}\beta$	$N_{2,2,1}^{-2,3}(\beta) = -\frac{4}{3}\beta^2$	$N_{2,1,2}^{-1,2}(\beta) = \frac{8}{3}\beta^2$
	$N_{2,2,2}^{-2,2}(\beta) = \frac{8}{7}\beta^2$	$N_{2,1,3}^{-1,1}(\beta) = -\frac{8}{7}\beta^2$	
$G_4(\beta) = \frac{8}{35}\beta^2$	$N_{4,2,2}^{-2,2}(\beta) = \frac{16}{35}\beta^2$	$N_{4,1,3}^{-1,1}(\beta) = -\frac{16}{35}\beta^2$	

general sum above, we are finally able to obtain the nonlinear counterpart of equation (2.108)

$$\begin{aligned}
1 + \xi_s(s_\perp, s_{||}, \mu) &= \\
&= \left\{ \left(1 + \frac{2}{3}\beta + \frac{1}{5}\beta^2\right) \xi_0^0 + \frac{2}{3}(\beta\xi_1^{-1}\xi_1^1 - \beta^2\xi_2^{-2}\xi_1^3) + 2\beta^2\xi_1^{-1}\xi_1^3 + \right. \\
&+ \frac{4}{3}\beta^2\xi_1^{-1}\xi_2^2 + \frac{7}{5}\beta^2(\xi_2^{-2}\xi_2^2 - \xi_1^{-1}\xi_3^1) \left. \right\} \mathcal{L}_0(\mu) + \\
&+ \left\{ -\left(\frac{4}{3}\beta + \frac{4}{7}\beta^2\right) \xi_2^0 + \frac{4}{3}(\beta\xi_1^{-1}\xi_1^1 - \beta^2\xi_2^{-2}\xi_1^3) + \frac{8}{3}\beta^2\xi_1^{-1}\xi_2^2 + \frac{8}{7}\beta^2(\xi_2^{-2}\xi_2^2 - \xi_1^{-1}\xi_3^1) \right\} \mathcal{L}_2(\mu) + \\
&+ \left\{ \frac{8}{35}\beta^2\xi_4^0 + \frac{16}{35}\beta^2(\xi_2^{-2}\xi_2^2 - \xi_1^{-1}\xi_3^1) \right\} \mathcal{L}_4(\mu)
\end{aligned} \tag{3.84}$$

Here we can notice that, like in the expansion (2.103), the angular dependence of each term in the equation above is stored into Legendre polynomials, while terms described by 2PCF multipoles have radial dependence only. Although incomplete¹¹, our multipole expansion shows that all the terms dropped in [34] (the ones coming from the second line of equation (3.71)) are indeed nonlinear. With equation (3.84) we can now give an *a posteriori* validation of the fact they were dropped in the former work [34]: since $\beta \propto f \simeq \Omega_m^{0.6}$, we have $\beta, \beta^2 \sim O(10^{-1})$ and therefore increasing powers of β determines smaller contributions in the multipole expansion; moreover, all the 2PCF multipoles are decreasing functions of r almost everywhere and all of them are reaching values between $O(10^{-2})$ and $O(10^{-3})$ already in the quasilinear regime ($r \sim 30 : 80 [h^{-1}\text{Mpc}]$) as shown in Figure 3.2. This implies that even the largest contributions coming from the second line of (3.71) are of order $O(10^{-5})$ against the smallest linear ones that were $O(10^{-4})$ [27].

From (3.84), we can see that accounting for nonlinear terms we improve the structures multiplying the Legendre polynomials, maintaining the even structure of the previous expansion as one should expect remaining in the plane-parallel approximation. A schematic representation of the angular behaviour of the even Legendre polynomials has been given already in the A. J. S. Hamilton review

¹¹Recall that our nonlinear multipole decomposition comes from the one of pairwise velocity moments of (3.72), which does not include contributions coming from the Bispectrum for σ_{12}^2 .

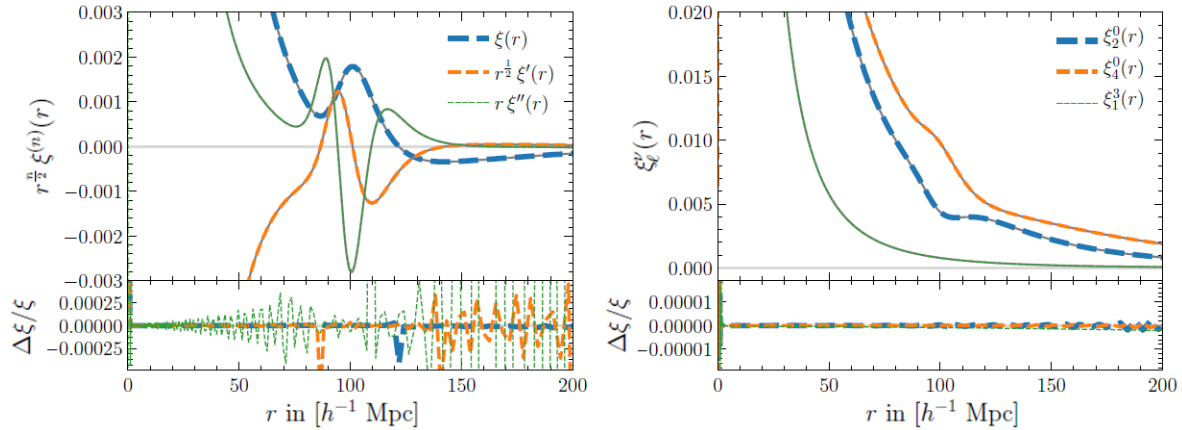


Figure 3.2: Radial dependence of ξ and its derivatives (left) and three $\xi_n^m(r)$ multipoles (right) as computed from the 2.FAST algorithm. Referring to equation (3.84), recall that ξ_1^{-1} multipoles come from terms of both first and second derivative of the 2PCF, equation (3.73), while ξ_2^{-2} are linked only to the second one (3.75). As it is visible in the Figure, an higher upper index of 2PCF multipoles determines a steeper r -dependence of the multipole itself. Relative residuals refer to the computation of the same quantities from their reference algorithm: `quadosc`. Figure taken from [27].

[29] (Figure 6 therein). We also highlight the fact that the computation the products of multipoles' magnitudes involves the integration of products between two spherical Bessel functions, which turns out to be complicated and time-consuming due to their highly oscillatory behaviour that delays the convergence of numerical integration. Recently [27], and [61] generalizing further the previous works, have proposed some acceleration methods to improve numerical integrations of such terms.

Since (3.84) follows the general trend set by [34], in Figure 3.3 we report the angular behaviour of the large scale redshift space 2PCF coming from their model to give a schematic visualization of our result: it shows the reconstruction of the BAO peak location in real space determined directly on the redshift space 2PCF; the dot-dashed line represents the isotropic real space location of the BAO peak, while the solid line marks its real space reconstruction from the redshift space 2PCF. Regarding the angular behaviour of (3.84)

Monopole: With $\mathcal{L}_0(\mu)$ being μ -independent, we have the monopole contribution being isotropic, with nonlinear terms modifying only the magnitude of the correction. Since each multipole reaches values of the order $O(10^{-3})$ for $r \simeq 100 [h^{-1}\text{Mpc}]$ [27], we can already say that their contribution is, as expected, smaller than the one given by assuming linear dynamics without the need of computing the various products coming from nonlinear terms.

Quadrupole: The additional terms follow an opposite trend with respect to the linear ones. However, given the considerations we have done for the monopole contribution, the whole quadrupole term is dominated by the linear contribution and, hence, it determines (recall that $\mathcal{L}_2(\mu = 0) = -1/2$ and $\mathcal{L}_2(\mu = 1) = 1$) an enhancement of the value of the 2PCF in the perpendicular direction and a reduction along the LOS [34].

Hexadecapole: With our description of nonlinearities, the hexadecapole receives an additional con-

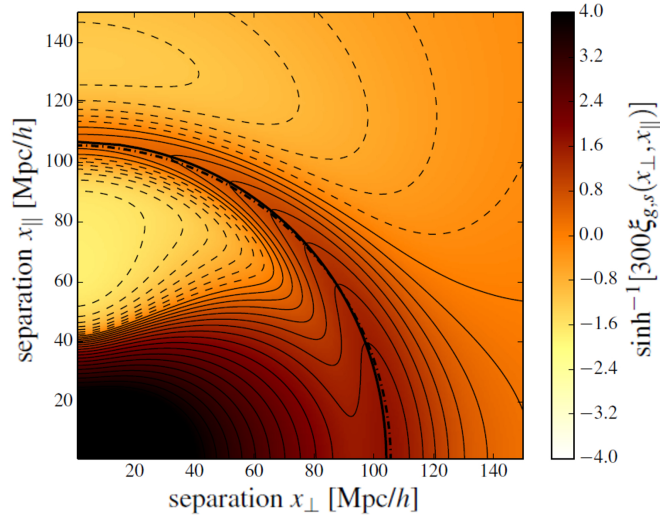


Figure 3.3: Reconstruction from a direct peak determination on (3.18). Brighter regions depict smaller values of the field, while darker ones depict higher ones. As shown in the right side of the picture, what is reported here is the arc-sine-hyperbolic of the corresponding function to make the colour variations noticeable. The dashed-dotted line marks the location of the real space isotropic BAO peak, while the bold solid one marks the location of the reconstructed BAO peak. Figure taken from [34].

tribution with respect to (2.108). Given the fact that $\mathcal{L}_4(\mu = 1) = 1$ and $\mathcal{L}_4(\mu = 0) = 3/8$, it enhances the 2PCF along the LOS while it suppress it in the perpendicular direction. Given the smaller magnitude with respect to the quadrupole, the hexadecapole leaves the overall behaviour of the redshift space correlation function unchanged.

3.5 The Shift of the BAO Peak

The purpose of all of our derivations comes clear once we recall that the BAO peak is an important feature of the 2PCF and, therefore, a deep understanding of the redshift space correlation function brings important information for the determination of the redshift space location, and features, of the BAO peak itself. Thanks to the fact that the redshift space 2PCF is a linear combination of multipoles inside equation (2.108), or (3.84) if one includes nonlinearities, these differences will be reflected to the BAO peak location; this feature is depicted in Figure 3.4 for the linear model of [34], with the monopole alone (black solid line) as well as all the three multipoles once shape of the no-wiggle 2PCF has been subtracted (red, green and blue solid lines)¹². Referring to the same Figure, vertical dashed lines report the location of the BAO peak for every function but the scaled local peculiar velocity $[u_{||}(x) - u_{||}^{nw}(x)]/x$.

To analyse the location of the BAO peak in redshift space, we first need to define it: from the considerations given in Section 1.5 we can define the peak as a local maximum at radial coordinate $r = 105.6 h^{-1}\text{Mpc}$ [6, 34, 62, 72]. The first characteristic to notice is that the dependence of (2.108) on

¹²The no-wiggle 2PCF for [34] has been calculated from equation (2.108) using the no-wiggle PS from [19].

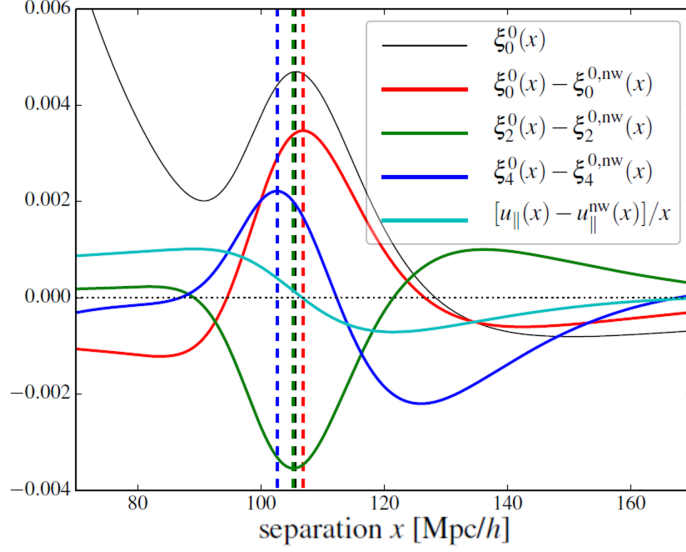


Figure 3.4: Real space location of the BAO peak for the monopole $\xi_0^0(r)$ (black line) and for the wiggly parts of $\xi_0^0(r)$ (red), $\xi_2^0(r)$ (green) and $\xi_4^0(r)$ (blue), with the no wiggle 2PCF determined using the PS of [19]. Vertical lines marks the peak location for the four curves: $r_{\text{BAO}} = 105.6, 106.8, 105.2$ and $102.6 h^{-1}\text{Mpc}$ of respectively $\xi_0^0(r)$, $\xi_0^0(r) - \xi_0^{\text{no-wiggle}}(r)$, $\xi_2^0(r) - \xi_2^{\text{no-wiggle}}(r)$ and $\xi_4^0(r) - \xi_4^{\text{no-wiggle}}(r)$. The cyan line shows the local peculiar velocity field rescaled by x . Figure taken from [34].

Legendre polynomials $\mathcal{L}_i(\mu)$, which in turn translates into an angular dependence, makes the redshift space 2PCF lose its isotropy. This novel angular dependence arises from the derivatives of velocity moments in the final equation (3.18) (but also (3.47), (3.61) and/or (3.70), dependently on the adopted model) [34]

$$\begin{aligned} \frac{d}{dr_{\parallel}} f v_{12}(1 + \xi) &= \frac{2}{3}\beta\xi_0^0 - \frac{4}{3}\beta\xi_2^0\mathcal{L}_2(\mu) \\ \frac{1}{2}\frac{d}{dr_{\parallel}} f^2\sigma_{12}^{\text{LD}}(1 + \xi) &= \beta^2 \left[\frac{1}{5}\xi_0^0 - \frac{4}{7}\xi_2^0\mathcal{L}_2(\mu) + \frac{8}{35}\xi_4^0\mathcal{L}_4(\mu) \right], \end{aligned} \quad (3.85)$$

with latter nonlinear descriptions determining even a more complex angular dependence (3.84). For the explicit relations between pairwise velocity moments and 2PCF multipoles expressed above we refer to equations (B.31) and (A.29), which are demonstrated step by step in Appendices A and B. By looking at (3.85), one can see that the net effect determines an enhancement of the 2PCF value along the the direction perpendicular to the LOS and a suppression along the parallel one [34, 62]. The nonlinear multipole expansion of equation (3.84) shows the same overall behaviour, with additional features coming from products of pairs of 2PCFs describing the even valued multipoles more deeply.

As visible in Figure 3.5, the BAO peak tend to follow the same pattern, with the maximum value of the distortions being at the two extrema of the direction cosine. Referring to Figure 3.5, it is important to notice that the various features of the redshift space 2PCF are sensitive to the method used to find the BAO peak [34]: they have found that the shift of the peak is of the order $\Delta_{\text{BAO}} \approx 1.5 h^{-1}\text{Mpc}$ for a direct peak extraction (red solid line), while it reduces to a value of $\Delta_{\text{BAO}} \approx 0.5 h^{-1}\text{Mpc}$

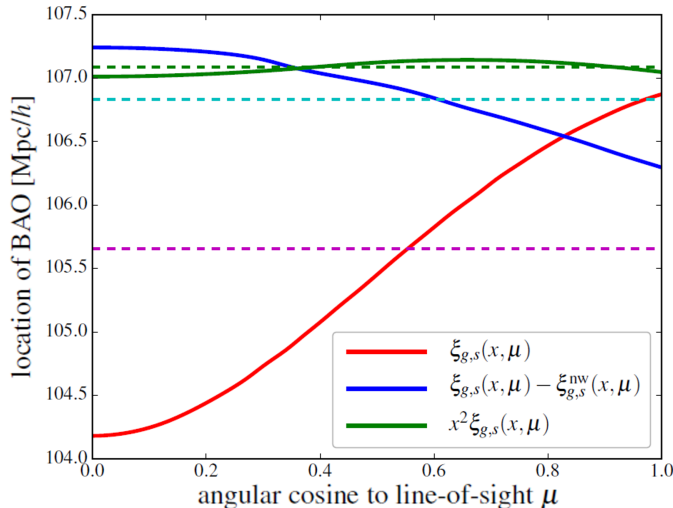


Figure 3.5: Location of the BAO peak as function of the angular cosine μ . The red solid line marks the behaviour of the peak for the direct peak extraction, the dashed magenta line shows the isotropic location of the peak in real space. Solid blue and dashed cyan lines are the BAO peak location measured from the wiggly redshift space 2PCF. Green solid and dashed lines follow the same convention for $r^2\xi(r, \mu)$. Figure taken from [34].

for a peak found by subtracting to the 2PCF the broadband shape of the BAO-less one, determined using the no-wiggle PS of [19] inside equation (2.106) (blue solid one). The green solid line shows distortions of the peak location of $r^2\xi(r)$, rather than just $\xi(r)$, it is much more stable: this is because the r^2 factor tends to cancel out the contribution due to the radial peculiar velocity, the first one in equation (3.85), leaving RSDs dependent on the velocity dispersion only, which has a much smaller magnitude [34, 69].

The peak presents also an additional variation in both intensity and width, namely it tend to shrink and become sharper along the LOS direction while we see the opposite behaviour as far as we approach the perpendicular direction: the reason of such a behaviour is that the peculiar velocity of galaxies around the BAO peak tend to be pointed towards the peak itself resulting in a more severe contribution in the two directional extrema, where we have those velocities aligned along the LOS in the former case and perpendicular to it in the latter [34, 69] as reported in the schematic picture in Figure 3.6. To better illustrate this further characteristics we report in Figure 3.7 the redshift space reconstruction of the BAO peak from the numerical simulation analysed in [69].

The BAO peak is highlighted also in Figure 3.8 where two different redshift space 2PCF have been compared, namely the one resulting from the simple combination of the nonlinear Kaiser model (2.43) with a Gaussian FOG exponential (2.40) (dashed lines) against the one including the additional terms from the TNS approach¹³ (2.131) (solid lines), with the effective velocity dispersion set to the best fitting values from cosmological analysis of Mock catalogues ($\sigma_{v, \text{eff}}^2 = 5.2_{-3.9}^{+2.9} [h^{-1}\text{Mpc}]$) [62]. It

¹³The two terms coming from the later analysis of [77], $T(k, \mu)$ and $F(k, \mu)$, have been omitted in Figures from [62]: this is because, as we were reporting in Section 2.7.3, they determine correction of the same magnitude but opposite sign, making their net contribution to the model negligible [57, 68, 77].

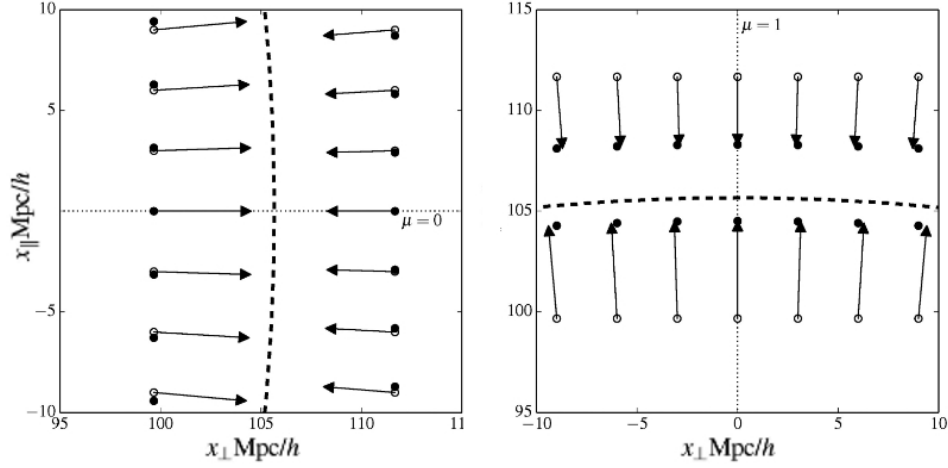


Figure 3.6: Schematic representation of the BAO peak sharpening mechanism in the direction perpendicular to the LOS (left panel) and along the LOS (right panel). The bold dashed line denotes the BAO peak at $x \sim 105 [h^{-1}\text{Mpc}]$, the white circles denote the galaxy coordinates in real space, while the black ones their coordinates in redshift space; the vectors depict the peculiar velocities of galaxies, always pointed toward the peak. To better visualize velocity features, their magnitude has been amplified by a factor 100. Figure taken from [34].

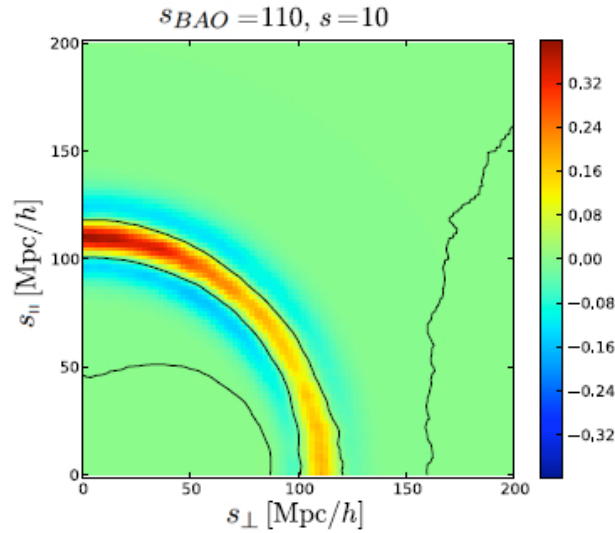


Figure 3.7: Redshift space reconstruction of the BAO peak from the Gaussian simulations discussed in [69]. The panel shows the linear theory redshift 2PCF flattened at a redshift coordinate of $s_{BAO} = 110 [h^{-1}\text{Mpc}]$ and for galaxies separated by $s = 10 [h^{-1}\text{Mpc}]$. Figure taken from [69]; labels have been modified to match with our definitions.

is possible to see that the peak is located at a coordinate $s_{\perp} \lesssim 105 [h^{-1}\text{Mpc}]$ in the perpendicular direction, while it reaches the LOS direction at $s_{\parallel} \gtrsim 105 [h^{-1}\text{Mpc}]$ following the angular dependence shown in Figure 3.5. The Figure shows that the two models agree at small scales but differ from each others as far as we move to large scales, with the major discrepancies being located at the BAO acoustic peak: this is due to the corrective terms $A(k, \mu)$ and $B(k, \mu)$ inserted by the TNS description, which start deviating from zero around the peak scale [68].

In Figure 3.9 it is illustrated the behaviour of the BAO peak under variations of the angular diameter distance D_A and the inverse of the Hubble parameter H^{-1} . These variations are important to understand because, as we were illustrating in Section 1.5.2, they are the quantities obtained from the Alcock-Paczynski test and are fundamental to probe DE properties. We know from Section 1.5.1 that if the correct distances of the objects are known, then the BAO peak form an invariant great circle. Following equation (1.83), if the angular diameter distance is unknown the BAO circle becomes uncertain transversely, being compressed when D_A decreases and stretched if D_A increases; the same modification affects the parallel direction for variations of the radial distance, which is directly dependent on the inverse of the Hubble expansion parameter H^{-1} . In principle the ratio between radial and transverse distances varies with the assumed cosmological models however, if the shape of an object is known a priori, it becomes possible to disentangle D_A and H improving significantly the results coming from the Alcock-Paczynski test [6, 62]. More explicitly, the scale of the measured 2PCF (in redshift space) $\{z_{\perp}, z_{\parallel}\}$, is related to the theoretical distance scale $\{s_{\perp}, s_{\parallel}\}$ (the one according to equation (1.83)) through [57, 62]

$$\begin{aligned} z_{\perp} D_A(z) &= s_{\perp} D_A^{fid}(z) \\ z_{\parallel} H^{fid}(z) &= s_{\parallel} H(z), \end{aligned} \tag{3.86}$$

where the *fid* label marks the quantity given the assumed cosmological model. From that, the relation between real and measured redshift separations reads

$$\begin{aligned} s &= \sqrt{s_{\perp}^2 + s_{\parallel}^2} = \left\{ \left(\frac{D_A(z)}{D_A^{fid}(z)} \right)^2 z_{\perp}^2 + \left(\frac{H^{fid}(z)}{H(z)} \right)^2 z_{\parallel}^2 \right\}^{1/2}, \\ \nu = \frac{s_{\parallel}}{s} &= \left(\frac{H^{fid}(z)}{H(z)} \right) z_{\parallel} \left\{ \left(\frac{D_A(z)}{D_A^{fid}(z)} \right)^2 z_{\perp}^2 + \left(\frac{H^{fid}(z)}{H(z)} \right)^2 z_{\parallel}^2 \right\}^{-1/2}. \end{aligned} \tag{3.87}$$

Then the measured 2PCF, $\xi_s^{fid}(z_{\perp}, z_{\parallel})$, is given in the fiducial parameter space $\{D_A^{fid}, H^{fid}\}$, while the theoretical 2PCF with arbitrary $\{D_A, H\}$ is fitted to $\xi_s^{fid}(z_{\perp}, z_{\parallel})$ using the equations above.

In conclusion, with the BAO acoustic peak being located at relatively large scales where RSDs can still be well described in a non perturbative way, a precise characterization of the redshift behaviour of the 2PCF turns out to be crucial to retrieve a huge amount of cosmological information and, thus, deepen our understanding of the Universe.

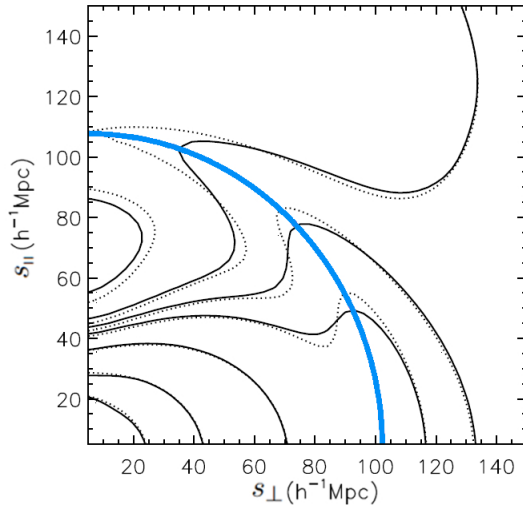


Figure 3.8: Comparison between the redshift 2PCF coming from the simple combination of the nonlinear Kaiser term with a Gaussian FOG exponential (dashed lines) and the one determined by the TNS model (solid lines). The bold cyan line describes the redshift BAO acoustic peak around $s \sim 105 [h^{-1}\text{Mpc}]$ and it respect the result given in Figure 3.5. Figure taken from [62], label have been modified to match with our definitions.

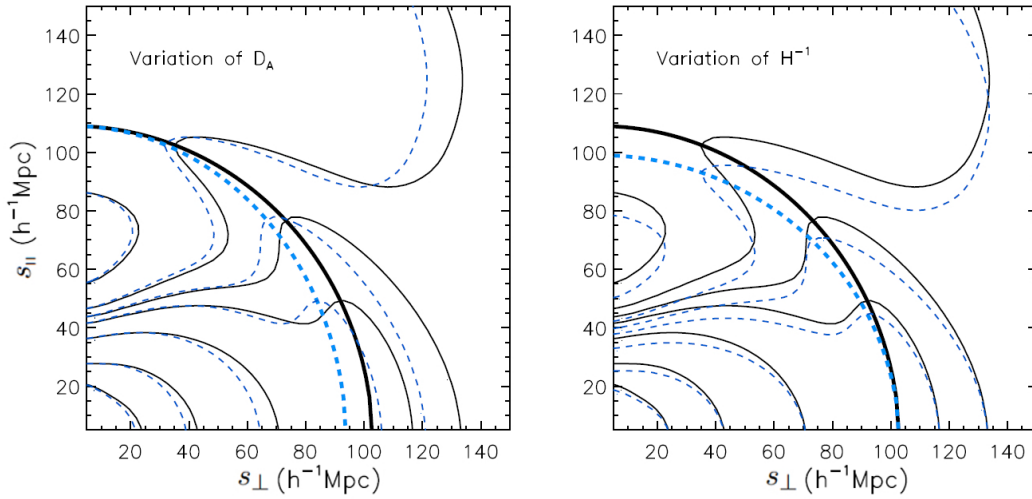


Figure 3.9: Both panels show how the redshift space 2PCF and BAO peak are modified from a 10% decrease of the estimated D_A (left) and H^{-1} (right). Thin black solid lines depict contours of the redshift space 2PCF from the TNS model and bold black solid line marks the location of the BAO peak. Thin dashed cyan lines depict the modification of the 2PCF contours when the respective parameter is varied, bold cyan dashed lines show instead the changes happening on the BAO acoustic peak. Figure taken from [62], labels have been modified to match our definitions.

4. Conclusions

With this work we have investigated RSDs and their implications for our understanding of the Universe. In particular, we have focused our attention toward a description in the non- and quasilinear regime using the plane-parallel approximation. It is clearly evident however, from all the various approaches reported and all the different assumptions available, that a completely analytical modelling of redshift space correlation functions and velocity statistics is a challenging and complex task to accomplish. Moreover, the difference between models is often more complex than a simple right/wrong, with different approaches becoming favourable over others once the scale of interest changes. With this final Chapter we want to give a final, brief summary on the major results of above and provide our take on possible improvements for this work.

4.1 Summary

BAOs are one of the most important feature of the matter, and radiation, PS. They are relics coming from a time prior to recombination, where the matter and radiation field were coupled together in a single fluid. They are product of the interaction between radiation pressure and gravity creating spherical acoustic waves in the primordial plasma which, in turn, determined the presence of over dense regions that later on favoured galaxy formation. Those spherical over densities, once projected in the sky plane, turns out to be the well known BAO acoustic rings. Their importance comes from the fact that their physical size of $\sim 105 [h^{-1}\text{Mpc}]$ can be measured by rather simple physics, make them an ideal standard ruler to measure the distances of the Universe.

With the BAOs information being determined by regions where the galaxy are slightly more dense than the average, they happen to be deeply linked with the galaxy (and, to be completely general, with the totality of matter) n -point correlation functions, a set of statistical functions telling us how much a given distribution differs from a random one. With this work we focused on the simplest among the correlation functions, namely the 2PCF, which analyse the galaxy statistics by looking at galaxy pairs. One of the major complexities in the characterization of the galaxy/matter 2PCF comes from the fact that our access to distance information comes from the Hubble law and, therefore, from redshift measurements. This complexity is ultimately determined by the peculiar velocity of galaxies that adds to the Hubble flow and perturbs redshift measurements introducing RSDs that need to be investigated, described and understood. From that comes the necessity to give a precise description of the 2PCF that the scientific community is trying to answer.

Chapter 2 has the purpose of illustrate the theory behind the 2-point statistics of the two main theoretical models used throughout the work, namely the Streaming model of Section 2.5 and the TNS one of Section 2.7. For both approaches we have explicitly shown their agreement with the large

scale Kaiser formula (2.31) for the PS. In Section 2.6 we have presented how the linear treatment of RSDs can be described with the multipole expansion of either the redshift space 2PCF or PS, showing redshift measurements done to access the third dimension in galaxy surveys determine a loss of isotropy of the galaxy clustering process. Section 2.8 closes the Chapter with

- a new definition of the pairwise generating function, $\mathcal{Z}(\lambda, \mathbf{r})$, which is able to simplify the comparison between different models,
- the step-by-step construction of the TNS generating function $\mathcal{Z}^{\text{TNS}}(\lambda, \mathbf{r})$ we have used later on in Chapter 3.

The main outcome of the Chapter is the 1 : 1 map between Streaming and TNS approach we have provided with equations (2.147) to (2.157): it shows that despite the different assumptions and thought processes behind their building they are describing the same quantities and, thanks to that, the comparison between them we have done in Chapter 3 is well motivated.

With Chapter 3 we carried out our derivations following both the general procedure proposed by R. Scoccimarro in [58] and the TNS model reported in Section 2.7. Namely

- In Section 3.1 we have derived results from [34] using our notation in order to have an easier comparison with nonlinear results later on in the Chapter

$$1 + \xi_s(s_\perp, s_\parallel) = 1 + \xi(r) - f \frac{dv_{12}}{dr_\parallel} + \frac{1}{2} f^2 \frac{d^2 \sigma_{12}^{\text{LD}}}{dr_\parallel^2} + \mathcal{O}(\xi^2).$$

- Starting from the generating function (2.172) we have converted the TNS description in configuration space, showing it is able to provide a description of the pairwise generating function comparable with the Gaussian streaming model of [34]. Furthermore it deepens the PDF description by making it dependent not only on the mean pairwise velocity v_{12} and the linear velocity dispersion of the Kaiser term σ_{12}^{LD} like the Gaussian case, but also on the velocity dispersion from the random motion of virialized objects $\sigma_{12}^{\text{virialized}}$, which is treated as a free parameter, and nonlinear contributions to the Kaiser velocity dispersion. All those dependencies enter in the large scales redshift space 2PCF expressed in equation (3.49)

$$1 + \xi_s^{\text{TNS}}(s_\perp, s_\parallel) \simeq 1 + \xi - f \frac{dv_{12}}{dr_\parallel} + \frac{1}{2} f^2 \frac{d^2 \sigma_{12}^{\text{LD}}}{dr_\parallel^2} + \frac{1}{2} f^2 \frac{d^2 \sigma_{12}^{\text{virialized}}}{dr_\parallel^2} + \frac{1}{2} f^2 \frac{d^2 \langle \Delta u_\parallel^2(\delta + \delta') \rangle}{dr_\parallel^2} + \mathcal{O}(\xi^2),$$

which shows it is able to reproduce equation (17) of [34] with the addition of nonlinearities.

- We also reported the B. Reid and M. White approach, which has been built in [55] from the Gaussian streaming model that was the starting point for the [34] derivation. We called it "a bridge" between Streaming and TNS approach because we have shown that, by adding a perturbative description of the pairwise velocity dispersion inside its formulation, it can recover a generating function very similar to the one from the latter starting from Gaussian results.

- We then further expanded the redshift space description of the large scale 2PCF accounting for nonlinear terms that were left outside from [34] calculations

$$1 + \xi_s(s_\perp, s_\parallel) \simeq 1 + \xi - f \frac{dv_{12}}{dr_\parallel} + \frac{1}{2} f^2 \frac{d^2 \sigma_{12}^{2\text{LD}}}{dr_\parallel^2} + \frac{1}{2} f^2 \frac{d^2 \langle \Delta u_\parallel^2 (\delta + \delta') \rangle}{dr_\parallel^2} + \frac{1}{2} f^2 \frac{d^2 \langle \Delta u_\parallel^2 \delta \delta' \rangle_c}{dr_\parallel^2} + \mathcal{O}(\xi^2).$$

The addition of nonlinear terms implies that, differently from (3.18), our large scale expansion depends on the *exact* pairwise velocity dispersion, σ_{12}^2 , rather than on the one described by assuming linear dynamics $\sigma_{12}^{2\text{LD}}$, accounting for nonlinear terms

$$\frac{1}{2} \frac{d^2 \langle \Delta u_\parallel^2 (\delta + \delta') \rangle}{dr_\parallel^2} \quad \& \quad \frac{1}{2} \frac{d^2 \langle \Delta u_\parallel^2 \delta \delta' \rangle_c}{dr_\parallel^2}$$

that were not completely considered in the previous derivation.

- Finally, from that we were able to rewrite the multipole expansion of the redshift space 2PCF of Section 2.6 in a way that is able to incorporate nonlinearities (3.84)

$$\begin{aligned} 1 + \xi_s(s_\perp, s_\parallel, \mu) &= \\ &= \left\{ \left(1 + \frac{2}{3}\beta + \frac{1}{5}\beta^2 \right) \xi_0^0 + \frac{2}{3}(\beta \xi_1^{-1} \xi_1^1 - \beta^2 \xi_2^{-2} \xi_1^3) + 2\beta^2 \xi_1^{-1} \xi_1^3 + \right. \\ &+ \left. \frac{4}{3}\beta^2 \xi_1^{-1} \xi_2^2 + \frac{7}{5}\beta^2 (\xi_2^{-2} \xi_2^2 - \xi_1^{-1} \xi_3^1) \right\} \mathcal{L}_0(\mu) + \\ &+ \left\{ - \left(\frac{4}{3}\beta + \frac{4}{7}\beta^2 \right) \xi_2^0 + \frac{4}{3}(\beta \xi_1^{-1} \xi_1^1 - \beta^2 \xi_2^{-2} \xi_1^3) + \frac{8}{3}\beta^2 \xi_1^{-1} \xi_2^2 + \frac{8}{7}\beta^2 (\xi_2^{-2} \xi_2^2 - \xi_1^{-1} \xi_3^1) \right\} \mathcal{L}_2(\mu) + \\ &+ \left\{ \frac{8}{35}\beta^2 \xi_4^0 + \frac{16}{35}\beta^2 (\xi_2^{-2} \xi_2^2 - \xi_1^{-1} \xi_3^1) \right\} \mathcal{L}_4(\mu) \end{aligned}$$

As one expects by our choice to remain in the plane-parallel approximation, this improved description of the angular behaviour is able to maintain the even structure of multipoles. Given their smaller magnitude with respect to linear terms inside (2.108) (recall that $\beta := f/b \simeq \Omega_m^{0.6}$ and 2PCF multipoles are, almost everywhere, decreasing function of r that reach values between $O(10^{-2})$ and $O(10^{-3})$ already in the quasilinear regime $r \sim 30 : 80 [h^{-1}\text{Mpc}]$ [27]), they are not able to invert the directional trend set by linear dynamics.

4.2 Outlook

In this final segment of the thesis we want to give an outlook on the possible ways that can be explored to improve our comprehension of RSDs. We start recalling the major assumptions made during the work, namely the single stream approximation for the closure of the Vlasov equation, equation (1.41), the plane-parallel approximation expressed in Section 2.2 and the Newtonian description of large scales structures. Moreover, the definition of the the pairwise velocity moments (2.68) we have given in this

work have been retrieved using the language of statistical field theory in terms of density and velocity perturbations. Even if these definitions give an extremely good approximation for particle DM and they can be generalized to multi streaming, it has been pointed out [39, 40] they determine a pairwise velocity PDF, as well as a moment generating function, which completely neglect velocity correlations. All the three assumptions before have the only purpose to simplify the calculations and hence they can be dropped in order to refine the resulting model with the drawback of a more complex mathematical formalism.

In addition to that, different approaches can be made to describe the shape of the pairwise velocity PDF: we cite for example two works by J. Kuruvilla and C. Porciani [39, 40], which have attempted to describe $\mathcal{P}(y, \mathbf{r})$ with a so called normal-variance mean mixture of distributions that was explored at first to describe particle velocities in an ideal relativistic gas; it consists in a convolution between a normal distribution and an hyperbolic one. With this approach they were able to describe the pairwise velocity PDF using the family of distribution function known as *Generalized Hyperbolic Distributions* that allowed them to reproduce with high precision the redshift space 2PCF at the cost of having five free parameters.

Regarding a more direct improvement of our results expressed using the completely general approach of Section 3.4, the first thing that comes to mind is to tackle the problem by perturbatively expand the description of the density and velocity fields and, then, propagate this description to all the derived quantities. Since with this work we chose to describe RSDs in a non perturbative way, most of those derivations were beyond the scope of this work; however, as one might expect, this way of thinking has already been highly explored in the literature: throughout this work we cited, among many others, the works of [7, 55, 62, 68, 71, 77].

Following the considerations given in Section 1.4, we want also to stress the 2PCF is the only non vanishing statistics only for the Gaussian case. As it comes clear by our derivations, which add onto the original considerations from R. Scoccimarro [58], Gaussianity is never truly reached in any realistic scenarios: in those settings we have usually conditions very close (but not exactly equal) to Gaussianity; therefore a more complete description of the clustering phenomenon, and in turn a better characterization of the RSDs, could be achieved by considering also higher statistics as the Bispectrum and Trispectrum of matter. To conclude this work, given the pure analytical setting we placed ourselves in, here we performed just the mathematical derivations behind the modelling of the redshift space 2PCF. To test the scientific validity of those derivations, it is then necessary to compare them against N-body simulations and real cosmological data.

Appendix A: Velocity Moment Relation with 2PCF Multipoles

Our starting point to reconnect equations (23) and (27) of the 2014 paper [34] with the general multipole expansion defined in equation (2.108) will be equation (3.18), which we report for convenience below

$$1 + \xi(s_{\perp}, s_{\parallel}) = 1 + \xi(r) - f \frac{dv_{12}}{dr_{\parallel}} + \frac{1}{2} f^2 \frac{d^2 \sigma_{12}^{2\text{LD}}(\mathbf{r})}{dr_{\parallel}^2}. \quad (\text{A.1})$$

With this Appendix we want to give a detailed step-by-step computation of the various terms inside the equation above in terms of ξ_n^m multipoles, each one separated from the others to give the reader the complete control over the various passages. Later on, in Appendix B, we will couple back together all the different multipole description of the quantities in (A.1) in order to obtain back equation (2.108)

First Derivative of the Mean Displacement

The first term we deal with is the one containing the derivative of the first velocity moment, v_{12} , defined in equation (2.68). Following Section 2.5.1, we take advantage once more of the linear order work done by R. Scoccimarro [58] and K. B. Fisher [24], between equations (2.79) and (2.81); explicitly we report (2.80) as our starting point¹

$$\begin{aligned} \langle v'_{\parallel} \delta \rangle &= -\hat{\mathbf{r}} \frac{aHf}{b} \int \frac{dk}{2\pi^2} k P_{\delta\theta}(k) j_1(kr) \\ \implies \langle u_{\parallel} \delta' \rangle &= \hat{\mathbf{r}} \frac{1}{b} \int \frac{dk}{2\pi^2} k P_{\delta\theta}(k) j_1(kr). \end{aligned} \quad (\text{A.2})$$

From that, if one exploits the fact both that density and velocity fields evaluated at the same coordinate are uncorrelated and the homogeneity of perturbations, it is possible to see that

$$\langle \Delta u_{\parallel}(\delta + \delta') \rangle = 2 \langle \Delta u_{\parallel} \delta' \rangle = -2\hat{\mathbf{r}} \frac{1}{b} \int \frac{dk}{2\pi^2} k P_{\delta\theta}(k) j_1(kr), \quad (\text{A.3})$$

where the minus sign arises from $\Delta u_{\parallel} := u'_{\parallel} - u_{\parallel}$. The left hand side of the equation above can be set equal to $v_{12}(1+\xi)$ according to the definition of the (2.68) thanks to the fact that $\langle \Delta u_{\parallel} \rangle = \langle \Delta u_{\parallel} \delta \delta' \rangle = 0$

¹Once more we drop the g label we used in Section 2.6 to refer to galaxies in order to avoid its proliferation and increase the clarity of the equations.

due to the symmetry property of the velocity field [8]. The right hand side can be lightened recalling the form of the 2PCF multipoles of equation (2.106), making the whole equation (A.3) [34]

$$fv_{12}(1 + \xi) = -2\hat{\mathbf{r}}r \frac{f}{b} \int \frac{dk}{2\pi^2} k^2 P_{\delta\theta}(k) \frac{j_1(kr)}{kr} = -2r_{\parallel} \beta \xi_1^1, \quad (\text{A.4})$$

thanks to $r_{\parallel} := \hat{\mathbf{r}}r$ and $\beta := f/b$. Considering equation (A.1) is the result of a large scale expansion, we can take advantage of $\xi \ll 1$ and write

$$-\frac{dfv_{12}}{dr_{\parallel}} \simeq -\frac{dfv_{12}(1 + \xi)}{dr_{\parallel}} = 2\beta\xi_1^1 + 2\beta r_{\parallel} \frac{d}{dr_{\parallel}} \xi_1^1. \quad (\text{A.5})$$

We can see equation (A.5) presents the radial derivative of the 1-1 multipole of the 2PCF, we can address its computation with the following properties of the spherical Bessel functions [3]

$$\frac{d}{dx} j_l(x) = \frac{l}{x} j_l(x) - j_{l+1}(x). \quad (\text{A.6})$$

For future reference, we also explicit the derivative dr/dr_{\parallel} from the definition of the galaxy separation $r^2 := r_{\perp}^2 + r_{\parallel}^2$

$$\frac{dr}{dr_{\parallel}} = \frac{1}{2} \frac{1}{\sqrt{r_{\perp}^2 + r_{\parallel}^2}} 2r_{\parallel} = \frac{r_{\parallel}}{r} := \mu. \quad (\text{A.7})$$

Implementing the calculations inside (A.5) we got

$$\begin{aligned} \frac{d}{dr_{\parallel}} \xi_1^1 &= \frac{d}{dr_{\parallel}} \int \frac{dk}{2\pi^2} k^2 P_{\delta\theta}(k) \frac{j_1(kr)}{(kr)^1} = \frac{dr}{dr_{\parallel}} \frac{d}{dr} \int \frac{dk}{2\pi^2} k^2 P_{\delta\theta}(k) \frac{j_1(kr)}{(kr)^1} \\ &= \mu \int \frac{dk}{2\pi^2} k^2 P_{\delta\theta}(k) \frac{dkr}{dr} \frac{d}{dkr} \frac{j_1(kr)}{(kr)^1} = \mu \int \frac{dk}{2\pi^2} k^2 P_{\delta\theta}(k) k \frac{d}{dkr} \frac{j_1(kr)}{(kr)^1} \\ &= \mu \int \frac{dk}{2\pi^2} k^2 P_{\delta\theta}(k) k \left[\frac{1}{(kr)^1} \left(\frac{1}{kr} j_1(kr) - j_2(kr) \right) - \frac{j_1(kr)}{(kr)^2} \right] \\ &= -\mu \int \frac{dk}{2\pi^2} k^2 P_{\delta\theta}(k) k \frac{j_2(kr)}{(kr)^1} = -\mu \frac{1}{r} \int \frac{dk}{2\pi^2} k^2 P_{\delta\theta}(k) kr \frac{j_2(kr)}{(kr)^1} \\ &= -\mu \frac{1}{r} \xi_2^0, \end{aligned} \quad (\text{A.8})$$

which inserted back in equation (A.5) gives

$$-\frac{dfv_{12}}{dr_{\parallel}} = 2\beta\xi_1^1 - 2\beta\mu^2\xi_2^0. \quad (\text{A.9})$$

We will see that the contribution given from ξ_1^1 can be written in terms of $(\xi_0^0 + \xi_2^0)$ (equation (B.30) of Section 4.2) making the derivative above

$$\frac{d}{dr_{\parallel}} f \langle \Delta u_{\parallel}(1 + \delta)(1 + \delta') \rangle = \frac{2}{3} \beta (\xi_0^0 + \xi_2^0) - 2\beta\mu^2\xi_2^0. \quad (\text{A.10})$$

First Derivative of the Velocity Dispersion

Regarding the second moment of the pairwise velocity we have, recalling equation (2.86),

$$f^2 \sigma_{12}^{\text{LD}}(1 + \xi) \simeq f^2 \sigma_{12}^{\text{LD}} = 2(\sigma_v^2 - \Psi_{\perp}(r)(1 - \mu^2) - \Psi_{\parallel}(r)\mu^2) \equiv 2(\sigma_v^2 - \psi_{\perp}(r) + \mu^2 \Delta\Psi(r)), \quad (\text{A.11})$$

where for the last equivalence we have used the definition of $\Delta\Psi(r)$ given in equation (2.73). To describe it in terms of the real space 2PCF multipoles (2.106), we will need to write back the $\Psi_{\perp}(r)$ and $\psi_{\parallel}(r)$ terms as integrals using their definitions of equation (2.72) [34, 58]

$$\begin{aligned} f^2 \sigma_{12}^{\text{LD}} &= 2 \left[\sigma_v^2 - (1 - \mu^2)\beta^2 \int \frac{d^3\mathbf{k}}{(2\pi)^3} \frac{P_{\theta\theta}(k)}{k^2} \frac{j_1(kr)}{kr} + \right. \\ &\quad \left. - \mu^2 \beta^2 \int \frac{d^3\mathbf{k}}{(2\pi)^3} \frac{P_{\theta\theta}(k)}{k^2} \left(j_0(kr) - 2 \frac{j_1(kr)}{kr} \right) \right] \\ &= 2 \left[\sigma_v^2 - \beta^2 \int \frac{d^3\mathbf{k}}{(2\pi)^3} \frac{P_{\theta\theta}(k)}{k^2} \left(\frac{j_1(kr)}{kr} - \mu^2 j_2(kr) \right) \right], \end{aligned} \quad (\text{A.12})$$

which is the form proposed in [34]. Looking back now at the definition of the multipoles (2.106), we can write

$$f^2 \sigma_{12}^{\text{LD}} = 2 [\sigma_v^2 - \beta^2 r^2 (\xi_1^3 - \mu^2 \xi_2^2)]. \quad (\text{A.13})$$

The β^2 factor in the previous equation is present even if $\sigma_{12}^2(1 + \xi)$ is dependent only on the velocity auto-correlation PS because we are in the linear description of the pairwise velocity moment and therefore we can set $P_{\theta\theta}(k) \sim P(k)$, which needs to account to the bias factor correction when we are describing galaxies as we stated in Sections 2.3.1 and 2.4. Since they will be useful, we report the form of some recurring derivatives of the real space separation r and the direction cosine of the separation μ

$$\begin{aligned} \frac{dr}{dr_{\parallel}} &= \frac{1}{2r} 2r_{\parallel} = \mu, \quad r := \sqrt{r_{\perp}^2 + r_{\parallel}^2} \quad \& \quad \mu := \frac{r_{\parallel}}{r} \\ \frac{dr^2}{dr_{\parallel}} &= 2r \frac{dr}{dr_{\parallel}} = 2r\mu \\ \frac{d}{dr_{\parallel}} \mu &= \frac{1}{r} - r_{\parallel} \frac{1}{r^2} \frac{1}{2r} 2r_{\parallel} = \frac{1}{r} (1 - \mu^2) \\ \frac{d}{dr_{\parallel}} \mu^2 &= 2\mu \frac{d}{dr_{\parallel}} \mu = 2\mu \frac{1}{r} (1 - \mu^2). \end{aligned} \quad (\text{A.14})$$

The first derivative of equation (A.13), needed to describe the last term of (A.1), reads

$$\begin{aligned} \frac{df^2 \sigma_{12}^{\text{LD}}}{dr_{\parallel}} &= -2\beta^2 \left[2r\mu(\xi_1^3 - \mu^2 \xi_2^2) + r^2 \frac{d}{dr_{\parallel}} (\xi_1^3 - \mu^2 \xi_2^2) \right] \\ &= -2\beta^2 \left[2r\mu(\xi_1^3 - \mu^2 \xi_2^2) + r^2 \frac{d\xi_1^3}{dr_{\parallel}} - r^2 \frac{d\mu^2}{dr_{\parallel}} \xi_2^2 - r^2 \mu^2 \frac{d\xi_2^2}{dr_{\parallel}} \right] \\ &= -2\beta^2 \left[2r\mu(\xi_1^3 - \mu^2 \xi_2^2) + r^2 \frac{d\xi_1^3}{dr_{\parallel}} - 2\mu r (1 - \mu^2) \xi_2^2 - r^2 \mu^2 \frac{d\xi_2^2}{dr_{\parallel}} \right]. \end{aligned} \quad (\text{A.15})$$

To deal with the derivatives of 2PCF multipoles, we use again the properties shown above, equation (A.6), obtaining

$$\begin{aligned}
\frac{d}{dr_{\parallel}} \xi_1^3 &= \mu \frac{d}{dr} \xi_1^3 = \mu \int \frac{dk}{2\pi^2} k^2 P_{\delta\theta}(k) \frac{d}{dr} \frac{j_1(kr)}{(kr)^3} \\
&= \mu \int \frac{dk}{2\pi^2} k^2 P_{\delta\theta}(k) k \left[\frac{1}{(kr)^3} \left(\frac{1}{kr} j_1(kr) - j_2(kr) \right) - 3 \frac{1}{(kr)^4} j_1(kr) \right] \\
&= \mu \int \frac{dk}{2\pi^2} k^2 P_{\delta\theta}(k) k \left[-2 \frac{1}{(kr)^4} j_1(kr) - \frac{1}{(kr)^3} j_2(kr) \right] \\
&= -\mu \frac{1}{r} (2\xi_1^3 + \xi_2^2)
\end{aligned} \tag{A.16}$$

and

$$\begin{aligned}
\frac{d}{dr_{\parallel}} \xi_2^2 &= \mu \frac{d}{dr} \xi_2^2 = \mu \int \frac{dk}{2\pi^2} k^2 P_{\delta\theta}(k) \frac{d}{dr} \frac{j_2(kr)}{(kr)^2} \\
&= \mu \int \frac{dk}{2\pi^2} k^2 P_{\delta\theta}(k) k \left[\frac{1}{(kr)^2} \left(\frac{2}{kr} j_2(kr) - j_3(kr) \right) - 2 \frac{1}{(kr)^3} j_2(kr) \right] \\
&= -\mu \frac{1}{r} \int \frac{dk}{2\pi^2} k^2 P_{\delta\theta}(k) \frac{j_3(kr)}{kr} = -\mu \frac{1}{r} \xi_3^1.
\end{aligned} \tag{A.17}$$

Thus equation (A.15) becomes

$$\begin{aligned}
\frac{df^2 \sigma_{12}^2 \text{LD}}{dr_{\parallel}} &= -2\beta^2 [2r\mu(\xi_1^3 - \mu^2 \xi_2^2) - r\mu(2\xi_1^3 + \xi_2^2) + \\
&\quad - 2r\mu(1 - \mu^2)\xi_2^2 + r\mu^3 \xi_3^1].
\end{aligned} \tag{A.18}$$

The previous equation will be our starting point for the computation of the second order derivative of the second cumulant done in the following subsection. Moreover, it corresponds to one of the three pairwise velocity contributions present in the second order term of the large scale redshift space 2PCF of equation (2.90), which is nonlinear and thus it can be dropped while performing a linear description as in [34].

Second Derivative of the Velocity Dispersion

Keeping in mind that our aim is simplifying equation (A.1), the next step will be computing the second derivative of the second pairwise velocity moment, which is equal to

$$\begin{aligned}
-\frac{1}{2\beta^2} \frac{d^2 f^2 \sigma_{12}^2 \text{LD}}{dr_{\parallel}^2} &= 2\mu^2(\xi_1^2 - \mu^1 \xi_2^2) + 2Q(\xi_1^3 - \mu^2 \xi_2^2) - 2\mu^2(2\xi_1^3 + \xi_2^2) - 4\mu^2 Q \xi_2^2 + 2\mu^2 \xi_3^1 + \\
&\quad - \mu^2(2\xi_1^3 + \xi_2^2) - Q(2\xi_1^3 + \xi_2^2) - 2\mu^2(2\xi_1^3 + \xi_2^2) + \mu^2 \xi_3^1 + \\
&\quad - 2\mu^2 Q \xi_2^2 - 2Q^2 \xi_2^2 + 4\mu^2 Q \xi_2^2 + 2\mu^2 \xi_3^1 + \\
&\quad + \mu^4 \xi_3^1 + 3\mu^2 Q \xi_3^1 + \mu^4(2\xi_3^1 - \xi_4^0),
\end{aligned} \tag{A.19}$$

where we have defined the quantity $Q := 1 - \mu^2$ to make the equation more compact; its derivative reads

$$\frac{dQ}{dr_{\parallel}} = -2\mu \frac{d\mu}{dr_{\parallel}} = -2\mu \frac{1}{r} Q. \quad (\text{A.20})$$

Each line of equation (A.19) comes from the Leibniz rule of derivatives applied on the respective term in equation (A.18), with the derivatives of ξ_1^3 and ξ_2^2 computed in equations (A.16) and (A.17). Here we highlight that, on top of equations (A.16) and (A.17), we need the computation of the derivative of ξ_3^1 . We show its derivation here below using, again, (A.6)

$$\begin{aligned} \frac{d}{dr_{\parallel}} \xi_3^1 &= \mu \frac{d}{dr} \xi_3^1 = \mu \int \frac{dk}{2\pi^2} k^2 P_{\delta\theta}(k) k \frac{d}{dkr} \frac{j_3(kr)}{kr} \\ &= \mu \int \frac{dk}{2\pi^2} k^2 P_{\delta\theta}(k) k \left[\frac{1}{kr} \left(\frac{3}{kr} j_3(kr) - j_4(kr) \right) - \frac{1}{(kr)^2} j_3(kr) \right] \\ &= \mu \frac{1}{r} \int \frac{dk}{2\pi^2} k^2 P_{\delta\theta}(k) \left[2 \frac{j_3(kr)}{kr} - j_4(kr) \right] = \mu \frac{1}{r} (2\xi_3^1 - \xi_4^0). \end{aligned} \quad (\text{A.21})$$

It is useful to simplify equation (A.19) before proceeding further, with some rearrangement of the various terms we have

$$\begin{aligned} -\frac{1}{2\beta^2} \frac{df^2 \sigma_{12}^{\text{LD}}}{dr_{\parallel}} &= 2(\xi_1^3 - \mu^2 \xi_2^2) - (2\xi_1^3 + \xi_2^2) + 2\mu^4 \xi_3^1 + \mu^2 \xi_3^1 + \\ &\quad - 2\mu^2 Q \xi_2^2 - 2Q^2 \xi_2^2 + 2\mu^2 Q \xi_3^1 + \mu^4 \xi_3^1 + \\ &\quad + 3\mu^2 Q \xi_3^1 + \mu^4 (2\xi_3^1 - \xi_4^0). \end{aligned} \quad (\text{A.22})$$

Grouping all the terms so we have ξ_n^m multipole times a polynomial of μ we get

$$\begin{aligned} -\frac{1}{2\beta^2} \frac{df^2 \sigma_{12}^{\text{LD}}}{dr_{\parallel}} &= -\mu^4 \xi_4^0 + \xi_2^2 (-2\mu^2 - 1 - 2\mu^2 Q - 2Q^2) + \\ &\quad + \xi_3^1 (2\mu^4 + \mu^2 + 2\mu^2 Q + \mu^4 + 3\mu^2 Q + 2\mu^4) \\ &= -\mu^4 \xi_4^0 - 3\xi_2^2 + 6\mu^2 \xi_3^1. \end{aligned} \quad (\text{A.23})$$

Equation (A.23), in the form presented above, does not provide much information: to understand its meaning we want to express it in terms of ξ_n^0 multipoles, rather than with the generic ξ_n^m ones. To do so we use an other property of spherical Bessel functions, namely [3, 34]

$$j_{l+1} + j_{l-1} = \frac{2l+1}{x} j_l(x). \quad (\text{A.24})$$

ξ_4^0 is already of the desired form, thus we have just to apply (A.24) to the other two terms

$$\begin{aligned} \xi_2^2 &= \int \frac{dk}{2\pi^2} k^2 P_{\delta\theta}(k) \frac{j_2(kr)}{(kr)^2} \\ &= \int \frac{dk}{2\pi^2} k^2 P_{\delta\theta}(k) \frac{1}{5kr} [j_1(kr) + j_3(kr)] \\ &= \int \frac{dk}{2\pi^2} k^2 P_{\delta\theta}(k) \frac{1}{5} \left[\frac{1}{3} (j_0(kr) + j_2(kr)) + \frac{1}{7} (j_2(kr) + j_4(kr)) \right] \\ &= \frac{1}{5} \left[\frac{1}{3} (\xi_0^0 + \xi_2^0) + \frac{1}{7} (\xi_2^0 + \xi_4^0) \right] \end{aligned} \quad (\text{A.25})$$

and

$$\begin{aligned}
\xi_3^1 &= \int \frac{dk}{2\pi^2} k^2 P_{\delta\theta}(k) \frac{j_3(kr)}{kr} \\
&= \int \frac{dk}{2\pi^2} k^2 P_{\delta\theta}(k) \frac{1}{7} [j_2(kr) + j_4(kr)] \\
&= \frac{1}{7} (\xi_2^0 + \xi_4^0).
\end{aligned} \tag{A.26}$$

Inserting everything together back inside equation (A.23) we obtain

$$\begin{aligned}
-\frac{1}{2\beta^2} \frac{df^2 \sigma_{12}^2 \text{LD}}{dr_{\parallel}} &= -\mu^4 \xi_4^0 - \frac{3}{5} \left[\frac{1}{3} (\xi_0^0 + \xi_2^0) + \frac{1}{7} (\xi_2^0 + \xi_4^0) \right] + 6\mu^2 \frac{1}{7} (\xi_2^0 + \xi_4^0) \\
&= -\frac{1}{5} \xi_0^0 + \left(-\frac{1}{5} - \frac{3}{35} + \frac{1}{7} 6\mu^2 \right) \xi_2^0 + \left(-\mu^4 - \frac{3}{35} + \frac{1}{7} 6\mu^2 \right) \xi_4^0 \\
&= -\frac{1}{5} \xi_0^0 + \frac{1}{35} (-7 - 3 + 30\mu^2) \xi_2^0 + \frac{1}{35} (-35\mu^4 - 3 + 30\mu^2) \xi_4^0,
\end{aligned} \tag{A.27}$$

where we can recognize the Legendre polynomials of order $l = 2$ and $l = 4$ multiplying the second and third term [3]

$$\begin{aligned}
\mathcal{L}_2(\mu) &= \frac{1}{2} (3\mu^2 - 1) \implies \frac{1}{35} (30\mu^2 - 10) = \frac{2}{7} (3\mu^2 - 1) = \frac{4}{7} \mathcal{L}_2(\mu) \\
\mathcal{L}_4(\mu) &= \frac{1}{8} (35\mu^4 - 30\mu^2 + 3) \implies \frac{1}{35} (-35\mu^4 + \mu^2 - 3) = -\frac{8}{35} \mathcal{L}_4(\mu).
\end{aligned} \tag{A.28}$$

Once inserted in the second derivative equation they give exactly the result found in [34]

$$\frac{1}{2} \frac{df^2 \sigma_{12}^2 \text{LD}}{dr_{\parallel}} = \beta^2 \left[\frac{1}{5} \xi_0^0 - \frac{4}{7} \xi_2^0 \mathcal{L}_2(\mu) + \frac{8}{35} \xi_4^0 \mathcal{L}_4(\mu) \right] \tag{A.29}$$

and reproduces correctly the β^2 terms in the multipole expansion of the 2PCF, proposed in equation (2.108). Once again, with the derivative expressed in this form we are able to retrieve information about the directional dependence of the velocity dispersion contribution to the redshift space 2PCF; first of all we see that the correction coming from the monopole is still isotropic which has to be paired with the directional behaviour of the other two. To do that we use the form of the Legendre polynomials given in equation (A.28), obtaining

$\mu = 1$: both \mathcal{L}_2 and \mathcal{L}_4 are equal to 1, determining an overall suppression for the direction parallel to the LOS.

$\mu = 0$: we have $\mathcal{L}_2 = -1/2$ and $\mathcal{L}_4 = 3/8$, both determining a positive correction and hence an enhancement to the 2PCF along the direction orthogonal to the LOS.

This trend is the same as the one presented in [34].

Appendix B: Reconstruction of the Redshift 2PCF Using Multipoles

With the results obtained in Appendix A we can now start expressing our large scales redshift space 2PCF expansion in terms of its real space multipoles: we apply property (A.24) to equation (A.9)

$$\begin{aligned}
\xi_1^1 &= \int \frac{dk}{2\pi^2} k^2 P_{\delta\theta}(k) \frac{j_1(kr)}{kr} \\
&= \int \frac{dk}{2\pi^2} k^2 P_{\delta\theta}(k) \frac{1}{3} [j_0(kr) + j_2(kr)] \\
&= \frac{1}{3} (\xi_0^0 + \xi_2^0),
\end{aligned} \tag{B.30}$$

which gives, thanks to (A.28),

$$\begin{aligned}
\frac{d}{dr_{\parallel}} f v_{12} (1 + \xi) &= \frac{2}{3} \beta \mu (\xi_0^0 + \xi_2^0) - 2\beta \mu^2 \xi_2^0 \\
&= \frac{2}{3} \beta \xi_0^0 + 2\beta \left(\frac{1}{3} - \mu^2 \right) \xi_2^0 \\
&= \frac{2}{3} \beta \xi_0^0 - \frac{4}{3} \beta \xi_2^0 \mathcal{L}_2(\mu).
\end{aligned} \tag{B.31}$$

Again, as we found out for the second cumulant before, this description of the 2PCF multipoles reproduces the exact form of the β terms in the ξ_n^0 multipole expansion of the 2PCF given in equation (2.108). We can see that the first order correction has two contributions: the first one is μ -independent and therefore it is isotropic, while the second one is direction-dependent and, recalling the form of the Legendre polynomials given in equation (A.28), brings an enhancement of the 2PCF along the direction parallel to the LOS, when $\mu = 1$, paired with a suppression of the 2PCF along the orthogonal one, when $\mu = 0$.

Here we can notice that the two anisotropic terms have opposite behaviours, with the quadrupole enhancing the 2PCF along the LOS and suppressing it in the perpendicular direction. Their difference in magnitude however, make the quadrupole contribution prevail over the hexadecapole one.

The term inside (2.108) which is not dependent on β corresponds, inside our large scale expansion (A.1), to the zeroth order $1 + \xi(r)$ term. With a procedure similar to the one used to determine $\langle v\delta' \rangle$ in Section 2.5, equation (2.83), it is possible to show that

$$\begin{aligned}
1 + \xi &= 1 + \langle \delta\delta' \rangle \equiv \langle \Delta u_{\parallel}^0 (1 + \delta)(1 + \delta') \rangle \\
&= \int \frac{d^3\mathbf{k}}{(2\pi)^3} e^{-i\mathbf{k}\cdot\mathbf{r}} P_{\delta\delta}(k),
\end{aligned} \tag{B.32}$$

where we have exploited the fact that 2PCF and PS are Fourier pairs. From here it is possible to retrieve the multipole description of $1 + \xi(r)$ if we recall the integral representation of spherical Bessel functions [3]

$$j_l(kr) = \frac{(-i)^l}{2} \int_{-1}^1 d \cos(\theta) e^{ikr \cos(\theta)} \mathcal{L}_l(\cos(\theta)), \quad (\text{B.33})$$

where we can identify $\cos(\theta)$ as the direction cosine μ . With such a description we can pass from an integration along $d \cos(\theta)$ to one along the colatitude $d\theta$ as follows

$$\int_0^\pi d\theta \sin(\theta) = \int_{-1}^1 d \cos(\theta) \quad (\text{B.34})$$

and recall the usual definition of the infinitesimal solid angle, $d\Omega = \sin(\theta)d\theta$, when we express the volume of the phase space $d^3\mathbf{k}$ as $d^3\mathbf{k} = k^2 dk \sin(\theta)d\theta d\phi = k^2 dk d\phi d\Omega$. Thus, equation (B.32) reads

$$\begin{aligned} 1 + \xi &= \int \frac{dk}{2\pi^2} k^2 P_{\delta\delta}(k) \int_0^{2\pi} \frac{d\phi}{2\pi} \frac{(-i)^0}{2} \int_{-1}^1 d\mu e^{-i\mathbf{k}\cdot\mathbf{r}} \mathcal{L}_0(\mu) \\ &= \int \frac{dk}{2\pi^2} k^2 P_{\delta\delta}(k) j_0(kr) = \xi_0^0, \end{aligned} \quad (\text{B.35})$$

where we have exploited $\mathcal{L}_0(\mu) = 1$.

Coupling together equations (A.29), (B.31) and (B.35) we are finally able to reproduce correctly the multipole expansion of the redshift space 2PCF given in Section 2.6, equation (2.108), up to β^2 terms as we expected

$$1 + \xi_s(s_\perp, s_\parallel) = \left(1 + \frac{2}{3}\beta + \frac{1}{5}\beta^2\right) \xi_0^0 \mathcal{L}_0(\mu) - \left(\frac{4}{3}\beta + \frac{4}{7}\beta^2\right) \xi_2^0 \mathcal{L}_2(\mu) + \frac{8}{35}\beta^2 \xi_4^0 \mathcal{L}_4(\mu). \quad (\text{B.36})$$

List of Abbreviations

Abbreviation	Description
2PCF	Two-Point Correlation Function
SDSS	Sloan Digital Sky Survey
DE	Dark Energy
BAO	Baryonic Acoustic Oscillations
PS	Power Spectrum
CMB	Cosmic Microwave background
CDM	Cold Dark Matter
DM	Dark Matter
PDF	Probability Distribution Function
FLRW	Friedmann-Lemaître-Robertson-Walker
RSD	Redshift Space Distortions
TNS	RSD model proposed by Taruya, Nishimichi and Saito
LOS	Line Of Sight
FOG	Finger Of God

Bibliography

- [1] Aghanim N. et al., *Planck 2018 results. I. Overview and the cosmological legacy of Planck*, Astronomy & Astrophysics **641** A1 (2020), arXiv preprint: 1807.06205
- [2] Alcock C., Paczynski B., *An evolution free test for non-zero cosmological constant*, Nature **281** p.358-359 (1979), codice DOI: 10.1038/281358a
- [3] Arfken G. B., Weber H. J., Harris F. E., *Mathematical Methods for Physicists*, Elsevier Inc. (2013), ISBN: 978-0-12-384654-9
- [4] Ballinger W. E., Peacock J. A., Heavens A. F., *Measuring the cosmological constant with redshift surveys*, Monthly Notices of the Astronomical Society **282** (1996), arXiv preprint: 9605017
- [5] Bardeen J. M., Bond J. R., Kaiser N., Szalay A. S., *The Statistics of Peaks of Gaussian Random Fields*, the Astrophysical Journal **333** p.78-89 (1988), codice DOI: 10.1086/164143
- [6] Bassett B. A., Hlozek B. A., *Baryon Acoustic Oscillations*, Dark energy: observational and theoretical approaches p.246 (2010), arXiv preprint: 0910.5224
- [7] Bernardeau F. et al., *Large-Scale Structure of the Universe and Cosmological Perturbation Theory*, Physics Reports **367** p.1-248 (2002), arXiv preprint: 0112551
- [8] Bharadwaj S., *Non-linear redshift distortions: the two-point correlation function*, Monthly Notices of the Astronomical Society **327** 2, p.577-587 (2001), arXiv preprint: 0105320
- [9] Blake C. et al., *The WiggleZ Dark Energy Survey: mapping the distance–redshift relation with baryon acoustic oscillations*, Monthly Notices of the Royal Astronomical Society **418** 3, p.1707-1724 (2011), arXiv preprint: 1108.2635
- [10] Cole S., Fisher K. B., Weinberg D. H., *Fourier analysis of redshift-space distortions and the determination of Ω* , Monthly Notices of the Astronomical Society **267** p.785-799 (1994), arXiv preprint: 9308003
- [11] Cole S., Fisher K. B., Weinberg D. H., *Constraints on Ω from the IRAS redshift surveys*, Monthly Notices of the Astronomical Society **275** p.515-526 (1995), arXiv preprint: 9412062
- [12] Coles P., Lucchin F., *Cosmology: The origin and evolution of cosmic structure*, John Wiley & Sons (2003), ISBN: 0471489093

- [13] Dam L., Bolejko K., Lewis G. F., *Exploring the redshift-space peculiar velocity field and its power spectrum*, Journal of Cosmology and Astroparticle Physics **2021** 09 (2021), arXiv preprint: 2105.12933
- [14] Davis M., Peebles P. J. E., *On the integration of the BBGKY equations for the development of strongly nonlinear clustering in an expanding universe*, Astrophysical Journal Supplement Series **34** p.425-450 (1977), codice DOI: 10.1086/190456
- [15] De la Torre S. et al., *The VIMOS Public Extragalactic Redshift Survey (VIPERS). Galaxy clustering and redshift-space distortions at $z=0.8$ in the first data release*, Astronomy & Astrophysics **557**, A54 (2013), arXiv preprint: 1303.2622
- [16] De Sainte Agathe V. et al., *Baryon acoustic oscillations at $z = 2.34$ from the correlations of Ly α absorption in eBOSS DR14*, Astronomy & Astrophysics **629**, A85 (2019), arXiv preprint: 1904.03400
- [17] Desjacques V., Jeong D., Schmidt F., *Large-scale galaxy bias*, Physics Reports **733** p.1-193 (2018), codice DOI: 0370-1573, arXiv preprint: 1611.09787
- [18] Dodelson S., *Modern Cosmology*, Academic press (2020), ISBN: 978-0-12-815948-4
- [19] Eisenstein D. J., Hu W., *Baryonic Features in the Matter Transfer Function*, The Astrophysical Journal **496** p.605-614 (1998), arXiv preprint: 9709112
- [20] Eisenstein D. J., Seo H. J., White M., *On the Robustness of the Acoustic Scale in the Low-Redshift Clustering of Matter*, The Astrophysical Journal **664** 2 (2007), arXiv preprint: 0604361
- [21] Eisenstein D. J. et al., *Detection of the Baryon Acoustic Peak in the large-Scale Correlation Function of SDSS Luminous Red Galaxies*, The Astrophysical Journal **633** 2 (2005), arXiv preprint: 0501171
- [22] Ellis G. F. R., Maartens R., MacCallum M. A. H., *Relativistic Cosmology*, Cambridge University Press (2012), ISBN: 978-0-521-38115-4
- [23] Fisher K. B. et al., *Clustering in the 1.2-Jy IRAS galaxy redshift survey - II. Redshift distortions and $\xi(r_p, \pi)$* , Monthly Notices of the Astronomical Society **267** p.927-948 (1994), arXiv preprint: 9308013
- [24] Fisher K. B., *On The Validity of the Streaming Model for the Redshift-Space Correlation Function in the Linear Regime*, The Astrophysical Journal **448** (1995), arXiv preprint: 9412081
- [25] Fixen D. J., *The Temperature of the Cosmic Microwave Background*, The Astrophysical Journal **707** 2 (2009), arXiv preprint: 0911.1955
- [26] Gatzanaga E., Scoccimarro R., *The three-point function in large-scale structure: redshift distortions and galaxy bias*, Monthly Notices of the Astronomical Society **361** p.824-836 (2005), arXiv preprint: 0501637

- [27] Grasshorn Gebhart H. S., Jeong D., *Fast and accurate computation of projected two-point functions*, Physical Review D **97** 2 (2018), arXiv preprint: 1709.02401
- [28] Gorski K., *On the Pattern of Perturbations of the Hubble Flow*, The Astrophysical Journal **332** L7 (1988), codice DOI: 10.1086/185255
- [29] Hamilton A. J. S., *Measuring Omega and the Real Correlation Function from the Redshift Correlation Function*, The Astrophysical Journal, Part 2 - Letters **385** L5 (1992), codice DOI: 10.1086/186264
- [30] Hamilton A. J. S., *Linear redshift distortions: a review*, D. (eds) The Evolving Universe. Astrophysics and Space Science Library **231** p.185-275 (1998), arXiv preprint: 9708102
- [31] Hamilton A. J. S., Culhane M., *Spherical Redshift Distortions*, Monthly Notices of the Astronomical Society **278** p.73 (1996), arXiv preprint: 9507021
- [32] Hlozek R., Cortes M., Clarkson C., Basset B., *Non-parametric Dark Energy Degeneracies*, General Relativity and Gravitation **40** p.285-300 (2008), arXiv preprint: 0801.3847
- [33] Hlozek R. et al., *The Atacama Cosmology Telescope: a measurement of the primordial power spectrum*, The Astrophysical Journal **749** 1 (2012), arXiv preprint: 1105.4887
- [34] Jeong D., Dai L., Kamionkowski M., Szalay A. S., *The redshift-space galaxy two-point correlation function and baryon acoustic oscillations*, Monthly Notices of the Royal Astronomical Society **449** 3 p.3312-3322 (2015), arXiv preprint: 1408.4648
- [35] Kaiser N., *On the Spatial Correlations of Abell Clusters*, The Astrophysical Journal, Part 2 - Letters **284** p.L9-L12 (1984), codice DOI: 10.1086/184341
- [36] Kaiser N., *Clustering in Real and Redshift Space*, Monthly Notices of the Astronomical Society **227** 1 (1987), codice DOI: 10.1093/mnras/227.1.1
- [37] Kazin E. A. et al., *The clustering of galaxies in the SDSS-III Baryon Oscillation Spectroscopic Survey: measuring $H(z)$ and $D_A(z)$ at $z = 0.57$ with clustering wedges*, Monthly Notices of the Astronomical Society **435** 1 p.64-86 (2013), arXiv preprint: 1303.4391
- [38] Kubo R., *Generalized Cumulant Expansion Method*, Journal of the Physical Society of Japan **17** 7, p.1100-1120 (1962), codice DOI: 10.1143/JPSJ.17.1100
- [39] Kuruvilla J., *Modelling redshift-space distortion effects on spatial clustering and velocity statistics*, Universitäts und Landesbibliothek Bonn (2020), 20.500.11811/8649
- [40] Kuruvilla J., Porciani C., *On the streaming model for redshift-space distortions*, Monthly Notices of the Astronomical Society **479** 2, p.2256-2276 (2018), arXiv preprint: 1710.09379
- [41] Kwan J., Lewis G. F., Linder E. V., *Mapping Growth and Gravity with Robust Redshift Space Distortions*, The Astrophysical Journal **748** 2 (2012), arXiv preprint: 1105.1194v2

- [42] Liddle A. R., Lyth D. H., *Cosmological Inflation and Large-Scale Structure*, Cambridge University Press (2000), ISBN: 0-521-66022-X
- [43] Magira H., Jing Y. P., Suto Y., *Cosmological Redshift-Space Distortion on Clustering of High-Redshift Objects: Correction for Nonlinear Effects in the Power Spectrum and Tests with N-Body Simulations*, The Astrophysical Journal **528** (2000), arXiv preprint: 9907438
- [44] Mann R. G., Peacock J. A., Heavens A. F., *Eulerian bias and the galaxy density field*, Monthly Notices of the Astronomical Society **293** 3, p.209-221 (1998), arXiv preprint: 9708031
- [45] Milne E. A., *Relativity, Gravitation and World-Structure*, Nature **135** p.635-636 (1935), codice DOI: 10.1038/135635a0
- [46] Mo H., van den Bosch F., White S., *Galaxy formation and Evolution*, Cambridge University Press (2010), ISBN: 978-0-521-85793-2
- [47] Mukhanov V., *Physical Foundations of Cosmology*, Cambridge University Press (2005), ISBN: 978-0-521-56398-7
- [48] Padmanabhan N., White M., *Constraining anisotropic baryon oscillations*, Physics Review D **77** 12 (2008), arXiv preprint: 0804.0799
- [49] Park C., Vogeley M. S., Geller M. J., Huchra J. P., *Power Spectrum, Correlation Function, and Tests for Luminosity Bias in the CfA Redshift Survey*, The Astrophysical Journal **431** (1994), codice DOI: 10.1086/174508
- [50] Peacock J. A., *Cosmological Physics*, Cambridge university press (1998), ISBN: 0 521 41072 X
- [51] Peebles P. J. E., *The Large-Scale Structure of the Universe*, Princeton university press (1980), ISBN: 0-691-08239-1
- [52] Peebles P. J. E., *Physical Cosmology*, Princeton University Press (1993), ISBN: 0-691-07428-3
- [53] Percival W. J., White M., *Testing cosmological structure formation using redshift-space distortions*, Monthly Notices of the Astronomical Society **393** 1, p.297-308 (2009), arXiv preprint: 0808.0003
- [54] Pritchard J. R., Furlanetto S. R., Kamionkowski M., *Galaxy surveys, inhomogeneous re-ionization and dark energy*, Monthly Notices of the Astronomical Society **374** 1 p.159-167 (2006), arXiv preprint: 0604358
- [55] Reid B. A., White M., *Towards an accurate model of the redshift-space clustering of haloes in the quasi-linear regime*, Monthly Notices of the Astronomical Society **417** 3, p.1913-1927 (2011), arXiv preprint: 1105.4165
- [56] Riley K. F., Hobson M. P., Bence S. J., *Mathematical Methods for Physics and Engineering*, Cambridge University Press (2006), ISBN: 978-0-521-86153-3

- [57] Saito S., *Galaxy Clustering in Redshift Space*, Lecture Series on Cosmology: MPA Garching (2016), Shun_Saito_on_RSD.pdf
- [58] Scoccimarro R., *Redshift-Space Distortions, Pairwise Velocities and Nonlinearities*, Physical Review D **70** 8 (2004), arXiv preprint: 0407214
- [59] Seo H. J., Eisenstein D. J., *Improved Forecasts for the Baryon Acoustic Oscillations and Cosmological Distance Scale*, The Astrophysical Journal **665** 1 (2007), arXiv preprint: 0701079
- [60] Shaw J. R., Lewis A., *Non-linear Redshift Space Power Spectra*, Physical Review **78** 10 (2008), arXiv preprint: 0808.1724
- [61] Slepian Z., Li Y., Schmittfull M., Vlah Z., *Rotation method for accelerating multiple-spherical Bessel function integrals against a numerical source function*, arXiv e-prints (2019), arXiv preprint: 1912.00065
- [62] Song Y. S., Okumura T., Taruya A., *Broadband Alcock-Paczynski test exploiting redshift distortions*, Physical Review D **89** 10 (2014), arXiv preprint: 1309.1162
- [63] Song Y. S., Zheng Y., Taruya A., Minji O., *Hybrid modeling of redshift space distortions*, Journal of Cosmology and Astroparticle Physics **7** (2018), arXiv preprint: 1801.04950
- [64] Springel V. et al., *Simulations of the formation, evolution and clustering of galaxies and quasars*, Nature **435** p.629-636 (2005), arXiv preprint: 0504097
- [65] Taruya A., Bernardeau F., Nishimichi T., Codis S., *Direct and fast calculation of regularized cosmological power spectrum at two-loop order*, Physical Review D **86** 10 (2012), arXiv preprint: 1208.1191
- [66] Taruya A., Nishimichi T., Bernardeau F., *Precision modeling of redshift-space distortions from multi-point propagator expansion*, Physical Review D **87** 8 (2013), arXiv preprint: 1301.3624
- [67] Taruya A., Nishimichi T., Saito S., Hiramatsu T., *Nonlinear Evolution of Baryon Acoustic Oscillations from Improved Perturbation Theory in Real and Redshift Spaces*, Physical Review D **80** 12 (2009), arXiv preprint: 0906.0507
- [68] Taruya A., Nishimichi T., Saito S., *Baryon Acoustic Oscillations in 2D: Modeling Redshift-space Power Spectrum from Perturbation Theory*, Physical Review D **82** 6 (2010), arXiv preprint: 1006.0699
- [69] Tian H. J., Neyrinck M. C., Budavári T., Szalay A. S., *REDSHIFT-SPACE ENHANCEMENT OF LINE-OF-SIGHT BARYON ACOUSTIC OSCILLATIONS IN THE SLOAN DIGITAL SKY SURVEY MAIN-GALAXY SAMPLE*, The Astrophysical Journal **728** 1 (2011), arXiv preprint: 1011.2481
- [70] Tinker J. L., *Redshift-space distortions with the halo occupation distribution – II. Analytic model*, Monthly Notices of the Astronomical Society **374** 2, p.477-492 (2006), arXiv preprint: 0604217

- [71] Tonegawa M., Appleby S., Park C., Sungwook H. E., Kim J., *The effects of non-linearity on the growth rate constraint from velocity correlation functions*, Monthly Notices of the Astronomical Society **529** 4, p.4787-4802 (2024), arXiv preprint: 2309.14457v2
- [72] Weinberg D. H. et al., *Observational Probes of Cosmic Acceleration*, Physics Reports **530** 2 p.87-255 (2013), arXiv preprint: 1201.2434
- [73] Weinberg S., *Gravitation and Cosmology: Principles and Applications of the General Theory of Relativity*, Wiley (1972), ISBN: 9780471925675
- [74] Weinberg S., *Cosmology*, Oxford University Press (2008), ISBN: 978-0-19-884528-7
- [75] White M. et al., *The Clustering of Massive Galaxies at $z \sim 0.5$ from the First Semester of BOSS Data*, The Astrophysical Journal **728** 2 (2011), arXiv preprint: 1010.4915
- [76] White M., *Redshift Space Distortions*, UC Berkley, mini_red_mjw.pdf
- [77] Zheng Y., Song Y. S., *Study on the mapping of dark matter clustering from real space to redshift space*, Journal of Cosmology and Astroparticle Physics **2016** 8 (2016), arXiv preprint: 1603.00101